A STUDY OF SOME TIME-DEPENDENT FLOWS IN MAGNETOHYDRODYNAMICS

BY

CLEMENT ADEDAYO APERE

DEPARTMENT OF MATHEMATICS
FACULTY OF SCIENCE
AHMADU BELLO UNIVERSITY
ZARIA, NIGERIA

APRIL, 2012

A STUDY OF SOME TIME-DEPENDENT FLOWS IN MAGNETOHYDRODYNAMICS

BY

CLEMENT ADEDAYO APERE

DEPARTMENT OF MATHEMATICS
FACULTY OF SCIENCE
AHMADU BELLO UNIVERSITY
ZARIA, NIGERIA

APRIL, 2012

A STUDY OF SOME TIME-DEPENDENT FLOWS IN MAGNETOHYDRODYNAMICS

BY

CLEMENT ADEDAYO APERE
BSc (NDA, 1990), MSc (UNILAG, 1998)
PHD/SCIE/00746/2006-07

A DISSERTATION SUBMITTED TO THE SCHOOL OF POSTGRADUATE STUDIES AHMADU BELLO UNIVERSITY ZARIA, NIGERIA IN PARTIAL FULFILLMENT OF THE REQUIREMENTS FOR THE AWARD OF
DOCTOR OF PHILOSOPHY IN MATHEMATICS

DEPARTMENT OF MATHEMATICS
FACULTY OF SCIENCE
AHMADU BELLO UNIVERSITY
ZARIA, NIGERIA

DECLARATION

I declare that the work in this dissertation titled "A Study of Some Time-dependent Flows in Magnetohydrodynamics" was performed by me in the Department of Mathematics under the supervision of Prof. B. K. Jha, Prof. D. Singh and Dr. J. Singh.

The information derived from the literature has been duly acknowledged in the text and a list of references provided. No part of this work has been presented for another degree or diploma at any institution.

Clement Adedayo Apere	Date

CERTIFICATION

This dissertation titled "A Study of Some Time-dependent Flows in Magnetohydrodynamics" by APERE, Clement Adedayo meets the regulation governing the award of Doctor of Philosophy of Ahmadu Bello University, Zaria and is approved for its contribution to knowledge and literary presentation.

Basant Kumar Jha — 24.04.2012

Prof. B. K. Jha
Chairman, Supervisory Committee — Date

25-04-12

Prof D. Singh
Member, Supervisory Committee — Date

24.04.2012.

Dr. J Singh
Member, Supervisory Committee — Date

24/4/2012

Prof. R. O. Ayeni
External Examiner — Date

25-04-12

Dr. B. Sani
Head of Department — Date

Prof. A. A. Joshua
Dean, School of Postgraduate Studies — Date

ACKNOWLEDGEMENTS

First and foremost, glory to God who bestowed upon me the potential to pursue a doctoral degree. Luck plays a very important role in my life especially in the choice of my dissertation supervisor, I have been extremely lucky to have Prof. B. K. Jha supervise my work. Without his guidance, dedication and encouragement, I would not have finished my programme so smoothly. He taught me to have tremendous passion and confidence in science research which I now know is priceless. Words are too limited to express my feelings to a person who sacrificed his health and private time to the successful completion of this work. To him, I say a big thank you.

I would also like to express my gratitude to other members of the Supervisory Committee, Prof. D. Singh and Dr. J. Singh for their invaluable contributions towards this study. My thanks go to the Head, Department of Mathematics, Dr. B. Sani and all the lecturers in the department for their friendly disposition and support throughout the period of my studies. I owe thanks in particular to Dr. O. Ajibade who was of immense assistance and a source of inspiration and also to Drs. A. M. Ibrahim and A. Mohammed for their involvement in different aspects of my research project, and many fruitful discussions. My gratitude also to many of my fellow researchers who took time away from their own busy schedules to provide feedback on this dissertation. I am reluctant to include such a list, as I will surely skip someone who deserves a mention.

I am eternally indebted to two personalities; Prof. K. Abubakar and Late Dr. H. Erhie. They both believed in my ability and encouraged me to pursue a doctoral study, without their motivation and insistence, I would not have started the course in the first place. Thanks also to members of my family who have been extremely understanding and supportive of my studies. I feel very lucky to have a family that shares my enthusiasm for academic pursuits. Finally, thanks to my wonderful wife, Sarah, who has encouraged me so much over the years.

DEDICATION

Devotion and relentless hard work were the key hallmarks for the completion of my doctoral dissertation, but even more was the support of my family. To my wife, Sarah and my adorable daughters; Chesna, Chemdiya and Chevonn. Today, I dedicate this important achievement to them, because without their support and understanding, I would not have achieved my goal. I love you all.

ABSTRACT

The motion of an electrically conducting fluid in two types of geometries is studied; namely a channel formed by two parallel plates and an annulus formed by two concentric cylinders. The fluid flow is assumed to be unsteady, laminar and incompressible with a magnetic field applied perpendicular to the flow direction. It is also assumed that no applied or polarization voltage exists. We have considered different physical situations and factored the effect of Hall and ion-slip currents in some cases. The system of partial differential equations describing the different flow problems has been formulated and unified closed form expressions are obtained for both cases of the applied magnetic field being fixed to either the fluid or the moving wall where applicable. The Laplace transform techniques are used to reduce the system of partial differential equations to ordinary differential equations; the resulting boundary value problems are then solved analytically. However, the Riemann-sum approximation method is used to invert the Laplace domain to the time domain where direct inversion is difficult. The corresponding steady state equations are derived where appropriate and solved analytically to double check the results. Also, the implicit finite difference method is used to verify the Riemann-sum approximation method. MATLAB programmes are written to compute and generate the graphs for the velocities and the skin frictions. A parametric study depicting the effect of the various dimensionless parameters on the velocity and skin friction is conducted. These parameters include the Ekman number *E*, the Hall parameter /3„ ion-slip parameter /3„ the suction/injection parameter S, the Hartmann number *Ha* and time *r*\ amongst others. The effects of changing the parameters mentioned above are observed either to increase, to decrease or to have no effect on the velocity profiles and the skin friction.

TABLE OF CONTENTS

ACKNOWLEDGEMENTS v

DEDICATION vi

ABSTRACT vii

LIST OF FIGURES xx

LIST OF TABLES xxi

NOMENCLATURE xxii

1 CHAPTER 1: INTRODUCTION 1

1.1 GOVERNING EQUATIONS OF MHD 5

1.1.1 Equation of Continuity 5

1.1.2 Maxwell's Equations 6

1.1.3 Navier-Stokes Equations 8

1.1.3.1 Geometric Configurations 10

1.1.4 Magnetic Induction Equation 12

1.2 BOUNDARY LAYER CONCEPT 12

1.3 ROTATING FRAME OF REFERENCE 14

1.4 MATHEMATICAL METHODS 17

1.4.1 Laplace Transform 17

1.4.1.1 Definition of Exponential Order 17

1.4.2 Riemann-sum Approximation 20

1.4.3 Finite Difference Method 22

1.5 OBJECTIVES OF THE STUDY 26

1.6 RESEARCH METHODOLOGY 27

1.7 OUTLINE OF THE DISSERTATION 28

2 CHAPTER 2: MHD COUETTE FLOW IN A ROTATING CHANNEL 30
2.1 TIME-DEPENDENT MHD COUETTE FLOW IN A ROTATING SYSTEM WITH SUCTION/INJECTION 33
2.1.1 Mathematical Analysis 34
2.1.2 Solution of the Problem 37
2.1.3 Skin Friction 40
2.1.4 Results and Discussion 42
2.2 COMBINED EFFECT OF HALL AND ION-SLIP CURRENTS ON MHD COUETTE FLOW IN A ROTATING SYSTEM 50
2.2.1 Mathematical Analysis 50
2.2.2 Solution of the Problem 53
2.2.3 Skin Friction 55
2.2.4 Steady State 56
2.2.5 Results and Discussion 57
2.3 HALL AND ION-SLIP EFFECTS ON UNSTEADY MHD COUETTE FLOW IN A ROTATING SYSTEM WITH SUCTION AND INJECTION . 66
2.3.1 Mathematical Analysis 66
2.3.2 Solution of the Problem 68
2.3.3 Skin Friction 70
2.3.4 Steady State 72
2.3.5 Results and Discussion 72
2.4 PARTICULAR CASES 83
2.5 CONCLUDING REMARKS 83

3 CHAPTER 3: MHD COUETTE FLOW IN AN ANNULUS 85
3.1 UNSTEADY MHD COUETTE FLOW IN AN ANNULUS: THE RIEMANN-SUM APPROXIMATION APPROACH 89
3.1.1 Mathematical Analysis 89
3.1.2 Solution of the Problem 91
3.1.3 Skin Friction 93
3.1.4 Results and Discussion 94
3.2 MHD COUETTE FLOW IN AN ANNULUS HAVING RAMP MOTION OF INNER CYLINDER 98
3.2.1 Mathematical Analysis 98

3.2.2 Skin Friction 102
3.2.3 Mass Flux 102
3.2.4 Steady State 103
3.2.5 Results and Discussion 104
3.3 UNSTEADY MHD TAYLOR-COUETTE FLOW WITH TRANSPIRATION 109
3.3.1 Mathematical Analysis 109
3.3.2 Solution of the problem 111
3.3.3 Skin Friction 114
3.3.4 Steady State 115
3.3.5 Results and Discussion 116
3.4 CONCLUDING REMARKS 123

4 CHAPTER 4: MHD TWO-PHASE COUETTE FLOW 124
4.1 UNSTEADY MHD TWO-PHASE COUETTE FLOW OF FLUID-PARTICLE SUSPENSION 127
4.1.1 Mathematical Analysis 127
4.1.2 Solution of the Problem 129
4.1.3 Skin Friction 134
4.1.4 Steady State 135
4.1.5 Result and Discussion 136
4.2 UNSTEADY MHD TWO-PHASE COUETTE FLOW OF FLUID-PARTICLE SUSPENSION IN AN ANNULUS 144
4.2.1 Mathematical Analysis 144
4.2.2 Analytical Solution 146
4.2.3 Skin Friction 150
4.2.4 Steady State Solution 151
4.2.5 Numerical Solution 153
4.2.6 Result and Discussion 156
4.3 CONCLUDING REMARKS 165

5 CHAPTER 5: MHD FREE CONVECTIVE FLOW 166
5.1 MHD FREE CONVECTIVE COUETTE FLOW WITH SUCTION AND INJECTION 169
5.1.1 Mathematical Analysis 169

5.1.2 Rate of Heat Transfer and Skin Friction 174
5.1.3 Validation of the Method 175
5.1.4 Results and Discussion 176
5.2 MHD TRANSIENT FREE CONVECTIVE FLOW IN A VERTICAL ANNULUS WITH THERMAL BOUNDARY CONDITION OF THE SECOND KIND 184
5.2.1 Mathematical Analysis 184
5.2.2 Solution of the Problem 187
5.2.3 Rate of Heat Transfer and Skin Friction 189
5.2.4 Steady State 190
5.2.5 Results and Discussion 191
5.3 CONCLUDING REMARKS 198

6 CHAPTER 6: SUMMARY, CONCLUSIONS AND FUTURE DIRECTIONS **199**
6.1 SUMMARY 199
6.2 CONCLUSIONS 200
6.3 FUTURE DIRECTIONS 202
6.3.1 Induced Magnetic Field 202
6.3.2 Non-Newtonian Fluid 203
6.3.3 Compressible Fluid 203
6.3.4 MHD in Fusion Plasma 204

I Appendix **206**

References **208**

LIST OF FIGURES

2.1 Schematic diagram of the model 34
2.2 Primary velocity u showing the effect of $\mathcal{S}$ with $K = 0$ and $K = 1$ represented by a and b respectively with fixed values of $\mathcal{H}a = 0.5$, $\mathcal{E} = 1$, $\eta = 0.4$ where $\mathcal{S} \in [-5, 5]$ 45
2.3 Secondary velocity v showing the effect of $\mathcal{S}$ with $K = 0$ and $K = 1$ represented by a and b respectively with fixed values of $\mathcal{H}a = 0.5$, $\mathcal{E} = 1$, $\eta = 0.4$ where $\mathcal{S} \in [-5, 5]$ 45
2.4 Primary velocity u showing the effect of $\mathcal{S}$ and $\mathcal{H}a$ with $K = 0$ and $K = 1$ represented by a and b respectively with fixed values of $z = 0.5$, $\mathcal{E} = 1$, $\eta = 0.4$ where $\mathcal{H}a \in [1, 5]$ 46
2.5 Secondary velocity v showing the effect of $\mathcal{S}$ and $\mathcal{H}a$ with $K = 0$ and $K = 1$ represented by a and b respectively with fixed values of $z = 0.5$, $\mathcal{E} = 1$, $\eta = 0.4$ where $\mathcal{H}a \in [1, 5]$ 46
2.6 Primary velocity u showing the effect of $\mathcal{S}$ and $\mathcal{E}$ with $K = 0$ and $K = 1$ represented by a and b respectively with fixed values of $z = 0.5$, $\mathcal{H}a = 1$, $\eta = 0.4$ where $\mathcal{E} \in [1, 5]$ 47
2.7 Secondary velocity v showing the effect of $\mathcal{S}$ and $\mathcal{E}$ with $K = 0$ and $K = 1$ represented by a and b respectively with fixed values of $z = 0.5$, $\mathcal{H}a = 1$, $\eta = 0.4$ where $\mathcal{E} \in [1, 5]$ 47
2.8 Primary velocity u showing the effect of $\mathcal{S}$ and η with $K = 0$ and $K = 1$ represented by a and b respectively with fixed values of $z = 0.5$, $\mathcal{H}a = 1$, $\mathcal{E} = 1$ where $\eta \in [0.1, 2]$ 48
2.9 Secondary velocity v showing the effect of $\mathcal{S}$ and η with $K = 0$ and $K = 1$ represented by a and b respectively with fixed values of $z = 0.5$, $\mathcal{H}a = 1$, $\mathcal{E} = 1$ where $\eta \in [0.1, 2]$ 48
2.10 Resultant skin friction at the plate where fluid is being injected ($z = 0$) with $K = 0$ and $K = 1$ represented by a and b respectively with fixed values of $\mathcal{H}a = 1$, $\mathcal{E} = 1$, where $\eta \in [0.1, 1]$ 49

2.11 Resultant skin friction at the plate where fluid is being sucked ($z = 1$) with $K = 0$ and $K = 1$ represented by a and b respectively with fixed values of $\mathcal{H}a = 1, \mathcal{E} = 1$, where $\eta \in [0.1, 1]$ 49
2.12 Primary velocity u showing the effect of Hall current in the presence of ion-slip current with $K = 0$ and $K = 1$ represented by a and b respectively with fixed values of $\mathcal{H}a = 35.0$, $\mathcal{E} = 1.0$, $\eta = 0.1$, $\beta_i = 5.0$ and $\beta_e \in [1.0, 10.0]$ 60
2.13 Secondary velocity v showing the effect of Hall current in the presence of ion-slip current with $K = 0$ and $K = 1$ represented by a and b respectively with fixed values of $\mathcal{H}a = 35.0$, $\mathcal{E} = 1.0$, $\eta = 0.1$, $\beta_i = 5.0$ and $\beta_e \in [1.0, 10.0]$ 60
2.14 Primary velocity u showing the effect of ion-slip current with $K = 0$ and $K = 1$ represented by a and b respectively with fixed values of $\mathcal{H}a = 35.0$, $\mathcal{E} = 1.0$, $\eta = 0.1$, $\beta_e = 10.0$ and $\beta_i \in [1.0, 5.0]$. 61
2.15 Secondary velocity v showing the effect of ion-slip current with $K = 0$ and $K = 1$ represented by a and b respectively with fixed values of $\mathcal{H}a = 35.0$, $\mathcal{E} = 1.0$, $\eta = 0.1$, $\beta_e = 10.0$ and $\beta_i \in [1.0, 5.0]$. 61
2.16 Primary velocity u showing the effect of Hall current over the ion-slip current with $K = 0$ and $K = 1$ represented by a and b respectively with fixed values of $z = 0.5$, $\eta = 0.1$, $\mathcal{H}a = 35.0$ and $\mathcal{E} = 1.0$ 62
2.17 Secondary velocity v showing the effect of Hall current over the ion-slip current with $K = 0$ and $K = 1$ represented by a and b respectively with fixed values $z = 0.5$, $\eta = 0.1$, $\mathcal{H}a = 35.0$ and $\mathcal{E} = 1.0$ 62
2.18 Primary velocity u showing the effect of time with $K = 0$ and $K = 1$ represented by a and b respectively with fixed values of $\mathcal{H}a = 35.0$, $\mathcal{E} = 1$, $\beta_e = 10.0$, $\beta_i = 5.0$ and $\eta \in [0.01, 0.15]$ 63
2.19 Secondary velocity v showing the effect of time with $K = 0$ and $K = 1$ represented by a and b respectively with fixed values of $\mathcal{H}a = 35.0$, $\mathcal{E} = 1$, $\eta = 0.4$, $\beta_e = 10.0$, $\beta_i = 5.0$ and $\eta \in [0.01, 0.15]$ . . 63
2.20 The resultant skin friction at $z = 0$ showing the effect of Hall and ion-slip parameter with $K = 0$ and $K = 1$ represented by a and b respectively with fixed values of $\mathcal{E} = 1$, $\mathcal{H}a = 35.0$ and $\eta = 0.1$ . . 64

2.21 The resultant skin friction at $z = 1$ showing the effect of Hall and ion-slip parameter with $K = 0$ and $K = 1$ represented by a and b respectively with fixed values of $\mathcal{E} = 1$, $\mathcal{H}a = 35.0$ and $\eta = 0.1$ . . 64
2.22 The resultant skin friction at $z = 0$ showing the effect of Hartmann number and time with $K = 0$ and $K = 1$ represented by a and b respectively with fixed values of $\mathcal{E} = 1$, $\beta_e = 10.0$, $\beta_i = 5.0$ and $\eta \in [0.01, 0.15]$ 65
2.23 The resultant skin friction at $z = 1$ showing the effect of Hartmann number and time with $K = 0$ and $K = 1$ represented by a and b respectively with fixed values of $\mathcal{E} = 1$, $\beta_e = 10.0$, $\beta_i = 5.0$ and $\eta \in [0.01, 0.15]$ 65
2.24 Primary velocity profile u showing the effect of rotation parameter with $K = 0$ and $K = 1$ represented by a and b respectively with fixed values of $\mathcal{S} = 0.5$, $\mathcal{H}a = 10.0$, $\eta = 0.1$, $\beta_e = 5.0$ and $\beta_i = 1.0$. 75
2.25 Secondary velocity profile v showing the effect of rotation parameter with $K = 0$ and $K = 1$ represented by a and b respectively with fixed values of $\mathcal{S} = 0.5$, $\mathcal{H}a = 10.0$, $\eta = 0.1$, $\beta_e = 5.0$ and $\beta_i = 1.0$ 76
2.26 Primary velocity u showing the effect of suction/injection parameter with $K = 0$ and $K = 1$ represented by a and b respectively with fixed values of $\mathcal{H}a = 10.0$, $\Omega = 2.0$, $\eta = 0.1$, $\beta_e = 5.0$ and $\beta_i = 1.0$ 76
2.27 Secondary velocity v showing the effect of suction/injection parameter with $K = 0$ and $K = 1$ represented by a and b respectively with fixed values $\mathcal{S} = 0.5$, $\mathcal{H}a = 10.0$ and $\Omega = 2.0$, $\eta = 0.1$, $\beta_e = 5.0$ and $\beta_i = 1.0$ 77
2.28 Primary velocity profile u showing the effect of Hall current in the presence of ion-slip current with $K = 0$ and $K = 1$ represented by a and b respectively with fixed values of $\mathcal{S} = 0.5$, $\mathcal{H}a = 10.0$, $\Omega = 2.0$, $\eta = 0.1$, $\beta_i = 1.0$ 77
2.29 Secondary velocity profile v showing the effect of Hall current in the presence of ion-slip current with $K = 0$ and $K = 1$ represented by a and b respectively with fixed values of $\mathcal{S} = 0.5$, $\mathcal{H}a = 10.0$, $\Omega = 2.0$, $\eta = 1.0$, $\beta_i = 1.0$ 78

2.30 Primary velocity profile u showing the effect of ion-slip current with $K = 0$ and $K = 1$ represented by a and b respectively with fixed values of $\mathcal{S} = 0.5$, $\mathcal{H}a = 10.0$, $\Omega = 2.0$, $\eta = 0.1$, $\beta_e = 5.0$ and $\beta_i = 1.0$ 78
2.31 Secondary velocity profile v showing the effect of ion-slip current with $K = 0$ and $K = 1$ represented by a and b respectively with fixed values of $\mathcal{S} = 0.5$, $\mathcal{H}a = 10.0$, $\Omega = 2.0$, $\eta = 1.0$, $\beta_e = 5.0$ and $\beta_i = 1.0$ 79
2.32 The resultant skin friction at $z = 0$ showing the effect of Hall and ion-slip parameter with $K = 0$ and $K = 1$ represented by a and b respectively with fixed values of $\mathcal{S} = 0.5$, $\mathcal{H}a = 10.0$, $\Omega = 2.0$ and $\eta = 0.1$ 79
2.33 The resultant skin friction at $z = 1$ showing the effect of Hall and ion-slip parameter with $K = 0$ and $K = 1$ represented by a and b respectively with fixed values of $\mathcal{S} = 0.5$, $\mathcal{H}a = 10.0$, $\Omega = 2.0$ and $\eta = 0.1$ 80
2.34 The resultant skin friction at $z = 0$ showing the effect of time and $\mathcal{S}$ with $K = 0$ and $K = 1$ represented by a and b respectively with fixed values of $\mathcal{H}a = 10.0$, $\Omega = 2.0$ $\beta_e = 5.0$ and $\beta_i = 1.0$. 80
2.35 The resultant skin friction at $z = 1$ showing the effect of time and $\mathcal{S}$ with $K = 0$ and $K = 1$ represented by a and b respectively with fixed values of $\mathcal{H}a = 10.0$, $\Omega = 2.0$ $\beta_e = 5.0$ and $\beta_i = 1.0$. 81
2.36 The secondary skin friction at $z = 0$ showing the effect of β_i and $\mathcal{S}$ with $K = 1$ and fixed values of $\mathcal{H}a = 10.0$, $\eta = 0.1$, $\Omega = 2.0$ and $\beta_e = 5.0$. 81
2.37 The secondary skin friction at $z = 1$ showing the effect of β_i and $\mathcal{S}$ with $K = 1$ and fixed values of $\mathcal{H}a = 10.0$, $\eta = 0.1$, $\Omega = 2.0$ and $\beta_e = 5.0$. 82

3.1 The velocity profile u showing the effect of $\mathcal{H}a$ with $K = 0$ and $K = 1$ represented by a and b respectively and $\eta = 5.0$. 95
3.2 The velocity profile u showing the effect of η and $K = 0$ and $K = 1$ represented by a and b respectively with $\mathcal{H}a = 0.3$. 96

3.3 The velocity profile u showing the effect of η and $K = 0$ and $K = 1$ represented by a and b respectively with $\mathcal{H}a = 4$. 96
3.4 The variation of the skin friction with η at the outer surface of the inner cylinder ($r = 1$) with $K = 0$ and $K = 1$ represented by a and b respectively. 97
3.5 The variation of the skin friction with η at the inner surface of the outer cylinder ($r = 2$) with $K = 0$ and $K = 1$ represented by a and b respectively. 97
3.6 The velocity profile u showing the effect of η with $K = 0$ and $K = 1$ represented by a and b respectively and $\eta_0 = 0.5$, $\mathcal{H}a = 1$. 106
3.7 The velocity profile u showing the effect of $\mathcal{H}a$ with $K = 0$ and $K = 1$ represented by a and b respectively and $\eta_0 = 0.5$, $\eta = 1$. . . 106
3.8 The skin friction at the outer surface of the inner cylinder ($r = 1$) showing the influence of $\mathcal{H}a$ and η with $K = 0$ and $K = 1$ represented by a and b respectively and $\eta_0 = 0.5$. 107
3.9 The skin friction at the inner surface of the outer cylinder ($r = 2$) showing the influence of $\mathcal{H}a$ and η with $K = 0$ and $K = 1$ represented by a and b respectively and $\eta_0 = 0.5$. 107
3.10 The dimensionless mass flux Q showing the influence of $\mathcal{H}a$ and η with $K = 0$ and $K = 1$ represented by a and b respectively and $\eta_0 = 1$. 108
3.11 Velocity v vs r with $\mathcal{S} = 0.5$, $\mathcal{H}a = 2.0$ and various values of β varying η. 119
3.12 Velocity v vs r with $\mathcal{S} = 0.5$, $\eta = 0.05$ and $\beta = 1.0$ for different values of $\mathcal{H}a$. 120
3.13 Velocity v vs r with $\mathcal{S} = 0.5$, $\mathcal{H}a = 2.0$ and $\eta = 0.05$ for different values of β. 120
3.14 Velocity v vs r with $\eta = 0.05$, $\mathcal{H}a = 2.0$ and $\beta = 1.0$ for different values of $\mathcal{S}$. 121
3.15 Velocity v vs $\mathcal{S}$ at the centerline of the annulus ($r = 1.5$) with $\mathcal{H}a = 2.0$, $\eta = 0.05$ for different values of β. 121
3.16 Skin friction τ vs $\mathcal{S}$ at outer surface of the inner cylinder ($r = 1.0$) with $\mathcal{H}a = 2.0$ and $\eta = 0.05$ for different values of β. 122

3.17 Skin friction τ vs S at the inner surface of the outer cylinder ($r = 2.0$) with $\mathcal{H}a = 2.0$ and $\eta = 0.05$ for different values of β. . . . 122

4.1 Profile of the fluid phase velocity u_f showing the effect of time with $K = 0$ and $K = 1$ represented by a and b respectively ($\mathcal{K} = 50.0$, $R_v = 1.0$, $R_c = 0.25$ and $\mathcal{H}a = 2$). 138
4.2 Profile of the particle phase velocity u_p showing the effect of time with $K = 0$ and $K = 1$ represented by a and b respectively ($\mathcal{K} = 50.0$, $R_v = 1.0$, $R_c = 0.25$ and $\mathcal{H}a = 2$). 139
4.3 Profile of the fluid phase velocity u_f showing the effect of $\mathcal{H}a$ with $K = 0$ and $K = 1$ represented by a and b respectively ($\mathcal{K} = 50.0$, $R_v = 1.0$, $R_c = 0.25$ and $\eta = 0.1$). 139
4.4 Profile of the particle phase velocity u_p showing the effect of $\mathcal{H}a$ with $K = 0$ and $K = 1$ represented by a and b respectively ($\mathcal{K} = 50.0$, $R_v = 1.0$, $R_c = 0.25$ and $\eta = 0.1$). 140
4.5 Profile of the fluid phase velocity u_f showing the effect of R_v and η ($\mathcal{K} = 50.0$, $R_c = 0.25$, $z = 0.5$ and $\mathcal{H}a = 2$). 140
4.6 Profile of the particle phase velocity u_p showing the effect of R_v and η ($\mathcal{K} = 50.0$, $R_c = 0.25$, $z = 0.5$ and $\mathcal{H}a = 2$). 141
4.7 Profile of the fluid phase velocity u_f showing the effect of R_c and η ($\mathcal{K} = 50.0$, $R_v = 1.0$, $z = 0.5$ and $\mathcal{H}a = 2$). 141
4.8 Profile of the particle phase velocity u_p showing the effect of R_c and η ($\mathcal{K} = 50.0$, $R_v = 1.0$, $z = 0.5$ and $\mathcal{H}a = 2$). 141
4.9 Variation of the fluid phase skin friction on the plate at $z = 0$ showing the effect of R_v and η ($\mathcal{K} = 50.0$, $\mathcal{H}a = 2.0$ and $R_c = 0.25$). 142
4.10 Variation of the particle phase skin friction on the plate at $z = 0$ showing the effect of R_v and η ($\mathcal{K} = 50.0$, $\mathcal{H}a = 2.0$ and $R_c = 0.25$). 142
4.11 Variation of the fluid phase skin friction on the plate at $z = 1$ showing the effect of R_v and η ($\mathcal{K} = 50.0$, $\mathcal{H}a = 2.0$ and $R_c = 0.25$). 142
4.12 Variation of the particle phase skin friction on the plate at $z = 1$ showing the effect of R_v and η ($\mathcal{K} = 50.0$, $\mathcal{H}a = 2.0$ and $R_c = 0.25$). 143
4.13 Schematic diagram of the problem 145

4.14 Profile of the fluid phase velocity u_f showing the effect of time with $K = 0$ and $K = 1$ represented by a and b respectively ($\mathcal{K} = 50.0$, $R_v = 1.0$, $R_c = 0.25$ and $\mathcal{H}a = 2$). 159
4.15 Profile of the particle phase velocity u_p showing the effect of time with $K = 0$ and $K = 1$ represented by a and b respectively ($\mathcal{K} = 50.0$, $R_v = 1.0$, $R_c = 0.25$ and $\mathcal{H}a = 2$). 159
4.16 Profile of the fluid phase velocity u_f showing the effect of $\mathcal{H}a$ with $K = 0$ and $K = 1$ represented by a and b respectively ($\mathcal{K} = 50.0$, $R_v = 1.0$, $R_c = 0.25$ and $\eta = 0.5$). 160
4.17 Profile of the fluid phase velocity u_p showing the effect of $\mathcal{H}a$ with $K = 0$ and $K = 1$ represented by a and b respectively ($\mathcal{K} = 50.0$, $R_v = 1.0$, $R_c = 0.25$ and $\eta = 0.5$). 160
4.18 Profile of the fluid phase velocity u_f showing the effect of R_v and η with $K = 0$ and $K = 1$ represented by a and b respectively ($\mathcal{K} = 50.0$, $r = 1.5$, $R_c = 0.25$, $\mathcal{H}a = 2.0$ and $\eta = 0.5$). 161
4.19 Profile of the fluid phase velocity u_p showing the effect of R_v and η with $K = 0$ and $K = 1$ represented by a and b respectively ($\mathcal{K} = 50.0$, $r = 1.5$, $R_c = 0.25$, $\mathcal{H}a = 2.0$ and $\eta = 0.5$). 161
4.20 Profile of the fluid phase velocity u_f showing the effect of R_c and η with $K = 0$ and $K = 1$ represented by a and b respectively ($\mathcal{K} = 50.0$, $r = 1.5$, $R_v = 1.0$, $\mathcal{H}a = 2.0$ and $\eta = 0.5$). 162
4.21 Profile of the particle phase velocity u_p showing the effect of R_c and η with $K = 0$ and $K = 1$ represented by a and b respectively ($\mathcal{K} = 50.0$, $r = 1.5$, $R_v = 1.0$, $\mathcal{H}a = 2.0$ and $\eta = 0.5$). 162
4.22 Variation of the fluid phase skin friction on the outer surface of the inner cylinder ($r = 1$) showing the effect of R_v and η ($\mathcal{K} = 50.0$, $\mathcal{H}a = 2.0$ and $R_c = 0.25$). 163
4.23 Variation of the particle phase skin friction on the outer surface of the inner cylinder ($r = 1$) showing the effect of R_v and η ($\mathcal{K} = 50.0$, $\mathcal{H}a = 2.0$ and $R_c = 0.25$). 163
4.24 Variation of the fluid phase skin friction on the inner surface of the outer cylinder ($r = 2$) showing the effect of R_v and η ($\mathcal{K} = 50.0$, $\mathcal{H}a = 2.0$ and $R_c = 0.25$). 164

4.25 Variation of the particle phase skin friction on the inner surface of the outer cylinder ($r = 2$) showing the effect of R_v and η ($K = 50.0$, $\mathcal{H}a = 2.0$ and $R_c = 0.25$). 164

5.1 Temperature profile θ showing the effect of η ($Pr = 0.71$ and $\mathcal{S} = 0.5$ 180

5.2 Temperature profile θ showing the effect of Pr and $\mathcal{S}$ at $\eta = 0.1$ at $z = 0.5$ 180

5.3 Velocity profile u for the cooling of the plate showing the effect of η with $K = 0$ and $K = 1$ represented by a and b respectively ($Pr = 0.71$, $\mathcal{S} = 0.5$, $Gr = 10$ and $\mathcal{H}_a = 2$). 181

5.4 Velocity profile u for the heating of the plate showing the effect of time η with $K = 0$ and $K = 1$ represented by a and b respectively ($Pr = 0.5$, $\mathcal{S} = 0.5$, Gr=-10 and $\mathcal{H}_a = 2$). 181

5.5 Velocity profile u for the cooling of the plate showing the effect of $\mathcal{H}_a$ and $\mathcal{S}$ with $K = 0$ and $K = 1$ represented by a and b respectively ($Gr = 10$, $Pr = 0.7$, $z = 0.5$ and $\eta = 0.1$). 181

5.6 Velocity profile u for the heating of the plate showing the effect of $\mathcal{H}_a$ and $\mathcal{S}$ with $K = 0$ and $K = 1$ represented by a and b respectively ($Gr = -10$, $Pr = 0.71$, $z = 0.5$ and $\eta = 0.1$. 182

5.7 Velocity profile u showing the effect of Gr and $\mathcal{S}$ with $K = 0$ and $K = 1$ represented by a and b respectively ($z = 0.5$, $Pr = 0.71$, $\eta = 0.1$ and $\mathcal{H}_a = 2$). 182

5.8 Rate of heat transfer at $z = 0$ showing the effect of Pr and $\mathcal{S}$ at $\eta = 0.1$. 182

5.9 Rate of heat transfer at $z = 1$ showing the effect of Pr and $\mathcal{S}$ at $\eta = 0.1$. 183

5.10 Skin friction on the plate at $z = 0$ showing the effect of Gr and $\mathcal{S}$ with $K = 0$ and $K = 1$ represented by a and b respectively ($Pr = 0.71$, $\eta = 0.1$ and $\mathcal{H}_a = 2$). 183

5.11 Skin friction on the plate at $z = 1$ showing the effect of Gr and $\mathcal{S}$ with $K = 0$ and $K = 1$ represented by a and b respectively ($Pr = 0.71$,$\eta = 0.1$ and $\mathcal{H}_a = 2$). 183

5.12 Schematic of the problem 186

5.13 Temperature profile θ showing the effect of η with $Pr = 0.71$ and $\mathcal{H}a = 2$. 194
5.14 Temperature profile θ showing the effect of Pr with $\eta = 0.2$ and $\mathcal{H}a = 2$. 194
5.15 Velocity profile u showing the effect of η with $Pr = 0.71$ and $\mathcal{H}a = 2.0$. 195
5.16 Velocity profile u showing the effect of Pr with $\eta = 0.2$ and $\mathcal{H}a = 2.195$
5.17 Velocity profile u showing the effect of $\mathcal{H}a$ with $Pr = 0.71$ and $\eta = 0.2$. 195
5.18 Contour graph of the rate of heat transfer at the inner surface of the outer cylinder ($r = 2$) showing the effect of Pr and η. 196
5.19 The skin friction at the outer surface of the inner cylinder ($r = 1$) showing the effect of $\mathcal{H}a$ and η. 196
5.20 The skin friction at inner surface of the outer cylinder ($r = 2$) showing the effect of $\mathcal{H}a$ and η. 197

LIST OF TABLES

4.1 Numerical values of the velocity obtained using the Riemann-sum approximation method and that obtained using finite difference method for both the fluid and the particle phases when $\eta = 0.2$, $K = 1$, $\mathcal{K} = 50$, $R_c = 0.25$ and $\mathcal{H}a = 2$. 155

4.2 Numerical values of the steady state skin friction obtained using the Riemann-sum approximation method and that obtained using finite difference method when $\mathcal{K} = 50$, $R_c = 0.25$ and $\mathcal{H}a = 2$. . . . 156

5.1 Numerical values of the velocity obtained analytically in Jha's problem and that of Riemann-sum approximation method when $Gr = 10$, $Pr = 7$ and $\mathcal{S} = 0$ in the present problem 177

5.2 Comparison of the numerical values of the transient state velocity obtained using the Riemann-sum approximation method and the steady state velocity obtained analytically when $\mathcal{H}a = 2$ and $Pr = 0.71$ 192

NOMENCLATURE

$\mathscr{A}$	closed surface
$\vec{B}$	total magnetic field
B_0	constant uniform magnetic field
c	substance quantity of mixture
C_p	specific heat at constant pressure
$\vec{E}$	electric field
$\mathcal{E}$	Ekmann number
g	acceleration due to gravity
Gr	Grashof number
$\vec{H}$	magnetic field intensity
$\mathcal{H}a$	Hartmann number
i, j, k	orthogonal unit vectors
I_0	zeroth-order modified Bessel function of the first kind
I_1	first-order modified Bessel function of the first kind
$\vec{J}$	electric current vector
K_0	zeroth-order modified Bessel function of the second kind
K_1	first-order modified Bessel function of the second kind
$\mathcal{K}'$	interaction coefficient
$\mathcal{K}$	dimensionless interaction coefficient
Nu	Nusselt number

Pr Prandtl number

q complex velocity

Ω constant heat flux

Q mass flux

r', θ', z' cylindrical coordinate

r, θ, z dimensionless cylindrical coordinate

s Laplace parameter

S suction/injection parameter

t dimensional time

T' Temperature of the fluid

T'_w Temperature of the plate

T_0 initial temperature

U constant

u', v', w' components of velocity in x', y', z' direction

u, v, w dimensionless components of velocity

$\mathcal{V}$ arbitrary volume

$\vec{V}$ phase velocity

x', y', z' cartesian coordinates

x, y, z dimensionless cartesian coordinates

∇^2 Laplacian

∇p pressure gradient

Greek Symbols

β ratio of the angular velocities

β_e Hall parameter

β_i ion-slip parameter

η dimensionless time

κ thermal conductivity

λ magnetic diffusivity

θ dimensionless temperature

μ dynamic viscosity

μ_0 magnetic permeability

ν kinematic viscosity

ξ coefficient of thermal expansion

ρ density

σ electrical conductivity

ς annulus dimension ratio

ϕ relative rotation of the outer to the inner cylinder

Ω' angular velocity

Ω rotation parameter

Subscripts

a accelerated

f fluid

i impulsive

p particle

s	steady state
t	transient
x	axial
y	transverse

CHAPTER 1

INTRODUCTION

Magnetohydrodynamics (MHD) is the study of the interaction of electrically conducting fluids and electromagnetic forces. Examples of such fluids include plasmas, liquid metals, and salt water or electrolytes. MHD describes the phenomena in electrically conducting fluids, where the velocity field $\vec{V}$, and the magnetic field $\vec{B}$, are coupled. Alfvén was the first to introduce the term "Magnetohydrodynamics" and he is also usually regarded as the father of MHD. He described such astrophysical phenomena as an independent scientific discipline[1]. However, the birth of incompressible fluid MHD is the study of the influence of a transverse uniform magnetic field on the flow of a viscous incompressible electrically conducting fluid between two infinite parallel stationary and insulating plates by Hartmann and Lazarus (1937). MHD problems arise in many natural phenomena in geophysics and astrophysics, for instance the generation of the magnetic field of planets and stars, the interaction of Earth's magnetic field with the solar wind as well as lightning. Its relevance is also found in engineering problems such as plasma confinement, liquid metal cooling of nuclear reactors, electromagnetic casting, the prediction

[1] Available online at
http://plasmauniverse.info/people/alfven.html.

of space weather to the damping of turbulent fluctuations in semiconductor melts during crystal growth and even the measurement of the flow rates of beverages in the food industry amongst others. Current research on methods to target chemotherapy drugs in the human body includes the investigation of biocompatible magnetic nanocarrier systems, for example magnetic liquids such as ferrofluids. The model developed to investigate an external magnetic field and its interaction with blood flow containing a magnetic carrier substance is based on the MHD equations; where a static magnetic field is coupled to fluid flow. Therefore, MHD is also very important in magnetic drug targeting.

The description of MHD flows involves the equations of fluid dynamics (Navier-Stokes equations) and the equations of electrodynamics (Maxwell's equations); which are mutually coupled through the Lorentz force and Ohm's law for moving electrical conductors. The flow between two boundaries due to the movemnt of one of the boundary is called Couette flow. There are two types of Couette flow; the flow between two walls one of which moves parallel to the other at a fixed distance. In this case, the modified pressure is constant or there is zero pressure gradient along the direction of flow, the velocity is zero everywhere for that flow field. In order to maintain a flow field, there is the need to set one of the walls in motion. This type of Couette flow in which the flow is driven only by the movement of one of the walls is known as plane Couette flow. However, if the flow is driven by both pressure and the movement of one of the walls the Couette motion is referred to as generalised Couette

flow. In this dissertation, we shall be concerned with the study of the MHD fluid flow relating to the plane Couette flow. Schlichting (1965) presented the analysis of flow formation in Couette motion as predicted by classical fluid mechanics. This problem reveals the relationship between the velocity and time and how the boundary layer spreads throghout the flow field. It also provides the exact solution of the non-linear Navier-Stokes equation. Couette flow can be used as a fundamental method for the measurement of viscosity and as a means of estimating the drag force in many wall driven applications according to Muzychka and Yovanovich (2006). The unsteady MHD Couette flow problem has been considered in several works considering various effects as in the work of Mazumder (1977a) who investigated the combined effect of Hall current and rotation on hydromagnetic flow over an oscillating plate in the presence of suction and injection. The importance of suction/injection on the boundary layer control in the field of aerodynamics and space science was emphasized by Singh (1984). It is well known that suction/injection can change the flow behaviour and as a consequence affect the skin friction. Injection tends to increase the velocity and the skin friction, while suction acts in the opposite way. Suction or injection also plays important role in the control of flow past an infinite plate or within parallel plates, hence its importance in practical problem involving film cooling, geophysical, biomedical, engineering and environmental applications. Shojaefard et al. (2005) carried out a numerical investigation of flow control by suction and injection on a a subsonic airfoil and came out with the conclusion

that suction significantly increases the lift coefficient while injection decreases the surface skin friction, which transitively resulted in a considerable reduction in energy consumed during flight of subsonic aircrafts.

The study of fluid/particle mixture is important in petroleum transport, powder technology, fluidization transport of solid particles by a liquid and liquid slurries in chemical and nuclear processing and metalized liquid fuel slurries for rocketry. Its relevance is also seen in the field of mining, agriculture and food technologies. The high possibility of particle entrainment in these flows made the formulation of the equation of motion for a two-phase fluid/particle system a necessity in order to understand the role of particles on the flow. The study of the effects of magnetic field on the free-convective flow is important in liquid-metals, electrolytes and ionized gases. For these reasons, the effect of magnetic field on the free convection flow has attracted many authors. Natural convection effects on Stokes problem was studied by Soundalgekar (1979). Ozoe and Maruo (1987) also investigated numerically the two-dimensional natural convection of a fluid under a magnetic field. The MHD flow and heat transfer problems have become important industrially, mainly due to the fact that many metallurgical processes involve the cooling of continuous strips or filaments by drawing them through an inactive fluid. Nanousis et al. (1980) inferred that a technological application of free convection can be found in the cooling of a nuclear reactor, providing heat sinks in turbine blades etc. The structures of stars and planets are also known according to Weir (1976) to be greatly influenced by

the thermal convection in their interior.

1.1 GOVERNING EQUATIONS OF MHD

In this dissertation, we are interested in the equation of an idealized version of the MHD system, wherein the fluid body has perfect conductivity, and so the local electric field is zero. The complete set of MHD equations for a Newtonian, constant property fluid flow includes the equation of mass continuity, the complete set of Maxwell's equations and the Navier-Stokes equations of motion (i.e. momentum equation).

1.1.1 Equation of Continuity

The basic tool in the study of fluid flow is the continuity equation otherwise known as the mass conservation. We consider an arbitrary volume of fluid $\mathscr{V}$, bounded by a closed surface $\mathscr{A}$; let the surface have an outward normal, $\hat{n}$. The mass within this volume is $\int_{\mathscr{V}} \rho d\mathscr{V}$, while the rate of change of this mass is

$$\frac{d}{dt}\int_{\mathscr{V}} \rho d\mathscr{V} \tag{1.1}$$

In the absence of sources and sinks, eq. (1.1) must be equal to zero. This integral can change with time in two ways (*i*) by intrinsic variation of $\rho, \partial\rho \neq 0$; or (*ii*) through flow into or out of the volume, at a rate $\rho\vec{V}\cdot\hat{n}$ per surface area. The sum

of (i) and (ii) must be zero:

$$\frac{d}{dt}\int_{\mathscr{V}} \rho d\mathscr{V} = \int_{\mathscr{V}} \frac{\partial \rho}{\partial t} d\mathscr{V} + \int_{\mathscr{A}} \rho \vec{V} \cdot \hat{n} d\mathscr{A} = 0 \tag{1.2}$$

The surface integral can be written as

$$\int_{\mathscr{A}} \rho \vec{V} \cdot \hat{n} d\mathscr{A} = \int_{\mathscr{A}} \nabla \cdot (\rho \vec{V}) = 0 \tag{1.3}$$

Since $\mathscr{V}$ is arbitrary, we can set the integrand to zero and get the differential form of this basic equation:

$$\frac{\partial \rho}{\partial t} + \nabla \cdot (\rho \vec{V}) = 0 \tag{1.4}$$

This is the mass continuity equation. However, for an incompressible fluid ρ is constant and thus the equation of continuity reduces to

$$\nabla \cdot \vec{V} = 0 \tag{1.5}$$

which is the form to be used in this dissertation.

1.1.2 Maxwell's Equations

The Maxwell's equations describes the behaviour of electric $\vec{E}$ and magnetic $\vec{B}$ fields, see Fleisch (2008) for a deeper comprehension of the Maxwell's equations. However, the following set of differential equations are the simplified form of

the Maxwell's equation:

$$\textit{Ampere's Circuital Law} \quad \nabla \times \vec{B} = \mu_0 \vec{J} \tag{1.6}$$

$$\textit{Charge Conservation} \quad \nabla \cdot \vec{J} = 0 \tag{1.7}$$

$$\textit{Faraday's Law} \quad \nabla \times \vec{E} = -\frac{\partial \vec{B}}{\partial t} \tag{1.8}$$

$$\textit{Solenoidal Constraint} \quad \nabla \cdot \vec{B} = 0 \tag{1.9}$$

$$\textit{Ohm's Law} \quad \vec{J} = \sigma(\vec{E} + \vec{V} \times \vec{B}) \tag{1.10}$$

$$\textit{Lorentz force} \quad \vec{F} = \vec{J} \times \vec{B} \tag{1.11}$$

It should be noted that the total magnetic field $\vec{B}$ is related to the magnetic field $\vec{H}$ as $\vec{B} = \mu_0 \vec{H}$. In the present study, the polarization effects are negligible ($\vec{E} = 0$) and the magnetic Reynolds number is very small i.e the induced magnetic field is also negligible. If the Hall and ion-slip currents are considered, Ohm's Law will be defined as follows:

$$\vec{J} = \sigma \left[\vec{V} \times B_0 - \beta_H (J \times B_0) + \frac{\beta_H \beta_I}{B_0} (J \times B_0) \times B_0 \right] \tag{1.12}$$

Equation (1.12) is normally referred to as generalized Ohm's Law.

1.1.3 Navier-Stokes Equations

It is a usual practice to obtain the Navier-Stokes equations from the Euler's equation. We will adopt this method here. Let us again consider the same surface $\mathscr{A}$ and enclosing volume $\mathscr{V}$ used in Subsection 1.1.1. The momentum within the surface is $\int_{\mathscr{V}} \rho \vec{V} d\mathscr{V}$. The net rate of change of this quantity again must reflect intrinsic ($\partial/\partial t \neq 0$) variation and advection (flow across the surface). Thus , the net rate of change of momentum is

$$\int_{\mathscr{V}} \frac{\partial}{\partial t}(\rho \vec{V}) d\mathscr{V} + \int_{\mathscr{A}} (\rho \vec{V}) \vec{V} \cdot \hat{n} d\mathscr{A} = \int_{\mathscr{V}} \frac{\partial}{\partial t}(\rho \vec{V}) d\mathscr{V} + \int_{\mathscr{V}} \nabla \cdot (\rho \vec{V} \vec{V}) d\mathscr{V} \qquad (1.13)$$

We have used the Gauss's Law for tensors (noting that $\rho \vec{V} \vec{V}$ is a second rank tensor). As it is the case with the continuity equation, the net rate of change of momentum in the volume must be equal to the net force exerted on the volume. We consider external forces which act throughout the volume (body forces, such as gravity, electomagnetism, bouyancy, radiation pressure if the fluid is optically thin; we let g be the net force per mass) and also the force exerted on the surface by the fluid outside $\mathscr{V}$. The net force on the volume $\mathscr{V}$ is, then

$$\int_{\mathscr{V}} \rho g d\mathscr{V} - \int_{\mathscr{A}} p \hat{n} d\mathscr{A} = \int_{\mathscr{V}} \rho g d\mathscr{V} - \int_{\mathscr{V}} \nabla p d\mathscr{V} \qquad (1.14)$$

In differential form, we have

$$\frac{\partial}{\partial t}(\rho\vec{V}) + \nabla \cdot (\rho\vec{V}\vec{V}) = -\nabla p + \rho g \tag{1.15}$$

It is a usual convention to expand the derivatives on the left hand side of eq. (1.15) and using eq. (1.4) to obtain

$$\rho\frac{\partial\vec{V}}{\partial t} + \rho(\vec{V}\cdot\nabla)\vec{V} = -\nabla p + \rho g \tag{1.16}$$

Equation (1.16) is known as Euler's equation, when we add viscous stresses to the equation, the equation is called Navier-Stokes equation, which is

$$\rho\frac{\partial\vec{V}}{\partial t} + \rho(\vec{V}\cdot\nabla)\vec{V} + \nabla p = \rho g + \rho\nu\nabla^2\vec{V} + (\rho\nu_b + \frac{1}{3}\rho\nu)\nabla(\nabla\cdot\vec{V}) \tag{1.17}$$

If Stoke's hypothesis holds, this equation simplifies to

$$\rho\frac{\partial\vec{V}}{\partial t} + \rho(\vec{V}\cdot\nabla)\vec{V} + \nabla p = \rho g + \rho\nu\nabla^2\vec{V} + \frac{1}{3}\rho\nu\nabla(\nabla\cdot\vec{V}) \tag{1.18}$$

In the absence of gravity and considering incompressibility (i.e $g = 0$ and $\nabla\cdot\vec{V} = 0$), the equation now becomes

$$\rho\frac{\partial\vec{V}}{\partial t} + \rho(\vec{V}\cdot\nabla)\vec{V} + \nabla p = \rho\nu\nabla^2\vec{V} \tag{1.19}$$

This is the normal Navier-Stokes equation for an incompressible fluid.

1.1.3.1 Geometric Configurations

The coordinate employed in applying the Navier-Stokes equations depends on the geometry of the problem involved; so that the equations are kept relatively simple. In this dissertation, we will use cartesian coordinates for flow between infinite flat plates and cylindrical coordinates are used for flow in an annulus. Based on the simplifications made in this study, the equation of continuity and the Navier-Stokes equation for an incompressible Newtonian fluid of constant viscosity are obtained by expanding equations (1.5) and (1.19) which are in vector forms as shown below:

Cartesian Coordinates

Continuity Equation

$$\frac{\partial u}{\partial x}+\frac{\partial v}{\partial y}+\frac{\partial w}{\partial z}=0 \tag{1.20}$$

x-momentum

$$\rho\left(\frac{\partial u}{\partial t}+u\frac{\partial u}{\partial x}+v\frac{\partial u}{\partial y}+z\frac{\partial u}{\partial z}\right)=-\frac{\partial p}{\partial x}+\mu\left(\frac{\partial^2 u}{\partial x^2}+\frac{\partial^2 u}{\partial y^2}+\frac{\partial^2 u}{\partial z^2}\right)+F_x \tag{1.21}$$

y-momentum

$$\rho\left(\frac{\partial v}{\partial t}+u\frac{\partial v}{\partial x}+v\frac{\partial v}{\partial y}+z\frac{\partial v}{\partial z}\right)=-\frac{\partial p}{\partial y}+\mu\left(\frac{\partial^2 v}{\partial x^2}+\frac{\partial^2 v}{\partial y^2}+\frac{\partial^2 v}{\partial z^2}\right)+F_y \tag{1.22}$$

z-momentum

$$\rho\left(\frac{\partial w}{\partial t}+u\frac{\partial w}{\partial x}+v\frac{\partial w}{\partial y}+z\frac{\partial w}{\partial z}\right)=-\frac{\partial p}{\partial z}+\mu\left(\frac{\partial^2 w}{\partial x^2}+\frac{\partial^2 w}{\partial y^2}+\frac{\partial^2 w}{\partial z^2}\right)+F_z \quad (1.23)$$

Cylindrical Coordinates

Continuity Equation

$$\frac{1}{r}\frac{\partial}{\partial r}(ru_r)+\frac{1}{r}\frac{\partial u_\theta}{\partial \theta}+\frac{\partial u_z}{\partial z}=0 \quad (1.24)$$

r-momentum

$$\begin{aligned}\rho\ &\left(\frac{\partial u_r}{\partial t}+u_r\frac{\partial u_r}{\partial r}+\frac{u_\theta}{r}\frac{\partial u_r}{\partial \theta}-\frac{u_\theta^2}{r}+u_z\frac{\partial u_r}{\partial z}\right)\\ =\ &-\frac{\partial p}{\partial r}+\mu\left[\frac{\partial}{\partial r}\left(\frac{1}{r}\frac{\partial}{\partial r}(ru_r)\right)+\frac{1}{r^2}\frac{\partial^2 u_r}{\partial \theta^2}-\frac{2}{r^2}\frac{\partial u_\theta}{\partial \theta}+\frac{\partial^2 u_r}{\partial z^2}\right]+F_r \quad (1.25)\end{aligned}$$

θ-momentum

$$\begin{aligned}\rho\ &\left(\frac{\partial u_\theta}{\partial t}+u_r\frac{\partial u_\theta}{\partial r}+\frac{u_\theta}{r}\frac{\partial u_\theta}{\partial \theta}+\frac{u_r u_\theta}{r}+u_z\frac{\partial u_\theta}{\partial z}\right)\\ =\ &-\frac{1}{r}\frac{\partial p}{\partial \theta}+\mu\left[\frac{\partial}{\partial r}\left(\frac{1}{r}\frac{\partial}{\partial r}(ru_\theta)\right)+\frac{1}{r^2}\frac{\partial^2 u_\theta}{\partial \theta^2}+\frac{2}{r^2}\frac{\partial u_r}{\partial \theta}+\frac{\partial^2 u_\theta}{\partial z^2}\right]+F_\theta \quad (1.26)\end{aligned}$$

z-momentum

$$\begin{aligned}\rho\ &\left(\frac{\partial u_z}{\partial t}+u_r\frac{\partial u_z}{\partial r}+\frac{u_\theta}{r}\frac{\partial u_z}{\partial \theta}+u_z\frac{\partial u_z}{\partial z}\right)\\ =\ &-\frac{\partial p}{\partial z}+\mu\left[\frac{1}{r}\frac{\partial}{\partial r}\left(r\frac{\partial u_z}{\partial r}\right)+\frac{1}{r^2}\frac{\partial^2 u_z}{\partial \theta^2}+\frac{\partial^2 u_z}{\partial z}\right]+F_z \quad (1.27)\end{aligned}$$

160026

A. B. U.
Library Services

where F is the body forces added to the equations.

1.1.4 Magnetic Induction Equation

Using the Ohm's Law to express the electric field we have

$$E = -V \times \vec{B} + \vec{J}/\sigma \tag{1.28}$$

Taking the curl of this expression and substituting into Maxwell's equation for $\nabla \times E$ and using Ampere's Law to substitute the current $\vec{J}$, we have the induction equation

$$\frac{\partial \vec{B}}{\partial t} = \nabla \times (\vec{V} \times \vec{B}) + \lambda \nabla^2 \vec{B} \tag{1.29}$$

where $\lambda = 1/\mu_0 \sigma$ and is the magnetic diffusivity

1.2 BOUNDARY LAYER CONCEPT

The theory of boundary layer effects was first presented by Ludwig Prandtl in the early 1900's. The general fluids equations had been known for many years, but solutions to the equations did not properly describe observed flow effects. Prandtl was the first to realize that the relative magnitude of the inertial and viscous forces changed from a layer very near the surface to a region far from the surface. He first proposed the interactively coupled, two layer solution which properly models many flow problems. As an object moves through a

fluid, or as a fluid moves past an object, the molecules of the fluid near the object are disturbed and move around the object. Aerodynamic forces are generated between the fluid and the object. The magnitude of these forces depend on the shape of the object, the speed of the object, the mass of the fluid going by the object and on two other important properties of the fluid; the viscosity, or stickiness, and the compressibility, or springiness, of the fluid. To properly model these effects, aerospace engineers use similarity parameters which are ratios of these effects to other forces present in the problem. If two experiments have the same values for the similarity parameters, then the relative importance of the forces are being correctly modeled.

Aerodynamic forces depend in a complex way on the viscosity of the fluid. As the fluid moves past the object, the molecules right next to the surface stick to the surface. The molecules just above the surface are slowed down in their collisions with the molecules sticking to the surface. These molecules in turn slow down the flow just above them. The farther one moves away from the surface, the fewer the collisions affected by the object surface. This creates a thin layer of fluid near the surface in which the velocity changes from zero at the surface to the free stream value away from the surface. Engineers call this layer the boundary layer because it occurs on the boundary of the fluid. The details of the flow within the boundary layer are very important for many problems in aerodynamics, including wing stall, the skin friction drag on an object, and the

heat transfer that occurs in high speed flight.[2]

1.3 ROTATING FRAME OF REFERENCE

Suppose that a given object has position vector $\vec{r}$ in some non-rotating inertial reference frame. Let us observe the motion of this object in a non-inertial reference frame which rotates with constant angular velocity $\vec{\Omega}$ about an axis passing through the origin of the inertial frame. Suppose, first of all, that our object appears stationary in the rotating reference frame. Hence, in the non-rotating frame, the object's position vector $\vec{r}$ will appear to precess about the origin with angular velocity $\vec{\Omega}$. It then follows, from the equation of motion that :

$$\frac{d\vec{r}}{dt} = \vec{\Omega} \times \vec{r} \tag{1.30}$$

Suppose, now, that our object appears to move in the rotating reference frame with instantaneous velocity $\vec{v}'$. It is fairly obvious that the appropriate generalization of the above equation is simply

$$\frac{d\vec{r}}{dt} = \vec{v}' + \vec{\Omega} \times \vec{r} \tag{1.31}$$

Let d/dt and d/dt' denote apparent time derivatives in the non-rotating and rotating frames of reference, respectively. Since an object which is stationary in the rotating reference frame appears to move in the non rotating frame, it is clear

[2] Available online at
http://www.grc.nasa.gov/WWW/k-12/airplane/boundlay.html.

that $d/dt \neq d/dt'$. Writing the apparent velocity, $\vec{v}'$, of our object in the rotating reference frame as $d\vec{r}/dt'$, the above equation takes the form

$$\frac{d\vec{r}}{dt} = \frac{d\vec{r}}{dt'} + \vec{\Omega} \times \vec{r} \tag{1.32}$$

or

$$\frac{d}{dt} = \frac{d}{dt'} + \vec{\Omega} \times \tag{1.33}$$

since $\vec{r}$ is a general position vector. Equation 1.33 expresses the relationship between apparent time derivatives in the non-rotating and rotating reference frames. Operating on the general position vector $\vec{r}$ with the time derivative 1.33, we get

$$\vec{v} = \vec{v}' + \vec{\Omega} \times \vec{r} \tag{1.34}$$

This equation relates the apparent velocity, $\vec{v} = d\vec{r}/dt$, of an object with position vector $\vec{r}$ in the non-rotating reference frame to its apparent velocity, $\vec{v}' = d\vec{r}/dt'$, in the rotating reference frame. Operating twice on the position vector $\vec{r}$ with the time derivative 1.33, we obtain

$$\vec{a} = \left(\frac{d}{dt'} + \vec{\Omega} \times \right) (v' + \vec{\Omega} \times \vec{r}) \tag{1.35}$$

or

$$\vec{a} = \vec{a}' + \vec{\Omega} \times (\vec{\Omega} \times \vec{r}) + 2\vec{\Omega} \times \vec{v}' \tag{1.36}$$

This equation relates the apparent acceleration, $\vec{a} = d^2\vec{r}/dt^2$, of an object with position vector $\vec{r}$ in the non-rotating reference frame to its apparent acceleration, $\vec{a}' = d^2\vec{r}/dt'^2$, in the rotating reference frame. Applying Newton's second law of motion in the inertial (i.e., non-rotating) reference frame, we obtain

$$\vec{F} = m\vec{a} \tag{1.37}$$

Here, m is the mass of our object, and F is the (non-fictitious) force acting on it. Note that these quantities are the same in both reference frames. Making use of Equation 1.36, the apparent equation of motion of our object in the rotating reference frame takes the form

$$m\vec{a}' = \vec{F} - m\vec{\Omega} \times (\vec{\Omega} \times \vec{r}) - 2m\vec{\Omega} \times \vec{v}' \tag{1.38}$$

The last two terms in the above equation are so-called "fictitious forces". Such forces are always needed to account for motion observed in non-inertial reference frames. Note that fictitious forces can always be distinguished from non-fictitious forces in Newtonian dynamics because the former have no associated reactions. The two fictitious forces appearing in Equation 1.38 are the centrifugal acceleration and coriolis force (Fitzpatrick 2011). Notice that the centrifugal acceleration depends on the frame rotation $\vec{\Omega}$ and the position vector $\vec{r}$, the coriolis force depends on the flow through the velocity vector $\vec{v}$. This is an important difference because it means we can simplify the appearance of the

centrifugal acceleration to something perhaps less threatening than a double cross-product

1.4 MATHEMATICAL METHODS

1.4.1 Laplace Transform

The Laplace transform is essentially a mathematical tool used to solve several mathematics and engineeering problems. This transform was first introduced by Laplace in his work on probability theorem. The main idea behind the Laplace Transformation is that we can solve an equation (or system of equations) containing differential and integral terms by transforming the equation in "t-space" to one in "s-space". This makes the problem much easier to solve. If needed we can find the inverse Laplace transform, which gives us the solution back in "t-space".

1.4.1.1 Definition of Exponential Order

Suppose $f(t)$ is piecewise continuous function and if it has an additional property that there exist a real number ε_0 and a finite number $\mathscr{Q}_1$ such that

$$\lim_{t\to\infty} |f(t)|e^{-\varepsilon t} \leq \mathscr{Q}_1 \; for \; \varepsilon > \varepsilon_0 \tag{1.39}$$

and the limit does not exist when $\varepsilon > \varepsilon_0$, then such a function is said to be of exponential order ε_0 also written as

$$|f(t)| = \mathcal{O}(e^{-\varepsilon_0 t}). \tag{1.40}$$

Variables such as velocity and current are always finite, which means that $f(t)$ is bounded. Thus, for any bounded function $f(t)$, $|f(t)|(e^{-\varepsilon_0 t}) \to 0$ for all $\varepsilon > 0$. The order of such a function is zero. However, variable such as electrical charge and mechanical displacement may increase without limit but of course proportional to t. Such functions are also of exponential order.

Definition

Let $f(t)$ be continuous and single valued function of the real variable t for all $0 < t < \infty$, and is of exponential order. Then the Laplace transform of $f(t)$ is defined as a function $\bar{f}(s)$ denoted by the integral

$$\mathscr{L}|f(t)| = \bar{f}(s) = \int_0^\infty f(t)e^{-st}dt,\ s > 0 \tag{1.41}$$

over that range of values of s for which the integral exist. Here s is a parameter, real or complex. Obviously, $\mathscr{L}|f(t)|$ is a function of s. Thus,

$$\mathscr{L}|f(t)| = \bar{f}(s)$$

$$f(t) = \mathscr{L}^{-1}[\bar{f}(s)] = \frac{1}{2\pi}\int_{\lambda_1 - j\infty}^{\lambda_1 + j\infty} \bar{f}(s)e^{st}ds, \tag{1.42}$$

where $\mathscr{L}$ is the operator which transforms $f(t)$ into $\bar{f}(s)$, called the Laplace transform operator, and $\mathscr{L}^{-1}$ is the inverse Laplace transform operator.

Theorem (Laplace transform)

If $f(t)$ is piecewise continuous in the range $t \geq 0$ and is of exponential order ε, then the Laplace transform $\bar{f}(s)$ of $f(t)$ exist for all $s > \varepsilon$.

Proof

From the definition of Laplace transform,

$$\mathscr{L}|f(t)| = \bar{f}(s) = \int_0^\infty f(t)e^{-st}dt = \int_0^{\mathscr{T}_1} f(t)e^{-st}dt + \int_{\mathscr{T}_1}^\infty f(t)e^{-st}dt = I_1 + I_2 \quad (1.43)$$

Since $f(t)$ is piecewise continuous on every finite interval $0 < \mathscr{T}_1 < t$, I_1 exists, whereas

$$I_2 \leq \int_{\mathscr{T}_1}^\infty f(t)e^{-st}dt \quad (1.44)$$

But $f(t)$ is a function of exponential order, therefore,

$$|f(t)| \leq \mathscr{Q}_1 e^{\varepsilon t} \text{ for } \varepsilon \text{ real.} \quad (1.45)$$

Hence

$$|e^{-st}f(t)| < \mathscr{Q}_1 e^{-(s-\varepsilon)t}. \quad (1.46)$$

Thus

$$|I_2| \leq \int_{\mathscr{T}_1}^\infty \mathscr{Q}_1 e^{-(s-\varepsilon)t}dt = \frac{\mathscr{Q}_1 e^{-(s-\varepsilon)t}}{s-\varepsilon},\ s > \varepsilon \quad (1.47)$$

In order words, I_2 can be made as small as we like provided $\mathcal{T}_1$ is large enough and therefore I_2 exists. Hence $\mathcal{L}[f(t)]$ exists for $s > \varepsilon$. (See Widder (1941)). The inverse Laplace transform which is used to return a Laplace transformed function to its original state are given in Abramowitz and Stegun (1965) and Churchill (1972).

1.4.2 Riemann-sum Approximation

An efficient and accurate method of Laplace inversion is the Riemann-sum approximation method of inverting difficult functions into their time domain. In applying this method, we use the Fourier-series (simplified by the Poisson summation formula) to replace the integral by a series which corresponds to the trapezoidal rule with a specified discretization error. The Fourier integral thus obtained can be approximated by its Riemann-sum. Denoting ω as the wave frequency and ι the half-period of its oscillations, i.e., $\omega = k\pi/\iota$ for the nth wave mode and $\triangle\omega_k = \pi/\iota$ for all modes

$$f(z,\eta) = \frac{e^{\gamma\eta}}{2\iota} \sum_{k=-\infty}^{\infty} \bar{f}(z, s = \gamma + \frac{ik\pi}{\iota}) e^{i(k\eta\pi/\iota)} \tag{1.48}$$

Since the series is nearly alternating, we apply Euler summation to accelerate convergence.

$$\begin{aligned} \bar{f}(z,\gamma+\frac{in\pi}{\iota})e^{i(k\eta\pi/\iota)} \;+\; & \bar{f}(z,\gamma-\frac{in\pi}{\iota})e^{-i(k\eta\pi/\iota)} \\ = \;& 2Re\left[\bar{f}(z,\gamma+\frac{ik\pi}{\iota})e^{i(k\eta\pi/\iota)}\right] \end{aligned} \tag{1.49}$$

eq. (1.48) can then be expressed as

$$f(z,\eta) = \frac{e^{\gamma\eta}}{\iota}\left[\frac{1}{2}\bar{f}(z,\gamma) + Re\sum_{k=1}^{\infty}\bar{f}(z,\gamma+\frac{ik\pi}{\iota})e^{i(k\eta\pi/\iota)}\right] \tag{1.50}$$

The Fourier-series method for numerically inverting Laplace transforms was first proposed by Dubner and Abate (1968). The use of the Euler summation in this context was proposed by Simon et al. (1972). Since the function $e^{i(k\eta\pi/\iota)}$ has a fundamental period of 2π, the physical domain of η in eq. (1.50) is $0 \leq \eta \leq 2\pi$. At $\eta = \iota$, more precisely, eq. (1.50) yields

$$f(z,\eta) \cong \frac{e^{\gamma\eta}}{\eta}\left[\frac{1}{2}\bar{f}(z,\gamma) + Re\sum_{k=1}^{N}\bar{f}(z,\gamma+\frac{ik\pi}{\eta})(-1)^k\right] \tag{1.51}$$

which is the inverse solution for $f(z,\eta)$. In eq. (1.51), *Re* refers to the 'real part of', $i = \sqrt{-1}$ is the imaginary number, N is the number of terms used in the Riemann-sum approximation. The Riemann-sum approximation for the Laplace inversion involves a single summation in the numerical process. Its accuracy depends on the value of $\gamma\eta$. and the truncation error dictated by N. The value of γ must be selected so that the Bromwich contour encloses all the baranch points. Any positive number can be selected for γ, because the branch points are all negative. For faster convergence, however, numerous numerical experiments have shown that the value of γ satisfying the relation

$$\gamma\eta \cong 4.7 \tag{1.52}$$

gives the most satisfactory results (Tzou (1997)). The criterion shown by eq. (1.52) is independent on the dimension η.

1.4.3 Finite Difference Method

The finite difference techniques are based upon the approximations that permit replacing differential equations by finite difference equations. These finite difference approximations are algebraic in form, and the solutions are related to grid points. Thus, a finite difference solution basically involves three steps:

a. Dividing the solution into grids of nodes.

b. Approximating the given differential equation by finite difference equivalence that relates the solutions to grid points.

c. Solving the difference equations subject to the prescribed boundary conditions and/or initial conditions.

Given a a function $f(x)$ and its derivatives which are single-valued, finite and continuous, then using Taylor's series.

$$\begin{aligned} f(x_0+\triangle x) &= f(x_0)+\triangle x f'(x_0)+\frac{1}{2!}(\triangle x)^2 f''(x_0) \\ &+ \frac{1}{3!}(\triangle x)^3 f'''(x_0)+\mathcal{O}(\triangle x)^4 \end{aligned} \tag{1.53}$$

$$\begin{aligned} f(x_0-\triangle x) &= f(x_0)-\triangle x f'(x_0)+\frac{1}{2!}(\triangle x)^2 f''(x_0) \\ &- \frac{1}{3!}(\triangle x)^3 f'''(x_0)+\mathcal{O}(\triangle x)^4 \end{aligned} \tag{1.54}$$

where prime indicates the differentiation with respect to x and $\mathcal{O}(\triangle x)^4$ is the error introduced by truncating the series. Subtract eqs. (1.53) from (1.54), we can obtain,

$$f'(x_0) \cong \frac{f(x_0+\triangle x) - f(x_0-\triangle x)}{2\triangle x} + \mathcal{O}(\triangle x)^2 \tag{1.55}$$

which is the central-difference formula. Note that $\mathcal{O}(\triangle x)^2$ means the truncation error is of the order of $\mathcal{O}(\triangle x)^2$ for the central -difference. The forward-difference and backward-difference could be obtained by re-arraanging eqs. (1.53) from (1.54) respectively, and we have for forward-difference

$$f'(x_0) \cong \frac{f(x_0+\triangle x) - f(x_0)}{\triangle x} + \mathcal{O}(\triangle x)^2 \tag{1.56}$$

and for backward difference

$$f'(x_0) \cong \frac{f(x_0) - f(x_0-\triangle x)}{\triangle x} + \mathcal{O}(\triangle x)^2 \tag{1.57}$$

Upon adding (1.53) and (1.54) we have

$$f''(x_0) \cong \frac{f(x_0+\triangle x) - 2f(x_0) + f(x_0-\triangle x)}{(\triangle x)^2} + \mathcal{O}(\triangle x)^2 \tag{1.58}$$

Higher order finite difference approximattion can be obtained by taking more terms in Taylor's series expansion.

Finite difference approximation to partial derivatives

We will approximate partial derivatives of f, a function of two independent continuous variables x and η, such as

$$\frac{\partial f}{\partial x}, \ \frac{\partial^2 f}{\partial x^2} \ \textit{and} \ \frac{\partial f}{\partial \eta} \ \textit{etc.} \tag{1.59}$$

by finite difference method. For this purpose, the continuous variable x and η are discretized, so we consider $f(x, \eta)$ to be evaluated only at the intersections P_l (mesh points) of the grid lines parallel to x and η axes. Let the coordinates (x, η) of the mesh point P_l be

$$x = i\triangle x; \quad t = j\triangle \eta, \tag{1.60}$$

where i, j are integers and $\triangle x, \triangle \eta$ are constant grid spacings in the x and η directions respectively. Let the value of f at P_l be denoted by

$$f_{i,j} = f(i\triangle x, j\triangle \eta). \tag{1.61}$$

We then borrow an analogy between ordinary and partial derivates from calculus and the concepts introduced earlier in this section, we now have the following centre-difference approximations to partial derivatives, each with a leading error

of order $(\triangle x)^2$

$$\begin{aligned}\left(\frac{\partial f}{\partial x}\right)_{i,j} &\cong \frac{1}{2\triangle x}[f(i+1)\triangle x, j\triangle\eta - f(i-1)\triangle x, j\triangle\eta)] \\ &\cong \frac{1}{2\triangle x}[f_{i+1,j} - f_{i-1,j}],\end{aligned} \tag{1.62}$$

$$\begin{aligned}\left(\frac{\partial^2 f}{\partial x^2}\right)_{i,j} &\cong \frac{1}{(\triangle x)^2}[f((i+1)\triangle x, j\triangle\eta) - 2f(i\triangle x, j\triangle\eta) \\ &+ f((i-1)\triangle x, j\triangle\eta)] \\ &\cong \frac{1}{(\triangle x)^2}[f_{i+1,j} - f_{i-1,j}],\end{aligned} \tag{1.63}$$

With this notation, the forward-difference approximation for $\partial f/\partial\eta$ at P_1 is

$$\frac{\partial f}{\partial \eta} \cong \frac{f_{i,j+1} - f_{i,j}}{\triangle\eta} \tag{1.64}$$

with leading error of the order $\triangle\eta$.

Average finite difference approximations to partial derivates

For a better approximations to partial derivates, we develop approximations to partial derivates at the mid-way between the time levels j and $j+1$. Furthermore, the function f is also approximated at the midpoint $(i\triangle x, (j+\frac{1}{2})\triangle\eta)$ as the average

$$f_{i,j+\frac{1}{2}} = \frac{1}{2}[f_{i,j+1} + f_{i,j}] \tag{1.65}$$

The temporal first derivative can be approximated at time level $j+\frac{1}{2}$

$$\left(\frac{\partial f}{\partial \eta}\right)_{i,j-\frac{1}{2}} = \frac{1}{k}\left[f_{i,j-1} - f_{i,j}\right] \tag{1.66}$$

The spatial first derivative can be determined at the midpoint by averaging the difference approximations at the jth and $(j+1)th$ time levels

$$\left(\frac{\partial f}{\partial x}\right)_{i,j+\frac{1}{2}} = \frac{1}{4\triangle x}\left[(f_{i+1,j+1} - f_{i-1,j+1}) + (f_{i+1,j} - f_{i+1,j})\right] \tag{1.67}$$

Similarly, the spatial second derivative can also be approximated at the midpoint by means of averaging as

$$\left(\frac{\partial^2 f}{\partial x^2}\right)_{i,j+\frac{1}{2}} = \frac{1}{2(\triangle x)^2}\left[(f_{i+1,j+1} - f_{i-1,j+1} - 2f_{i,j+1}) + (f_{i+1,j} - 2f_{i,j} + f_{i-1,j})\right] \tag{1.68}$$

For a thorough study of the finite difference method, see Leveque (2007).

1.5 OBJECTIVES OF THE STUDY

The aim of this dissertation is to study the motion of an electrically conducting, viscous and incompressible fluid flowing in a channel formed by two parallel plates and an annulus formed by two concentric cylinders with a magnetic field applied perpendicular to the flow direction. The specific objectives are

a. To analyse the MHD Couette flow in a rotating porous channel.

b. To examine the effect of Hall and ion-slip currents in a rotating channel.

c. To consider the Hall and ion-slip effect in a rotating channel with porous walls.

d. To study the MHD Couette flow in an annulus.

e. To obtain the solution of the unsteady MHD Taylor-Couette flow with transpiration.

f. To analyse the problem of two-phase MHD flow in both parallel and annular channels.

g. To examine the influence of free convection on MHD flow.

1.6 RESEARCH METHODOLOGY

The methodologies adopted in the realization of the above objectives are enumerated below in sequential order:

a. Review existing literatures and extend them to include different boundary conditions and physical situation.

b. Solve the BVPs analytically where possible and use the Riemann-sum approximation approach if otherwise.

c. Obtain the numerical values of the analytical or semi-anlytical solutions to the BVPs using MATLAB.

d. Derive the corresponding steady state equations where appropriate and solve analytically to double check the results.

e. Generate line graphs or contours for the numerical values using MATLAB.

f. Interpret the plots in order to explain flow behaviours in the physical situations and draw conclusions.

1.7 OUTLINE OF THE DISSERTATION

In this Chapter, we have provided a background information on the basic equations describing coupled MHD behaviour. We then gave some underlying physics common to the motion of fluid and MHD. This Chapter also describe the mathematical methods used in the dissertation. Motivated by the facts in Chapter 1, the rest of this dissertation is divided into five chapters. In Chapter 2 we look at the MHD Couette flow in a rotating channel by considering three problems; the first problem is concerned with the time-dependent MHD Couette flow in a rotating porous channel, the second is the combined effect of Hall and ion-slip currents on MHD Couette flow in a rotating system while the last problem extended the second to include the effect of suction and injection.

In Chapter 3, we commenced the study on the annular geometry by considering three problems; the first is the unsteady MHD Couette flow in an annulus, the second is the MHD Couette flow in an annulus having ramp motion of inner cylinder and the last is on the MHD Taylor–Couette flow in a porous annulus. The intent of Chapter 4 is to analyse a two–phase unsteady MHD Couette flow considering the effect of the particle–phase viscous stresses. In Chapter 5, we have carried out an analysis of the unsteady MHD free convective

flow of a viscous incompressible electrically conducting fluid. Literature survey suggests that no previous attempts have been made to examine the problems studied in Chapters 2–5. Finally, the summary, conclusions and direction for future work are given in Chapter 6. A whole lot of reasonable advancement has been made in the context of MHD flow both analytically and semi-analytically in this dissertation. It is hoped that this dissertation will give further insight into the problems of MHD flows with great applications in industries.

CHAPTER 2

MHD COUETTE FLOW IN A ROTATING CHANNEL

The MHD channel flow was first investigated by Hartmann (1937) who considered plane Poiseuille flow with a transverse magnetic field. Since then, the study of MHD flow has received considerable attention due to its importance from the energy generation point of view and one may envisage MHD generators for power generation. MHD Couette flow is also important in the design of high temperature cooling systems for reactors, turbine blades, MHD power pumps, aerodynamic heating and in the purification of crude oil. Katagiri (1962) investigated the formation of Couette flow of a viscous, incompressible and electrically conducting fluid between two infinite parallel plane walls in the presence of transverse magnetic field. Muhuri (1963) extended the problem by imposing uniform suction velocity on the walls. Singh and Kumar (1983) studied the unsteady MHD Couette flow by assuming that the magnetic lines of force are fixed relative to the moving plate for both impulsive and accelerated motion of the moving plates and came out with the deduction that magnetic field increases the velocity field in both cases. A study on oscillatory Couette flow in the presence of an inclined magnetic field was carried out by Guria et al. (2009).

The study of the interaction of the Coriolis force with the electromagnetic force is important in MHD Couette flows. Rotating MHD problems are found in turbo machinery, solidification process in metallurgy and in some astrophysical problems. Taking these facts into account, the effect of rotation on the unsteady MHD Couette flow when one of the plates has been set into impulsive motion was examined by Chandran et al. (1993), they noticed a decrease in velocity due to rotation and an increase due to magnetic field. The transient features of the Couette flow of an electrically conducting fluid when one of the plates is set into an accelerated motion was studied by Singh et al. (1994). Seth et al. (1982) investigated the unsteady MHD flow of an electrically conducting viscous incompressible fluid in a rotating system under the influence of a uniform transverse magnetic field when one of the plates is set into motion with a time-dependent velocity in its own plane. Guria et al. (2006) carried out a study on the unsteady Couette flow in a rotating system. The steady MHD Couette flow of a viscous incompressible electrically conducting fluid in a rotating system in the presence of an inclined magnetic field was studied by Seth et al. (2009). Das et al. (2009) studied the unsteady MHD Couette flow in a rotating system. Many other authors Jana et al. (1977), Seth and Jana (1980), Singh (1983), Mazumder (1991), Ghosh (1993) and Guria et al. (2006) amongst several others have discussed the MHD Couette flow in a rotating system.

In partially ionised gases, the phenomenon of Hall currents occurs when the magnetic field is high or when the collision frequency is low (Sutton and

Sherman 1965). The current induced in a fluid is usually carried predominantly by electrons, which undergo successive collisions with other charged or neutral particles and are usually more mobile than ions. The electron drift velocity in most cases, leads to a second component of velocity, which in turn leads to a secondary force and causes anisotropic electrical conductivity in the flow. The current component created by this anisotropic conductivity is known as the Hall current. The dimensionless product $\omega_e\tau_e$ often called the Hall parameter, is an important characteristic number in MHD design, where ω_e is the electron cyclotron frequency and τ_e is the electron collision mean free time.

On a microscopic scale, the Hall parameter indicates the average angular travel of electrons between collisions, while on a macroscopic scale, the value of $\omega_e\tau_e$ indicates the relative importance of the Hall field and Hall current. If both the electron $\omega_e\tau_e$ and ion $\omega_i\tau_i$ Hall parameters are large simulataneously as is the case in some weakly ionised gases, the conductivity is then reduced due to a phenomenon called ion slip. Though, τ_i is ordinarily larger than τ_e, ω_i is much smaller than ω_e, such that the product $\omega_i\tau_i$ is usually negligible (Tillack and Morley (1998)). These Hall effects play a very important role in determining the flow features. Ahmad and Kumari (2009) studied the effects of Hall current on steady MHD Couette flow within a parallel plate channel in a rotating system in the presence of a uniform magnetic field applied perpendicular to the plane of the plate. Deka (2008) investigated the simultaneous effect of rotation and Hall currents on the hydrodynamic flow past an accelerated horizontal plate

relative to a rotating fluid. The Hall effects on MHD Couette flow in a rotating system were variously investigated by Ghosh and Pop (2004). Debnath et al. (1979), Mandal and Mandal (1983), Tiwari and Singh (1983) and Ghosh and Pop (2003) under varying conditions. The MHD Couette flow with temperature dependent viscosity and the ion-slip was investigated by Attia (2005b). Attia (2005a) also examined the unsteady Couette flow with heat transfer considering ion-slip while Ram (1995) studied the effect of Hall and ion-slip currents on free convective heat generating flow in a rotating fluid. The unsteady hydromagnetic Couette flow of a viscous incompressible electrically conducting fluid in a rotating system in the presence of a uniform transverse magnetic field was recently studied by ?.

2.1 TIME-DEPENDENT MHD COUETTE FLOW IN A ROTATING SYSTEM WITH SUCTION/INJECTION[1]

In this Section, the motion of a viscous, incompressible and electrically conducting fluid filling the gap between two infinite porous plates is considered. An exact solution for the accelerated motion of the lower bounding plate is formulated. Analytical solution of the governing equation is obtained by using the Laplace transform technique. The analysis of the results obtained shows that the primary velocity increases with increase in the suction/injection parameter

[1]Jha and Apere (2011c) Published in
ZAMM - Journal of Applied Mathematics and Mechanics/Zeitschrift für Angewandte Mathematik und Mechanik **91** 832 (2011); doi: 10.1002/zamm.201000049

490026

A. B. U.

while the secondary velocity increases in magnitude near the moving plate and decreases in magnitude near the fixed plate.

2.1.1 Mathematical Analysis

A Cartesian coordinate system (x', y', z') rotating about the z'-axis with an angular velocity Ω' is introduced. The motion of a viscous, incompressible and electrically conducting fluid filling the gap between two infinite porous plates is considered. The two plates are located on z'-axis at distance h apart. At time $t \leq 0$, the fluid, the porous plates and the magnetic lines of force are assumed to be at rest. When $t > 0$ the lower porous plate begins to move in its own plane with a velocity Ut^n where U is a constant and the upper plate remains fixed. The fluid flows between the two porous plates in the x'-direction with a uniform suction applied from above and injection from below and a uniform magnetic field B_0 acting perpendicular to the plates, the z'-axis is assumed to be normal to the porous plates (see Figure 2.1). Adding the Coriolis force and the

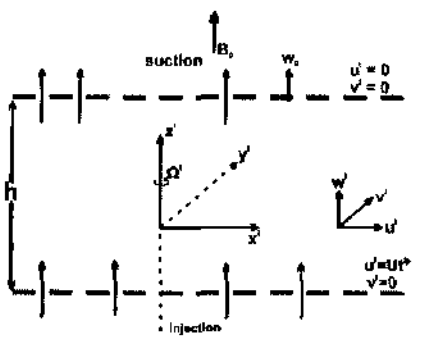


Figure 2.1: Schematic diagram of the model

Lorenz force to eq. (1.12), the basic equation governing the flow of the fluid in

the present problem is as follows

$$\frac{\partial \vec{V}}{\partial t} + (\vec{V}.\nabla)\vec{V} + 2\Omega' \kappa \times \vec{V} = -\frac{1}{\rho}\nabla P + \nu \nabla^2 V + \frac{1}{\rho}\vec{J} \times \vec{B}. \tag{2.1}$$

Since the porous plates are infinite, all physical variables except the pressure are functions of z' and t only. Integrating the equation of continuity eq. (1.5), we have $w' = w_0$, the constant w_0 representing the normal velocity at the plate is positive for injection and negative for suction. The induced magnetic field is neglected by assuming a small magnetic Reynolds number as shown in Pai (1962), therefore, the uniform magnetic field $\vec{B}$ is a constant $\vec{B} \equiv (0, 0, B_0)$ and is considered as the total magnetic field acting on the fluid. The equation for the conservation of electric charge $\nabla \cdot \vec{J} = 0$, results to $J_{z'}$= constant where $\vec{J} = (J_{x'}, J_{y'}, J_{z'})$.

In the case of vertical velocity, we immediately see that $J_{z'} = 0$. Thus, from eq. (1.12 on page 7), we obtain

$$J_{x'} = \sigma B_0 v' \ \ and \ \ J_{y'} = -\sigma B_0 u' \tag{2.2}$$

. Under these assumptions, the equations in the component form are obtained

$$\frac{\partial u'}{\partial t} + w_0 \frac{\partial u'}{\partial z'} - 2\Omega' v' = \nu \frac{\partial^2 u'}{\partial z'^2} - \frac{\sigma B_0^2}{\rho} u' \tag{2.3}$$

$$\frac{\partial v'}{\partial t'} + w_0 \frac{\partial v'}{\partial z'} + 2\Omega' u' = \nu \frac{\partial^2 v'}{\partial z'^2} - \frac{\sigma B_0^2}{\rho} v'. \tag{2.4}$$

The initial and boundary conditions for the present problem are

$$\begin{aligned} u' &= v' = 0,\ 0 \le z' \le h \text{ and } t \le 0, \\ u' &= Ut^n,\ v' = 0,\ \text{at } z' = 0, t > 0; \\ u' &= v' = 0,\ \text{at } z' = h,\ t > 0. \end{aligned} \tag{2.5}$$

Eq. (2.3) is valid when the magnetic lines of force are fixed relative to the fluid. If the magnetic field is fixed relative to the moving plate, eq. (2.3) can be replaced with

$$\frac{\partial u'}{\partial t} + w_0 \frac{\partial u'}{\partial z'} - 2\Omega' v' = \nu \frac{\partial^2 u'}{\partial z'^2} - \frac{\sigma B_0^2}{\rho}(u' - Ut^n), \tag{2.6}$$

eqs. (2.3) and (2.6) can be combined together to obtain

$$\frac{\partial u'}{\partial t'} + w_0 \frac{\partial u'}{\partial z'} - 2\Omega' v' = \nu \frac{\partial^2 u'}{\partial z'^2} - \frac{\sigma B_0^2}{\rho}(u' - KUt^n), \tag{2.7}$$

where

$$K = \begin{cases} 0 & \text{when } B_0 \text{ is fixed relative to the fluid} \\ 1 & \text{when } B_0 \text{ is fixed relative to the moving plate} \end{cases}$$

If we define the complex velocity $q' = u' + iv'$ subject to the boundary conditions

above; eqs. (2.4) and (2.7) now becomes

$$\frac{\partial q'}{\partial t} + w_0 \frac{\partial q'}{\partial z'} - 2i\Omega' q' = \nu \frac{\partial^2 q'}{\partial z'^2} - \frac{\sigma B_0^2}{\rho}(q' - KUt^n). \tag{2.8}$$

The initial and boundary conditions become

$$\begin{aligned} q' &= 0,\ 0 \le z' \le h \text{ and } t \le 0, \\ q' &= Ut^n \text{ at } z' = 0,\ t > 0; \\ q' &= 0, \text{ at } z' = h,\ t > 0. \end{aligned} \tag{2.9}$$

Eq. (2.8) subject to the boundary condition (2.9) is the general representation of the velocity distribution for the MHD Couette flow between two infinite parallel porous plates in a rotating system. Now we have to find the solution of eq. (2.8). We have considered the uniformly accelerated movement of the lower plate ($n = 1$).

2.1.2 Solution of the Problem

Substitute $n = 1$ in eq (2.8) the equation reduces to

$$\frac{\partial q}{\partial \eta} + \mathcal{S}\frac{\partial q}{\partial z} + \frac{2i}{\mathcal{E}} q = \frac{\partial^2 q}{\partial z^2} - \mathcal{H}a^2(q - K\eta). \tag{2.10}$$

The equation is subject to the following dimensionless initial and boundary conditions

$$\begin{aligned} q &= 0,\ 0 \leq z \leq 1 \ and\ \eta \leq 0 \\ q &= \eta \ at\ z = 0,\ \eta > 0; \\ q &= 0,\ at\ z = 1,\ \eta > 0. \end{aligned} \tag{2.11}$$

The dimensionless quantities used are as follows $z = z'/h,\ q = \nu q'/(Uh^2),\ \eta = \nu t/h^2,\ \mathcal{H}a^2 = B_0 h\sqrt{\sigma/\nu\rho},\ \mathcal{E} = \nu/\Omega' h^2, S = hw_0/\nu.$

The solution of eq. (2.10) can be obtained using the Laplace transforms technique. Define the following transform variables

$$\bar{q}(z,s) = \int_0^\infty q(z,\eta)e^{-s\eta}d\eta,\ (s>0) \quad \textit{where s is the Laplace parameter,}$$

and taking the Laplace transform of eq. (2.10) with the corresponding boundary conditions (2.11) we obtain the following ordinary differential equation,

$$\frac{d^2\bar{q}}{dz^2} - S\frac{d\bar{q}}{dz} - (m+s)\bar{q} = -\frac{\mathcal{H}a^2 K}{s^2}, \tag{2.12}$$

where $m = \mathcal{H}a + 2i/\mathcal{E}$. The boundary condition now becomes

$$\bar{q} = s^{-2}\ at\ z = 0,\ and\ \bar{q} = 0\ at\ z = 1. \tag{2.13}$$

The solution of (2.12) subject to the boundary condition (2.13) is

$$\begin{aligned}\bar{q}(z,s) &= e^{Sz/2}\sum_{n=0}^{\infty}\left(\frac{e^{-a\delta}}{s^2}-\frac{e^{-b\delta}}{s^2}\right)+\frac{\mathcal{H}a^2Ke^{Sz/2}}{m}\Big[\sum_{n=0}^{\infty}\left(\frac{e^{-b\delta}}{m(s+m)}+\frac{e^{-b\delta}}{s^2}-\frac{e^{-b\delta}}{sm}\right)\\ &- \sum_{n=0}^{\infty}\left(\frac{e^{-a\delta}}{m(s+m)}+\frac{e^{-a\delta}}{s^2}-\frac{e^{-a\delta}}{sm}\right)\Big]-\frac{\mathcal{H}a^2Ke^{(S(z-1)/2}}{m}\\ &\times \Big[\sum_{n=0}^{\infty}\left(\frac{e^{-c\delta}}{m(s+m)}+\frac{e^{-c\delta}}{s^2}-\frac{e^{-c\delta}}{sm}\right)-\sum_{n=0}^{\infty}\left(\frac{e^{-d\delta}}{m(s+m)}+\frac{e^{-d\delta}}{s^2}-\frac{e^{-d\delta}}{sm}\right)\Big]\\ &+ \frac{\mathcal{H}a^2K}{m}\Big\}. \qquad (2.14)\end{aligned}$$

where $a=2n+z$, $b=2n+2-z$, $c=2n+1-z$, $d=2n+1+z$, $k=S^2/4+m$ and $\delta=\sqrt{s+k}$.

We can then obtain the velocity distribution $q(z,\eta)$ on inversion of the above equation as

$$\begin{aligned}q(z,\eta) &= e^{Sz/2}\sum_{n=0}^{\infty}\left[f_1(\eta,a,k)-f_1(\eta,b,k)\right]+A_1e^{Sz/2}\sum_{n=0}^{\infty}\left[f_2(\eta,b,k)\right.\\ &- \left.f_2(\eta,a,k)\right]+A_1e^{S(z-1)/2}\sum_{n=0}^{\infty}\left[f_2(\eta,d,k)-f_2(\eta,c,k)\right]\\ &+ A_2e^{Sz/2}\sum_{n=0}^{\infty}\left[f_1(\eta,b,k)-f_1(\eta,a,k)\right]+A_2e^{S(z-1)/2}\\ &\times \sum_{n=0}^{\infty}\left[f_1(\eta,d,k)-f_1(\eta,c,k)\right]+A_3, \qquad (2.15)\end{aligned}$$

where A_1, A_2, A_3 and the functionals f_1 and f_2 are set in Appendix I.

2.1.3 Skin Friction

The primary and the secondary components of the skin friction can be obtained from the following expression.

$$\tau = \tau_x + i\tau_y. \tag{2.16}$$

τ is obtained by differentiating eq. (2.15) with respect to z and expressed in the following form

$$\begin{aligned}
\frac{\partial q}{\partial z} &= e^{Sz/2}\left\{\sum_{n=0}^{\infty}\left[f_3(\eta,a,k)-f_3(\eta,b,k)\right]+\frac{S}{2}\sum_{n=0}^{\infty}\left[f_1(\eta,a,k)-f_1(\eta,b,k)\right]\right\} \\
&+ A_1 e^{Sz/2}\left\{\sum_{n=0}^{\infty}\left[f_4(\eta,b,k)-f_4(\eta,a,k)\right]+\frac{S}{2}\sum_{n=0}^{\infty}\left[f_2(\eta,b,k)-f_2(\eta,a,k)\right]\right\} \\
&+ A_1 e^{(S(z-1)/2}\left\{\sum_{n=0}^{\infty}\left[f_4(\eta,d,k)-f_4(\eta,c,k)\right]+\frac{S}{2}\sum_{n=0}^{\infty}\left[f_2(\eta,d,k)\right.\right. \\
&- \left.\left.f_2(\eta,c,k)\right]\right\}+A_2 e^{Sz/2}\left\{\sum_{n=0}^{\infty}\left[f_3(\eta,b,k)-f_3(\eta,a,k)\right]+\frac{\eta}{2}\sum_{n=0}^{\infty}\left[f_1(\eta,b,k)\right.\right. \\
&- \left.\left.f_1(\eta,a,k)\right]\right\}+A_2 e^{(S(z-1)/2}\left\{\sum_{n=0}^{\infty}\left[f_3(\eta,d,k)-f_3(\eta,c,k)\right]\right. \\
&+ \left.\frac{S}{2}\sum_{n=0}^{\infty}\left[f_1(\eta,d,k)-f_1(t,c,k)\right]\right\}.
\end{aligned} \tag{2.17}$$

Eq. (2.17) represent the general expression for the skin friction between different layers of fluid flow within the channel. On the wall where fluid is being injected

into the channel ($z = 0$) we have the skin friction to be

$$\begin{aligned}
\frac{\partial q}{\partial z}\Big|_{z=0} &= \sum_{n=0}^{\infty}\left[f_3(\eta,a_1,k) - f_3(\eta,b_1,k)\right] + \frac{\mathcal{S}}{2}\sum_{n=0}^{\infty}\left[f_1(\eta,a_1,k) - f_1(\eta,b_1,k)\right] \\
&+ A_1\Big\{\sum_{n=0}^{\infty}\left[f_4(\eta,b_1,k) - f_4(\eta,a_1,k)\right] + \frac{\mathcal{S}}{2}\sum_{n=0}^{\infty}\left[f_2(\eta,b_1,k) - f_2(\eta,a_1,k)\right]\Big\} \\
&+ A_1 e^{-\mathcal{S}/2}\Big\{\sum_{n=0}^{\infty}\left[f_4(\eta,d_1,k) - f_4(\eta,c_1,k)\right] + \frac{\mathcal{S}}{2}\sum_{n=0}^{\infty}\left[f_2(\eta,d_1,k)\right. \\
&- \left. f_2(\eta,c_1,k)\right]\Big\} + A_2\Big\{\sum_{n=0}^{\infty}\left[f_3(\eta,b_1,k) - f_3(\eta,a_1,k)\right] \\
&+ \frac{\mathcal{S}}{2}\sum_{n=0}^{\infty}\left[f_2(\eta,b_1,k) - f_2(\eta,a_1,k)\right]\Big\} + A_2 e^{\ \mathcal{S}/2}\Big\{\sum_{n=0}^{\infty}\left[f_3(\eta,d_1,k)\right. \\
&- \left. f_3(\eta,c_1,k)\right] + \frac{\mathcal{S}}{2}\sum_{n=0}^{\infty}\left[f_1(\eta,d_1,k) - f_1(t,c_1,k)\right]\Big\}. \qquad (2.18)
\end{aligned}$$

where $a_1 = 2n$, $b_1 = 2n+2$ and $c_1 = d_1 = 2n+1$. The functionals f_3 *and* f_4 are defined in the Appendix I.

while on the wall with suction ($z = 1$), we have

$$\begin{aligned}
\frac{\partial q}{\partial z}\Big|_{z=1} &= e^{s/2}\Big\{\sum_{n=0}^{\infty}\left[f_3(t,a_2,k) - f_3(t,b_2,k)\right] + \frac{\mathcal{S}}{2}\sum_{n=0}^{\infty}\left[f_1(t,a_2,k) - f_1(t,b_2,k)\right]\Big\} \\
&+ A_1 e^{\mathcal{S}/2}\Big\{\sum_{n=0}^{\infty}\left[f_4(t,b_2,k) - f_4(t,a_2,k)\right] + \frac{\mathcal{S}}{2}\sum_{n=0}^{\infty}\left[f_2(t,b_2,k) - f_2(t,a_2,k)\right]\Big\} \\
&+ A_1\Big\{\sum_{n=0}^{\infty}\left[f_4(t,d_2,k) - f_4(t,c_2,k)\right] + \frac{\mathcal{S}}{2}\sum_{n=0}^{\infty}\left[f_2(t,d_2,k) - f_2(t,c_2,k)\right]\Big\} \\
&+ A_2 e^{\mathcal{S}/2}\Big\{\sum_{n=0}^{\infty}\left[f_3(t,b_2,k) - f_3(t,a_2,k)\right] + \frac{\mathcal{S}}{2}\sum_{n=0}^{\infty}\left[f_1(t,b_2,k) - f_1(t,a_2,k)\right]\Big\} \\
&+ A_2\Big\{\sum_{n=0}^{\infty}\left[f_3(t,d_2,k) - f_3(t,c_2,k)\right] + \frac{\mathcal{S}}{2}\sum_{n=0}^{\infty}\left[f_1(t,d_2,k) - f_1(t,c_2,k)\right]\Big\} \qquad (2.19)
\end{aligned}$$

where $a_2 = b_2 = 2n+1$, $c_2 = 2n$ and $d_2 = 2n+2$.

We can then obtain the primary and the secondary velocities and the associated

skin friction components by separating the real and imaginary parts of the complex equations obtained in equations (2.15), (2.18) and (2.19) using MATLAB. The resultant skin friction is obtained by taking the absolute value of the axial τ_x and the transverse τ_y skin frictions using MATLAB, the results are then computed and are presented in Section 2.1.4.

2.1.4 Results and Discussion

In order to have a physical insight into the problem, we have written a MATLAB programme to compute and generate the graphs for the primary and secondary velocities and the associated skin frictions. The dimensionless parameters used to analyse the fluid flow inside the channel are the suction/injection parameter $\mathcal{S}$, with the suction and injection applied simultaneously at the opposite porous plates of the channel at the same rate, the Hartmann $\mathcal{H}a$ and the Ekman numbers $\mathcal{E}$. The different values of the dimensionless parameters used in calculations are as follows: $\mathcal{H}a = 1.0$, $\mathcal{E} = 1.0$ and $\eta = 0.4$, except otherwise stated. Some representative results are presented in the form of contour graphs in Figures 2.2–2.11 to interpret the effects of these parameters. A comparative analysis is made when the magnetic field is fixed relative to the moving plate on the right panels of the figures. Figures 2.2 and 2.3 show the profile of the primary velocity u and the secondary velocity v respectively for various values of $\mathcal{S}$.

The primary velocity decreases from its initial value at the boundary to zero at the fixed porous plate through layers of different depths, while the

magnitude of the secondary velocity first increases and then decreases to zero at the upper fixed porous plate. It is observed that increasing injection result into the enhancement of the primary velocity and the magnitude of the secondary velocity, while suction tends to retard both components of the velocity. A marginal increase in the magnitude of both the primary and secondary velocities is noticed when the magnetic lines of force are fixed relative to the moving plate on the (b) part of the figures. It can be deduced that both the primary and the secondary velocities are sensitive to suction and injection. We set out to study the flow behaviour at the middle of the channel ($z = 0.5$) towards the different dimensioness parameters in Figures 2.4–2.9. The influence of $\mathcal{E}$ over $\mathcal{H}a$ on the flow behaviour is presented in Figures 2.4 and 2.5. The primary velocity is observed in Figure 2.4 to decay with suction as the magnetic field is strengthened when $K = 0$ and increases with injection as the magnetic field is further increased when $K = 1$. We noticed that for high values of $\mathcal{H}a$, the impact of $\mathcal{S}$ on the flow field becomes negligible, the effect of $\mathcal{S}$ on the flow behaviour eventually vanishes when $\mathcal{H}a$ is large enough. The behaviour of the flow field towards $\mathcal{H}a$ is in consonant with earlier results obtained by Singh and Kumar (1983) and Das et al. (2009).

The combined effect of the $\mathcal{S}$ and $\mathcal{E}$ on the flow behaviour is shown in Figures 2.6 and 2.7. It is noticed as expected in Figure 2.6a that $\mathcal{E}$ has no significant effect on the primary velocity when the magnetic field is fixed relative to the fluid but when it is fixed relative to the moving plate in Figure 2.6b, it is interesting to

note that the Ekman number has an increasing effect on the primary velocity. This phenomenon is due to the time-dependent motion of the magnetic field as such phenomenon did not occur when magnetic lines of force are moving with constant velocity in the impulsive case. Figure 2.7 reveals that the magnitude of the secondary velocity reduces as the Ekman number and the suction/injection parameter is increased. This can be explained physically; Ekman number is inversely proportional to rotation and therefore an increase would result to a reduction in rotation which predictably reduces the secondary velocity. We also observed that as $\mathcal{S}$ is increased negatively (that is the system is subjected to more suction), the effect of $\mathcal{E}$ reduces and eventually disappears. It is observed in Figure 2.8 that the primary velocity increases with time as $\mathcal{S}$ is increased while the magnitude of the secondary velocity also increases with time for the two cases under consideration (i.e for $K = 0$ and $K = 1$).

The resultant skin frictions on the two plates are presented in Figures 2.10 and 2.11. It is discovered that on both plates and irrespective of where the magnetic field is fixed relative to, the resultant skin friction increases with time. On the plate ($z = 0$) where injection takes place, the resultant skin friction decreases as the suction/injection parameter is increased as shown in Figure 2.10 and approaches zero as $\mathcal{S}$ is further increased. On the stationary plate ($z = 1$) however, it increases with $\mathcal{S}$ for the two cases considered. It is noticed that the skin friction on the plate ($z = 1$) vanishes as $\mathcal{S}$ is increased negatively. The decrease in skin fricion is a contributing factor to the enhanced velocity noticed

near the plate where injection of fluid takes place.

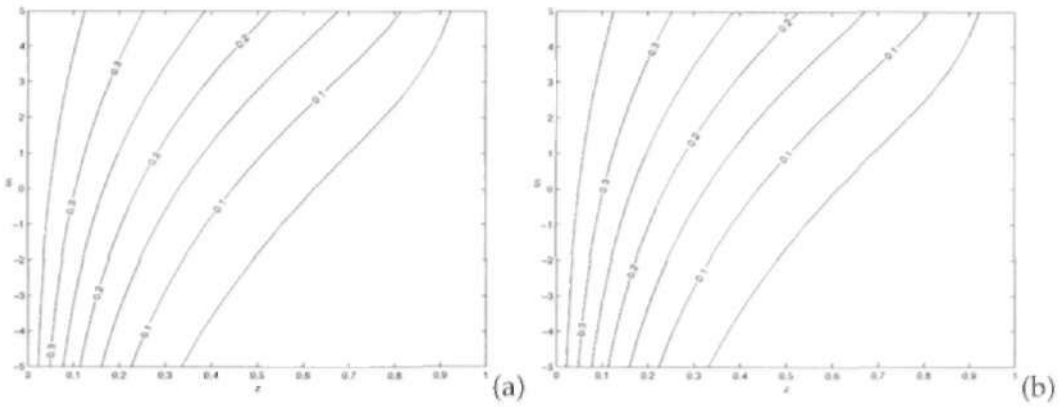


Figure 2.2: Primary velocity u showing the effect of $\mathcal{S}$ with $K = 0$ and $K = 1$ represented by a and b respectively with fixed values of $\mathcal{H}a = 0.5$, $\mathcal{E} = 1$, $\eta = 0.4$ where $\mathcal{S} \in [-5, 5]$

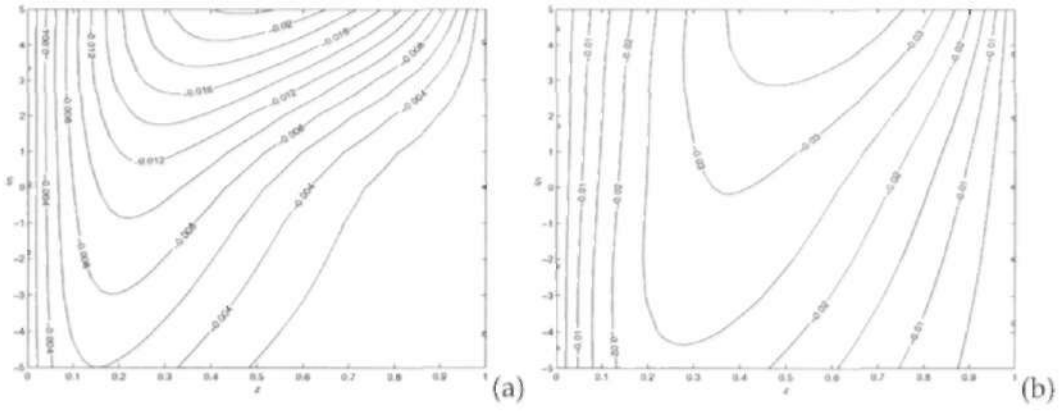


Figure 2.3: Secondary velocity v showing the effect of $\mathcal{S}$ with $K = 0$ and $K = 1$ represented by a and b respectively with fixed values of $\mathcal{H}a = 0.5$, $\mathcal{E} = 1$, $\eta = 0.4$ where $\mathcal{S} \in [-5, 5]$

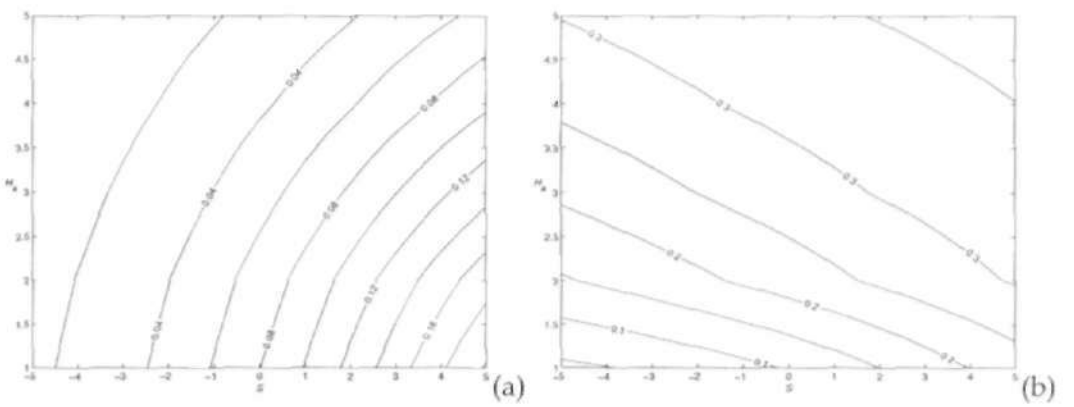


Figure 2.4: Primary velocity u showing the effect of $\mathcal{S}$ and $\mathcal{H}a$ with $K = 0$ and $K = 1$ represented by a and b respectively with fixed values of $z = 0.5$, $\mathcal{E} = 1$, $\eta = 0.4$ where $\mathcal{H}a \in [1,5]$

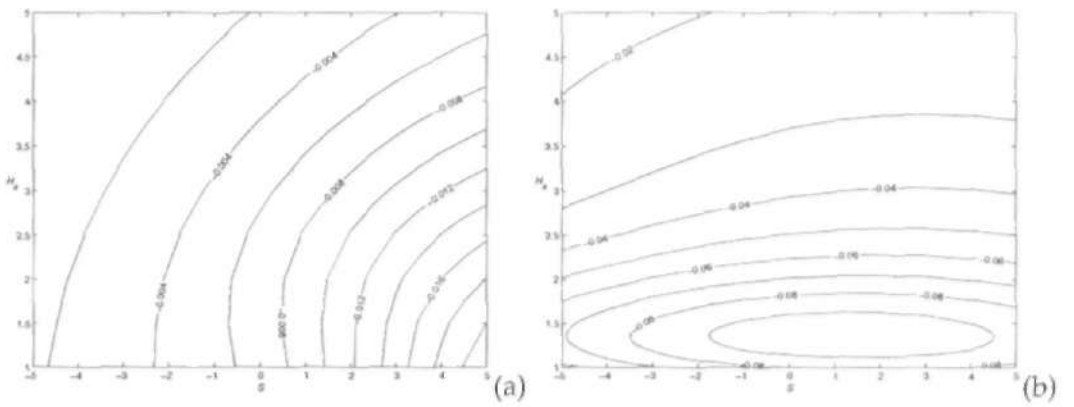


Figure 2.5: Secondary velocity v showing the effect of $\mathcal{S}$ and $\mathcal{H}a$ with $K = 0$ and $K = 1$ represented by a and b respectively with fixed values of $z = 0.5$, $\mathcal{E} = 1$, $\eta = 0.4$ where $\mathcal{H}a \in [1,5]$

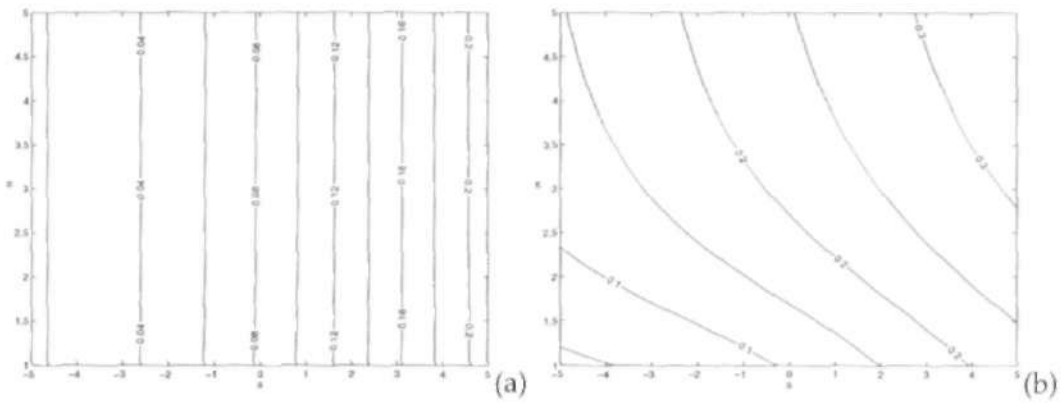


Figure 2.6: Primary velocity u showing the effect of $\mathcal{S}$ and $\mathcal{E}$ with $K = 0$ and $K = 1$ represented by a and b respectively with fixed values of $z = 0.5$, $\mathcal{H}a = 1$, $\eta = 0.4$ where $\mathcal{E} \in [1,5]$

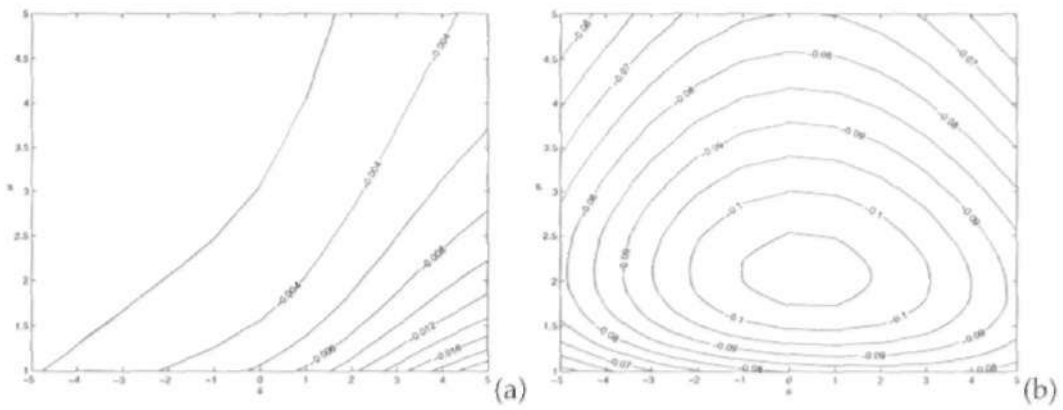


Figure 2.7: Secondary velocity v showing the effect of $\mathcal{S}$ and $\mathcal{E}$ with $K = 0$ and $K = 1$ represented by a and b respectively with fixed values of $z = 0.5$, $\mathcal{H}a = 1$, $\eta = 0.4$ where $\mathcal{E} \in [1,5]$

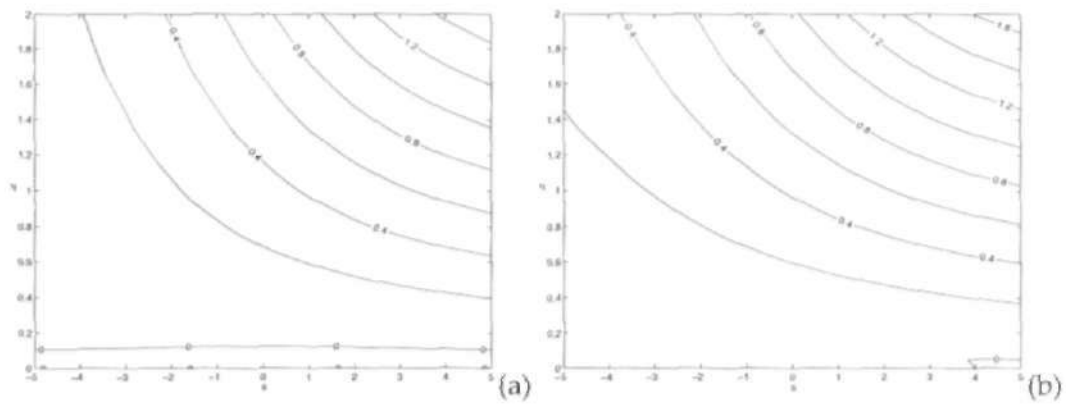


Figure 2.8: Primary velocity u showing the effect of S and η with $K = 0$ and $K = 1$ represented by a and b respectively with fixed values of $z = 0.5$, $\mathcal{H}a = 1$, $\mathcal{E} = 1$ where $\eta \in [0.1, 2]$

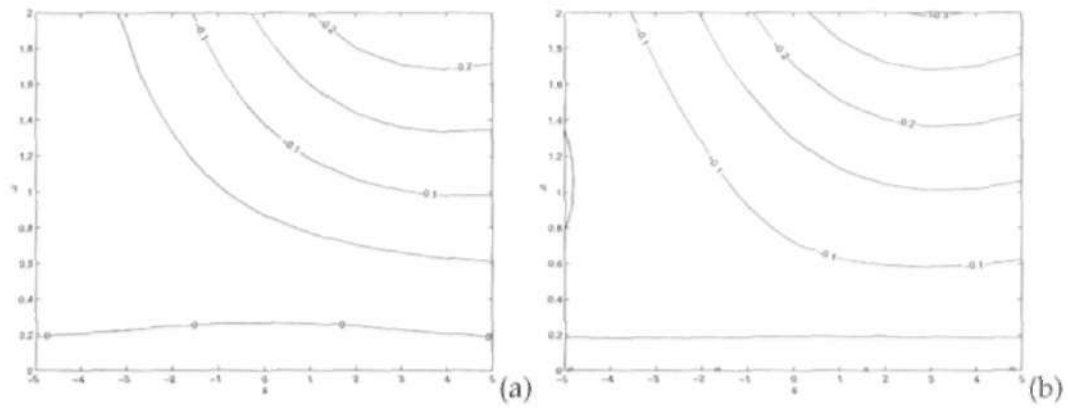


Figure 2.9: Secondary velocity v showing the effect of S and η with $K = 0$ and $K = 1$ represented by a and b respectively with fixed values of $z = 0.5$, $\mathcal{H}a = 1$, $\mathcal{E} = 1$ where $\eta \in [0.1, 2]$

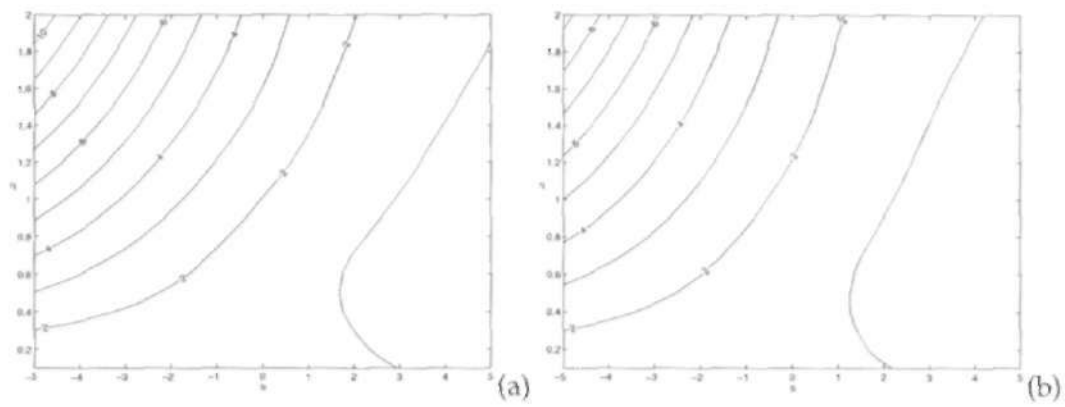


Figure 2.10: Resultant skin friction at the plate where fluid is being injected ($z = 0$) with $K = 0$ and $K = 1$ represented by a and b respectively with fixed values of $\mathcal{H}a = 1, \mathcal{E} = 1$, where $\eta \in [0.1, 1]$

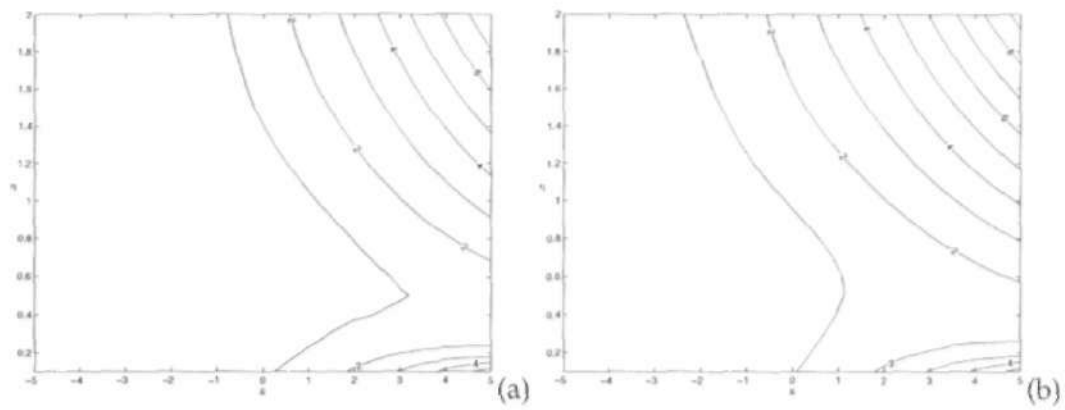


Figure 2.11: Resultant skin friction at the plate where fluid is being sucked ($z = 1$) with $K = 0$ and $K = 1$ represented by a and b respectively with fixed values of $\mathcal{H}a = 1, \mathcal{E} = 1$, where $\eta \in [0.1, 1]$

2.2 COMBINED EFFECT OF HALL AND ION-SLIP CURRENTS ON MHD COUETTE FLOW IN A ROTATING SYSTEM[2]

We develop an exact solution for the MHD Couette flow in a rotating system considering Hall and ion-slip currents. We consider the same physical situation as in Section 2.1. However, the plates are impermeable and the electron-atom collision frequency is assumed to be relatively high, so that the Hall and the ion-slip currents effect cannot be neglected. The combined effect of Hall and ion-slip currents gives rise to a velocity in the y'-axis. It is found that the influence of the Hall and ion slip parameters have a retarding effect on the magnitude of the secondary velocity especially when the magnetic lines of force are fixed relative to the moving plate. It is also interesting to note that the presence of Hall and ion-slip currents led to an increase in the time it took both the primary and the secondary velocities to achieve their steady state values.

2.2.1 Mathematical Analysis

For the case under consideration $w' = 0$. Recall the generalised Ohm's Law with Hall and ion-slip currents from eq. (1.12 on page 7)

$$J = \sigma \left[\vec{V} \times B_0 - \beta_H (J \times B_0) + \frac{\beta_H \beta_i}{B_0} (J \times B_0) \times B_0 \right] \tag{2.20}$$

[2]Jha and Apere (2010a) Published in
J. Phys. Soc. Jpn. **79** 104401 (2010); doi: 10.1143/JPSJ.79.104401

Under the assumptions given, we now have

$$J_x = \sigma B_0(\chi u' + \vartheta v') \tag{2.21}$$

$$J_y = \sigma B_0(\chi v' - \vartheta u'), \tag{2.22}$$

where

$$\vartheta = \frac{1+\beta_e\beta_i}{(1+\beta_e\beta_i)^2+\beta_e^2} \tag{2.23}$$

$$\chi = \frac{\beta_e}{(1+\beta_e\beta_i)^2+\beta_e^2}, \tag{2.24}$$

and $\beta_e = \sigma\beta_H B_0$ is the Hall parameter and β_H is the Hall factor. The Navier-Stokes equations of motion in a rotating frame of reference under this condition are

$$\frac{\partial u'}{\partial t} - 2\Omega' v' = \nu\frac{\partial^2 u'}{\partial z'^2} + \frac{\sigma B_0^2}{\rho}(\chi v' - \vartheta u') \tag{2.25}$$

$$\frac{\partial v'}{\partial t} + 2\Omega' u' = \nu\frac{\partial^2 v'}{\partial z'^2} - \frac{\sigma B_0^2}{\rho}(\chi u' + \vartheta v'). \tag{2.26}$$

The initial and boundary conditions for the present problem are

$$\begin{aligned} u' &= v' = 0,\ 0 \le z' \le h \text{ and } t \le 0, \\ u' &= Ut^n,\ v' = 0,\ \text{at } z' = 0, t > 0; \\ u' &= v' = 0,\ \text{at } z' = h,\ t > 0. \end{aligned} \tag{2.27}$$

Equations (2.25) and (2.26) are valid when the magnetic lines of force are fixed relative to the fluid. If the magnetic field is also accelerated with the same velocity as the plate, we must account for the relative motion. Thus, eqs. (2.25) and (2.26) turn to

$$\frac{\partial u'}{\partial t} - 2\Omega' v' = \nu \frac{\partial^2 u'}{\partial z'^2} - \frac{\sigma B_0^2}{\rho}[\chi v' - \vartheta(u' - KUt'^n)] \tag{2.28}$$

$$\frac{\partial v'}{\partial t'} + 2\Omega' u' = \nu \frac{\partial^2 v'}{\partial z'^2} - \frac{\sigma B_0^2}{\rho}[\chi(u' - KUt'^n) + \vartheta v'], \tag{2.29}$$

where K is as defined in Section 2.1. If we define the complex velocity $q' = u' + iv'$ subject to the boundary conditions above; equations (2.28) and (2.29) now becomes

$$\frac{\partial q'}{\partial t} - 2i\Omega' q' = \nu \frac{\partial^2 q'}{\partial z'^2} - \frac{\sigma B_0^2}{\rho}(\vartheta + i\chi)q' + \frac{\sigma B_0^2}{\rho}(\vartheta + i\chi)KUt'^n. \tag{2.30}$$

The initial and boundary conditions (2.27) also become

$$\begin{aligned} q' &= 0,\ 0 \le z' \le h \text{ and } t \le 0, \\ q' &= Ut'^n \text{ at } z' = 0,\ t > 0; \\ q' &= 0, \text{ at } z' = h,\ t > 0. \end{aligned} \tag{2.31}$$

Equation (2.30) describes the general flow in that the initial motion of the moving plate is given by a power law in the time variable. The equations are valid for both cases of when the magnetic lines of force are fixed relative to the fluid and when fixed relative to the moving plate. We are going to solve the above equation for the impulsive motion of the moving plate which corresponds to when $n = 0$ in eq. (2.30).

2.2.2 Solution of the Problem

Using the following dimensionless quantities and setting $n = 0$ in eq. (2.30) $z = z'/h,\ q = q'/U,\ \eta = \nu t/h^2,\ \mathcal{H}a = B_0 h\sqrt{\sigma/\nu\rho},\ \mathcal{E} = \nu/\Omega' h^2$. We now have

$$\frac{\partial^2 q}{\partial z^2} - \frac{\partial q}{\partial \eta} - \left[\mathcal{H}a^2(\vartheta + i\chi) + 2i/\mathcal{E}\right] q = -\mathcal{H}a^2 K(\vartheta + i\chi), \tag{2.32}$$

subject to the following dimensionless initial and boundary conditions

$$\begin{aligned} q &= 0,\ 0 \leq z \leq 1 \ and\ \eta \leq 0 \\ q &= 1\ at\ z = 0,\ \eta > 0; \\ q &= 0,\ at\ z = 1,\ \eta > 0. \end{aligned} \tag{2.33}$$

Taking the Laplace transform of eq. (2.32) with the corresponding boundary conditions, we obtain the following ordinary differential equation

$$\frac{d^2\bar{q}}{dz^2} - (m+s)\bar{q} = -\frac{\mathcal{H}a^2K(\vartheta+i\chi)}{s}, \tag{2.34}$$

where $m = \mathcal{H}a^2(\vartheta+i\chi)+2i/\mathcal{E}$. The boundary condition now becomes

$$\bar{q} = s^{-1} \text{ at } z = 0, \text{ and } \bar{q} = 0 \text{ at } z = 1. \tag{2.35}$$

The solution of eq. (2.34) subject to the boundary condition is

$$\begin{aligned} \bar{q}(z,s) &= \frac{1}{s}\sum_{k=0}^{\infty}\left(e^{-a\delta} - e^{-b\delta}\right) + \frac{\mathcal{H}a^2K(\vartheta+i\chi)}{s\delta^2} \\ &\times \left[1 - \sum_{k=0}^{\infty}(-1)^k\left[e^{-c\delta} + e^{-d\delta}\right]\right], \end{aligned} \tag{2.36}$$

where $\delta = \sqrt{m+s}$, $a = 2k+z$, $b = 2k+2-z$, $c = k+z$, *and* $d = k+1-z$. We can then obtain the velocity distribution $q(z,\eta)$ on inversion of the above equation,

$$\begin{aligned} q(z,\eta) &= \sum_{k=0}^{\infty}\left[f_2(\eta,a,m) - f_2(\eta,b,m)\right] + A_4e^{-m\eta}\sum_{k=0}^{\infty}(-1)^k\left[f_5(\eta,c,m)\right. \\ &+ \left. f_5(\eta,d,m)\right] - A_4\sum_{k=0}^{\infty}(-1)^k\left[f_2(\eta,c,m) + f_2(\eta,d,m)\right] \\ &+ A_4(1-e^{-m\eta}), \end{aligned} \tag{2.37}$$

where A_4 and the functionals f_2 and f_5 are set in the Appendix. The primary and the secondary velocities are obtained by separating the real and imaginary parts of the complex equations obtained in eq. (2.37) using MATLAB.

2.2.3 Skin Friction

The skin friction τ is defined as $\frac{\partial q}{\partial z}$, which is obtained by differentiating eq. (2.37) with respect to z as

$$\begin{aligned}\tau = \frac{\partial q}{\partial z} &= \sum_{k=0}^{\infty}[f_4(\eta,a,m) - f_4(\eta,b,m)] + A_4 e^{-m\eta}\sum_{k=0}^{\infty}(-1)^k\big[f_6(\eta,c,m) \\ &+ f_6(\eta,d,m)\big] - A_4\sum_{k=0}^{\infty}(-1)^k\big[f_4(\eta,c,m) + f_4(\eta,d,m)\big]. \qquad (2.38)\end{aligned}$$

The axial τ_x and the transverse τ_y skin frictions can be obtained by separating the real and imaginary parts in equation (2.38) using MATLAB.

$$\tau = \tau_x + i\tau_y \qquad (2.39)$$

Equation (2.38) represents the general expression for the skin friction between different fluid layers within the channel. On the lower plate ($z = 0$) we have the skin friction to be

$$\begin{aligned}\tau_0 = \frac{\partial q}{\partial z}\Big|_{z=0} &= \sum_{k=0}^{\infty}[f_4(\eta,a_1,m) - f_4(\eta,b_1,m)] + A_4 e^{-m\eta}\sum_{k=0}^{\infty}(-1)^k\big[f_6(\eta,c_1,m) \\ &+ f_6(\eta,d_1,m)\big] - A_4\sum_{k=0}^{\infty}(-1)^k\big[f_4(\eta,c_1,m) + f_4(\eta,d_1,m)\big], \qquad (2.40)\end{aligned}$$

where $a_1 = 2k$, $b_1 = 2k+2$, $c_1 = k$ and $d_1 = k+1$. The functionals f_5 *and* f_6 are defined in Appendix I.

460026

A. B. U.
Library Services

while on the upper plate ($z = 1$), we have

$$\tau_1 = \frac{\partial q}{\partial z}\Big|_{z=1} = \sum_{k=0}^{\infty}[f_4(\eta, a_2, m) - f_4(\eta, b_2, m)] + A_4 e^{-m\eta}\sum_{k=0}^{\infty}(-1)^k[f_6(\eta, c_2, m) + f_6(\eta, d_2, m)] - A_4\sum_{k=0}^{\infty}(-1)^k[f_4(\eta, c_2, m) + f_4(\eta, d_2, m)], \quad (2.41)$$

where $a_2 = 2k+1$, $b_2 = 2k+1$, $c_2 = k+1$ and $d_2 = k$.

The resultant skin friction is obtained by taking the absolute values of the axial τ_x and the transverse τ_y skin frictions.

2.2.4 Steady State

The expression for the steady state velocity q_s is obtained by setting $\partial q/\partial t$ in eq. (2.32) to be zero. We now have the following ordinary differential equation:

$$\frac{d^2 q_s}{dz^2} - m\bar{q}_s = -\mathcal{H}a^2 K(\vartheta + i\chi) \quad (2.42)$$

The solution of the above equation with the boundary condition (2.33) yields,

$$q_s(z) = \frac{e^{-\sqrt{m}z} - e^{-\sqrt{m}(2-z)}}{1 - e^{-2\sqrt{m}}} + \frac{\mathcal{H}a^2 K(\vartheta + i\chi)}{m}\left[1 - \frac{e^{-\sqrt{m}z} + e^{-\sqrt{m}(1-z)}}{1 + e^{-\sqrt{m}}}\right]. \quad (2.43)$$

The corresponding skin friction τ_s for the steady state is obtained by differentiating equation (2.43) with respect to z

$$\tau_s = \frac{\partial q_s}{\partial z} = -\sqrt{m}\frac{(e^{-\sqrt{m}z} + e^{\xi z})}{1 - e^{-2\sqrt{m}}} + \frac{\mathcal{H}a^2 K(\vartheta + i\chi)}{\sqrt{m}}\left[\frac{e^{-\sqrt{m}z} - e^{\sqrt{m}z}}{1 + e^{-\sqrt{m}}}\right]. \quad (2.44)$$

2.2.5 Results and Discussion

In order to discuss the results, some numerical calculations are carried out for the dimensionless velocities and the skin friction. The general expressions for the velocity and the skin friction are given by eqs. (2.37), and (2.38). The solution given in the equations are in complex form; so with MATLAB, one can separate both the velocity and skin friction into real and imaginary parts and then calculate the numerical values of the primary and secondary velocities and the associated skin frictions. Contour and line graphs of the velocity profiles and skin friction are presented in Figures 2.12–2.23 to reveal the influences of the governing parameters. The value of the Ekman number $\mathcal{E}$ is fixed throughout as one in order to concentrate on the effect of the Hall and ion slip currents.

Figure 2.12 shows the effect of the Hall current in the presence of ion-slip current on the primary velocity for fixed values of $\mathcal{H}a = 35.0$, $\mathcal{E} = 1.0$, $t = 0.1$ and $\beta_i = 5.0$. From Figure 2.12a, the primary velocity u is observed to increase as the Hall current increases when the magnetic field is fixed relative to the fluid ($K = 0$), the reverse is the case when the magnetic field is fixed relative to the moving plate ($K = 1$). In Figure 2.13a, the secondary velocity reduces as the Hall current increases when $K = 0$, while for $K = 1$, three distinctive regions can be noticed. Near the moving lower plate, it is observed that v decreases with an increase in the Hall parameter, while at the middle of the channel it increase. A reversal of this trend is noticed as we move towards the stationary

plate. Figure 2.14 and Figure 2.15 shows the effect of the ion-slip current on the velocity profiles for fixed values of $\mathcal{H}a = 35.0$, $\mathcal{E} = 1.0$, $\eta = 0.1$ and $\beta_e = 10.0$. The effect of the ion-slip parameter on the primary veloicty as observed in Figure 2.14 is similar to the effect the Hall current have on the primary velocity as seen in Figure 2.12. However, the secondary velocity v when the magnetic field is fixed relative to the fluid ($K = 0$), is seen in Figure 2.15a to increase with the ion-slip parameter close to the plate at $z = 0$ (i.e the moving plate). As the ion-slip parameter is increased further and close to the stationary plate, the effect of the ion slip on the flow behaviour is reduced to the barest minimum. An opposite behaviour is noticed when the magnetic field is fixed relative to the moving plate ($K = 1$) as observed in Figure 2.15b.

The primary velocity u is seen in Figure 2.16 to increase with both the Hall and the ion-slip currents when $K = 0$, while when $K = 1$, it decreases with both Hall and ion-slip currents. The behaviour of the secondary velocity with respect to Hall and ion-slip current is depicted in Figure 2.17. The ion-slip current is a decreasing function of the secondary velocity at all times, the Hall current behaves in a similar manner when $K = 0$. However, the behaviour of the Hall current towards the secondary velocity when $K = 1$ is somehow erratic, it reduces with Hall current close to the moving plate until it reaches zero at the middle of the plate and started increasing at the other half of the channel. Figure 2.18 shows that the primary velocity increases with time until it reaches its steady state for both cases. However, the primary velocity is seen to attain its steady

state quicker in the case when $K = 0$ than when $K = 1$. The secondary velocity behaves in an opposite manner towards time as seen in Figure 2.19.

The influence of the governing parameters on the skin friction are presented in Figures 2.20-2.23. The skin friction on the moving plate ($z = 0$) decreases with increase in both the Hall and ion-slip parameters for fixed values of $\mathcal{E} = 1$, $\mathcal{H}a = 35.0$ and $\eta = 0.1$ when $K = 0$ as seen in Figure 2.20a, while the opposite behaviour is noticed in Figure 2.20b when $K = 1$. At the stationary plate ($z = 1$), we noticed that when the magnetic field is fixed relative to the fluid ($K = 0$) in Figure 2.21a, the skin friction tends to zero as both the Hall and ion-slip parameter are decreased. However, the influence of the Hall and ion-slip parameter on the skin friction on the stationary plate when ($K = 1$) is the same as when ($K = 0$) on the moving plate. Figures 2.22 and 2.23 reflect that the skin friction decreases with time on both porous plates when magnetic field is fixed with respect to the moving porous plate. Moreover, the skin friction decreases with time at the moving porous plate when the magnetic field is fixed to the fluid while the role of time is just contrast at the stationary plate.The skin friction when the magnetic field is fixed relative to the moving plate is seen to behave in an exact opposite manner to that of the accelerated motion studied by Jha and Apere (2012b).

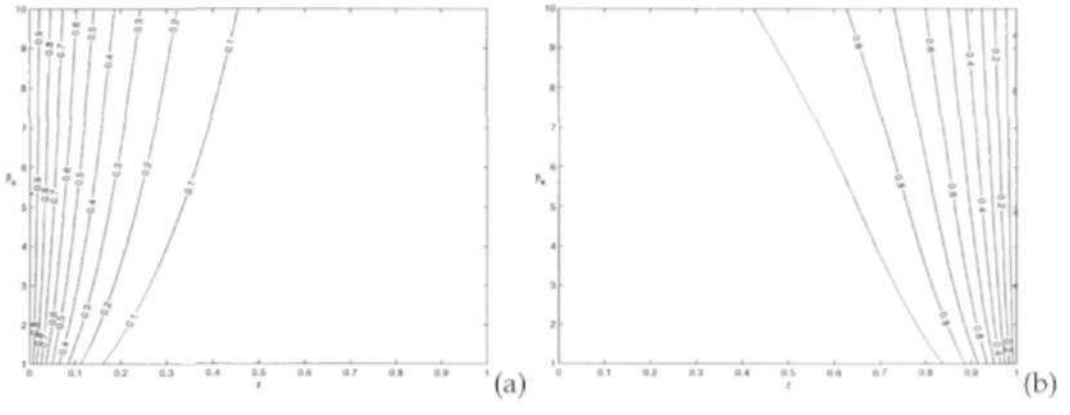


Figure 2.12: Primary velocity profile u showing the effect of Hall current in the presence of ion-slip current with $K = 0$ and $K = 1$ represented by a and b respectively with fixed values of $\mathcal{H}a = 35.0$, $\mathcal{E} = 1.0$, $\eta = 0.1$, $\beta_i = 5.0$ and $\beta_e \in [1.0, 10.0]$

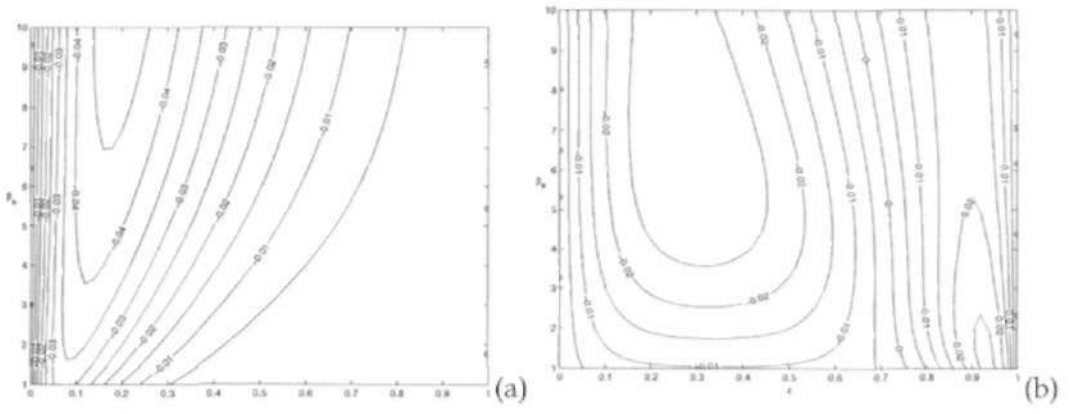


Figure 2.13: Secondary velocity profile v showing the effect of Hall current in the presence of ion-slip current with $K = 0$ and $K = 1$ represented by a and b respectively with fixed values of $\mathcal{H}a = 35.0$, $\mathcal{E} = 1.0$, $\eta = 0.1$, $\beta_i = 5.0$ and $\beta_e \in [1.0, 10.0]$

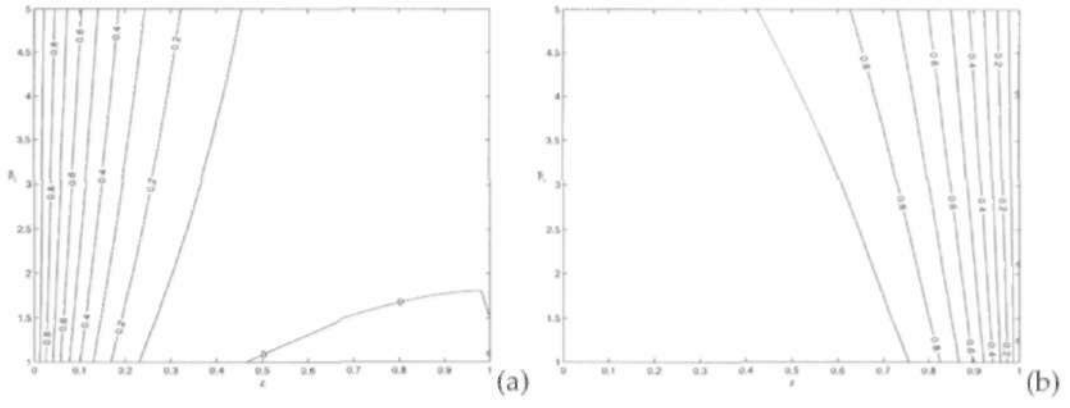


Figure 2.14: Primary velocity u showing the effect of ion-slip current with $K = 0$ and $K = 1$ represented by a and b respectively with fixed values of $\mathcal{H}a = 35.0$, $\mathcal{E} = 1.0$, $\eta = 0.1$, $\beta_e = 10.0$ and $\beta_i \in [1.0, 5.0]$

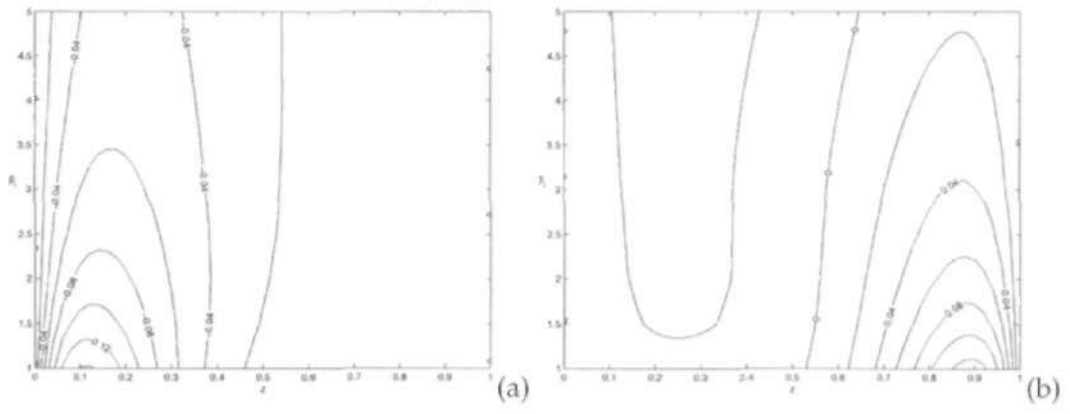


Figure 2.15: Secondary velocity v showing the effect of ion-slip current with $K = 0$ and $K = 1$ represented by a and b respectively with fixed values of $\mathcal{H}a = 35.0$, $\mathcal{E} = 1.0$, $\eta = 0.1$, $\beta_e = 10.0$ and $\beta_i \in [1.0, 5.0]$

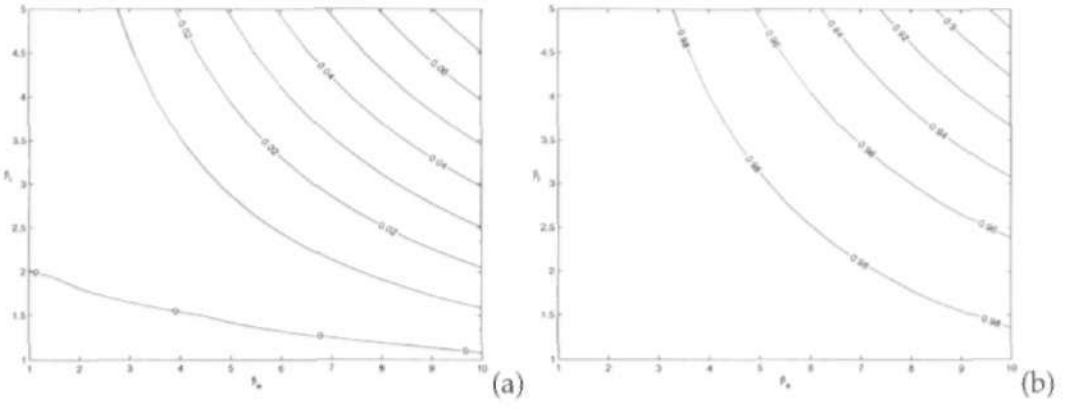


Figure 2.16: Primary velocity u showing the effect of Hall current over the ion-slip current with $K = 0$ and $K = 1$ represented by a and b respectively with fixed values of $z = 0.5$, $\eta = 0.1$, $\mathcal{H}a = 35.0$ and $\mathcal{E} = 1.0$

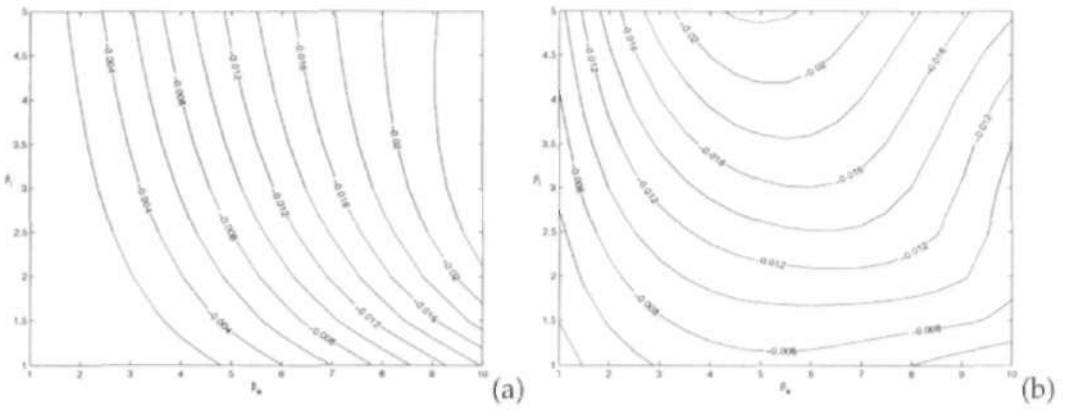


Figure 2.17: Secondary velocity v showing the effect of Hall current over the ion-slip current with $K = 0$ and $K = 1$ represented by a and b respectively with fixed values $z = 0.5$, $\eta = 0.1$, $\mathcal{H}a = 35.0$ and $\mathcal{E} = 1.0$

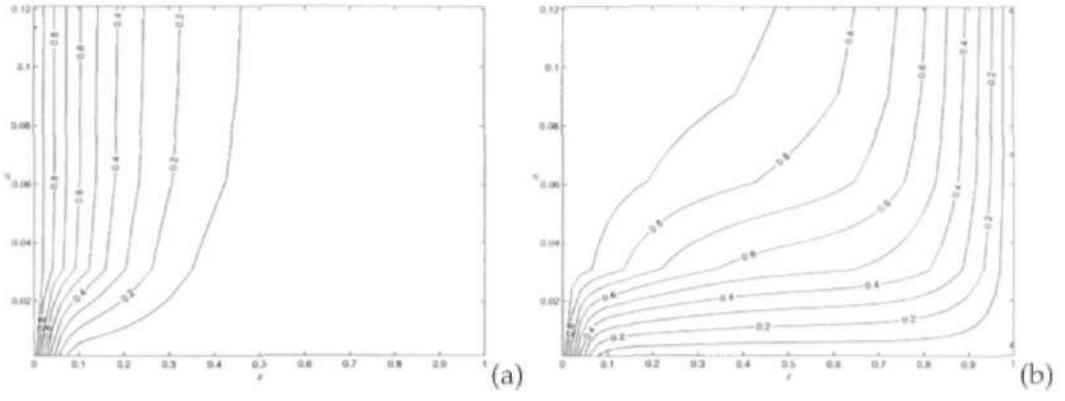


Figure 2.18: Primary velocity u showing the effect of time with $K = 0$ and $K = 1$ represented by a and b respectively with fixed values of $\mathcal{H}a = 35.0$, $\mathcal{E} = 1$, $\beta_e = 10.0$, $\beta_i = 5.0$ and $\eta \in [0.01, 0.15]$

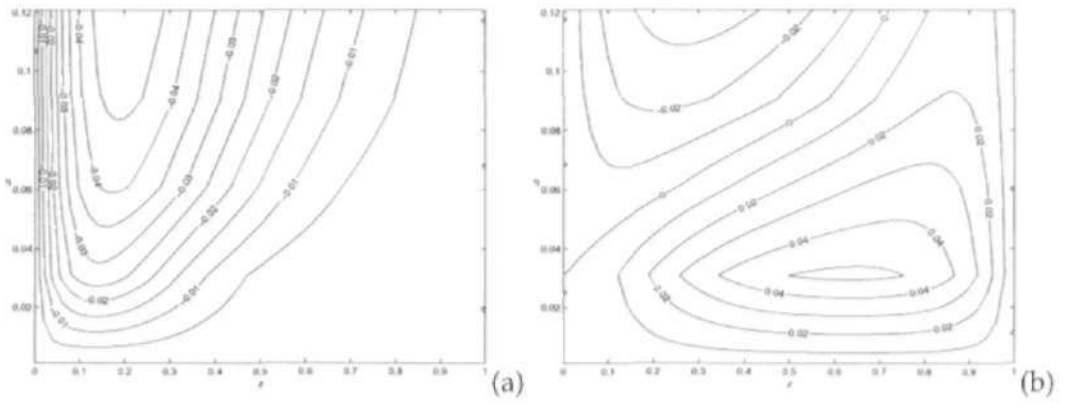


Figure 2.19: Secondary velocity v showing the effect of time with $K = 0$ and $K = 1$ represented by a and b respectively with fixed values of $\mathcal{H}a = 35.0$, $\mathcal{E} = 1$, $\eta = 0.4$, $\beta_e = 10.0$, $\beta_i = 5.0$ and $\eta \in [0.01, 0.15]$

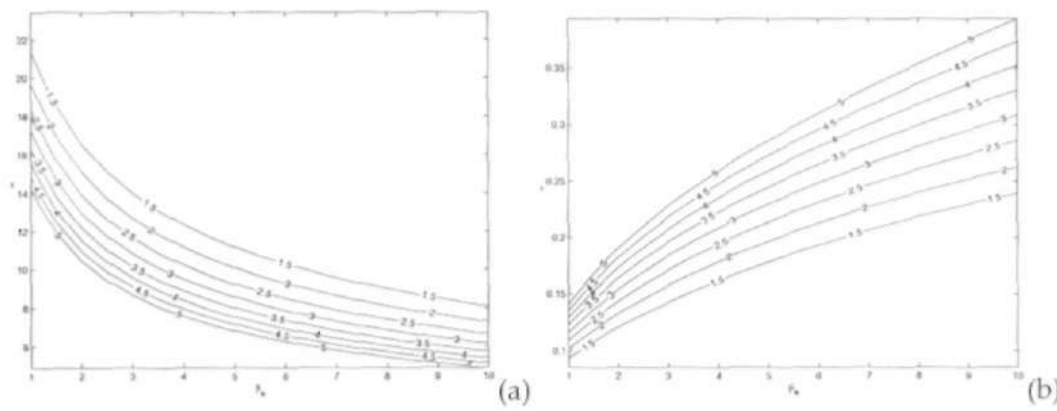


Figure 2.20: The resultant skin friction at $z = 0$ showing the effect of Hall and ion-slip parameter with $K = 0$ and $K = 1$ represented by a and b respectively with fixed values of $\mathcal{E} = 1$, $\mathcal{H}a = 35.0$ and $\eta = 0.1$

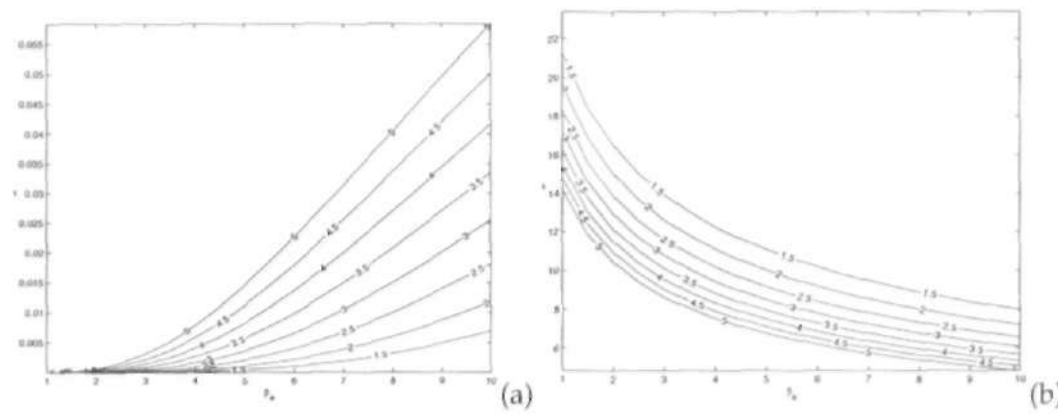


Figure 2.21: The resultant skin friction at $z = 1$ showing the effect of Hall and ion-slip parameter with $K = 0$ and $K = 1$ represented by a and b respectively with fixed values of $\mathcal{E} = 1$, $\mathcal{H}a = 35.0$ and $\eta = 0.1$

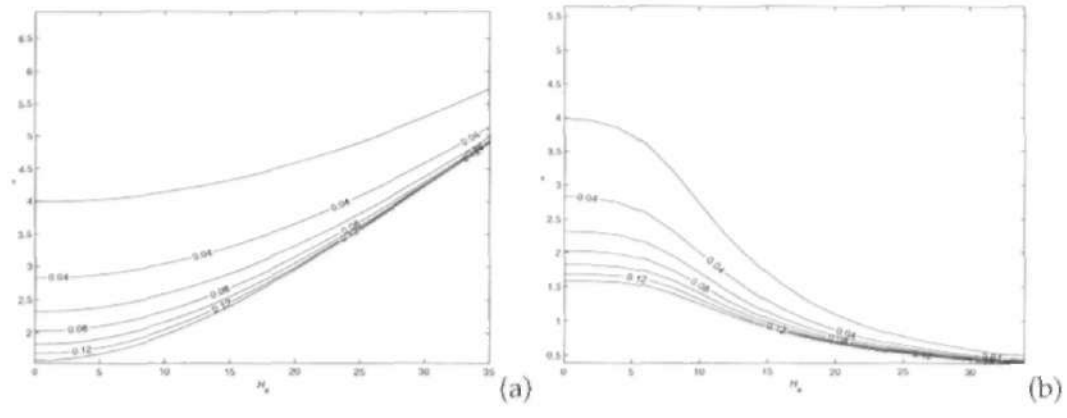


Figure 2.22: The resultant skin friction at $z = 0$ showing the effect of Hartmann number and time with $K = 0$ and $K = 1$ represented by a and b respectively with fixed values of $\mathcal{E} = 1$, $\beta_e = 10.0$, $\beta_i = 5.0$ and $\eta \in [0.01, 0.15]$

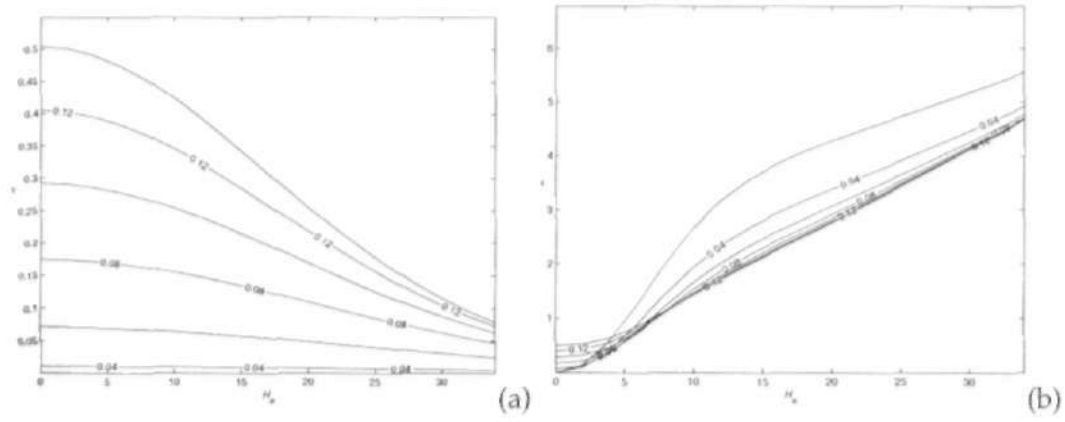


Figure 2.23: The resultant skin friction at $z = 1$ showing the effect of Hartmann number and time with $K = 0$ and $K = 1$ represented by a and b respectively with fixed values of $\mathcal{E} = 1$, $\beta_e = 10.0$, $\beta_i = 5.0$ and $\eta \in [0.01, 0.15]$

2.3 HALL AND ION-SLIP EFFECTS ON UNSTEADY MHD COUETTE FLOW IN A ROTATING SYSTEM WITH SUCTION AND INJECTION[3]

Despite the effects the integration of suction/injection, Hall and ion-slip currents and rotation is known to have on MHD flow and their applications in cosmical fluid dynamics and solar physics, the combined effects of these parameters appears not to have been given adequate attention. With this fact in mind, we have extended the approach of Section 2.2 to include the effect of suction/injection in this section. However, the lower porous plate is stationary in this case, while the upper porous plate is moving. From investigation, we observed that fixing the magnetic field relative to the moving porous plate always results into the phenomenon of backflow on the secondary velocity.

2.3.1 Mathematical Analysis

The fluid and the porous plates of the channel are in a state of rigid body rotation about the z'-axis with uniform angular velocity Ω'. At time $t \leq 0$, the fluid, the plates and the magnetic lines of force are assumed to be at rest. When $t > 0$ the upper plate ($z' = h$) begins to move in its own plane with a velocity Ut^n where U is a constant and the lower plate ($z' = 0$) remains fixed. The z'-axis is assumed to be normal to the porous plates. Then the equation of continuity, on integration

[3]Jha and Apere (2011a) Published in
J. Phys. Soc. Jpn. **80** 114401 (2011); doi: 10.1143/JPSJ.80.114401

gives

$$w' = constant = w_0'. \tag{2.45}$$

where w_0' is the normal velocity of suction or injection at the plate according as $w_0' < 0$ or $w_0' > 0$ respectively and $w_0' = 0$ represents the case of non-permeable plate. Under the assumptions made, the present problem which is a combination of the physical situations in Sections 2.1 and 2.2 is governed by the following equations:

$$\frac{\partial u'}{\partial t} - 2\Omega' v' + w_0' \frac{\partial u'}{\partial z'} = \nu \frac{\partial^2 u'}{\partial z'^2} + \frac{\sigma B_0^2}{\rho}[\chi v' - \vartheta(u' - KUt'^n)] \tag{2.46}$$

$$\frac{\partial v'}{\partial t} + 2\Omega' u' + w_0' \frac{\partial v'}{\partial z'} = \nu \frac{\partial^2 v'}{\partial z'^2} - \frac{\sigma B_0^2}{\rho}[\chi(u' - KUt'^n) + \vartheta v']. \tag{2.47}$$

The initial and boundary conditions for the present problem are

$$\begin{aligned} u' &= v' = 0, \ at\ t < 0 \quad 0 \le z' \le h \\ u' &= 0, \ v' = 0, \ at\ t > 0\ and\ z' = 0 \\ u' &= Ut'^n, \ v' = 0, \ at\ t > 0 \quad and\ z' = h. \end{aligned} \tag{2.48}$$

Defining a complex velocity $q' = u' + iv'$, eqs. (2.46) and (2.47) now becomes

$$\frac{\partial q'}{\partial t} - 2i\Omega' q' + w_0 \frac{\partial q'}{\partial z'} = \nu \frac{\partial^2 q'}{\partial z'^2} - \frac{\sigma B_0^2}{\rho}(\vartheta + i\chi)q' + \frac{\sigma B_0^2}{\rho}(\vartheta + i\chi)KUt'^n. \tag{2.49}$$

The initial and boundary conditions also become

$$\begin{aligned} q' &= = 0, \ at\ t < 0 \quad 0 \le z' \le h \\ q' &= 0, \ at\ t > 0\ and\ z' = 0 \\ q' &= Ut'^{n}, \ at\ t > 0 \quad and\ z' = h. \end{aligned} \tag{2.50}$$

We are set out to determine the solution for the impulsive motion where $n = 0$.

2.3.2 Solution of the Problem

Using the same dimensionless quantities used in Section 2.2 and S as defined in Section 2.1, we now have

$$\frac{\partial q}{\partial \eta} + \mathcal{S}\frac{\partial q}{\partial z} + \left[\mathcal{H}a^2(\vartheta + i\chi) + 2i\Omega\right] q = \frac{\partial^2 q}{\partial z^2} + \mathcal{H}a^2 K(\vartheta + i\chi). \tag{2.51}$$

The corresponding initial and boundary conditions of the differential equations are

$$\begin{aligned} q &= = 0, \ at\ \eta < 0 \quad 0 \le z \le 1 \\ q &= 0, \ at\ \eta > 0\ and\ z = 0 \\ q &= 1, \ at\ \eta > 0 \quad and\ z = 1. \end{aligned} \tag{2.52}$$

Applying the Laplace transform, we obtain the following ordinary differential equations

$$\frac{d^2\bar{q}}{dz^2} - S\frac{d\bar{q}}{dz} - (m+s)\bar{q} = -\frac{\mathcal{H}a^2K(\vartheta+i\chi)}{s}, \tag{2.53}$$

where $m = \mathcal{H}a^2(\vartheta+i\chi) + 2i\Omega$. The boundary condition now becomes

$$\bar{q} = 0 \text{ at } z = 0, \text{ and } \bar{q} = s^{-1} \quad \text{at } z = 1. \tag{2.54}$$

The solution of eq. (2.53) together with the boundary condition (2.54) is

$$\begin{aligned}\bar{q}(z,s) &= \frac{e^{S(z-1)/2}}{s}\Big[\frac{e^{-\delta(1-z)} - e^{-\delta(1+z)}}{1-e^{-2\delta}}\Big] + \frac{\mathcal{H}a^2K(\vartheta+i\chi)}{s(m+s)} \\ &\times \Big[1 - e^{S(z-1)/2}\Big(\frac{e^{-\delta(1-z)} - e^{-\delta(1+z)}}{1-e^{-2\delta}}\Big) \\ &- e^{Sz/2}\Big(\frac{e^{-\delta z} - e^{-\delta(2-z)}}{1-e^{-2\delta}}\Big)\Big].\end{aligned} \tag{2.55}$$

Using the series expansion for $(1-e^{-2\delta})$, eq. (2.55) can be written in the following form

$$\begin{aligned}\bar{q}(z,s) &= e^{(sz-s)/2}\sum_{n=0}^{\infty}\Big(\frac{e^{-a\delta}}{r} - \frac{e^{-b\delta}}{s}\Big) + \frac{\mathcal{H}a^2K(\vartheta+i\chi)e^{S(z-s)/2}}{m} \\ &\times \Big[\sum_{n=0}^{\infty}\Big(\frac{e^{-a\delta}}{s+m} - \frac{e^{-b\delta}}{s+m}\Big) - \sum_{n=0}^{\infty}\Big(\frac{e^{-a\delta}}{s} - \frac{e^{-b\delta}}{s}\Big)\Big] + \frac{\mathcal{H}a^2K(\vartheta+i\chi)e^{Sz/2}}{m} \\ &\times \Big[\sum_{n=0}^{\infty}\Big(\frac{e^{-c\delta}}{s+m} - \frac{e^{-d\delta}}{s+m}\Big) - \sum_{n=0}^{\infty}\Big(\frac{e^{-c\delta}}{s} - \frac{e^{-a\delta}}{s}\Big)\Big] \\ &+ \frac{\mathcal{H}a^2K(\vartheta+i\chi)}{m}\Big(\frac{1}{s} - \frac{1}{s+m}\Big),\end{aligned} \tag{2.56}$$

where $\delta = \sqrt{s+k}$, $k = S^2/4 + m$, $a = 1 + 2n - z$, $b = 1 + 2n + z$, $c = 2n + z$, *and* $d = 2 + 2n - z$. We can then obtain the velocity distribution $q(z,\eta)$ on inversion of the above equation as:

$$\begin{aligned} q(z,\eta) &= e^{S(z-1)/2}\sum_{n=0}^{\infty}[f_7(\eta,a,k) - f_7(\eta,b,k)] + Ae^{S(z-1)/2} \\ &\times \sum_{n=0}^{\infty}\Big\{e^{-m\eta}[f_7(\eta,a,k) - f_7(\eta,b,k)] - [f_7(\eta,a,k) - f_7(\eta,b,k)]\Big\} \\ &+ A_4 e^{Sz/2}\sum_{n=0}^{\infty}\Big\{e^{-m\eta}[f_7(\eta,c,k) - f_7(\eta,d,k)] \\ &- [f_7(\eta,c,k) - f_7(\eta,d,k)]\Big\} + A_4(1 - e^{-m\eta}), \end{aligned} \tag{2.57}$$

where

$$A_4 = \frac{\mathcal{H}a^2 K(\vartheta + i\chi)}{m} \tag{2.58}$$

and the functional f_7 is defined as

$$\begin{aligned} f_7(x_1,x_2,x_3) &= \frac{1}{2}\Big[\exp(x_2\sqrt{x_3})\mathrm{erfc}\Big(\frac{x_2}{2\sqrt{x_1}} + \sqrt{x_1 x_3}\Big) \\ &+ \exp(-x_2\sqrt{x_3})\mathrm{erfc}\Big(\frac{x_2}{2\sqrt{x_1}} - \sqrt{x_1 x_3}\Big)\Big]. \end{aligned}$$

2.3.3 Skin Friction

The skin friction can now be calculated. This is given by

$$\frac{\partial q}{\partial z} = \tau = \frac{\partial u}{\partial z} + i\frac{\partial v}{\partial z}. \tag{2.59}$$

It is obtained by differentiating eq. (2.57) with respect to z and expressed in the following form

$$\begin{aligned}
\frac{\partial q}{\partial z} &= e^{S(z-1)/2}\Big\{\sum_{n=0}^{\infty}\left[f_8(\eta,a,k)-f_8(\eta,b,k)\right]+\frac{S}{2}\sum_{n=0}^{\infty}\left[f_7(\eta,a,k)-f_7(\eta,b,k)\right]\Big\} \\
&+ A_4e^{S(z-1)-s)/2}\Big\{\sum_{n=0}^{\infty}e^{-m\eta}\left[f_8(\eta,a,k)-f_8(t,b,k)\right]-\left[\left(f_8(t,a,k)-f_8(t,b,k)\right]\right. \\
&+ \frac{S}{2}\sum_{n=0}^{\infty}e^{-m\eta}\left[f_7(\eta,a,k)-f_7(\eta,b,k)\right]-\left[\left(f_7(\eta,a,k)-f_7(\eta,b,k)\right]\right\} \\
&+ A_4e^{Sz/2}\Big\{\sum_{n=0}^{\infty}e^{\ m\eta}\left[f_8(\eta,c,k)-f_8(\eta,d,k)\right]-\left[\left(f_8(\eta,c,k)-f_8(\eta,d,k)\right]\right. \\
&+ \frac{S}{2}\sum_{n=0}^{\infty}e^{-m\eta}\left[f_7(\eta,c,k)-f_7(\eta,d,k)\right]-\left[\left(f_7(\eta,c,k)-f_7(\eta,d,k)\right]\right\}, \qquad (2.60)
\end{aligned}$$

where the functional f_8 is

$$\begin{aligned}
f_8(x_1,x_2,x_3) &= \frac{1}{2}\Big[\sqrt{x_3}\exp(x_2\sqrt{x_3})\mathrm{erfc}\Big(\frac{x_2}{2\sqrt{x_1}}+\sqrt{x_1x_3}\Big) \\
&- \sqrt{x_3}\exp(-x_2\sqrt{x_3})\mathrm{erfc}\Big(\frac{x_2}{2\sqrt{x_1}}-\sqrt{x_1x_3}\Big) \\
&- \frac{2}{\sqrt{\pi x_1}}\exp\Big(\frac{-x_2^2}{4}-x_1x_3\Big)\Big].
\end{aligned}$$

Equation (2.60) represents the general expression for the skin friction between different layers of fluid flow within the channel. The skin frictions at the upper plate and that at the lower plate can then be obtained by substituting $z = 1$ and $z = 0$ respectively in eq. (2.60).

The primary and the secondary velocities and the associated skin friction components are obtained by separating the real and imaginary parts of the complex equations obtained in eqs. (2.57) and (2.60) using MATLAB. The

resultant skin friction is obtained by taking the absolute value of the axial and the transverse skin friction, the results are then computed and are presented in Section 5. The real part of eq. (2.60) is τ_x $(\frac{\partial u}{\partial z})$ while the imaginary part is τ_y $(\frac{\partial v}{\partial z})$.

2.3.4 Steady State

Following the same approach as in Section 2.2, we obtain the steady state equation to be

$$\frac{d^2 q_s}{dz^2} - S\frac{dq_s}{dz} - mq_s = -\mathcal{H}a^2 K(\vartheta + i\chi). \tag{2.61}$$

Equation (2.61) is solved with eq. (2.52) to obtain the steady state velocity thus

$$\begin{aligned} q_s(z) &= \frac{e^{S(z-1)/2}\left[e^{-\delta(1-z)} - e^{-(\delta(1+z)}\right]}{1-e^{-2\delta}} + \frac{\mathcal{H}a^2 K(\vartheta + i\chi)}{m} \\ \times &\quad \left[1 - \frac{e^{Sz/2}\left[(e^{-\delta z} - e^{-\delta(2-z)})\right]}{1-e^{-2\delta}}\right. \\ - &\quad \left.\frac{e^{S(z-1))/2}\left[(e^{-\delta(1\ \ z)} - e^{-\delta(1+z)})\right]}{1-e^{-2\delta}}\right]. \end{aligned} \tag{2.62}$$

The numerical results of eq.(2.62) is found to be in excellent agreement with that of eq (2.57) when the value of η is large.

2.3.5 Results and Discussion

In order to study the effects of Hall and ion-slip currents and suction/injection on the flow field, the velocity profiles for the primary u and the secondary v flows are drawn for various values of rotation parameter Ω, suction/injection

parameter $\mathcal{S}$ and Hall β_e and ion-slip β_i parameters in Figures 2.24–2.31. It is shown in Figure 2.24a that u decreases with increase in Ω when $K = 0$. However, in Figure 2.24b, the opposite trend is noticed when $z < 0.4$, after which u is again observed to decrease with an increase in Ω. The secondary velocity is seen in Figure 2.25 to increase in magnitude with Ω. This is expected as v is as a result of coriolis force. It is interesting to note in Figure 2.25b that a backflow occurs for small values of the Ω when the magnetic field is fixed relative to the moving porous plate. Figure 2.26 depicts the effect of $\mathcal{S}$ on u. We observe that for suction, u increases with $\mathcal{S}$, while for injection it decreases with an increase in the value of $\mathcal{S}$. This behaviour is consistent for both $K = 0$ and $K = 1$. In Figure 2.27, v increases in magnitude with an increase in $\mathcal{S}$ for suction and decreases in magnitude for injection. It is however observed in Figure 2.27b that fixing the magnetic field relative to the moving porous plate results into the occurrence of a backflow. The primary velocity is noticed in Figure 2.28a to increase with increase in β_e when the magnetic field is fixed relative to the fluid, however, a decrease in u as a result of an increase in β_e is noticed when the magnetic field is fixed relative to the moving porous plate.

In Figure 2.29 it is seen that v increases in magnitude as the β_e is increased when $K = 0$, although, the effect of the β_e is seen to be negligible close to the moving porous plate. For $K = 1$ in Figure 2.29b, v decreases in magnitude as β_e is increased while the effect of β_e is observed to be insignificant close to the stationary plate. The phenomenon of backflow is also observed in Figure 2.29b.

Figure 2.30a shows that u increases with an increase in β_i for $K = 0$ and decreases with it when $K = 1$. A decrease in the magnitude of the v is noticed in Figure 2.31a as β_e is increased while the opposite behaviour occurs when $K = 1$ in Figure 2.31b with a backflow everywhere within the channel. Although not shown, it is observed that it took both u and v a longer time to achieve their steady state values in the presence of Hall and ion-slip currents and suction/injection.

The absolute skin friction τ at the two plates are presented in Figures 2.32-2.35. The skin friction on the stationary plate (z=0) is shown in Figure 2.32. It is observed in Figure 2.32a that the τ increases with β_e. It also increases with β_i for small values of β_e, but as the value of β_e is further increased, τ is seen to decrease with increase in the value of β_i. However, when K=1 as shown in Figure 2.32b, τ decreases steadily with both β_e and β_i. On the moving porous plate ($z = 1$), τ decreases with both β_e and β_i when $K = 0$ as seen in Figure2.33a, although, the effect of β_i is seen to wane as the value of β_e get bigger. Figure 2.33b depicts the behaviour of τ when $K = 1$, the figure shows that for small values of β_i (< 0.4), τ increases with β_e, but as the value of β_i is increased further, a decrease in the value of τ is noticed at small values of β_e. Further increase in β_e however leads to a reverse behaviour. The response of τ to time and the suction/injection parameter S is depicted in Figures 2.34 and 2.35. In Figure 2.34a, we observe on the stationary plate (z=0) that for suction, an increase in S leads to an increase in τ while for injection it leads to a decrease in τ.

It is also noticed that when $\eta < 0.25$, τ decreases with time, but the effect

of time on τ is observed to dissappear soon after. In Figure 2.34b, τ increases with time for a while, and thereafter the effect of time remains constant. The effect of time on τ when $K = 0$ on the moving porous plate is almost constant throughout the channel as seen in Figure 2.35a, though a marginal decrease at very small time is noticed. The skin friction however increases with increase in $\mathcal{S}$ for injection and decreases for suction for both $K = 0$ and $K = 1$. It is however interesting to note the reaction of τ with respect to time when $K = 1$; at $\eta < 0.2$, τ decreases with time and between $0.2 < \eta < 0.3$, τ is observed to increase with time and from this point onwards the effect of time remains constant. In order to assure the existence of backflow, the graph of τ_y is plotted against $\mathcal{S}$ as a function of β_i in Figures 2.36 and 2.37 for $z = 0$ and $z = 1$ respectively. We noticed that positive values of τ_y is obtained on the moving porous plate ($z = 0$), which actually confirms the existence of a backflow for the secondary velocity.

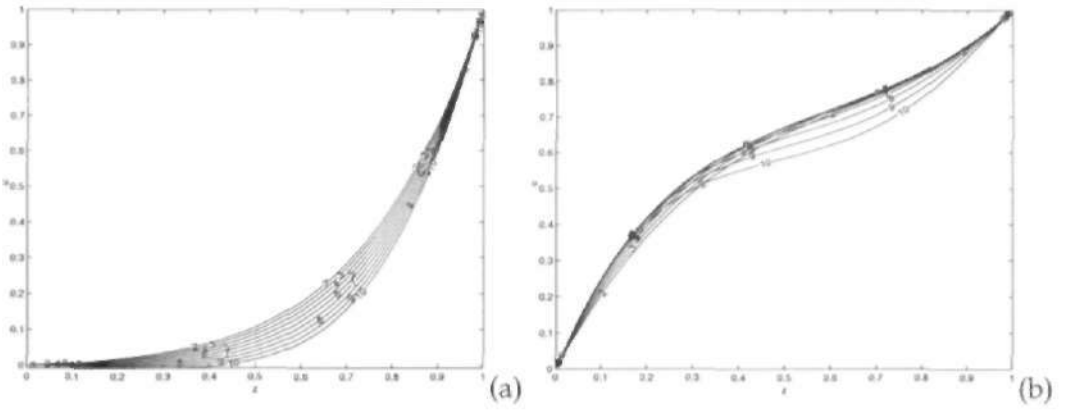


Figure 2.24: Primary velocity profile u showing the effect of rotation parameter with $K = 0$ and $K = 1$ represented by a and b respectively with fixed values of $\mathcal{S} = 0.5$, $\mathcal{H}a = 10.0$, $\eta = 0.1$, $\beta_e = 5.0$ and $\beta_i = 1.0$

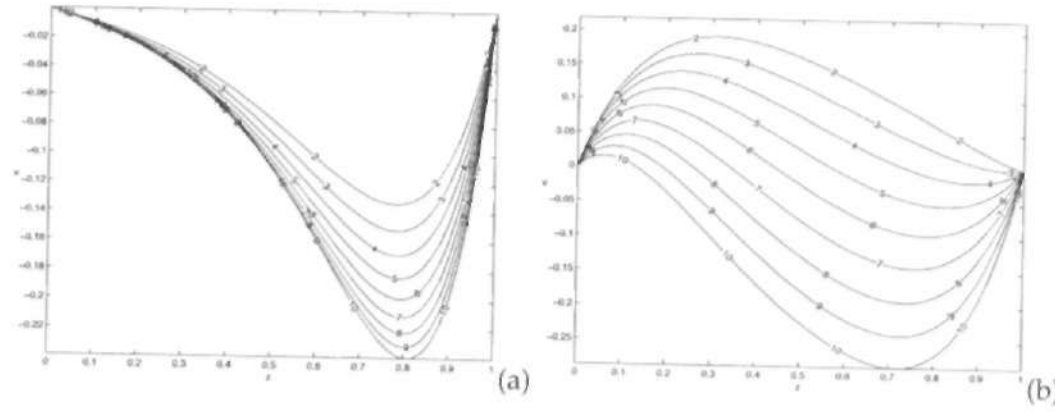


Figure 2.25: Secondary velocity profile v showing the effect of rotation parameter with $K = 0$ and $K = 1$ represented by a and b respectively with fixed values of $S = 0.5$, $\mathcal{H}a = 10.0$, $\eta = 0.1$, $\beta_e = 5.0$ and $\beta_i = 1.0$

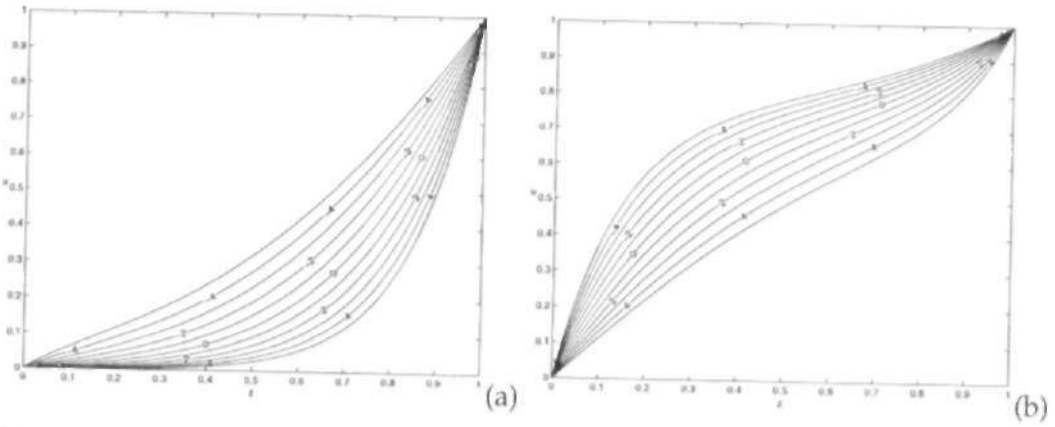


Figure 2.26: Primary velocity u showing the effect of suction/injection parameter with $K = 0$ and $K = 1$ represented by a and b respectively with fixed values of $\mathcal{H}a = 10.0$, $\Omega = 2.0$, $\eta = 0.1$, $\beta_e = 5.0$ and $\beta_i = 1.0$

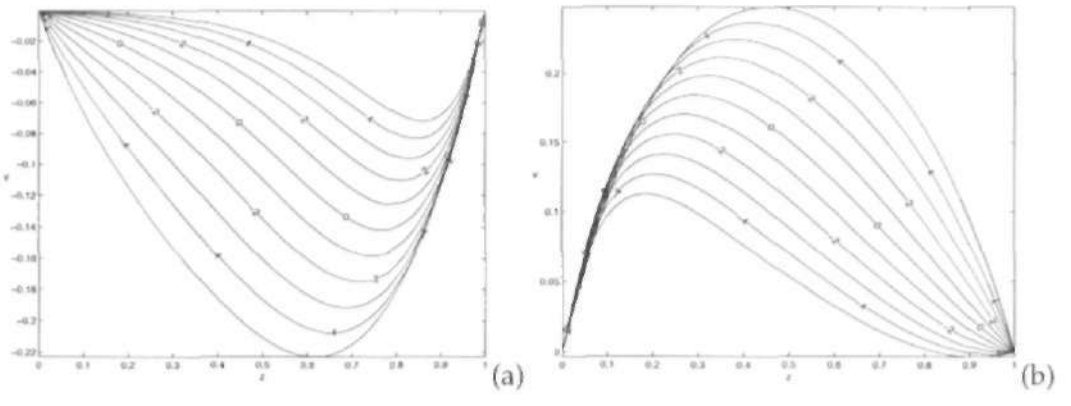


Figure 2.27: Secondary velocity v showing the effect of suction/injection parameter with $K = 0$ and $K = 1$ represented by a and b respectively with fixed values $\mathcal{S} = 0.5$, $\mathcal{H}a = 10.0$ and $\Omega = 2.0$, $\eta = 0.1$, $\beta_e = 5.0$ and $\beta_i = 1.0$

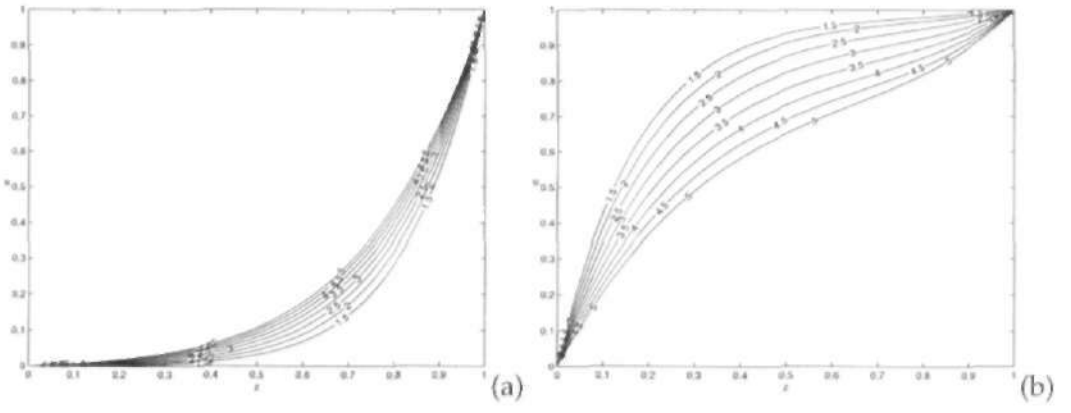


Figure 2.28: Primary velocity profile u showing the effect of Hall current in the presence of ion-slip current with $K = 0$ and $K = 1$ represented by a and b respectively with fixed values of $S = 0.5$, $\mathcal{H}a = 10.0$, $\Omega = 2.0$, $\eta = 0.1$, $\beta_i = 1.0$

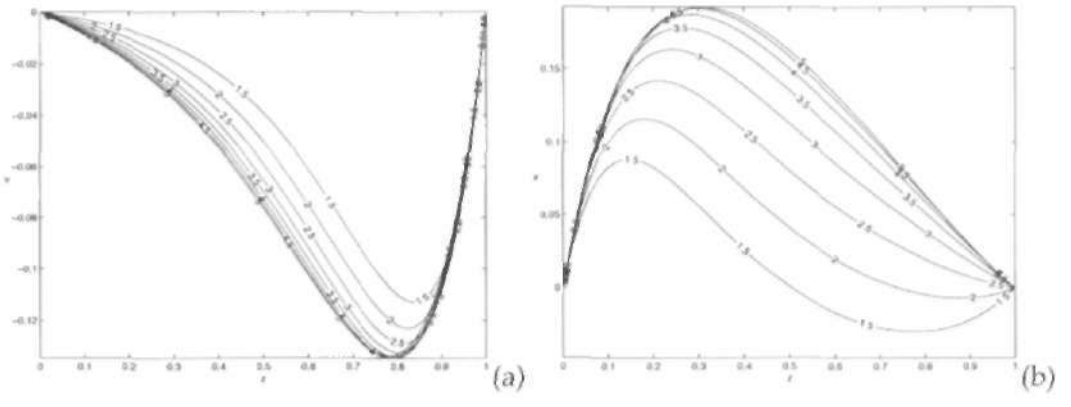


Figure 2.29: Secondary velocity profile v showing the effect of Hall current in the presence of ion-slip current with $K = 0$ and $K = 1$ represented by a and b respectively with fixed values of $S = 0.5$, $\mathcal{H}a = 10.0$, $\Omega = 2.0$, $\eta = 1.0$, $\beta_i = 1.0$

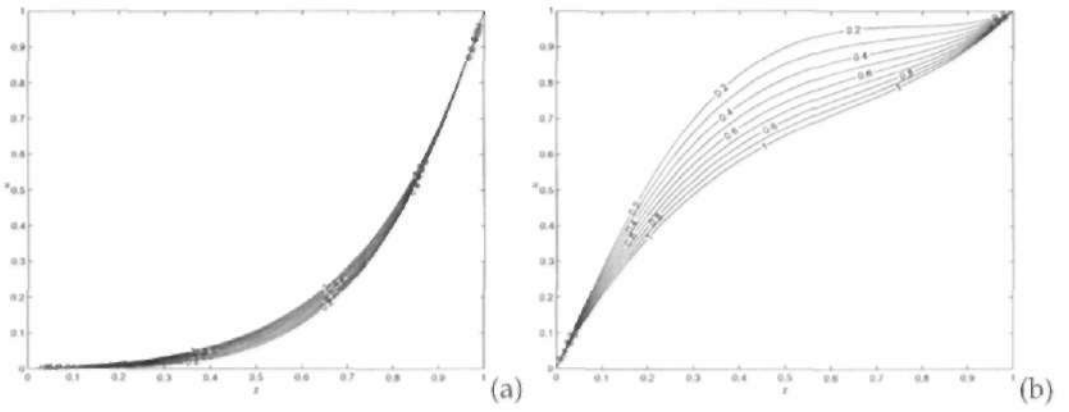


Figure 2.30: Primary velocity profile u showing the effect of ion-slip current with $K = 0$ and $K = 1$ represented by a and b respectively with fixed values of $S = 0.5$, $\mathcal{H}a = 10.0$, $\Omega = 2.0$, $\eta = 0.1$, $\beta_e = 5.0$ and $\beta_i = 1.0$

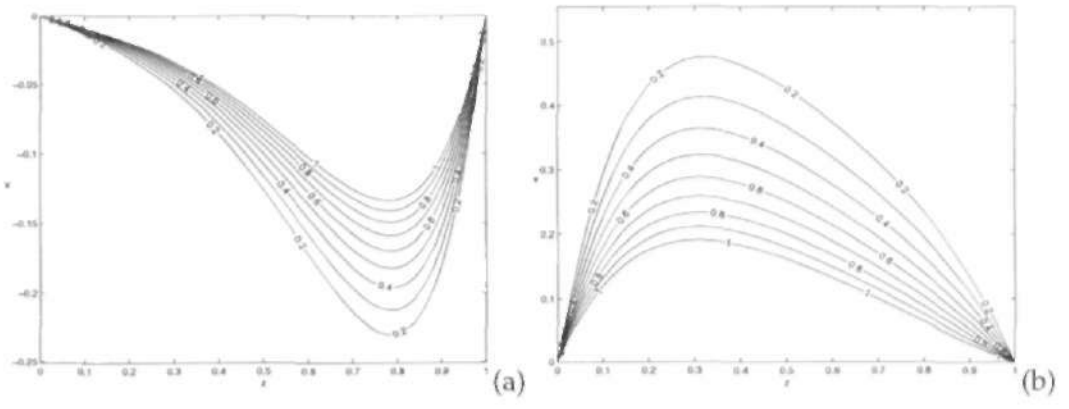


Figure 2.31: Secondary velocity profile v showing the effect of ion-slip current with $K = 0$ and $K = 1$ represented by a and b respectively with fixed values of $\mathcal{S} = 0.5$, $\mathcal{H}a = 10.0$, $\Omega = 2.0$, $\eta = 1.0$, $\beta_e = 5.0$ and $\beta_i = 1.0$

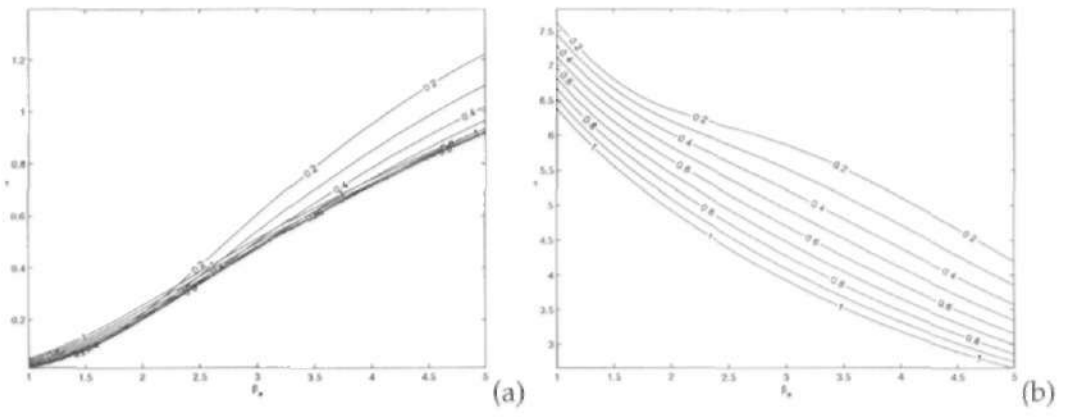


Figure 2.32: The resultant skin friction at $z = 0$ showing the effect of Hall and ion-slip parameter with $K = 0$ and $K = 1$ represented by a and b respectively with fixed values of $\mathcal{S} = 0.5$, $\mathcal{H}a = 10.0$, $\Omega = 2.0$ and $\eta = 0.1$

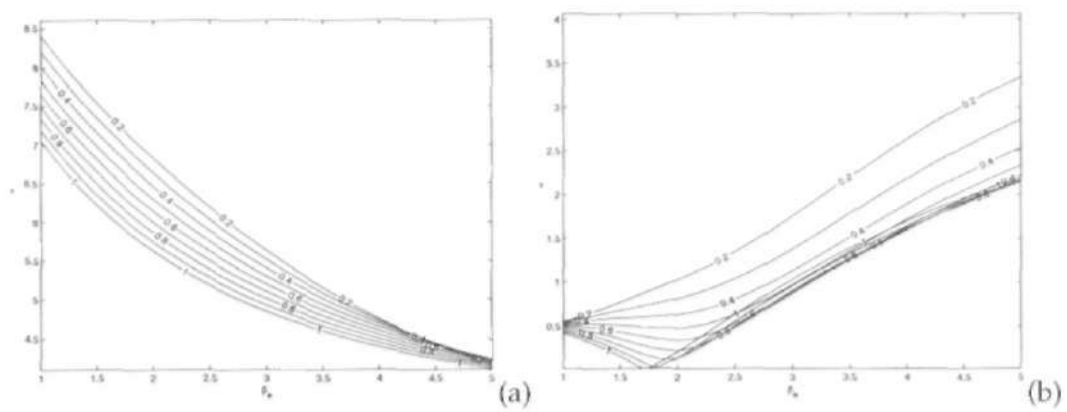


Figure 2.33: The resultant skin friction at $z = 1$ showing the effect of Hall and ion-slip parameter with $K = 0$ and $K = 1$ represented by a and b respectively with fixed values of $S = 0.5$, $\mathcal{H}a = 10.0$, $\Omega = 2.0$ and $\eta = 0.1$

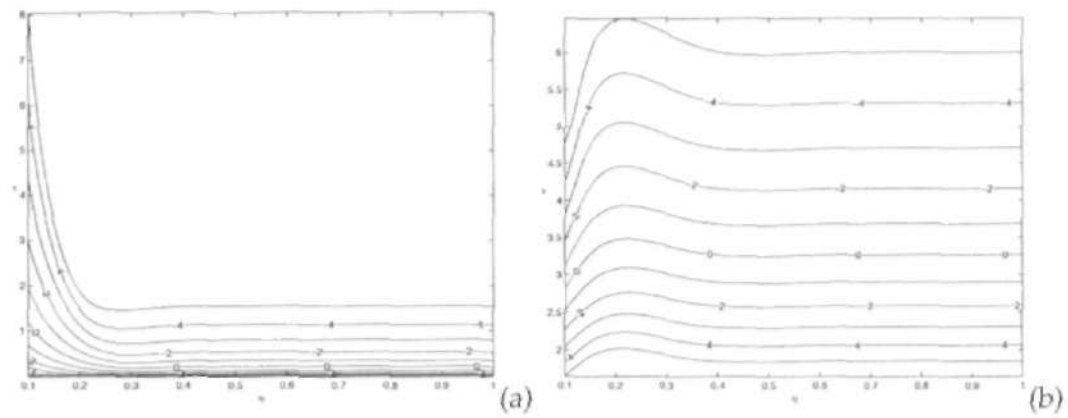


Figure 2.34: The resultant skin friction at $z = 0$ showing the effect of time and S with $K = 0$ and $K = 1$ represented by a and b respectively with fixed values of $\mathcal{H}a = 10.0$, $\Omega = 2.0$ $\beta_e = 5.0$ and $\beta_i = 1.0$.

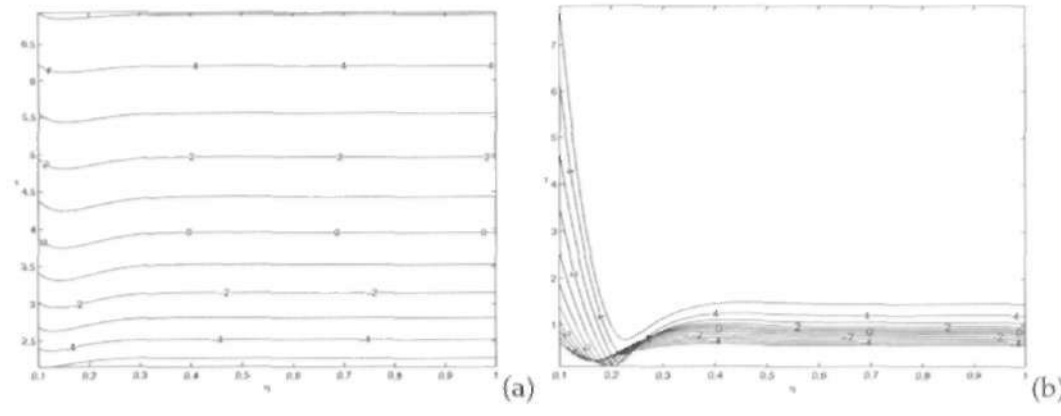


Figure 2.35: The resultant skin friction at $z = 1$ showing the effect of time and $\mathcal{S}$ with $K = 0$ and $K = 1$ represented by a and b respectively with fixed values of $\mathcal{H}a = 10.0$, $\Omega = 2.0$ $\beta_e = 5.0$ and $\beta_i = 1.0$.

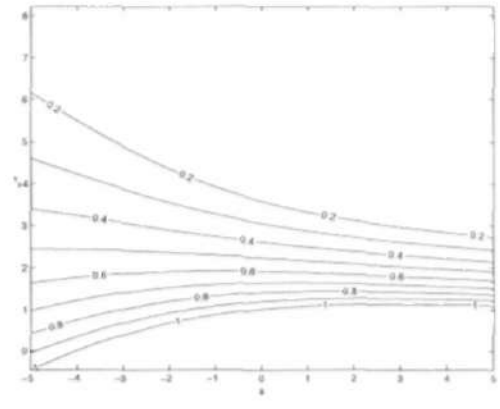


Figure 2.36: The secondary skin friction at $z = 0$ showing the effect of β_i and $\mathcal{S}$ with $K = 1$ and fixed values of $\mathcal{H}a = 10.0$, $\eta = 0.1$, $\Omega = 2.0$ and $\beta_e = 5.0$.

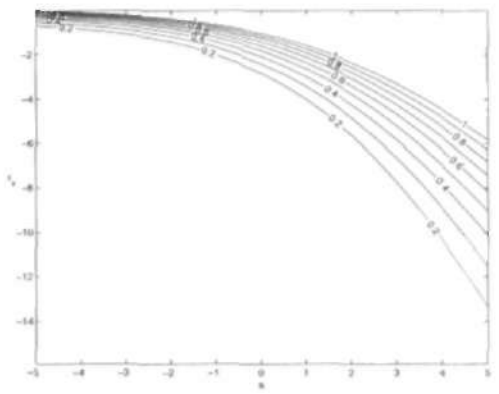


Figure 2.37: The secondary skin friction at $z = 1$ showing the effect of β_i and S with $K = 1$ and fixed values of $\mathcal{H}a = 10.0$, $\eta = 0.1$, $\Omega = 2.0$ and $\beta_e = 5.0$.

2.4 PARTICULAR CASES

a. In the case of impermeable plates i.e. $S = 0$, the results of Section 2.3 are reduced to that of Seth et al. (2011).

b. In the absence of Hall and ion-slip currents i.e $\beta_e = 0$, $\beta_i = 0$, the result of Section 2.3 are reduced to that of Section 2.2 (Jha and Apere 2010a).

c. In the case of a impermeable plates and in the absence of Hall and ion-slip currents i.e $S = 0$, $\beta_e = 0$, $\beta_i = 0$ and $K = 0$, the results of Section 2.3 are reduced to those obtained by Das et al. (2009).

d. In the case of impermeable plates and in the absence of magnetic field i.e $S = 0$, $Ha = 0$ and $K = 0$, the results of Section 2.3 are reduced to those obtained by Guria et al. (2006).

e. In the case of non-permeable plate and in the absence of Hall and ion-slip currents and rotation i.e. $S = 0$, $\beta_e = 0$, $\beta_i = 0$ and $\Omega = 0$ respectively; the results of Section 2.3 are reduced to those obtained by Singh and Kumar (1983).

2.5 CONCLUDING REMARKS

The unsteady MHD Couette flow of a viscous incompressible electrically conducting fluid between parallel plates in a rotating system is considered. Three problems have been discussed in this Chapter, the first is the time-dependent

MHD Couette flow with suction/injection, while the second is the combined effect of Hall and ion-slip currents and the last problem took into consideration the effect of suction/injection, Hall and ion-slip currents. It has been observed that injection has an increasing effect on both the primary velocity and the magnitude of the secondary velocity while suction has the opposite effect. It is fascinating to note that the Ekman number has an increasing effect on the primary velocity when the magnetic lines of force are fixed relative to the moving plate; this is due to the time-dependent motion of the magnetic field. An increase in injection leads to a decrease in the resultant skin friction on the plate with injection, while it increases on the plate with suction, suction has the opposite effect on the flow behaviour. It is observed that the effect of both the Hall and ion-slip parameters is to increase the primary velocity and reduce the secondary velocity.

The resultant skin friction on the moving plate decreases with increase in both the Hall and ion-slip parameters when the magnetic field is fixed relative to the fluid, while the opposite behaviour is noticed when the magnetic field is fixed relative to the moving plate. On the stationary plate however, the skin friction increases with both the Hall and ion-slip currents when ($K = 0$), an opposite behaviour is observed when ($K = 1$). We also observed that fixing the magnetic field relative to the moving porous plate always results into the phenomenon of backflow on the secondary velocity due to the presence of the Hall and ion-slip currents.

CHAPTER 3

MHD COUETTE FLOW IN AN ANNULUS

The analysis of the fully developed laminar MHD flow in an annular channel by Globe (1959) is believed to be the first MHD flow problem in an annulus. Jain and Mehta (1962) extended the problem by imposing suction/injection on the walls. An exact solution of electrically conducting viscous incompressible flow in an annulus with porous walls under an external radial magnetic field was obtained by Nandi (1973). Antimirov and Kolyshkin (1984) studied the unsteady MHD flow in an annular channel with radial magnetic field while Takhar et al. (1989) examined the stability of MHD Couette flow in a narrow gap annulus. The flow of an electrically conducting fluid through a channel or a circular pipe in the presence of a transverse magnetic field is encountered in a variety of applications such as MHD generators, pumps, accelerators, and flow meters. The annular geometry is also widely employed in the gas cooled nuclear reactors in which the cylindrical fissionable fuel elements are placed axially in vertical coolants channel within the graphite moderators and the cooling gas is flowing along the channel parallel to the fuel elements (Singh et al. (1997)) and also in drilling operation of oil and gas well. Makinde et al. (2009) studied the steady, axisymmetric, MHD flow of a viscous, Newtonian, incompressible,

electrically-conducting fluid through an isotropic, homogenous porous medium located in the annular zone between two concentric rotating cylinders in the presence of a radial magnetic field. The unsteady MHD generalized Couette flow and heat transfer characteristics of a reactive variable viscosity incompressible electrically conducting third grade fluid in a channel with asymmetric convective cooling at the walls in the presence of uniform transverse magnetic field was investigated by Makinde and Chinyoka (2011).

The first attempt to study the laminar flow in a uniformly porous rectangular channel is believed to be that of Bearman (1953); where he showed that a solution for the flow between porous plates with constant and equal suction at both walls could be obtained by assuming that the velocity component normal to the walls was independent of the distance along the channel. Bearman (1958) extended his investigation to the annular space by considering the Navier–Stokes equations for the case of steady state in an annulus with porous walls assuming constant influx through one wall is equal to the efflux through the other. Folllowing Berman's pioneering effort, many other authors has investigated laminar flow in a porous annulus.

Mention can be made of the work of Wang (1971) who extended Bearman's work to the case of the pulsating flow in a porous channel (between parallel walls) and for the corresponding problem in a porous annulus. Banks and Zaturska (1992) studied theoretically the axisymmetric flow of a viscous fluid through a porous annular pipe with constant and equal fluxes through each

pipe wall; while Zaturska and Banks (1995) studied the axisymmetric flow of a viscous fluid through a porous pipe driven by suction at the pipe wall. They investigated the temporal stability of known exact similarity solutions of the Navier–Stokes equations for various values of the Reynolds number and stable and unstable parts of the solution branches are delineated. Verma and Bansal (1969) investigated the laminar flow in an annulus with porous walls of different permeability.

The analytical solutions of the equations of motion of a Newtonian fluid for the fully developed laminar flow between two concentric cylinders when an oscillating circumferential pressure gradient is imposed (finite gap oscillating Dean flow) was presented by Tsangaris et al. (2006). Tsangaris and Vlachakis (2007) extended the problem to the case when the walls of the cylinders are porous. A general review of the exact solutions of the Navier–Stokes equations including those with porous boundaries can be found in the articles of Wang (1989, 1991). All the aforementioned works does not consider the situation where either one or both cylinders are rotating. The flow of viscous fluid in the annular gap between two rotating cylinders is normally referred to as Taylor–Couette flow.

Taylor (1923) showed that when the angular velocity of the inner cylinder is increased above a certain threshold, Couette flow becomes unstable and a secondary steady state characterized by axisymmetric toroidal vortices emerges, this phenomenon is known as Taylor vortex flow. Further increase in the angular

velocity of the cylinder result into the system undergoing a progression of instabilities which lead to states with greater spatio-temporal complexity, with the next state being known as wavy vortex flow. If the cylinders rotate in different directions then spiral vortex flow arises. Beyond a certain Reynolds number there is the onset of turbulence. The study of fluid flow in a rotating annulus is very important, because of its many application in electrical, mechanical and nuclear engineering field and other related fields.

The applications of the rotating annulus is found in rotating extractors, rotating membrane filters, co-axial rotating heat pipes, cylindrical bearings, rotating power transmission systems and drilling operation of oil and gas wells etc. (Sukumaran et al. (2010)). The transient flow in a rotating porous annulus due to suction at the walls was investigated by Aruna Prasad and Venkatasiva Murthy (1991). In their study, they use the Brinkman's law to represent the fluid motion and obtained exact solution of the unsteady flow using the Laplace method. Dizaji et al. (2008) studied the flow field of a third grade non–Newtonian fluid in the annulus of rotating concentric cylinders in the presence of magnetic field and obtained numerical solutions using the finite difference method. The same problem was treated by Ellahi et al. (2009); albeit analytically with and without magnetic field. Flow fields in an annulus between two rotating cylinders with a porous lining have also been numerically examined by Subotic and Lai (2010). They assume in their study that the outer cylinder is stationary while the inner cylinder is rotating with a constant angular speed. Survey of literatures on

the annulus problem revealed that there are few works that address flow problem in the annulus of two rotating concentric porous cylinders in the presence of magnetic field.

3.1 UNSTEADY MHD COUETTE FLOW IN AN ANNULUS: THE RIEMANN-SUM APPROXIMATION APPROACH[1]

The unsteady MHD Couette flow of a viscous incompressible electrically conducting fluid between two concentric horizontal cylinders of infinite length have been analysed when the outer cylinder has been set into uniform accelerated motion. A unified closed form expressions are derived corresponding to the cases of the magnetic field fixed relative to the fluid or to the accelerated outer cylinder. The well known Laplace transform technique is applied to solve the time-dependent governing equations, while the method of Riemann-sum approximation is employed to invert the Laplace domain to the time domain in order to obtain the velocity and the skin friction. The variations of the velocity and the skin friction with respect to the Hartmann number and time have been discussed.

3.1.1 Mathematical Analysis

We consider the motion of a viscous, incompressible and electrically conducting fluid filling the gap between two horizontal concentric cylinders of infinite

[1]Jha and Apere (2010b) Published in
J. Phys. Soc. Jpn. **79** 124403 (2010); doi: 10.1143/JPSJ.79.124403

length. The inner and the outer cylinders have radii a and b respectively. The motion of the fluid is due to the sudden movement of the outer cylinder in the presence of magnetic field acting perpendicular to the flow direction. The z'-axis is assumed to be on the axis of the cylinders in the horizontal direction and r'-axis is on the radial direction. At time $t \leq 0$, the fluid and the cylinders are assumed to be at rest, when $t > 0$ the outer cylinder is set into motion with a velocity Ut^n where U is a constant and the inner cylinder remains at rest. All physical variables are functions of r' and t.

$$\frac{\partial u'}{\partial t} = \nu \left[\frac{\partial^2 u'}{\partial r'^2} + \frac{1}{r'} \frac{\partial u'}{\partial r'} \right] - \frac{\sigma B_0^2}{\rho} u' \tag{3.1}$$

Eq. (3.1) is valid when the magnetic field is fixed relative to the fluid. If the magnetic field is fixed relative to the moving cylinder, Eq. (3.1) can be replaced with

$$\frac{\partial u'}{\partial t} = \nu \left[\frac{\partial^2 u'}{\partial r'^2} + \frac{1}{r'} \frac{\partial u'}{\partial r'} \right] - \frac{\sigma B_0^2}{\rho} (u' - Ut^n) \tag{3.2}$$

Eqs. (3.1) and (3.2) can be combined together to obtain

$$\frac{\partial u'}{\partial t} = \nu \left[\frac{\partial^2 u'}{\partial r'^2} + \frac{1}{r'} \frac{\partial u'}{\partial r'} \right] - \frac{\sigma B_0^2}{\rho} (u' - KUt^n), \tag{3.3}$$

where

$$K = \begin{cases} 0 & when\ B_0\ is\ fixed\ relative\ to\ the\ fluid \\ 1 & when\ B_0\ is\ fixed\ relative\ to\ the\ moving\ cylinder \end{cases}$$

The initial and boundary conditions for the problem are

$$\begin{aligned} u' &= 0,\ a \leq r' \leq b\ and\ t \leq 0, \\ u' &= 0,\ at\ r' = a, t > 0; \\ u' &= Ut^n,\ at\ r' = b,\ t > 0. \end{aligned} \tag{3.4}$$

The flow described by eqs. (3.3) and (3.4) is the general representation of the velocity distribution for the Couette flow between two infinite concentric cylinders of any conducting medium due to the movement of the outer cylinder. In order to analyse the specific flow profiles, we have considered the case when $n = 1$, which correspond to the accelerated motion.

3.1.2 Solution of the Problem

Introducing the following dimensionless quantities;

$r = r'/a,\ u = u'\nu/Ua^2,\ \eta = \nu t/a^2,\ \mathcal{H}a = B_0 a\sqrt{\sigma/\nu\rho}\ and\ \varsigma = b/a$

where $\mathcal{H}a$ is the Hartmann number and a and b are the radii of the inner and the outer cylinders respectively and ς is the annulus dimension ratio and is fixed as

2 in this problem. Eq. (3.3) can then be written in dimensionless form as

$$\frac{\partial u}{\partial \eta} = \frac{\partial^2 u}{\partial r^2} + \frac{1}{r}\frac{\partial u}{\partial r} - \mathcal{H}a^2(u - K\eta) \tag{3.5}$$

subject to the following dimensionless initial and boundary conditions

$$\begin{aligned} u &= 0,\ 1 \le r \le \varsigma \ and\ \eta \le 0, \\ u &= 0,\ at\ r = 1,\ \eta > 0; \\ u &= \eta,\ at\ r = \varsigma,\ \eta > 0. \end{aligned} \tag{3.6}$$

Taking the Laplace transform of Eq. (3.5) with the corresponding boundary conditions (3.6). Eq. (3.5) then become

$$\frac{d^2\bar{u}}{dr^2} + \frac{1}{r}\frac{d\bar{u}}{dr} - (s + \mathcal{H}a^2)\bar{u} = -\frac{\mathcal{H}a^2 K}{s^2}. \tag{3.7}$$

The solution of eq. (3.7) which is a Bessel equation under the modified boundary condition (3.6) is

$$\bar{u}(r,s) = C_1 I_0(\delta r) + C_2 K_0(\delta r) + \frac{\mathcal{H}a^2 K}{s^2\delta^2}, \tag{3.8}$$

where

$$\delta = \sqrt{s + \mathcal{H}a^2} \tag{3.9}$$

$$C_1 = -\frac{K_0(\delta)}{\beta_1 s^2} - \frac{\mathcal{H}a^2 K}{\beta_1 s^2 \delta^2}\left[K_0(\delta\varsigma) - K_0(\delta)\right] \tag{3.10}$$

$$C_2 = \frac{I_0(\delta)}{\beta_1 s^2} + \frac{\mathcal{H}a^2 K}{\beta_1 s^2 \delta^2}\left[I_0(\delta\varsigma)) - I_0(\delta)\right] \tag{3.11}$$

$$\beta_1 = K_0(\delta\varsigma)I_0(\delta) - I_0(\delta\varsigma)K_0(\delta). \tag{3.12}$$

Using the Riemann-sum approximation for the inversion of Laplace transform, eq. (3.8) can be inverted to the time domain as follows:

$$u(r,\eta) = \frac{e^{\gamma\eta}}{\eta}\left[\frac{1}{2}\bar{u}(r,\gamma) + Re\sum_{n=1}^{N}\bar{u}(r,\gamma+\frac{ik\pi}{\eta})(-1)^k\right]. \tag{3.13}$$

3.1.3 Skin Friction

The skin friction τ is defined as $\frac{\partial u}{\partial r}$, it is obtained by differentiating eq. (3.13) with respect to r as

$$\tau = \frac{\partial u}{\partial r} = \frac{e^{\gamma\eta}}{\eta}\left[\frac{1}{2}\bar{u}_1(r,\gamma) + Re\sum_{n=1}^{N}\bar{u}_1(r,\gamma+\frac{ik\pi}{\eta})(-1)^k\right], \tag{3.14}$$

where

$$\bar{u}_1(r,s) = [C_1 I_1(\delta r) - C_2 K_1(\delta r)]\delta. \tag{3.15}$$

Eq. (3.14) represent the general expression for the skin friction between different fluid layers amidst the two cylinders. The skin frictions at the outer surface of the inner cylinder ($r = 1$) and that at the inner surface of the outer cylinder ($r = 2$) can then be obtained from eq. (3.14).

3.1.4 Results and Discussion

In order to understand the effects of the Hartmann number $\mathcal{H}a$ and time η in the problem, a MATLAB programme is written to compute and generate the graphs for the velocity and the skin friction. The velocity profiles and the skin-friction have been discussed by assigning numerical values to the two parameters. Figure 3.1 shows the velocity profiles against r (which is on the radial direction). It depicts the effects of $\mathcal{H}a$ on the velocity. It is observed in Figure 3.1a that the velocity decreases with increasing $\mathcal{H}a$ when the magnetic field is fixed relative to the fluid ($K = 0$) and in Figure 3.1b increases when fixed relative to the moving outer cylinder ($K = 1$). The velocity is also observed to increase exponentially from the outer surface of the inner cylinder until it reaches its maximum value at the inner surface of the outer cylinder.

Figure 3.2 shows the effect of time η on the velocity against r when $\mathcal{H}a = 0.3$, while Figure 3.3 is depicted for the value of $\mathcal{H}a = 4$. It is obvious from the figures that as time moves on, the velocity shows a significant increase in its value and also increases steadily until it reaches its equilibrium value. It can also be seen that the effect of fixing the magnetic field to either the fluid or the moving cylinder is very pronounced and distinct at high values of $\mathcal{H}a$ as shown in Figure 3.3 as this is not the case in Figure 3.2 when $\mathcal{H}a = 0.3$. The behaviour of the velocity inside the annulus is similar to that of the channel as earlier studied by Singh et al. (1994).

The skin-friction τ against $\mathcal{H}a$ is presented in Figures 3.4 and 3.5. In Figure 3.4a, we see that increasing η results to an increase in τ at the outer surface of the inner cylinder when $K = 0$, while an increase in $\mathcal{H}a$ lead to a decrease in the value of τ. However, when $K = 1$ as shown in Figure 3.4b, τ is observed to increase steadily with both time and the magnetic field. Similarly, on the inner surface of the outer cylinder, τ increases with both time and magnetic field as illustrated in Figure 3.5a when $K = 0$, but for the case of $K = 1$, it is noticed that although τ increases with time, it was found to decrease with the magnetic field.

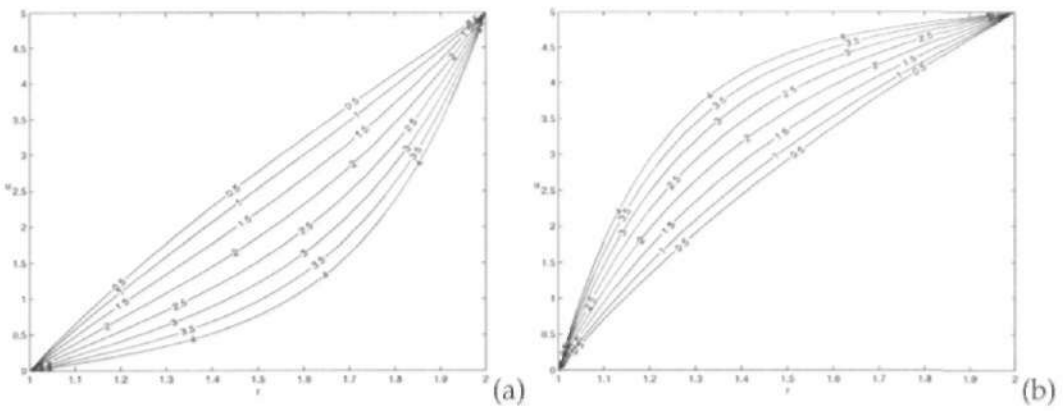


Figure 3.1: The velocity profile u showing the effect of $\mathcal{H}a$ with $K = 0$ and $K = 1$ represented by a and b respectively and $\eta = 5.0$.

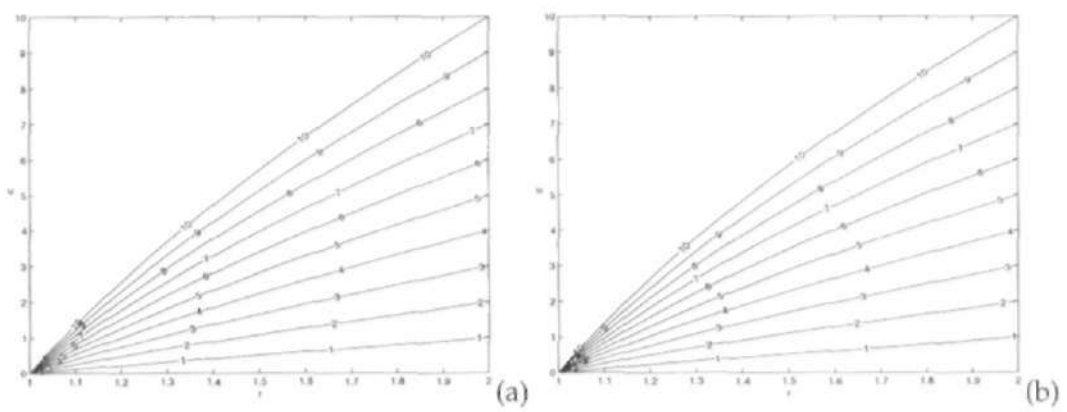


Figure 3.2: The velocity profile u showing the effect of η and $K = 0$ and $K = 1$ represented by a and b respectively with $\mathcal{H}a = 0.3$.

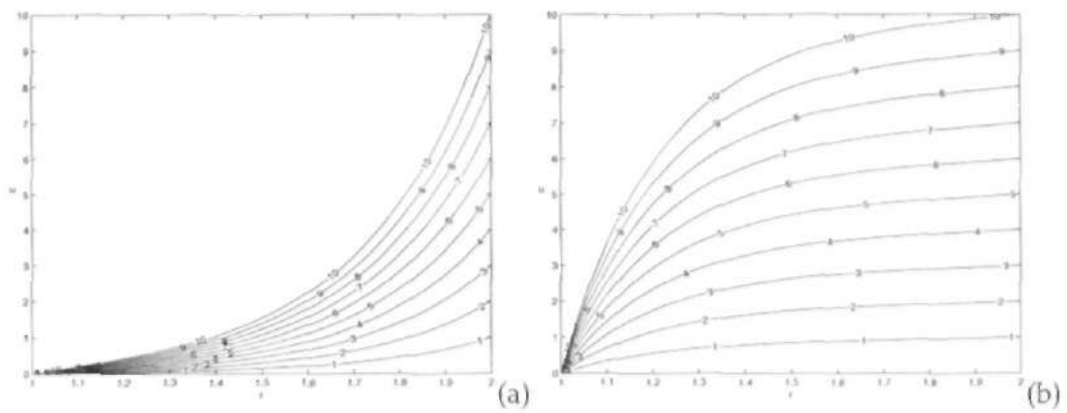


Figure 3.3: The velocity profile u showing the effect of η and $K = 0$ and $K = 1$ represented by a and b respectively with $\mathcal{H}a = 4$.

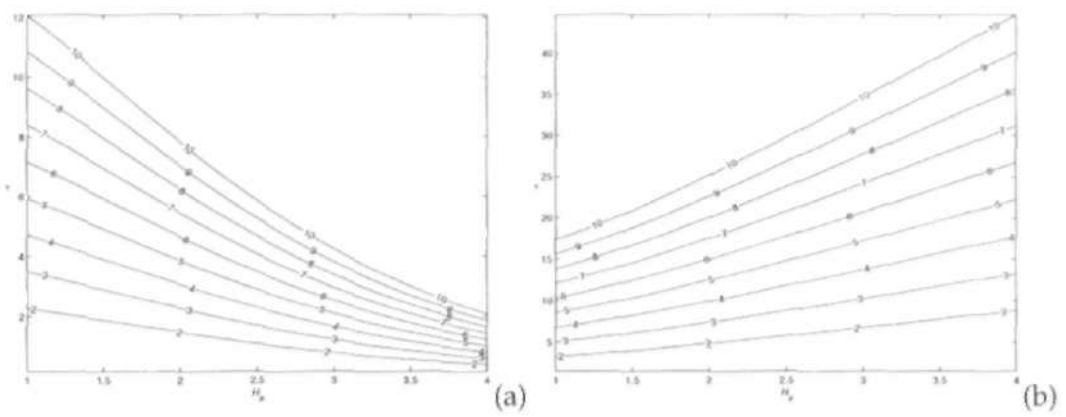


Figure 3.4: The variation of the skin friction with η at the outer surface of the inner cylinder ($r = 1$) with $K = 0$ and $K = 1$ represented by a and b respectively.

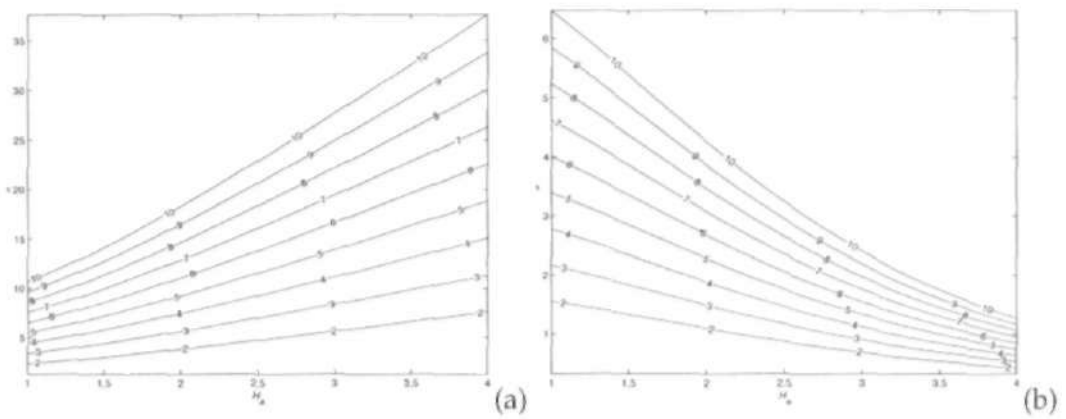


Figure 3.5: The variation of the skin friction with η at the inner surface of the outer cylinder ($r = 2$) with $K = 0$ and $K = 1$ represented by a and b respectively.

3.2 MHD COUETTE FLOW IN AN ANNULUS HAVING RAMP MOTION OF INNER CYLINDER[2]

A semi-analytical solution for the unsteady MHD Couette flow of a viscous incompressible electrically conducting fluid between two concentric horizontal cylinders of infinite length whose inner cylinder is moving with ramp motion is presented in this Section. Unified closed form expressions are derived for the velocity and the skin friction corresponding to the cases of the magnetic field being fixed relative to the fluid or to the moving inner cylinder. The combination of the Laplace transform technique and the Riemann-sum approximation method have been used to solve the time-dependent governing equations. The variations of the velocity and the skin friction with respect to the Hartmann number and time have been discussed.

3.2.1 Mathematical Analysis

The same model in the previous section is still being considered. However, in this section, the fluid flow is induced by the inner cylinder which is set into ramp motion with a velocity $Uf(t)$ where U is a constant having the dimension of velocity and the outer cylinder remains at rest. Since the cylinders are of infinite length and the flow is fully developed, all physical variables are functions of r' and t. Under these assumptions, the mathematical model governing the problem

[2]Under consideration in
Applied Mathimatical Letters

is given as

$$\frac{\partial u'}{\partial t} = \nu \left[\frac{\partial^2 u'}{\partial r'^2} + \frac{1}{r'}\frac{\partial u'}{\partial r'}\right] - \frac{\sigma B_0^2}{\rho} u'. \tag{3.16}$$

Eq. (3.16) is valid when the magnetic field is fixed relative to the fluid. If the magnetic field is fixed relative to the moving cylinder, eq. (3.16) can be replaced with

$$\frac{\partial u'}{\partial t} = \upsilon \left[\frac{\partial^2 u'}{\partial r'^2} + \frac{1}{r'}\frac{\partial u'}{\partial r'}\right] - \frac{\sigma B_0^2}{\rho}[u' - Uf(t)] \tag{3.17}$$

Eqs. (3.16) and (3.17) can be combined together to obtain

$$\frac{\partial u'}{\partial t} = \nu \left[\frac{\partial^2 u'}{\partial r'^2} + \frac{1}{r'}\frac{\partial u'}{\partial r'}\right] - \frac{\sigma B_0^2}{\rho}[u' - KUf(t)], \tag{3.18}$$

where

$$K = \begin{cases} 0 & when\ B_0\ is\ fixed\ relative\ to\ the\ fluid \\ 1 & when\ B_0\ is\ fixed\ relative\ to\ the\ moving\ cylinder \end{cases}$$

The initial and boundary conditions for the problem are

$$\begin{aligned} u' &= 0,\ a \le r' \le b\ and\ t \le 0, \\ u' &= Uf(t),\ at\ r' = a, t > 0; \\ u' &= 0,\ at\ r' = b,\ t > 0. \end{aligned} \tag{3.19}$$

where $f(t)$ is defined as

$$f(t) = \begin{cases} \frac{t}{t_0} & at \ \ t \leq t_0 \\ 1 & at \ \ t > t_0 \end{cases}.$$

Therefore

$$f(t) = \frac{t}{t_0}H(t) - \frac{1}{t_0}(t - t_0)H(t - t_0),$$

where $H(t)$ is the unit step function.

Introducing the following dimensionless quantities in eqs. (3.18) and (3.19);

$r = r'/a, \ u = u'/U, \ \eta = \nu t/a^2, \ t_0 = \nu t_0/a^2, \ \mathcal{H}a = B_0 a\sqrt{\sigma/\nu\rho}$ *and* $\varsigma = b/a$.

We now have

$$\frac{\partial u}{\partial \eta} = \frac{\partial^2 u}{\partial r^2} + \frac{1}{r}\frac{\partial u}{\partial r} - \mathcal{H}a^2[u - Kf(\eta)] \tag{3.20}$$

subject to the following dimensionless initial and boundary conditions

$$\begin{aligned} u &= 0, \ 1 \leq r \leq \varsigma \ and \ \eta \leq 0, \\ u &= f(\eta), \ at \ r = 1, \ \eta > 0; \\ u &= 0, \ at \ r = \varsigma, \ \eta > 0, \end{aligned} \tag{3.21}$$

where

$$f(\eta) = \frac{\eta}{\eta_0}H(\eta) - \frac{1}{\eta_0}(\eta - \eta_0)H(\eta - \eta_0).$$

Using the Laplace transforms technique, eq. (3.20) then becomes

$$\frac{d^2\bar{u}}{dr^2} + \frac{1}{r}\frac{d\bar{u}}{dr} - (s + \mathcal{H}a^2)\bar{u} = -\mathcal{H}a^2 K f(s), \tag{3.22}$$

where

$$f(s) = \frac{1}{\eta_0}\left[\frac{1 - \exp(-s\eta_0)}{s^2}\right]$$

The solution of eq. (3.22) which is a non-homogeneous Bessel equation is

$$\bar{u}(r,s) = C_1 I_0(\delta r) + C_2 K_0(\delta r) + \frac{\mathcal{H}a^2 K f(s)}{\delta^2}. \tag{3.23}$$

Using the boundary condition eq. (3.21), C_1 and C_2 are obtained as follows:

$$C_1 = -f(s)\frac{K_0(\varsigma\delta)}{\beta_1} + f(s)\frac{\mathcal{H}a^2 K}{\beta_1 \delta^2}\left[K_0(\delta\varsigma) - K_0(\delta)\right] \tag{3.24}$$

$$C_2 = f(s)\frac{I_0(\varsigma\delta)}{\beta_1} - f(s)\frac{\mathcal{H}a^2 K}{\beta_1 \delta^2}\left[I_0(\delta\varsigma) - I_0(\delta)\right], \tag{3.25}$$

where

$$\delta = \sqrt{s + \mathcal{H}a^2} \tag{3.26}$$

and

$$\beta_1 = I_0(\delta\varsigma)K_0(\delta) - K_0(\delta\varsigma)I_0(\delta). \tag{3.27}$$

Using the Riemann-sum approximation for the inversion of Laplace transform,

480026

Services

eq. (3.23) can be inverted to the time domain as follows:

$$u(r,\eta) = \frac{e^{\gamma\eta}}{\eta}\left[\frac{1}{2}\bar{u}(r,\gamma) + Re\sum_{k=1}^{N}\bar{u}(r,\gamma+\frac{ik\pi}{\eta})(-1)^k\right]. \tag{3.28}$$

3.2.2 Skin Friction

The skin friction τ is defined as $\frac{\partial u}{\partial r}$, it is obtained by differentiating eq. (3.28) with respect to r as

$$\tau = \frac{\partial u}{\partial r} = \frac{e^{\gamma\eta}}{\eta}\left[\frac{1}{2}\bar{u}_1(r,\gamma) + Re\sum_{k=1}^{N}\bar{u}_1(r,\gamma+\frac{ik\pi}{\eta})(-1)^k\right], \tag{3.29}$$

where

$$\bar{u}_1(r,s) = \delta[C_1 I_1(\delta r) - C_2 K_1(\delta r)]. \tag{3.30}$$

Eq. (3.29) represent the general expression for the skin friction between different fluid layers amidst the two cylinders.The skin frictions at the outer surface of the inner cylinder (τ_1) and that at the inner surface of the outer cylinder (τ_ς) can then be obtained by substituting $r = 1$ and $r = 2$ respectively in eq. (3.29).

3.2.3 Mass Flux

Another very important quantitity for this problem is the non-dimensional mass flux. These is defined by the following:

$$Q = 2\pi\int_1^{\varsigma} r\bar{u}(r,s)dr, \tag{3.31}$$

which is obtained from eq. (3.23) as

$$Q = 2\pi\left[\frac{C_1}{\delta}\{\varsigma I_1(\delta\varsigma) - I_1(\delta)\} - \frac{C_2}{\delta}\{\varsigma K_1(\delta\varsigma) - K_1(\delta)\} + \frac{\mathcal{H}a^2 K f(s)}{2\delta^2}(\varsigma^2 - 1)\right]. \tag{3.32}$$

3.2.4 Steady State

In order to confirm the accuracy of the Riemann-sum approximation method, we set out to find the solution of the steady state, which should coincide with the transient solution at large time. The expression for the steady state velocity distribution u at this state is obtained by setting $\partial u/\partial\eta$ in eq. (3.20) to zero. We then obtain the following ordinary differential equation

$$\frac{d^2u}{dr^2} + \frac{1}{r}\frac{du}{dr} - \mathcal{H}a^2 u = -\mathcal{H}a^2 K. \tag{3.33}$$

The solution of eq. (3.33) together with the boundary condition (3.21) is

$$u(r) = C_3 I_0(\mathcal{H}ar) + C_4 K_0(\mathcal{H}_a r) + K, \tag{3.34}$$

where

$$C_3 = -\frac{K_0(\varsigma\mathcal{H}a)}{\beta_2} - \frac{K}{\beta_2}[K_0(\varsigma\mathcal{H}a) - K_0(\mathcal{H}a)] \tag{3.35}$$

$$C_4 = \frac{I_0(\varsigma\mathcal{H}a)}{\beta_2} - \frac{K}{\beta_2}[I_0(\varsigma\mathcal{H}a) - I_0(\mathcal{H}a)] \tag{3.36}$$

$$\beta_2 = I_0(\varsigma\mathcal{H}a)K_0(\mathcal{H}a) - K_0\varsigma\mathcal{H}a)I_0(\mathcal{H}a). \tag{3.37}$$

The corresponding skin friction τ_s for the steady state is obtained by differentiating eq. (4.18) with respect to r as

$$\tau_s = \frac{du}{dr} = \mathcal{H}a[C_3 I_1(\mathcal{H}ar) - C_4 K_1(\mathcal{H}ar)] \tag{3.38}$$

while the steady state mass flux is

$$Q_s = 2\pi \left[\frac{C_3}{\mathcal{H}a}\{\varsigma I_1(\mathcal{H}a\varsigma) - I_1(\mathcal{H}a)\} - \frac{C_4}{\mathcal{H}a}\{\varsigma K_1(\mathcal{H}a\varsigma) - K_1(\mathcal{H}a)\} + \frac{K}{2}(\varsigma^2 - 1) \right]. \tag{3.39}$$

The results obtained for the velocity, skin friction and the mass flux for the steady state are found to be in excellent agreement with those of eqs. (3.28), (3.29) and (3.31) when the value of η is large.

3.2.5 Results and Discussion

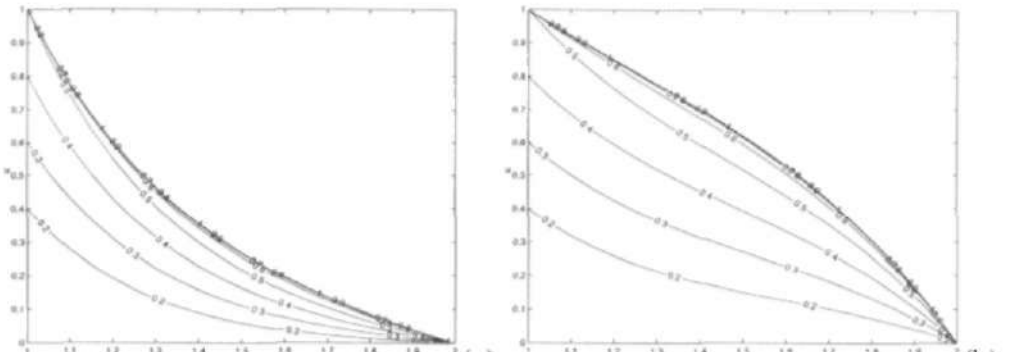
In order to see the effect of the controlling parameters occuring in this problem, we have presented the variation of the velocity and the skin friction for different values of these dimensionless parameters. The variation of the velocity with respect to the dimensionless time has been shown in Figure 3.6. It can be seen that the velocity increases with η until it reaches its steady state around $\eta = 0.6$. We also noticed that the velocity decreases steadily from its peak value on the outer surface of the inner cylinder to zero on the inner surface of the outer cylinder. A close study of Figure 3.6 also reveals that the ramp motion of the cylinder is accelerated motion when $\eta < \eta_0$ and impulsive when $\eta \geq \eta_0$. This

pattern of behaviour is synonymous for both when $K = 0$ and when $K = 1$. We have also presented the velocity profiles for various values of the Hartmann number $\mathcal{H}a$ in Figure 3.7. It is clear from this figure that the velocity of the fluid decreases with $\mathcal{H}a$ when $K = 0$. However, when $K = 1$, a reversal in this behaviour is noticed.

The skin friction τ at the outer surface of the inner cylinder and that at the inner surface of the outer cylinder are presented in Figures 3.8 and 3.9. From Figure 3.8, we observed that when $K = 0$, the magnitude of τ increases with time unitil when $\eta = 0.5$ when we see a reversal in behaviour, this reversal is as a result of the ramp motion changing from accelerated to impulsive at this point. A stagnation in τ is however noticed when $\eta = 0.6$ where a further increase in the value of η does not have any effect on the skin friction. The magnitude of τ is also seen to increase with $\mathcal{H}a$ in this case. A similar behaviour towards η is noticed for the case when $K = 1$, we however noticed an increase in the magnitude of τ when $\mathcal{H}a$ is increased. On the inner surface of the outer cylinder, we notice that the magnitude of τ decreases with $\mathcal{H}a$ when $K = 0$ and increases with $\mathcal{H}a$ when $K = 1$. For both cases however, an increase in $\mathcal{H}a$ leads to an increase in the magnitude of τ.

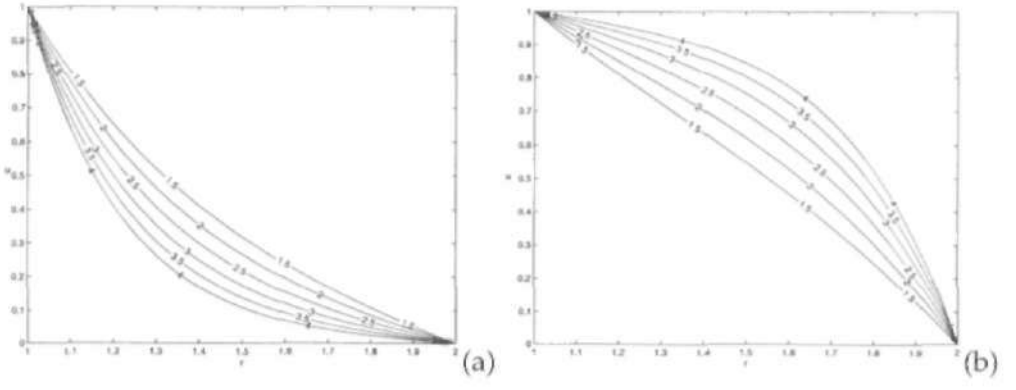
Figure 3.10 shows the dimensionless mass flux within the annulus against the dimensionless time for different values of the Hartmann number $\mathcal{H}a$. It is observed that an increase in $\mathcal{H}a$ when $(K = 0)$ lead to a decrease in mass flux, this is due to the retarding nature of the Lorentz force which tends to slow down

the fluid motion and hence the mass mass flux. However, when the magnetic field is fixed relative to the moving cylinder ($K = 1$), an increase in $\mathcal{H}a$ leads to an increase in mass flux. This is as a result of the ramp motion of the magnetic field which acts in support of the velocity, thereby enhancing the mass flux. The mass flux is also noticed to increase with time until it reaches its steady state for both cases.



(a) (b)

Figure 3.6: The velocity profile u showing the effect of η with $K = 0$ and $K = 1$ represented by a and b respectively and $\eta_0 = 0.5$, $\mathcal{H}a = 1$.



(a) (b)

Figure 3.7: The velocity profile u showing the effect of $\mathcal{H}a$ with $K = 0$ and $K = 1$ represented by a and b respectively and $\eta_0 = 0.5$, $\eta = 1$.

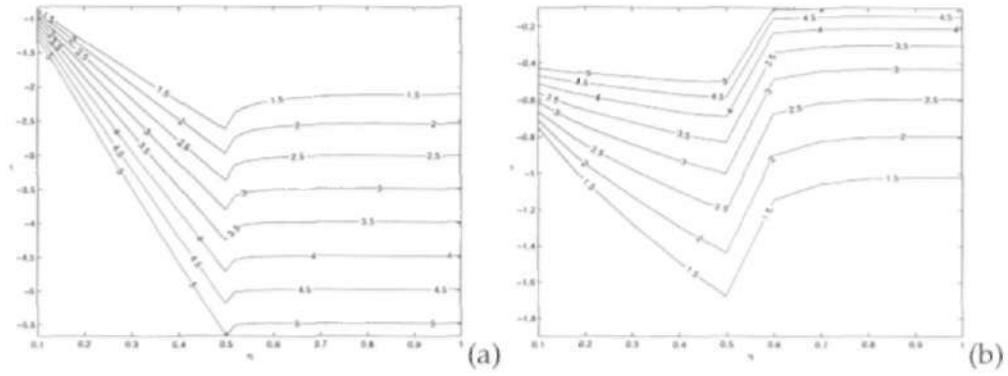


Figure 3.8: The skin friction at the outer surface of the inner cylinder ($r = 1$) showing the influence of $\mathcal{H}a$ and η with $K = 0$ and $K = 1$ represented by a and b respectively and $\eta_0 = 0.5$.

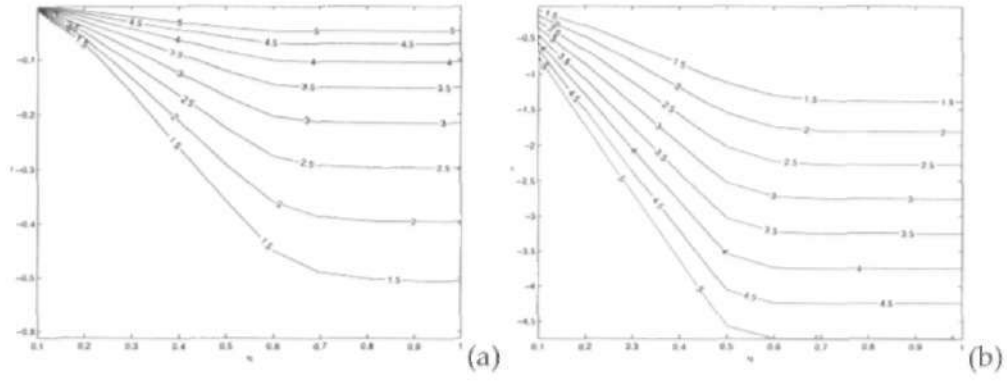


Figure 3.9: The skin friction at the inner surface of the outer cylinder ($r = 2$) showing the influence of $\mathcal{H}a$ and η with $K = 0$ and $K = 1$ represented by a and b respectively and $\eta_0 = 0.5$.

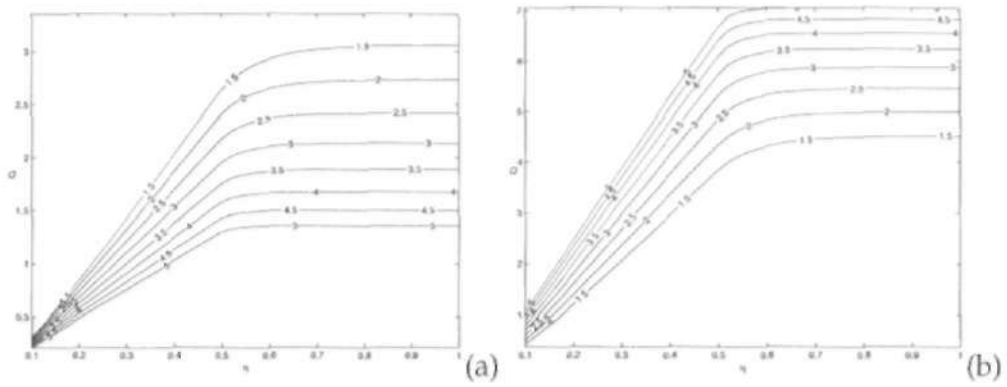


Figure 3.10: The dimensionless mass flux Q showing the influence of $\mathcal{H}a$ and η with $K = 0$ and $K = 1$ represented by a and b respectively and $\eta_0 = 1$.

3.3 UNSTEADY MHD TAYLOR-COUETTE FLOW WITH TRANSPIRATION[3]

In this section, we have presented a semi-analytical solution for the unsteady MHD flow of an incompressible laminar fluid in an annulus of two co-rotaing concentric porous cylinders. The fluid motion is due to the angular rotation of both cylinders with different angular velocities. The solution of the problem is obtained using the Laplace transform technique in conjuction with the Riemann-sum approximation method of Laplace inversion. The analytical solution of the steady state is derived separately to validate the solution. The effects of the various dimensionless parameters entering into the problem are studied with the aid of graphs.

3.3.1 Mathematical Analysis

We consider the motion of an incompressible and electrically conducting fluid filling the gap between two horizontal concentric porous cylinders of infinite length in the presence of magnetic field acting perpendicularly to the flow direction. The inner and the outer cylinders have radii a and b respectively. At time $t \leq 0$, the fluid and the cylinders are assumed to be at rest, when $t > 0$ the inner and the outer cylinders are impulsively rotated at constant angular velocity ω_1 and ω_2 respectively, which are lower than the threshold required to initiate Taylor vortices. In the absence of pressure and gravity, the flow is

[3]Under consideration in
IEEE

governed by the following equations in vector form

$$\nabla \cdot \vec{V} = 0 \tag{3.40}$$

$$\rho \frac{\partial \vec{V}}{\partial t} + \rho(\vec{V} \cdot \nabla)\vec{V} = \rho \nu \nabla^2 \vec{V} + \vec{J} \times \vec{B} \tag{3.41}$$

$$\vec{J} = \sigma(\vec{E} + \vec{V} \times \vec{B}). \tag{3.42}$$

The z'-axis is assumed to be on the horizontal axis of the cylinders while r' and θ' are on the radial and tangential axes respectively. We assume that there is no applied and polarisation voltage (i.e., $\vec{E} = 0$) and that the induced magnetic field is negligible which translates to only a constant uniform magnetic field B_0 acting on the fluid. Therefore

$$J'_r = \sigma B_0 v' \quad and \quad J'_\theta = -\sigma B_0 u'. \tag{3.43}$$

Based on the assumptions made; eqs. (3.40) and (3.41) are simplified in cylindrical polar coordinate as follows:

$$\frac{\partial}{\partial r'}(r'u') = 0 \tag{3.44}$$

$$\left(\frac{\partial v'}{\partial t} + u'\frac{\partial v'}{\partial r} + \frac{u'v'}{r'}\right) = \nu\left[\frac{\partial^2 v'}{\partial r'^2} + \frac{1}{r'}\frac{\partial v'}{\partial r'} - \frac{v'}{r'^2}\right] - \frac{\sigma B_0^2}{\rho}v'. \tag{3.45}$$

490026

Integrating eq. (3.44), the radial velocity distribution at the outer surface of the inner cylinder ($r' = a$) is defined as

$$u' = \frac{u_0 a}{r'} \tag{3.46}$$

Substituting u' into eq. (3.45), we have

$$\frac{\partial v'}{\partial t} + u_0 a \left[\frac{1}{r'}\frac{\partial v'}{\partial r'} + \frac{v'}{r'^2}\right] = \nu \left[\frac{\partial^2 v'}{\partial r'^2} + \frac{1}{r'}\frac{\partial v'}{\partial r'} - \frac{v'}{r'^2}\right] - \frac{\sigma B_0^2}{\rho} v', \tag{3.47}$$

subject to the following initial and boundary conditions

$$\begin{aligned} v' &= 0,\ a \le r' \le b \text{ and } t \le 0, \\ v' &= a\omega_1',\ \text{at } r' = a, t > 0; \\ v' &= b\omega_2',\ \text{at } r' = b,\ t > 0. \end{aligned} \tag{3.48}$$

3.3.2 Solution of the problem

Introducing the following dimensionless variables in eqs. (3.47) and (3.48)

$r = r'/a,\ v = v'/a\omega_1',\ \eta = \nu t/a^2,\ \mathcal{H}a = B_0 a\sqrt{\sigma/\nu\rho},\ \mathcal{S} = u_0 a/\nu,\ \varsigma = b/a,\ \beta = \frac{\omega_2'}{\omega_1'}$

and $\phi = \beta\varsigma$, we have

$$\frac{\partial v}{\partial \eta} + \mathcal{S}\left[\frac{1}{r}\frac{\partial v}{\partial r} + \frac{v}{r^2}\right] = \frac{\partial^2 v}{\partial r^2} + \frac{1}{r}\frac{\partial v}{\partial r} - \frac{v}{r^2} - \mathcal{H}a^2 v, \tag{3.49}$$

and the initial and boundary conditions also become

$$\begin{aligned} v &= 0,\ 1 \le r \le \varsigma \ and\ \eta \le 0, \\ v &= 1,\ at\ r = 1, \eta > 0; \\ v &= \phi,\ at\ r = \varsigma,\ \eta > 0. \end{aligned} \tag{3.50}$$

The solution of eq. (3.49) can be obtained using the Laplace transforms technique as follows:

$$\frac{d^2\bar{v}}{dr^2} + \frac{1}{r}(1-\mathcal{S})\frac{d\bar{v}}{dr} - \left[r^2(s+\mathcal{H}a^2) + (\mathcal{S}+1)\right]\frac{v}{r^2} = 0 \tag{3.51}$$

and the following boundary condition,

$$\begin{aligned} \bar{v} &= 0,\ 1 \le r \le \varsigma \ and\ \eta \le 0, \\ \bar{v} &= \frac{1}{s},\ at\ r = 1,\ \eta > 0; \\ \bar{v} &= \frac{\phi}{s},\ at\ r = \varsigma,\ \eta > 0. \end{aligned} \tag{3.52}$$

Using the approach of Tsangaris et al. (2006), eq. (3.51) can be reduced by using the following transformation variable

$$\bar{v}(r,s) = r^{\frac{\mathcal{S}}{2}}\bar{f}(r), \tag{3.53}$$

to the following Bessel equation

$$\frac{d^2\bar{f}}{dr^2}+\frac{1}{r}\frac{d\bar{f}}{dr}-\left[(\frac{\mathcal{S}}{2}+1)^2+r^2(s+\mathcal{H}a^2)\right]\frac{\bar{f}}{r^2}=0. \tag{3.54}$$

The solution of eq. (3.54) is

$$\bar{f}(r,s)=C_1I_\iota(\delta r)+C_2K_\iota(\delta r). \tag{3.55}$$

Here I_ι and K_ι are the modified Bessel's function of the ι-th order of the first and second kinds respectively and

$$\iota=\frac{\mathcal{S}}{2}+1. \tag{3.56}$$

$$\delta=\sqrt{s+\mathcal{H}a^2}. \tag{3.57}$$

Substitute $\bar{f}$ into eq. (3.53) we have

$$\bar{v}(r,s)=r^{\frac{\mathcal{S}}{2}}[C_1I_\iota(\delta r)+C_2K_\iota(\delta r)]. \tag{3.58}$$

Using the boundary condition (eq. 3.52), C_1 and C_2 are obtained as shown below:

$$C_1=\frac{\left[\beta\varsigma^{(-\frac{\mathcal{S}}{2}+1)}K_\iota(\delta)-K_\iota(\varsigma\delta)\right]}{s[I_\iota(\varsigma\delta)K_\iota(\delta)-K_\iota(\varsigma\delta)I_\iota(\delta)]} \tag{3.59}$$

$$C_2=-\frac{\left[\beta\varsigma^{(-\frac{\mathcal{S}}{2}+1)}I_\iota(\delta)-I_\iota(\varsigma\delta)\right]}{s[I_\iota(\varsigma\delta)K_\iota(\delta)-K_\iota(\varsigma\delta)I_\iota(\delta)]}. \tag{3.60}$$

It is difficult to invert eq. (3.58) in closed form, we then use the Riemann-sum approximation to carry out the inversion as follows:

$$v(r,\eta) = \frac{e^{\gamma\eta}}{\eta}\left[\frac{1}{2}\bar{v}(r,\gamma) + Re\sum_{k=1}^{N}\bar{v}(r,\gamma+\frac{ik\pi}{\eta})(-1)^k\right]. \tag{3.61}$$

3.3.3 Skin Friction

The skin friction is obtained from eq. (3.61) as follows:

$$\begin{aligned}\tau &= \left[\frac{dv}{dr} - \frac{v}{r}\right] \\ &= \frac{e^{\gamma\eta}}{\eta}\left[\frac{1}{2}\bar{v}_1(r,\gamma) + Re\sum_{k=1}^{N}\bar{v}_1(r,\gamma+\frac{ik\pi}{\eta})(-1)^k\right],\end{aligned} \tag{3.62}$$

where

$$\begin{aligned}\bar{v}_1 &= \left(\frac{S}{2}-1\right)r^{(\frac{S}{2}-1)}\left[C_1 I_1(\delta r) + C_2 K_1(\delta r)\right] \\ &+ \delta r^{\frac{S}{2}}\left[C_1 I_{1+1}(\delta r) - C_2 K_{1+1}(\delta r)\right].\end{aligned} \tag{3.63}$$

On the outer surface of the inner cylinder ($r = 1$), $\bar{v}_1$ is simplified as

$$\begin{aligned}\bar{v}_1|_{r=1} &= \left(\frac{S}{2}-1\right)\left[C_1 I_1(\delta) + C_2 K_1(\delta)\right] \\ &+ \delta\left[C_1 I_{1+1}(\delta) - C_2 K_{1+1}(\delta)\right],\end{aligned} \tag{3.64}$$

while on the inner surface of the outer cylinder v_1 is obtained by setting $r = 2$ in eq. 3.63 as shown below.

$$\begin{aligned} \bar{v}_1|_{r=2} &= \left(\frac{\mathcal{S}}{2} - 1\right) 2^{(\frac{\mathcal{S}}{2}-1)} [C_1 I_t(2\delta) + C_2 K_t(2\delta)] \\ &+ \delta 2^{\frac{\mathcal{S}}{2}} [C_1 I_{t+1}(2\delta) - C_2 K_{t+1}(2\delta)]. \end{aligned} \tag{3.65}$$

3.3.4 Steady State

The expression for the steady state velocity distribution v_s is obtained by setting $\partial v/\partial \eta$ in eq. (3.49) to zero. We then obtain the following ordinary differential equation,

$$\frac{d^2 v_s}{dr^2} + \frac{1}{r}(1-\mathcal{S})\frac{dv_s}{dr} - [\mathcal{H}a^2 r^2 + (\mathcal{S}+1)]\frac{v_s}{r^2} = 0, \tag{3.66}$$

using the following transformation variable

$$v_s(r) = r^{\frac{\mathcal{S}}{2}} f_s(r), \tag{3.67}$$

the above equation is transformed into the following homogeneous differential equation

$$\frac{d^2 f_s}{dr^2} + \frac{1}{r}\frac{df_s}{dr} - \left[(\frac{S}{2}+1)^2 + \mathcal{H}a^2 r^2\right]\frac{f_s}{r^2} = 0. \tag{3.68}$$

The solution of eq. (3.68) is

$$f_s(r) = C_3 I_t(\mathcal{H}_a r) + C_4 K_t(\mathcal{H}_a r), \tag{3.69}$$

substitute eq. (3.69) into eq. (3.67) we have the velocity for the steady state v_s to be

$$v_s(r) = r^{\frac{\mathcal{S}}{2}}[C_3 I_t(\mathcal{H}ar) + C_4 K_t(\mathcal{H}ar)], \tag{3.70}$$

where C_3 and C_4 are obtained using eq. (3.50) as shown below

$$C_3 = \frac{\left[\beta\varsigma^{(-\frac{\mathcal{S}}{2}+1)}K_t(\mathcal{H}a) - K_t(\varsigma\mathcal{H}a)\right]}{[I_t(\varsigma\mathcal{H}a)K_t(\mathcal{H}a) - K_t(\varsigma\mathcal{H}a)I_t(\mathcal{H}a)]} \tag{3.71}$$

$$C_4 = -\frac{\left[\beta\varsigma^{(-\frac{\mathcal{S}}{2}+1)}I_t(\mathcal{H}a) - I_t(\varsigma\mathcal{H}a)\right]}{[I_t(\varsigma\mathcal{H}a)K_t(\mathcal{H}a) - K_t(\varsigma\mathcal{H}a)I_t(\mathcal{H}a)]}. \tag{3.72}$$

The steady state skin friction τ_s is obtained similarly as follows

$$\begin{aligned}\tau_s &= \left(\frac{\mathcal{S}}{2} - 1\right) r^{(\frac{\mathcal{S}}{2}-1)}[C_1 I_t(\mathcal{H}_a r) + C_2 K_t(\mathcal{H}_a r)] \\ &+ \mathcal{H}_a r^{\frac{\mathcal{S}}{2}}[C_1 I_{t+1}(\mathcal{H}_a r) - C_2 K_{t+1}(\mathcal{H}_a r)].\end{aligned} \tag{3.73}$$

3.3.5 Results and Discussion

The variation of the velocity v profiles with time η for different values of the ratio of the angular velocities β is shown in Figure 3.11 when $\mathcal{S} = 0.5$ and $\mathcal{H}a = 2.0$. Figure 3.11(a)–(c) shows the velocity profile when the cylinders move in the same direction (+ve values of β) and Figure 3.11(d)–(f), when the cylinders move in the opposite direction (-ve values of β). It is observed in Figure 1(a); when the inner cylinder is moving at an angular velocity twice that of the outer cylinder (i.e $\beta = 0.5$) that the fluid velocity on the outer surface of the inner cylinder

and that on the inner surface of the outer cylinder are the same. However, we noticed in Figure 3.11(b) that when the two cylinders are moving at the same velocities ($\beta = 1.0$), v on the inner surface of the outer cylinder is twice that on the outer surface of the inner cylinder. We also noticed in Figure 3.11(c) that the v on the inner surface of the outer cylinder is $3\times$ that on the inner cylinder when $\beta = 1.5$. For the case of the cylinders moving in the opposite directions as depicted in Figure 3.11(d)–(f), we observed that the v decreases monotonically from one on the inner cylinder to the negative of their corresponding values when the cylinders are moving in the same directions as earlier explained. The velocities are found to increase with η when the cylinders are moving in the same directions (i.e for positive values of β) and decreases with η for negative values of β. But for the case when $\beta = -0.5$, an initial increase in v is noticed and thereafter a turnaround in behaviour around the middle of the annulus.

In Figure 3.12, we observed that the velocity reduces with increase in $\mathcal{H}a$. This is expected as increase in $\mathcal{H}a$ results into an increase in the Lorentz force which is known to retard fluid motion. The behaviour of the velocity with respect to β for a fixed $\eta = 0.05$ is shown in Figure 3.13, the result obtained is in tandem with that of Figure 3.11. The effect of the suction parameter $\mathcal{S}$ is presented in Figure 3.14 for a fixed value of $\beta = 1$. The effect of $\mathcal{S}$ on v is found to be quite remarkable; we observe an increase in v when $\mathcal{S}$ is increased positively and a decrease when $\mathcal{S}$ is increased negatively, a reversal in behaviour is however noticed around $r = 1.4$. The combined effect of $\mathcal{S}$ and β on the flow

field at the centreline of the annulus ($r = 1.5$) is depicted in Figure 3.15. It is shown in this figure that for small values of β (=0.2 for example), an increase in S leads to an increase in v. If β is however increased, v is found to decrease with increase in S.

The changes in skin friction τ with S and β on both the outer surface of the inner cylinder and on the inner surface of the outer cylinder are shown in Figures 3.16 and 3.17. These figures shows the variations of τ for $\eta = 0.05$, since changes are more pronounced at small time. It is seen in Figure 3.16 that τ increases marginally with S on the outer surface of the inner cylinder and then start to decrease steadily with it. We also noticed that increasing β leads to a decrease in the magnitude of τ for negative values of S. The effect of β on τ is seen to gradually disappear as S is further increased. On the inner surface of the outer cylinder, we noticed that the magnitude of τ decrease with an increase in S but increase with increase in β. The rate of change τ with respect to S is found to be obvious at $r = 1$, while it is more pronounced with respect to β at $r = 2$.

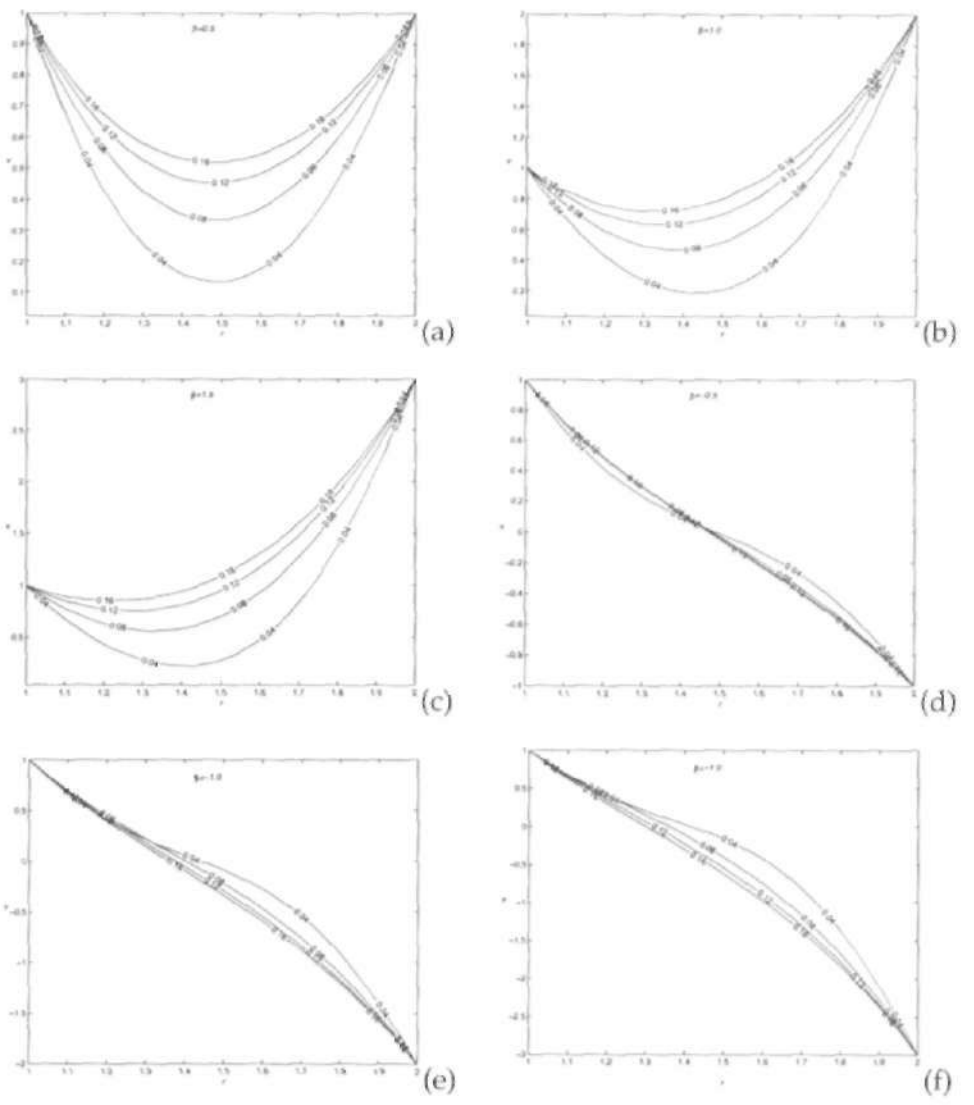


Figure 3.11: Velocity v vs r with $\mathcal{S} = 0.5$, $\mathcal{H}a = 2.0$ and various values of β varying η.

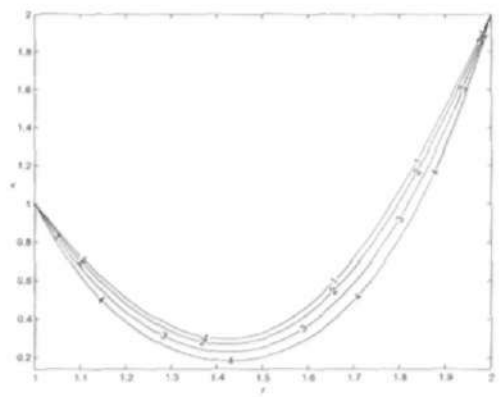


Figure 3.12: Velocity v vs r with $\mathcal{S} = 0.5$, $\eta = 0.05$ and $\beta = 1.0$ for different values of $\mathcal{H}a$.

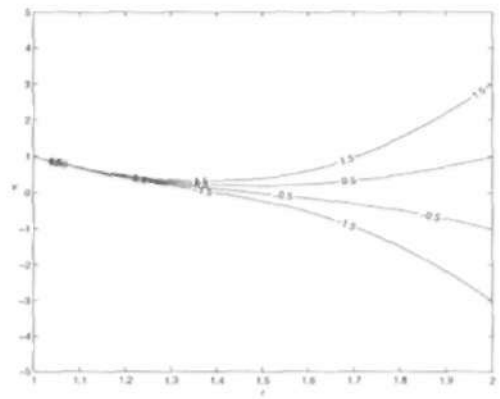


Figure 3.13: Velocity v vs r with $\mathcal{S} = 0.5$, $\mathcal{H}a = 2.0$ and $\eta = 0.05$ for different values of β.

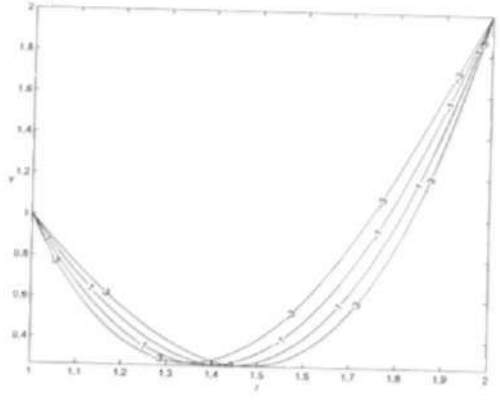


Figure 3.14: Velocity v vs r with $\eta = 0.05$, $\mathcal{H}a = 2.0$ and $\beta = 1.0$ for different values of $\mathcal{S}$.

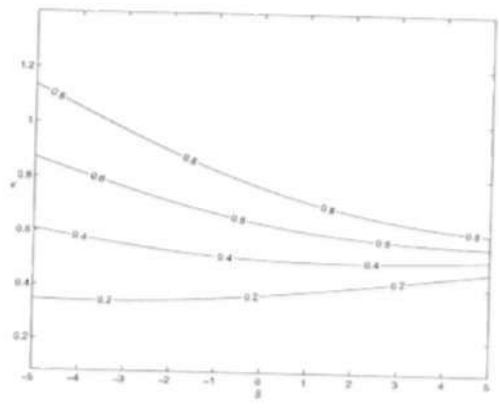


Figure 3.15: Velocity v vs $\mathcal{S}$ at the centerline of the annulus ($r = 1.5$) with $\mathcal{H}a = 2.0$, $\eta = 0.05$ for different values of β.

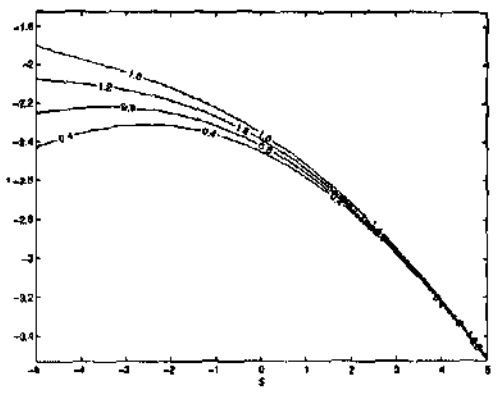


Figure 3.16: Skin friction τ vs S at outer surface of the inner cylinder ($r = 1.0$) with $\mathcal{H}a = 2.0$ and $\eta = 0.05$ for different values of β.

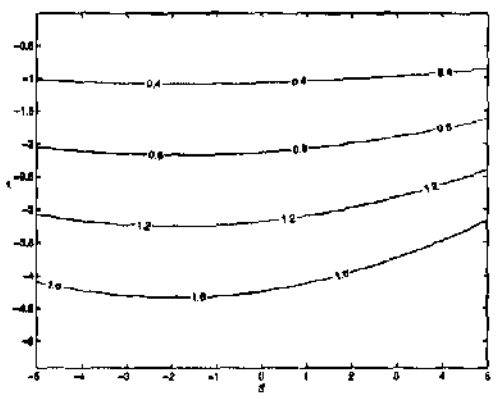


Figure 3.17: Skin friction τ vs S at the inner surface of the outer cylinder ($r = 2.0$) with $\mathcal{H}a = 2.0$ and $\eta = 0.05$ for different values of β.

3.4 CONCLUDING REMARKS

We have analysed the fluid flow between two concentric horizontal cylinders of infinite length. We have considered three problems; the first is due to the sudden movement of the outer cylinder, the second is due to the ramp motion of the inner cylinder and the last problem is the unsteady MHD Taylor–Couette flow in the presence of suction and injection. A unified closed form expressions are derived for each problem corresponding to the cases of the magnetic field being fixed relative to the fluid or to the moving cylinder. It is observed that the velocity decreases with increase in Hartmann number when the magnetic field is fixed relative to the fluid; this is expected, as the magnetic field has a retarding influence on the flow fields.

The skin friction increases with time, while it decreases with Hartmann number on the outer surface of the inner cylinder when $K = 0$ and on the inner surface of the outer cylinder when $K = 1$. An opposite behaviour is noticed on the inner surface of the outer cylinder. For the MHD Taylor–Couette flow, we have observed that increasing β leads to a decrease in the magnitude of the skin friction for negative values of S on the outer surface of the inner cylinder. This effect of β on the skin friction is seen to vanish as S is further increased. It is also evident form the results that rate of change τ with respect to S is found to be more pronounced on the outer surface of the inner cylinder, while it is more pronounced with respect to β on the inner surface of the outer cylinder.

CHAPTER 4

MHD TWO-PHASE COUETTE FLOW

Two-phase flow is a particular example of a multiphase flow, Multiphase flow is a generalisation of the modelling used in two-phase flow where the two phases are not chemically related (e.g. dusty gases) or where more than two phases are present. Each of the phases is considered to have a separately defined volume fraction (the sum of which is unity), and velocity field. Strictly speaking all flow are multi-phase since no fluid is so clean. In describing flow, one of the challenges we face is therefore deciding whether we need a multi-phase model or not. Some examples of two-phase flow are; bubbles rising in a carbonated drink, raindrops falling through the air, gasoline and air reacting in an automobile engine, water and steam circulating in a nuclear reactor and in petrochemical industries amongst others.

Rahmatulin (1956) developed a model which examines the unstable movement between fluid and particles and thereby included the particle-phase viscosity term in his model. Saffman (1962) observed the effect of dust particles on the laminar flow of an incompressible fluid with mass concentration of dust particles. The equations he obtained neglected the interaction between the individual dust particles and also assumed that in the continuum hypothesis,

the cloud of dust particles form a pseudo-fluid and therefore excluded the viscosity of the particle phase. However, in Rahmatulin's model, each phase of the suspension has a local velocity and material properties, also, the phases are assumed to interact mutually in a continuous manner and the phases are homogeneous and evenly distributed per unit volume of the mixture. The following partial differential equations describe the unstable movements of the two-phase incompressible fluids for a plane channel geometry according to Rahmatulin.

$$\rho_f \frac{\partial \vec{V}_f}{\partial t} = -f_f P + f_f \mu_1 \nabla^2 \vec{V}_f + K(\vec{V}_p - \vec{V}_f); \quad \nabla \cdot \vec{V}_f = 0 \tag{4.1}$$

$$\rho_p \frac{\partial \vec{V}_p}{\partial t} = -f_p P + f_p \mu_1 \nabla^2 \vec{V}_p + K(\vec{V}_f - \vec{V}_p); \quad \nabla \cdot \vec{V}_p = 0 \tag{4.2}$$

Using Saffman's model; Nag et al. (1979) studied the Couette flow of a dusty gas between two parallel infinite plates for both the impulsive and the accelerated start of one of the plates. Singh and Dube (1973) studied the laminar flow of an unsteady, incompressible viscous fluid with uniform distribution of dust particles through a circular pipe under the influence of pressure gradient. The effect of particulate diffusion on the compressible boundary-layer flow of a two-phase suspension over a horizontal surface was examined by Chamkha (1998). Makinde and Chinyoka (2010) investigated the unsteady flow and heat transfer of a dusty fluid between two parallel plates with variable viscosity and electric conductivity. Several other researchers; Gireesha et al. (2007), Rashmi

et al. (2007) and Ghosh and Ghosh (2008) studied the flow of dusty fluids under varying condition. All of these studies excluded the paticle-phase viscous effects.

The Rahmatulin (1956) model has been improved by Fayzullyev (1966), Latipov (1963) and Drew (1983) among other researchers under different conditions. Other works which use the concept of the particle–phase viscosity includes Gidaspow (1986), Gadiraju et al. (1992) and Chamkha and Ramadan (1998). Chamkha (2000) studied the unsteady laminar flow and heat transfer of a particulate suspension in an electrically conducting fluid through channels and circular pipes in the presence of uniform transverse magnetic field which is formulated using a two-phase continuum model. He assumed the particle-phase viscosity to be constant in order to obtain a closed form solutions. Recebli and Kurt (2008) examined the effect of the electrical and magnetic field applied perpendicular to the flow and each other on the two–phase steady flow in a gas pipe. Gupta and Gupta (1975) discussed the flow of a dusty gas in the annular space between two concentric cylinders when both cylinders are moving with arbitrary time-dependent velocities. The flow and heat transfer of a dusty fluid within the annulus of circular cylinders under a pulsatile pressure gradient has been studied by Datta and Dalai (1995).

The problem of two-phase unsteady MHD Couette flow between two concentric cylinders of infinite length has been analysed when the outer cylinder is impulsively started. The system of partial differential equations describing the flow problem is formulated taking the viscosity of the particle phase into

consideration. Unified closed form expressions are obtained for the velocities and the problem is solved using a combination of the Laplace transform technique, D'Alemberts and the Riemann-sum approximation methods. The governing equations are also solved using the implicit finite difference method to verify the method used for the inversion. The variation of the velocity and the skin friction with the dimensionless parameters occuring in the problem are illustrated graphically and discussed for both phases.

4.1 UNSTEADY MHD TWO-PHASE COUETTE FLOW OF FLUID-PARTICLE SUSPENSION[1]

4.1.1 Mathematical Analysis

The motion of an unsteady, laminar, viscous fluid/particle suspension between two infinite horizontal plates located at the $z' = 0$ and $z' = h$ planes is considered. The fluid phase is assumed to be electrically conducting, while the channel walls are assumed to be electrically non-conducting. A uniform transverse magnetic field is applied normal to the flow direction and it is assumed that no applied or polarization voltage exists. When $t > 0$ the lower plate ($z' = 0$) begins to move in its own plane with a velocity Ut'' where U is a constant and the upper plate ($z' = h$) remains fixed. The magnetic Reynolds number is assumed to be small so that the induced magnetic field and the Hall effects of MHD are negligible.

[1]Under consideration in
Applied Mathematical Modelling

It is assumed that the fluid and the particles are interacting as a continuum. Following Rahmatulin's model, the equation of motion with electromagnetic force added is given as shown below

$$\rho_f \frac{\partial \vec{V}_f}{\partial t} = -c_f P + c_f \mu_f \nabla^2 \vec{V}_f + K'(\vec{V}_p - \vec{V}_f) + \vec{J} \times \vec{B}; \quad \nabla \cdot \vec{V}_f = 0 \tag{4.3}$$

$$\rho_p \frac{\partial \vec{V}_p}{\partial t} = -c_p P + c_p \mu_p \nabla^2 \vec{V}_p + K'(\vec{V}_f - \vec{V}_p); \quad \nabla \cdot \vec{V}_p = 0, \tag{4.4}$$

where $\vec{V}_f = (u'_f, v'_f, w'_f)$ and $\vec{V}_p = (u'_p, v'_p, w'_p)$ denotes respectively the velocity components of the fluid and the particles and $\vec{J} = \sigma(\vec{E} + \vec{V}_f \times \vec{B})$.

Under the assumptions made in the present problem eqs. (4.3) and (4.4) becomes

$$\frac{\partial u'_f}{\partial t} = \nu_f c_f \frac{\partial^2 u'_f}{\partial z'^2} + K'(u'_p - u'_f) - \frac{\sigma B_0^2}{\rho} u'_f \tag{4.5}$$

$$\frac{\partial u'_p}{\partial t} = \nu_p c_p \frac{\partial^2 u'_p}{\partial z'^2} + K'(u'_f - u'_p). \tag{4.6}$$

Equation (4.5) is valid when the magnetic field is fixed relative to the fluid. If the magnetic field is also accelerated with the same velocity as the plate, we must account for the relative motion. Thus, eq. (4.5) turn to

$$\frac{\partial u'_f}{\partial t} = \nu_f c_f \frac{\partial^2 u'_f}{\partial z'^2} + K'(u'_p - u'_f) - \frac{\sigma B_0^2}{\rho}(u'_f - Ut^n) \tag{4.7}$$

Eqs. (4.5) and (4.7) are combined together to obtain

$$\frac{\partial u'_f}{\partial t} = \nu_f c_f \frac{\partial^2 u'_f}{\partial z'^2} + K'(u'_p - u'_f) - \frac{\sigma B_0^2}{\rho}(u'_f - UKt^n), \tag{4.8}$$

where

$$K = \begin{cases} 0 & when\ B_0\ is\ fixed\ relative\ to\ the\ fluid \\ 1 & when\ B_0\ is\ fixed\ relative\ to\ the\ moving\ plate \end{cases}.$$

The initial and boundary conditions for the present problem are

$$\begin{aligned} u'_f &= u'_p = 0, \quad 0 \le z' \le h \text{ and } t \le 0, \\ u'_f &= u'_p = Ut^n, \text{ at } z' = 0,\ t > 0; \\ u'_f &= u'_p = 0, \text{ at } z' = h,\ t > 0. \end{aligned} \tag{4.9}$$

4.1.2 Solution of the Problem

It is convenient to non-dimensionalise the equations by using the following

$$z = z'/h,\ u'_f; u'_p = (u'_f; u'_p)/U,\ \eta = tc_f\nu_1/h^2, \quad \mathcal{H}a = B_0 h\sqrt{\sigma/\nu_f\rho_f c_f}, \quad K = K'h^2/\nu_f c_f.$$

Considering the impulsive motion of the lower plate which corresponds to $n = 0$ and substituting the dimensionless quantities into the governing equations and the boundary condition, the following dimensionless equation results,

$$\frac{\partial u_f}{\partial \eta} = \frac{\partial^2 u_f}{\partial z^2} + K(u_p - u_f) - \mathcal{H}a^2(u_f - K) \tag{4.10}$$

$$\frac{\partial u_p}{\partial \eta} = R_c R_v \frac{\partial^2 u_p}{\partial z^2} + \mathcal{K}(u_f - u_p), \tag{4.11}$$

where the parameters used in eq. (4.11) are defined as $R_c = c_p/c_f$ and $R_v = \nu_p/\nu_f$.

The initial and boundary conditions (4.9) also become

$$\begin{aligned} u_f &= u_p = 0, \quad 0 \le z \le 1 \text{ and } \eta \le 0, \\ u_f &= u_p = 1, \text{ at } z = 0, \ \eta > 0; \\ u_f &= u_p = 0, \text{ at } z = 1, \ \eta > 0. \end{aligned} \tag{4.12}$$

Taking the Laplace transform of eqs. (4.10) and (4.11) we have the following ordinary differential equations

$$\frac{d^2\bar{u}_f}{dz^2} - (s + \mathcal{H}a^2 + \mathcal{K})\bar{u}_f + \mathcal{K}\bar{u}_p = -\mathcal{H}a^2 K \tag{4.13}$$

$$\frac{d^2\bar{u}_p}{dz^2} - \frac{(s+\mathcal{K})}{R_c R_v}\bar{u}_p + \frac{\mathcal{K}}{R_c R_v}\bar{u}_f = 0, \tag{4.14}$$

where

$$\bar{u}_f = \int_0^\infty u_f(z,\eta)e^{-s\eta}d\eta \qquad \text{and} \qquad \bar{u}_p = \int_0^\infty u_p(z,\eta)e^{-s\eta}d\eta,$$

and $s > 0$.

The Laplace transformation of the initial and boundary conditions are

$$\begin{aligned} \bar{u}_f &= \bar{u}_p = 0, \quad 0 \le z \le 1 \text{ and } \eta \le 0, \\ \bar{u}_f &= \bar{u}_p = 1/s, \text{ at } z = 0, \ \eta > 0; \\ \bar{u}_f &= \bar{u}_p = 0, \text{ at } z = 1, \ \eta > 0. \end{aligned} \tag{4.15}$$

We choose the D'Alembert's method to obtain the solutions of eqs. (4.13) and (4.14). In order to solve the equations, we multiply eq. (4.13) by A and add it to eq. (4.14).

$$\frac{d^2}{dz^2}(A\bar{u}_f + \bar{u}_p) - \delta^2(A\bar{u}_f + \bar{u}_p) = -\frac{\mathcal{H}a^2AK}{s}, \tag{4.16}$$

where

$$A = \frac{\left[A(s + \mathcal{H}a^2 + \mathcal{K}) - \frac{\mathcal{K}}{R_c R_v}\right]}{\left[\frac{(s+\mathcal{K})}{R_c R_v} - \mathcal{K}A\right]} \tag{4.17}$$

The general solution of eq. (4.16) is

$$A\bar{u}_f + \bar{u}_p = C_1 cosh(\delta z) + C_2 sinh(\delta z) + \frac{\mathcal{H}a^2AK}{s\delta^2}. \tag{4.18}$$

Using the boundary condition (4.15), C_1 and C_2 are obtained as follows

$$C_1 = \frac{(1+A)}{s} - \frac{\mathcal{H}a^2AK}{s\delta^2} \tag{4.19}$$

$$C_2 = -\left[\frac{(1+A)}{s} - \frac{\mathcal{H}a^2AK}{s\delta^2}\right]\frac{cosh(\delta)}{sinh(\delta)} - \frac{\mathcal{H}a^2AK}{s\delta^2 sinh(\delta)}, \tag{4.20}$$

where

$$\delta^2 = \left[\frac{(s+\mathcal{K})}{R_c R_v} - \mathcal{K}A\right]. \tag{4.21}$$

Upon substituting C_1 and C_2 into eq. (4.18), the general solution now becomes

$$\begin{aligned} A\bar{u}_f + \bar{u}_p &= (1+A)\frac{sinh(\delta(1-z))}{ssinh(\delta)} + \mathcal{H}a^2 AK\left[\frac{1}{s} - \frac{sinh(\delta z)}{s\delta^2 sinh(\delta)}\right] \\ &+ \mathcal{H}a^2 AK\frac{sinh(\delta(1-z))}{s\delta^2 sinh(\delta)}. \end{aligned} \tag{4.22}$$

From eq. (4.17) we have

$$A^2 + A\left[\frac{(s+\mathcal{H}a^2+\mathcal{K})}{\mathcal{K}} - \frac{(s+\mathcal{K})}{\mathcal{K}R_c R_v}\right] - \frac{1}{R_c R_v} = 0. \tag{4.23}$$

The roots of eq. (4.23) are

$$\begin{aligned} A_1; A_2 &= \frac{1}{2}\left[-\left(\frac{(s+\mathcal{H}a^2+\mathcal{K})}{\mathcal{K}} - \frac{(s+\mathcal{K})}{\mathcal{K}R_c R_v}\right)\right] \\ &\pm \frac{1}{2}\left[\sqrt{\left(\frac{(s+\mathcal{H}a^2+\mathcal{K})}{\mathcal{K}} - \frac{(s+\mathcal{K})}{\mathcal{K}R_c R_v}\right)^2 + \frac{4}{R_c R_v}}\right]. \end{aligned} \tag{4.24}$$

Replacing A with A_1 and A_2 one after the other in eq. (4.21) and (4.22) the following are obtained

$$\begin{aligned} A_1\bar{u}_f + \bar{u}_p &= (1+A_1)\frac{sinh(\delta_1(1-z))}{ssinh(\delta_1)} + \mathcal{H}a^2 AK\left[\frac{1}{s} - \frac{sinh(\delta_1 z)}{s\delta_1^2 sinh(\delta_1)}\right] \\ &+ \mathcal{H}a^2 A_1\mathcal{K}\frac{sinh(\delta_1(1-z))}{s\delta_1^2 sinh(\delta_1)} \end{aligned} \tag{4.25}$$

$$A_2\bar{u}_f+\bar{u}_p = (1+A_2)\frac{sinh(\delta_2(1-z))}{ssinh(\delta_2)}+\mathcal{H}a^2AK\left[1-\frac{sinh(\delta_2 z)}{s\delta_2^2 sinh(\delta_2)}\right] + \mathcal{H}a^2A_2K\frac{sinh(\delta_2(1-z))}{s\delta_2^2 sinh(\delta_2)}. \quad (4.26)$$

Solving eqs. (4.25) and (4.26) we have

$$\begin{aligned}\bar{u}_f &= \frac{1}{s(A_1-A_2)}\left[(1+A_1)\frac{sinh(\delta_1(1-z))}{sinh(\delta_1)}-(1+A_2)\frac{sinh(\delta_2(1-z))}{sinh(\delta_2)}\right] \\ &+ \frac{\mathcal{H}a^2K}{s(A_1-A_2)}\left[\frac{A_1}{\delta_1^2}\left(1-\frac{sinh(\delta_1 z)}{sinh(\delta_1)}\right)-\frac{A_2}{\delta_2^2}\left(1-\frac{sinh(\delta_2 z)}{sinh(\delta_2)}\right)\right] \\ &+ \frac{\mathcal{H}a^2K}{s(A_1-A_2)}\left[\frac{A_1}{\delta_1^2}\left(\frac{sinh(\delta_1(z-1))}{sinh(\delta_1)}\right)-\frac{A_2}{\delta_2^2}\left(\frac{sinh(\delta_2(z-1))}{sinh(\delta_2)}\right)\right] \quad (4.27)\end{aligned}$$

$$\begin{aligned}\bar{u}_p &= \frac{1}{s(A_2-A_1)}\left[(A_2+A_1A_2)\frac{sinh(\delta_1(1-z))}{sinh(\delta_1)}-(A_1+A_1A_2)\frac{sinh(\delta_2(1-z))}{sinh(\delta_2)}\right] \\ &+ \frac{\mathcal{H}a^2A_1A_2K}{s(A_2-A_1)}\left[\frac{1}{\delta_1^2}\left(1-\frac{sinh(\delta_1 z)}{sinh(\delta_1)}\right)-\frac{1}{\delta_2^2}\left(1-\frac{sinh(\delta_2 z)}{sinh(\delta_2)}\right)\right] \\ &+ \frac{\mathcal{H}a^2A_1A_2K}{s(A_2-A_1)}\left[\frac{1}{\delta_1^2}\left(\frac{sinh(\delta_1(z-1))}{sinh(\delta_1)}\right)-\frac{1}{\delta_2^2}\left(\frac{sinh(\delta_2(z-1))}{sinh(\delta_2)}\right)\right]. \quad (4.28)\end{aligned}$$

Eqs. (4.27) and (4.28) are inverted using the Riemann-sum approximation method of Laplace inversion as follows:

$$u_f(z,\eta)=\frac{e^{\gamma\eta}}{\eta}\left[\frac{1}{2}\bar{u}_f(z,\gamma)+Re\sum_{k=1}^{N}\bar{u}_f(z,\gamma+\frac{ik\pi}{\eta})(-1)^k\right] \quad (4.29)$$

$$u_p(z,\eta)=\frac{e^{\gamma\eta}}{\eta}\left[\frac{1}{2}\bar{u}_p(z,\gamma)+Re\sum_{k=1}^{N}\bar{u}_p(z,\gamma+\frac{ik\pi}{\eta})(-1)^k\right]. \quad (4.30)$$

4.1.3 Skin Friction

The dimensionless skin friction on the plates for the fluid and the particle phases are obtained by differentiating eqs. (4.29) and (4.30) respectively with respect to z as

$$\tau_f = \frac{\partial u_f}{\partial r} = \frac{e^{\gamma\eta}}{\eta}\left[\frac{1}{2}z_1(z,\gamma) + Re\sum_{k=1}^{N} z_1(z,\gamma+\frac{ik\pi}{\eta})(-1)^k\right] \tag{4.31}$$

$$\tau_p = \frac{\partial u_p}{\partial r} = \frac{e^{\gamma\eta}}{\eta}\left[\frac{1}{2}z_2(z,\gamma) + Re\sum_{k=1}^{N} z_2(z,\gamma+\frac{ik\pi}{\eta})(-1)^k\right], \tag{4.32}$$

where

$$\begin{aligned} z_1 &= \frac{1}{s(A_1-A_2)}\left[-\delta_1(1+A_1)\frac{cosh(\delta_1(1-z))}{sinh(\delta_1)} + \delta_2(1+A_2)\frac{cosh(\delta_2(1-z))}{sinh(\delta_2)}\right] \\ &+ \frac{\mathcal{H}a^2K}{s(A_1-A_2)}\left[-\frac{A_1}{\delta_1}\left(\frac{cosh(\delta_1 z)}{sinh(\delta_1)}\right) + \frac{A_2}{\delta_2}\left(\frac{cosh(\delta_2 z)}{sinh(\delta_2)}\right)\right] \\ &+ \frac{\mathcal{H}a^2K}{s(A_1-A_2)}\left[\frac{A_1}{\delta_1}\left(\frac{cosh(\delta_1(y-1))}{sinh(\delta_1)}\right) - \frac{A_2}{\delta_2}\left(\frac{cosh(\delta_2(z-1))}{sinh(\delta_2)}\right)\right] \end{aligned} \tag{4.33}$$

$$\begin{aligned} z_2 &= \frac{1}{s(A_2-A_1)}\left[-\delta_1(A_2+A_1A_2)\frac{cosh(\delta_1(1-z))}{sinh(\delta_1)} + \delta_2(A_1+A_1A_2)\frac{cosh(\delta_2(1-z))}{sinh(\delta_2)}\right] \\ &+ \frac{\mathcal{H}a^2A_1A_2K}{s(A_1-A_2)}\left[-\frac{1}{\delta_1}\left(\frac{cosh(\delta_1 z)}{sinh(\delta_1)}\right) + \frac{1}{\delta_2}\left(\frac{cosh(\delta_2 z)}{sinh(\delta_2)}\right)\right] \\ &+ \frac{\mathcal{H}a^2A_1A_2K}{s(A_1-A_2)}\left[\frac{1}{\delta_1}\left(\frac{cosh(\delta_1(z-1))}{sinh(\delta_1)}\right) - \frac{1}{\delta_2}\left(\frac{cosh(\delta_2(z-1))}{sinh(\delta_2)}\right)\right]. \end{aligned} \tag{4.34}$$

The skin friction on the upper and lower plates for the two phases can then be obtained by substituting $z = 0$ and $z = 1$ respectively in eqs. (4.31) and (4.32).

4.1.4 Steady State

We set out to validate the accuracy of the Riemann-sum approximation method employed in this present problem by obtaining analytically the solution of the steady state. The expression for the steady state velocities for the two phases are obtained by setting $\partial()/\partial\eta$ in eqs. (4.10) and (4.11) to zero. The following ordinary differential equations then results

$$\frac{d^2u_{sf}}{dz^2} - (\mathcal{K} + \mathcal{H}a^2)u_{sf} + \mathcal{K}u_{sp} = -\mathcal{H}a^2K \tag{4.35}$$

$$\frac{d^2u_{sp}}{dz^2} - \frac{\mathcal{K}}{R_cR_v}u_{sp} + \frac{\mathcal{K}}{R_cR_v}u_{sf} = 0. \tag{4.36}$$

The solutions of eqs. (4.35) and (4.36) using D'Alembert's method are

$$\begin{aligned} u_{sf} &= \frac{1}{(B_1 - B_2)}\left[(1+B_1)\frac{sinh(\alpha_1(1-z))}{sinh(\alpha_1)} - (1+B_2)\frac{sinh(\alpha_2(1-z))}{sinh(\alpha_2)}\right] \\ &+ \frac{\mathcal{H}^2K}{(B_1 - B_2)}\left[\frac{B_1}{\alpha_1^2}\left(1 - \frac{sinh(\alpha_1 z)}{sinh(\alpha_1)}\right) - \frac{B_2}{\alpha_2^2}\left(1 - \frac{sinh(\alpha_2 z)}{sinh(\alpha_2)}\right)\right] \\ &+ \frac{\mathcal{H}^2K}{(B_1 - B_2)}\left[\frac{B_1}{\alpha_1^2}\left(\frac{sinh(\alpha_1(z-1))}{sinh(\alpha_1)}\right) - \frac{B_2}{\alpha_2^2}\left(\frac{sinh(\alpha_2(z-1))}{sinh(\alpha_2)}\right)\right] \end{aligned} \tag{4.37}$$

$$
\begin{aligned}
u_{sp} &= \frac{1}{(B_2-B_1)}\left[(B_2+B_1B_2)\frac{sinh(\alpha_1(1-z))}{sinh(\alpha_1)}-(B_1+B_1B_2)\frac{sinh(B_2(1-z))}{sinh(\alpha_2)}\right] \\
&+ \frac{\mathcal{H}^2B_1B_2K}{(B_2-B_1)}\left[\frac{1}{\alpha_1^2}\left(1-\frac{sinh(\alpha_1 z)}{sinh(\alpha_1)}\right)-\frac{1}{\alpha_2^2}\left(1-\frac{sinh(\alpha_2 z)}{sinh(\alpha_2)}\right)\right] \\
&+ \frac{\mathcal{H}a^2B_1B_2K}{(B_2-B_1)}\left[\frac{1}{\alpha_1^2}\left(\frac{sinh(\alpha_1(z-1))}{sinh(\alpha_1)}\right)-\frac{1}{\alpha_2^2}\left(\frac{sinh(\alpha_2(z-1))}{sinh(\alpha_2)}\right)\right], \qquad (4.38)
\end{aligned}
$$

where

$$\alpha^2 = \left[\frac{\mathcal{K}}{R_cR_v}-\mathcal{K}B\right] \qquad (4.39)$$

$$B = \frac{\left[B(\mathcal{H}a^2+\mathcal{K})-\frac{\mathcal{K}}{R_cR_v}\right]}{\left[\frac{\mathcal{K}}{R_cR_v}-\mathcal{K}B\right]} \qquad (4.40)$$

$$B_1;B_2 = \frac{1}{2}\left[-\left(\frac{(\mathcal{H}a^2+\mathcal{K})}{\mathcal{K}}-\frac{1}{R_cR_v}\right)\pm\sqrt{\left(\frac{(\mathcal{H}a^2+\mathcal{K})}{\mathcal{K}}-\frac{1}{R_cR_v}\right)^2+\frac{4}{R_cR_v}}\right]. \qquad (4.41)$$

The numerical values obtained for both u_{sf} and u_{sp} are the same with those obtained from eqs. (4.29) and (4.30) at large time.

4.1.5 Result and Discussion

In order to have a physical insight into the problem, we have written a MATLAB programme to compute and generate the graphs for the velocity of the two different phases and the skin frictions. The different values of the dimensionless parameters used in calculations are as follows: $\mathcal{K} = 50.0$, $R_v = 1.0$, $R_c = 0.25$, $\eta = 0.1$ and $\mathcal{H}a = 2$. Some representative results are presented in the form of line graphs in Figures 4.1–4.12 to interpret the effects of these parameters. A comparative analysis is made when a marked difference is noticed on the

behaviour of the flow when the magnetic field is fixed relative to the moving plate; this is depicted on right panels of the affected figures. We observe in Figure 4.1 that an increase in time leads to an increase in the fluid phase velocity when $K = 0$ and $K = 1$. The velocity of the particle phase is also noticed to follow the same trend in Figure 4.2. The fluid phase velocity is noticed in Figure 4.3 to decrease with increase in $\mathcal{H}a$ for both when $K = 0$ and $K = 1$. Figure 4.4 shows that the particle phase velocity also decreases with increase in $\mathcal{H}a$. It is observed that the effect of $\mathcal{H}a$ on the flow last longer when $K = 1$ than when $K = 0$. We can conclude from both Figures 4.3 and 4.4 that the veocities can be controlled by increasing or decreasing the magnetic field.

Figures 4.5 and 4.6 depict the variation in the values of u_f and u_p respectively brought about by the changes in the ratio of the kinematic viscosity R_ν. As R_ν increases, which translates to an increase in the particle phase viscosity, the velocity of the two phases decreases. The effect of the substance quantity of mixture on the flow field is shown in Figures 4.7 and 4.8. We observe that an increase in R_c when $K = 0$, result into an increase in the velocity of both velocities. Also, at small time ($\eta < 0.4$), when $K = 1$, the same trend is observed. However, as the time is increased further we observe in the "b" part of the figures that an increase in the particle concentration slows down the flow. It is found out that the fluid velocity is always greater than that of the particle for all the dimensional quantities considered.

The response of the skin friction to the ratio of the viscosities R_ν and time η is

depicted in Figures 4.9–4.12. In Figure 4.9, we observe that on the moving plate ($z = 0$), an increase in both R_v and η leads to a decrease in τ_f, the same pattern of behaviour is noticed for the particle phase skin friction τ_p in Figure 4.10. In order to observe the accurate behaviour of the skin friction on the stationary plate, we set $R_c = 1$, τ_f and τ_p are seen in Figures 4.11 and 4.12 respectively to increase with R_v but decreases with η until the flow reaches its steady state.

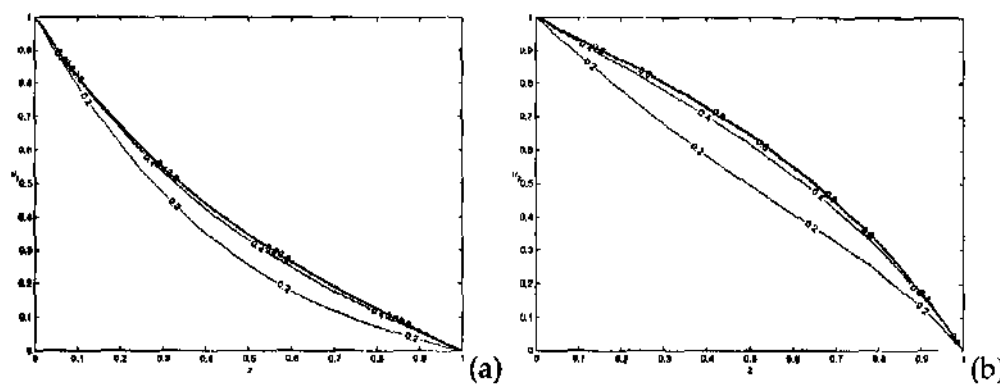


Figure 4.1: Profile of the fluid phase velocity u_f showing the effect of time with $K = 0$ and $K = 1$ represented by a and b respectively ($\mathcal{K} = 50.0$, $R_v = 1.0$, $R_c = 0.25$ and $\mathcal{H}a = 2$).

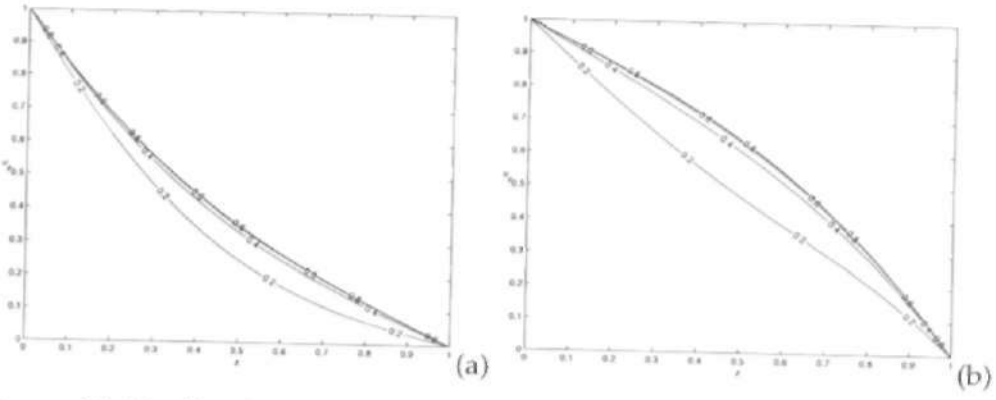


Figure 4.2: Profile of the particle phase velocity u_p showing the effect of time with $K = 0$ and $K = 1$ represented by a and b respectively ($\mathcal{K} = 50.0$, $R_v = 1.0$, $R_c = 0.25$ and $\mathcal{H}a = 2$).

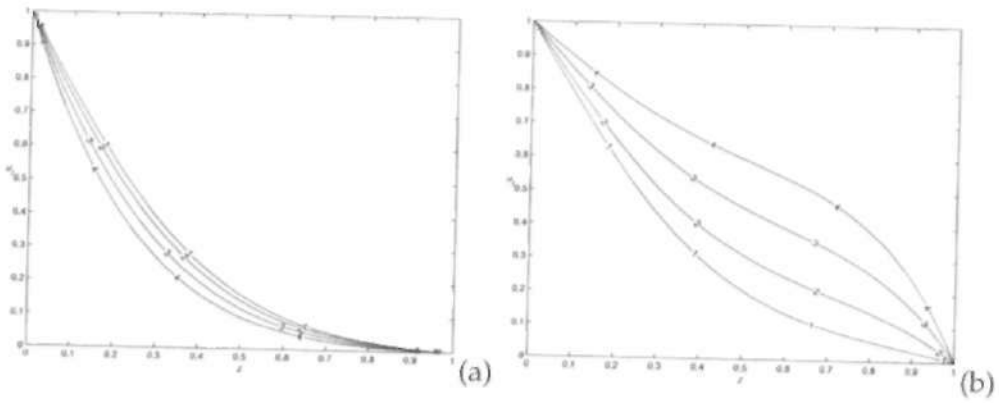


Figure 4.3: Profile of the fluid phase velocity u_f showing the effect of $\mathcal{H}a$ with $K = 0$ and $K = 1$ represented by a and b respectively ($\mathcal{K} = 50.0$, $R_v = 1.0$, $R_c = 0.25$ and $\eta = 0.1$).

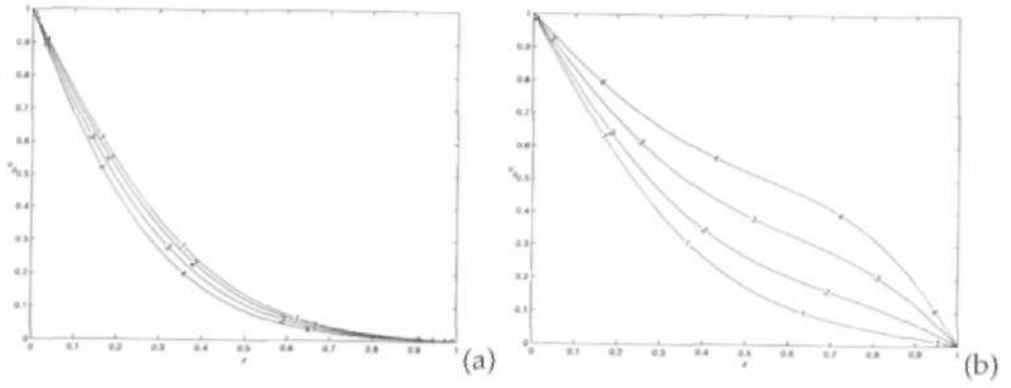


Figure 4.4: Profile of the particle phase velocity u_p showing the effect of $\mathcal{H}a$ with $K = 0$ and $K = 1$ represented by a and b respectively ($\mathcal{K} = 50.0$, $R_v = 1.0$, $R_c = 0.25$ and $\eta = 0.1$).

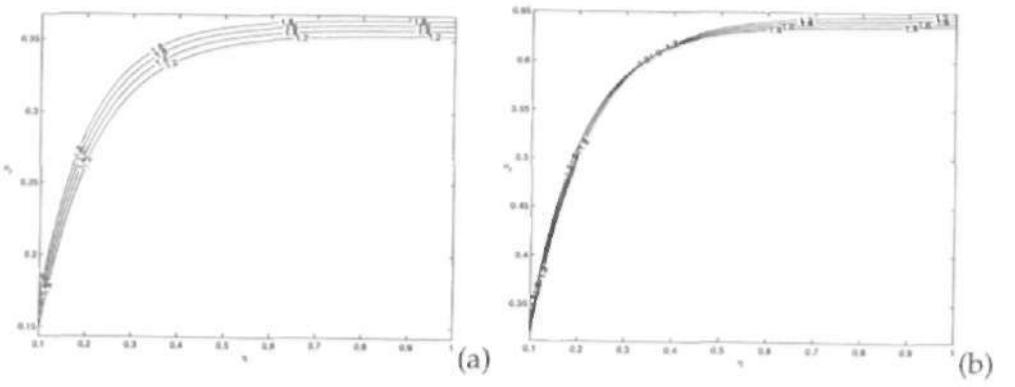


Figure 4.5: Profile of the fluid phase velocity u_f showing the effect of R_v and η ($\mathcal{K} = 50.0$, $R_c = 0.25$, $z = 0.5$ and $\mathcal{H}a = 2$).

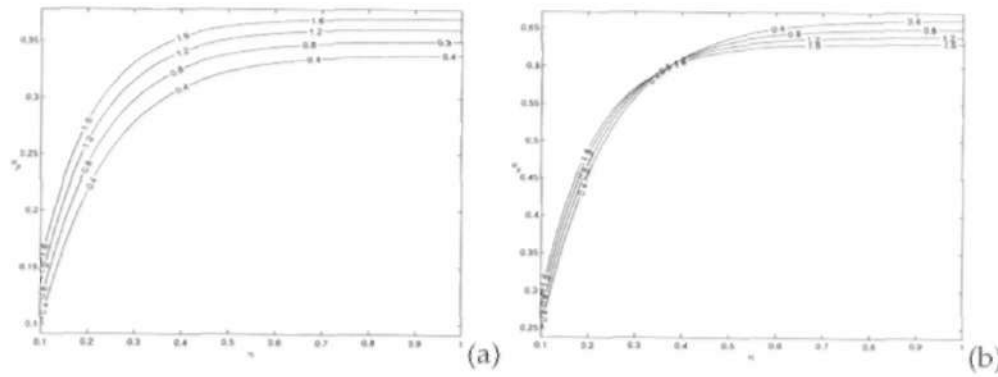


Figure 4.6: Profile of the particle phase velocity u_p showing the effect of R_v and η ($\mathcal{K} = 50.0$, $R_c = 0.25$, $z = 0.5$ and $\mathcal{H}a = 2$).

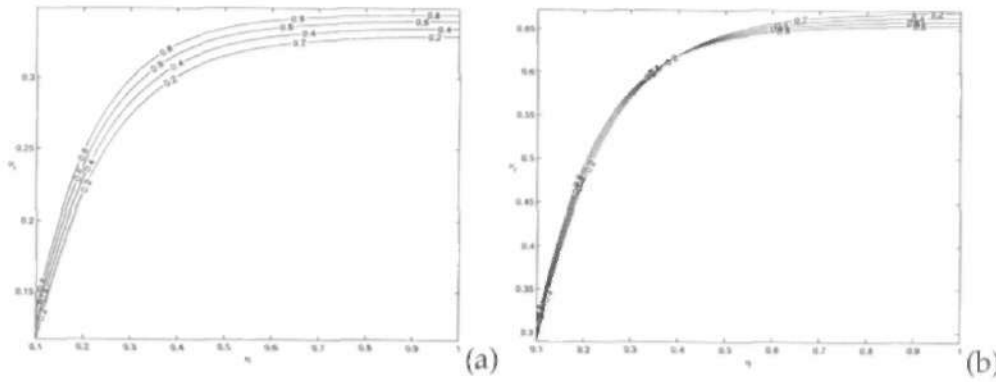


Figure 4.7: Profile of the fluid phase velocity u_f showing the effect of R_c and η ($\mathcal{K} = 50.0$, $R_v = 1.0$, $z = 0.5$ and $\mathcal{H}a = 2$).

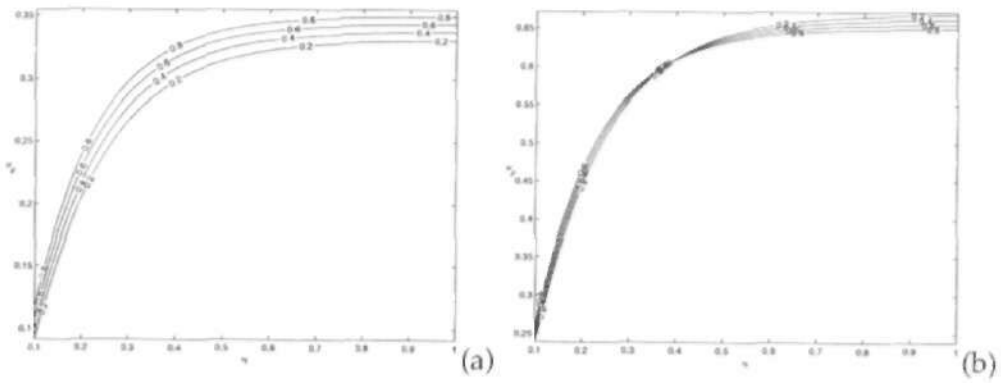


Figure 4.8: Profile of the particle phase velocity u_p showing the effect of R_c and η ($\mathcal{K} = 50.0$, $R_v = 1.0$, $z = 0.5$ and $\mathcal{H}a = 2$).

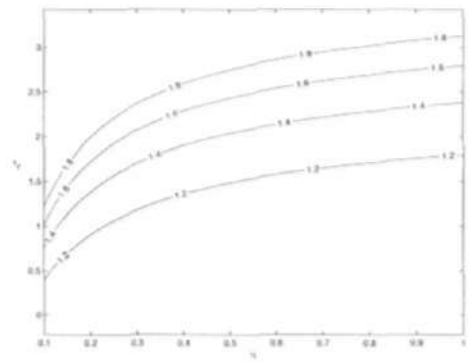


Figure 4.9: Variation of the fluid phase skin friction on the plate at $z = 0$ showing the effect of R_v and η ($\mathcal{K} = 50.0$, $\mathcal{H}a = 2.0$ and $R_c = 0.25$).

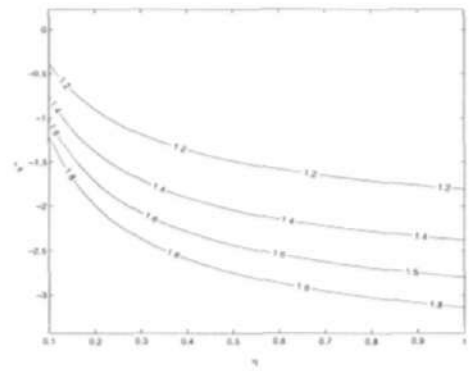


Figure 4.10: Variation of the particle phase skin friction on the plate at $z = 0$ showing the effect of R_v and η ($\mathcal{K} = 50.0$, $\mathcal{H}a = 2.0$ and $R_c = 0.25$).

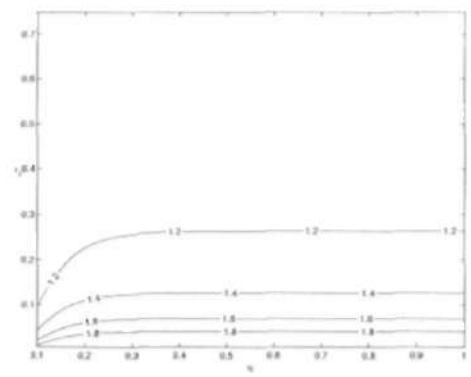


Figure 4.11: Variation of the fluid phase skin friction on the plate at $z = 1$ showing the effect of R_v and η ($\mathcal{K} = 50.0$, $\mathcal{H}a = 2.0$ and $R_c = 0.25$).

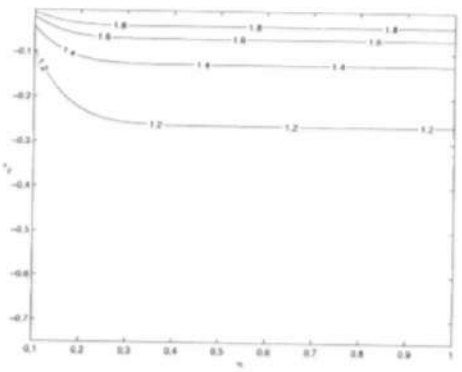


Figure 4.12: Variation of the particle phase skin friction on the plate at $z = 1$ showing the effect of R_v and η ($\mathcal{K} = 50.0$, $\mathcal{H}a = 2.0$ and $R_c = 0.25$).

4.2 UNSTEADY MHD TWO-PHASE COUETTE FLOW OF FLUID-PARTICLE SUSPENSION IN AN ANNULUS[2]

4.2.1 Mathematical Analysis

Consider the motion of an unsteady, laminar, viscous fluid/particle suspension between two concentric cylinders of infinite length. The fluid phase is assumed to be electrically conducting, while the particles are assumed to be electrically non-conducting. The z'-axis is assumed to be on the axis of the cylinders in the horizontal direction and r'-axis is on the radial direction. The fluid-particle suspension exists in the region $a \leq r' \leq b$ between the two cylinders in the presence of magnetic field acting perpendicular to the flow direction, where a and b are the radii of the inner and the outer cylinders respectively. Initially, the fluid, the particles and the two cylinders were at rest. However, when $t > 0$, the outer cylinder begins to move in its own plane with a velocity Ut^n, where U is a constant and the inner cylinder remains at rest. Since the cylinders are of infinite length and the flow is time dependent fully developed one-dimensional flow, all physical variables are functions of r' and t. The magnetic Reynolds number is assumed to be small so that the induced magnetic field and the Hall effects of MHD are negligible. It is further assumed that the fluid and the particles are interacting as a continuum. See Figure 4.13 for the schematic diagram of the problem.

[2]Jha and Apere (2011d) Published in
AIP Advances **1**, 042121 (2011); doi: 10.1063/1.3657509

Under the assumptions made in the present problem and using Rahmatulin's

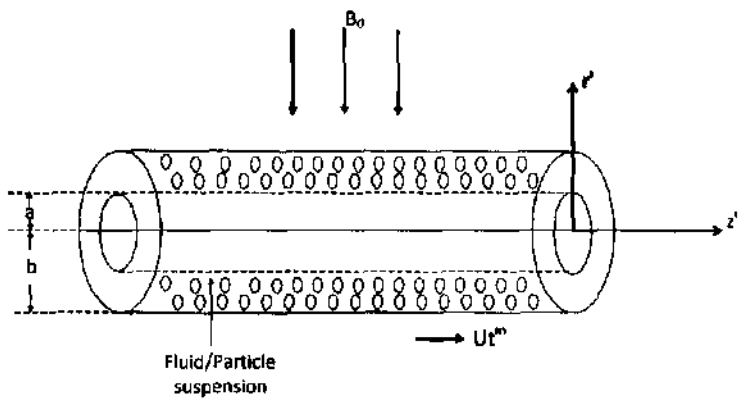


Figure 4.13: Schematic diagram of the problem

model for a cylindrical geometry, the equation of motion for the problem is

$$\frac{\partial u'_f}{\partial t} = \frac{\mu_f}{\rho_f} c_f \left[\frac{\partial^2 u'_f}{\partial r'^2} + \frac{1}{r'} \frac{\partial u'_f}{\partial r'} \right] + K'(u'_p - u'_f) - \frac{\sigma B_0^2}{\rho_f} u'_f \tag{4.42}$$

$$\frac{\partial u'_p}{\partial t} = \frac{\mu_p}{\rho_p} c_p \left[\frac{\partial^2 u'_p}{\partial r'^2} + \frac{1}{r'} \frac{\partial u'_p}{\partial r'} \right] + K'(u'_f - u'_p), \tag{4.43}$$

where all the parameters used are defined in the nomenclature. Eq. (4.42) is valid when the magnetic field is fixed relative to the fluid. If the magnetic field is also moving with the same velocity as the moving outer cylinder, we must

account for the relative motion. Thus, eq. (4.42) turn to

$$\frac{\partial u'_f}{\partial t} = \nu_f c_f \left[\frac{\partial^2 u'_f}{\partial r'^2} + \frac{1}{r'}\frac{\partial u'_f}{\partial r'}\right] + K'(u'_p - u'_f) - \frac{\sigma B_0^2}{\rho_f}(u'_f - Ut'^n). \tag{4.44}$$

Eqs. (4.42) and (4.44) can be written as one to obtain

$$\frac{\partial u'_f}{\partial t} = \nu_f c_f \left[\frac{\partial^2 u'_f}{\partial r'^2} + \frac{1}{r'}\frac{\partial u'_f}{\partial r'}\right] + K'(u'_p - u'_f) - \frac{\sigma B_0^2}{\rho_f}(u'_f - UKt'^n), \tag{4.45}$$

where

$$K = \begin{cases} 0 & \textit{when } B_0 \textit{ is fixed relative to the fluid} \\ 1 & \textit{when } B_0 \textit{ is fixed relative to the moving cylinder} \end{cases}$$

The initial and boundary conditions for the present problem are

$$\begin{aligned} u'_f &= u'_p = 0, \quad a \le r' \le b \textit{ and } t \le 0, \\ u'_f &= u'_p = 0, \quad \textit{at} \quad r' = a, t > 0; \\ u'_f &= u_p = Ut'^n, \textit{ at } r' = b, \ t > 0. \end{aligned} \tag{4.46}$$

4.2.2 Analytical Solution

It is convinient to non-dimensionalise the equations by using the following

$r = r'/a$, $u_f; u_p = (u'_f; u'_p)/U$, $\eta = tc_f\nu_f/a^2$, $Ha = B_0 a\sqrt{\sigma/\upsilon_1\rho_1 c_f}$,

$K = K'a^2/\nu_f c_f$ *and* $\varsigma = b/a$.

Considering the impulsive motion of the outer cylinder which corresponds to

$n = 0$ and substituting the dimensionless quantities into the governing eqs. (4.45) and (4.43) and the boundary condition, the following dimensionless equations result,

$$\frac{\partial u_f}{\partial \eta} = \frac{\partial^2 u_f}{\partial r^2} + \frac{1}{r}\frac{\partial u_f}{\partial r} + \mathcal{K}(u_p - u_f) - \mathcal{H}a^2(u_f - K) \tag{4.47}$$

$$\frac{\partial u_p}{\partial \eta} = R_c R_\nu \left[\frac{\partial^2 u_2}{\partial r^2} + \frac{1}{r}\frac{\partial u_p}{\partial r}\right] + \mathcal{K}(u_f - u_p), \tag{4.48}$$

where the parameters used in eq. (4.48) are defined as $R_c = c_p/c_f$ and $R_\nu = \nu_p/\nu_f$.

The initial and boundary conditions (4.46) also become

$$\begin{aligned} u_f &= u_p = 0, \quad 1 \le r \le \varsigma \text{ and } \eta \le 0, \\ u_f &= u_p = 0, \quad \text{at} \quad r = 1, \ \eta > 0; \\ u_f &= u_p = 1, \text{ at } r = \varsigma, \ \eta > 0. \end{aligned} \tag{4.49}$$

$$\frac{d^2\bar{u}_f}{dr^2} + \frac{1}{r}\frac{d\bar{u}_f}{dr} - (s + \mathcal{H}a^2 + \mathcal{K})\bar{u}_f + \mathcal{K}\bar{u}_p = -\frac{\mathcal{H}a^2 K}{s} \tag{4.50}$$

$$\frac{d^2\bar{u}_p}{dr^2} + \frac{1}{r}\frac{d\bar{u}_p}{dr} - \frac{(s+\mathcal{K})}{R_c R_\nu}\bar{u}_p + \frac{\mathcal{K}}{R_c R_\nu}\bar{u}_f = 0 \tag{4.51}$$

The Laplace transformation of the initial and boundary conditions are

$$\begin{aligned} \bar{u}_f &= \bar{u}_p = 0,\ 1 \le r \le \varsigma \ and\ \eta \le 0, \\ \bar{u}_f &= \bar{u}_p = 0,\ at\ r = 1,\ \eta > 0; \\ \bar{u}_f &= \bar{u}_p = 1/s,\ at\ r = \varsigma,\ \eta > 0. \end{aligned} \tag{4.52}$$

We choose the D'Alembert's method to obtain the solutions of eqs. (4.50) and (4.51). In order to solve the equations , we multiply eq. (4.50) by A and add it to eq. (4.51) which gives:

$$\frac{d^2}{dr^2}(A\bar{u}_f + \bar{u}_p) + \frac{1}{r}\frac{d}{dr}(A\bar{u}_f + \bar{u}_p) - \delta^2(A\bar{u}_f + \bar{u}_p) = -\frac{\mathcal{H}a^2 AK}{s}, \tag{4.53}$$

where

$$A = \frac{\left[A(s + \mathcal{H}a^2 + \mathcal{K}) - \frac{K}{R_c R_v}\right]}{\left[\frac{(s+\mathcal{K})}{R_c R_v} - \mathcal{K}A\right]} \tag{4.54}$$

The solution of eq. (4.53) is

$$A\bar{u}_f + \bar{u}_p = C_1 I_0(\delta r) + C_2 K_0(\delta r) + \frac{\mathcal{H}a^2 AK}{s\delta^2}. \tag{4.55}$$

Using the boundary condition (4.52), C_1 and C_2 are obtained as follows

$$C_1 = \frac{\mathcal{H}a^2 AK}{s\alpha\delta^2}[K_0(\delta) - K_0(\varsigma\delta] - \frac{(1+A)}{s\alpha}K_0(\delta) \tag{4.56}$$

$$C_2 = \frac{\mathcal{H}a^2 AK}{s\alpha\delta^2}[I_0(\varsigma\delta) - I_0(\delta)] + \frac{(1+A)}{s\alpha} I_0(\delta), \tag{4.57}$$

where

$$\delta = \sqrt{\left[\frac{(s+\mathcal{K})}{R_c R_v} - \mathcal{K}A\right]} \tag{4.58}$$

$$\alpha = K_0(\varsigma\delta)I_0(\delta) - K_0(\delta)I_0(\varsigma\delta) \tag{4.59}$$

From eq. (4.54) we have

$$A^2 + A\left[\frac{(s+\mathcal{H}a^2+\mathcal{K})}{\mathcal{K}} - \frac{(s+\mathcal{K})}{\mathcal{K}R_c R_v}\right] - \frac{1}{R_c R_v} = 0. \tag{4.60}$$

The roots of eq. (4.60) are

$$\begin{aligned} A_1; A_2 &= \frac{1}{2}\left[-\left(\frac{(s+\mathcal{H}a^2+\mathcal{K})}{\mathcal{K}} - \frac{(s+\mathcal{K})}{\mathcal{K}R_c R_v}\right)\right] \\ &\pm \frac{1}{2}\left[\sqrt{\left(\frac{(s+\mathcal{H}a^2+\mathcal{K})}{\mathcal{K}} - \frac{(s+\mathcal{K})}{\mathcal{K}R_c R_v}\right)^2 + \frac{4}{R_c R_v}}\right] \end{aligned} \tag{4.61}$$

Replacing A with A_1 and A_2 in eq. (4.53) and δ with δ_1 and δ_2. The following are obtained:

$$A_1\bar{u}_f + \bar{u}_p = D_1 I_0(\delta_1 r) + D_2 K_0(\delta_1 r) + \frac{\mathcal{H}a^2 A_1 K}{s\delta_1^2} \tag{4.62}$$

$$A_2\bar{u}_f + \bar{u}_p = D_3 I_0(\delta_2 r) + D_4 K_0(\delta_2 r) + \frac{\mathcal{H}a^2 A_2 K}{s\delta_2^2}, \tag{4.63}$$

where D_1 and D_2 are obtained by substituting δ_1 in C_1 and C_2 respectively while D_3 and D_4 are also obtained by substituting δ_2 in C_1 and C_2. Solving eqs. (4.62) and (4.63) we have

$$\begin{aligned} \bar{u}_f &= \frac{D_1 I_0(\delta_1 r) - D_3 I_0(\delta_2 r) + D_2 K_0(\delta_1 r) - D_4 K_0(\delta_2 r)}{A_1 - A_2} \\ &+ \frac{\mathcal{H} a^2 K}{s(A_1 - A_2)} \left[\frac{A_1}{\delta_1^2} - \frac{A_2}{\delta_2^2} \right] \end{aligned} \tag{4.64}$$

$$\begin{aligned} \bar{u}_p &= \frac{[D_1 I_0(\delta_1 r) + D_2 K_0(\delta_1 r)]A_2 - [D_3 I_0(\delta_2 r) + D_4 K_0(\delta_2 r)]A_1}{A_2 - A_1} \\ &+ \frac{\mathcal{H} a^2 A_1 A_2 K}{s(A_2 - A_1)} \left[\frac{1}{\delta_1^2} - \frac{1}{\delta_2^2} \right]. \end{aligned} \tag{4.65}$$

Eqs. (4.64) and (4.65) are inverted using the Riemann-sum approximation method of Laplace inversion as follows:

$$u_f(r,\eta) = \frac{e^{\gamma\eta}}{\eta} \left[\frac{1}{2} \bar{u}_f(r,\gamma) + Re \sum_{k=1}^{N} \bar{u}_f(r, \gamma + \frac{ik\pi}{\eta})(-1)^k \right] \tag{4.66}$$

$$u_p(r,\eta) = \frac{e^{\gamma\eta}}{\eta} \left[\frac{1}{2} \bar{u}_p(r,\gamma) + Re \sum_{k=1}^{N} \bar{u}_p(r, \gamma + \frac{ik\pi}{\eta})(-1)^k \right]. \tag{4.67}$$

4.2.3 Skin Friction

The dimensionless skin friction for the fluid and the particle phases are obtained by differentiating eqs. (4.66) and (4.67) respectively with respect to r as

$$\tau_f = \frac{\partial u_f}{\partial r} = \frac{e^{\gamma\eta}}{\eta}\left[\frac{1}{2}z_1(r,\gamma) + Re\sum_{k=1}^{N} z_1(r,\gamma+\frac{ik\pi}{\eta})(-1)^k\right] \tag{4.68}$$

$$\tau_p = \frac{\partial u_p}{\partial r} = \frac{e^{\gamma\eta}}{\eta}\left[\frac{1}{2}z_2(r,\gamma) + Re\sum_{k=1}^{N} z_2(r,\gamma+\frac{ik\pi}{\eta})(-1)^k\right], \tag{4.69}$$

where

$$z_1 = \frac{\delta_1[D_1 I_1(\delta_1 r) - D_2 K_1(\delta_1 r)] + \delta_2[D_4 K_1(\delta_2 r) - D_3 I_1(\delta_2 r)}{A_1 - A_2} \tag{4.70}$$

$$z_2 = \frac{[D_1 I_1(\delta_1 r) - D_2 K_1(\delta_1 r)]A_2\delta_1 - [D_3 I_1(\delta_2 r) - D_4 K_1(\delta_2 r)]A_1\delta_2}{A_2 - A_1}. \tag{4.71}$$

The skin frictions at the outer surface of the inner cylinder and that at the inner surface of the outer cylinder for both the fluid and the particles can then be obtained by substituting $r = 1$ and $r = 2$ respectively in eqs. (4.70) and (4.71).

4.2.4 Steady State Solution

We set out to validate the accuracy of the Riemann-sum approximation method employed in this present problem by obtaining analytically the solution of the steady state. The expression for the steady state velocities for the two phases are obtained by setting $\partial()/\partial t$ in eqs. (4.45) and (4.46) to zero. The following

ordinary differential equations then results

$$\frac{d^2u_f}{dr^2}+\frac{1}{r}\frac{du_f}{dr}-(\mathcal{K}+\mathcal{H}a^2)u_f+\mathcal{K}u_p=-\mathcal{H}a^2K \tag{4.72}$$

$$\frac{d^2u_p}{dr^2}+\frac{1}{r}\frac{du_p}{dr}-\frac{\mathcal{K}}{R_cR_v}u_p+\frac{\mathcal{K}}{R_cR_v}u_f=0. \tag{4.73}$$

The solutions of eqs. (4.72) and (4.73) using D'Alembert's method are

$$\begin{aligned} u_f(r) &= \frac{F_1I_0(\gamma_1r)-F_3I_0(\gamma_2r)+F_2K_0(\gamma_1r)-F_4K_0(\gamma_2r)}{B_1-B_2} \\ &+ \frac{\mathcal{H}a^2K}{(B_1-B_2)}\left[\frac{B_1}{\gamma_1^2}-\frac{B_2}{\gamma_2^2}\right] \end{aligned} \tag{4.74}$$

$$\begin{aligned} u_p(r) &= \frac{[F_1I_0(\gamma_1r)+F_2K_0(\gamma_1r)]B_2-[F_3I_0(\gamma_2r)+F_4K_0(\gamma_2r)]B_1}{B_2-B_1} \\ &+ \frac{\mathcal{H}a^2B_1B_2K}{(B_2-B_1)}\left[\frac{1}{\gamma_1^2}-\frac{1}{\gamma_2^2}\right]. \end{aligned} \tag{4.75}$$

F_1 and F_2 are obtained by substituting γ_1 in E_1 and E_2 respectively while F_3 and F_4 are also obtained by substituting γ_2 in E_1 and E_2 while E_1 and E_2 are obtained using the boundary condition (4.49) as

$$E_1=\frac{\mathcal{H}a^2BK}{\alpha}[K_0(\gamma)-K_0(\varsigma\gamma]-\frac{(1+B)}{\alpha}K_0(\gamma) \tag{4.76}$$

$$E_2=\frac{\mathcal{H}a^2BK}{\alpha}[I_0(\varsigma\gamma)-I_0(\gamma)]+\frac{(1+B)}{\alpha}I_0(\gamma) \tag{4.77}$$

and

$$\gamma^2 = \left[\frac{\mathcal{K}}{R_c R_v} - \mathcal{K}B\right] \tag{4.78}$$

$$B = \frac{\left[B(\mathcal{H}a^2+\mathcal{K}) - \frac{\mathcal{K}}{R_c R_v}\right]}{\left[\frac{\mathcal{K}}{R_c R_v} - \mathcal{K}B\right]} \tag{4.79}$$

$$B_1; B_2 = \frac{1}{2}\left[-\left(\frac{(\mathcal{H}a^2+\mathcal{K})}{\mathcal{K}} - \frac{1}{R_c R_v}\right) \pm \sqrt{\left(\frac{(\mathcal{H}a^2+\mathcal{K})}{\mathcal{K}} - \frac{1}{R_c R_v}\right)^2 + \frac{4}{R_c R_v}}\right]. \tag{4.80}$$

4.2.5 Numerical Solution

The momentum equations for fluid and dust particles given by eqs. (4.47) and (4.48) under the initial and boundary conditions (4.49) are solved numerically using implicit finite difference method. The procedure involves the replacement of the partial differential eqs. (4.47) and (4.48) into the finite difference equations at the grid point. They are in order as follows:

$$\begin{aligned}\frac{u_f(i,j)-u_f(i,j-1)}{\triangle\eta} &= \frac{[u_f(i+1,j)-2u_f(i,j)+u_f(i-1,j)]}{(\triangle r)^2} \\ &+ \frac{1}{r(i)}\frac{[u_f(i+1,j)-u_f(i-1,j)]}{2\triangle r} \\ &+ \mathcal{K}[u_p(i,j)-u_f(i,j)] - \mathcal{H}a^2[u_f(i,j)-K]\end{aligned} \tag{4.81}$$

$$\begin{aligned}\frac{u_p(i,j)-u_p(i,j-1)}{\triangle\eta} &= \frac{R_c R_v[u_p(i+1,j)-2u_p(i,j)+u_p(i-1,j)]}{(\triangle r)^2} \\ &+ \frac{R_c R_v}{r(i)}\frac{[u_p(i+1,j)-u_p(i-1,j)]}{2\triangle r} \\ &+ \mathcal{K}[u_f(i,j)-u_p(i,j)].\end{aligned} \tag{4.82}$$

Here the index i refers to r and j refers to η. The time derivative is replaced by the backward difference formula, while the spatial derivatives are replaced by central difference formula. The above equations are solved by Thomas algorithm by manipulating into a system of linear algebraic equations in the tridiagonal form. At each time step, the process of numerical integration for every dependent variable starts from the first neighbouring grid point of the outer surface of the inner cylinder at $r = 1$ and proceeds towards the inner surface of the outer cylinder at $r = \varsigma$. The process of computation is advanced until a steady state is approached by satisfying the following convergence criterion:

$$\frac{\sum |A_{i,j+1} - A_{i,j}|}{M^* |A|_{max}} \leq 10^{-6} \tag{4.83}$$

with respect to the fluid and dust particle velocity fields.

Here $A_{i,j}$ stands for the velocity field of the fluid and dust particle, M^* is the number of interior grid points and $|A|_{max}$ is the maximum absolute value of $A_{i,j}$. In the numerical computation special attention is needed to specify $\triangle\eta$ to get steady state solution as rapid as possible, yet small enough to avoid instabilities. It is set, which is suitable for the present computation, as

$$\triangle\eta = Stabr \times (\triangle r)^2 \tag{4.84}$$

The parameter *Stabr* is determined by numerical experimentation in order to achieve convergence and stability of the solution procedure. Numerical

experiments show that the value 2 is suitable for the present numerical computation. In order to confirm the validity of the numerical solution, the numerical results are compared with analytical solution derived for steady state problem. The obtained numerical values using implicit finite difference method at steady state are in excellent agreement with numerical values obtained from analytical solutions. Also, the result obtained using implicit finite difference and Riemann-sum for fluid and dust particle velocity and skin-friction are presented in Tables I & II respectively. These tables reveal that there is an excellent agreement in numerical values for both method. An alternative accurate and also efficient numerical method of solving this problem is the pseudo-spectral methods. This method was used by Avilla et al. (2007) in the stability control and catastrophic transition in a forced Taylor-Couette system, details can be found in Fornberg (1998).

Table 4.1: Numerical values of the velocity obtained using the Riemann-sum approximation method and that obtained using finite difference method for both the fluid and the particle phases when $\eta = 0.2$, $K = 1$, $\mathcal{K} = 50$, $R_c = 0.25$ and $\mathcal{H}a = 2$.

		Velocity			
		Riemann − sum		*Finite Difference*	
r	R_v	*Fluid*	*Particle*	*Fluid*	*Particle*
1.2	1.0	0.2669	0.2448	0.2650	0.2426
	1.5	0.2735	0.2508	0.2716	0.2486
	2.0	0.2796	0.2567	0.2778	0.2546
1.4	1.0	0.4523	0.4264	0.4493	0.4229
	1.5	0.4651	0.4411	0.4622	0.4377
	2.0	0.4763	0.4538	0.4735	0.4506
1.6	1.0	0.6254	0.6023	0.6223	0.5987
	1.5	0.6397	0.6199	0.6369	0.6165
	2.0	0.6518	0.6343	0.6490	0.6311
1.8	1.0	0.8103	0.7969	0.8084	0.7946
	1.5	0.8197	0.8086	0.8179	0.8065
	2.0	0.8273	0.8179	0.8257	0.8159

Table 4.2: Numerical values of the steady state skin friction obtained using the Riemann-sum approximation method and that obtained using finite difference method when $\mathcal{K} = 50$, $R_c = 0.25$ and $\mathcal{H}a = 2$.

			Steady state skin friction			
			Riemann − sum		*Finite difference*	
r	K	R_v	*Fluid*	*Particle*	*Fluid*	*Particle*
1.0	0	1.0	1.6659	1.4403	1.6637	1.4456
		1.5	1.6200	1.3605	1.6176	1.3647
		2.0	1.5828	1.2987	0.7884	0.9935
	1	1.0	0.4416	0.4487	0.4414	0.4486
		1.5	0.4592	0.4694	0.4591	0.4693
		2.0	0.4744	0.4873	0.4743	0.4872
2.0	0	1.0	0.8831	0.8974	0.8825	0.8968
		1.5	0.9185	0.9388	0.9178	0.9382
		2.0	0.9489	0.9746	0.9483	0.9740
	1	1.0	2.3919	2.1660	2.3880	2.1705
		1.5	2.3458	2.0858	2.3416	2.0892
		2.0	2.3083	2.0237	2.3041	2.0265

4.2.6 Result and Discussion

In order to get a physical insight into the problem, a MATLAB programme is written to compute and generate the graphs for the velocity of both phases and their skin frictions. Unless otherwise stated, we employed the following parameters: $\mathcal{K} = 50.0$, $R_v = 1.0$, $R_c = 0.25$, $\mathcal{H}a = 2$, $\varsigma = 2$ and $\eta = 0.5$ in generating the line graphs in Figures 4.14–4.25. We however plotted contour graphs where necessary in order to see clearly the effect some parameters. It is important to know that the graphs on the left side of the figures corresponds to when $K = 0$, while that on the right corresponds to when $K = 1$. Figure 4.14 shows the effect of time η on the fluid phase velocity u_f. In Figure 4.14a, we see that u_f increases with time until it reaches its steady state, similarly, when $K = 1$ as observed in Figure 4.13b, u_f also increases with time. The particle phase

velocity u_p follows the same pattern of behaviour in Figure 4.15. The velocity of both the fluid and the particle phases increases from their initial value at the boundary to one at the moving cylinder through layers of different depths. The numerical values obtained for the velocities are always less when the magnetic field is fixed relative to the fluid than when fixed relative to the moving cylinder. The variation of u_f against the Hartmann number $\mathcal{H}a$ is shown in Figure 4.16, u_f is observed in Figure 4.16a to decrease with an increase in $\mathcal{H}a$ when $K = 0$, however, in Figure 4.16b, an increase in $\mathcal{H}a$ is seen to lead to an increase in u_f. This physical facts can be explained because the magnetic field is supporting the fliud motion when the magnetic lines of force are fixed relative to the moving cylinder. In Figure 4.17a, u_p is seen to follow the same trend of behaviour as u_f. The effect of the viscosity ratio R_v and time η on both u_f and u_p are depicted in Figures 4.18 and 4.19 respectively at the centre of the annulus gap ($r = 1.5$), u_f is seen to increase with R_v and η for $K = 0$ and $K = 1$. Figures 4.20 and 4.21 shows the effect of R_c ($= f_p/f_f$) on the behaviour of both fluid and particle velocities, where f_f and f_p depicts the substance quantity of mixture of fluid and particle respectively. We observe that an increase in R_c when $K = 0$, results into an increase in the velocities of both phases. However, when $K = 1$ the same trend is observed only at small time ($\eta < 0.5$). As the time is further increased, an increase in the particle concentration leads to a decrease in the velocities of both the fluid and the particle phases as observed in Figures 4.20b and 4.21b.

The skin frictions for both phases at the outer surface of the inner cylinder

($r = 1$) and at the inner surface of the outer cylinder ($r = 2$) are presented in Figures 4.22–4.25. The variation of the fluid-phase skin friction τ_1 is observed in Figure 4.22 to increase with time on the stationary cylinder for both $K = 0$ and $K = 1$. It also increases with R_v when $K = 0$, however, when $K = 1$, we noticed in Figure 4.22b that at small time, the effect of R_v on the skin friction is negligible. As the time is increased, a decrease in τ_1 due to an increase in R_v is noticed. The particle phase skin friction, τ_2 is observed in Figure 4.23 to follow a similar trend with that of the fluid phase. On the inner surface of the outer cylinder ($r = 2$), we noticed in Figure 4.24a that τ_f decreases with R_v and increases with time when $K = 0$. In Figure 4.24b when $K = 1$, an increase in the magnitude of τ_f due to an increase in R_v is noticed. However, a reversal in behaviour is seen when $\eta > 0.5$; where an increase in R_v leads to a decrease in the magnitude of τ_f. The response of τ_p to R_v is depicted in Figure 4.25, the magnitude of τ_p is seen to decrease with R_v and decreases with time when $K = 0$ and $K = 1$. The behaviour of the skin friction is in agreement with the behaviour of the velocities of the two phases earlier discussed. In addition, a careful study of Figures 4.22–4.25 reveals that the skin frictions at the opposite cylinders are seen to be of opposite sign; at the outer surface of the inner cylinder it is positive and negative at the inner surface of the outer cylinder.

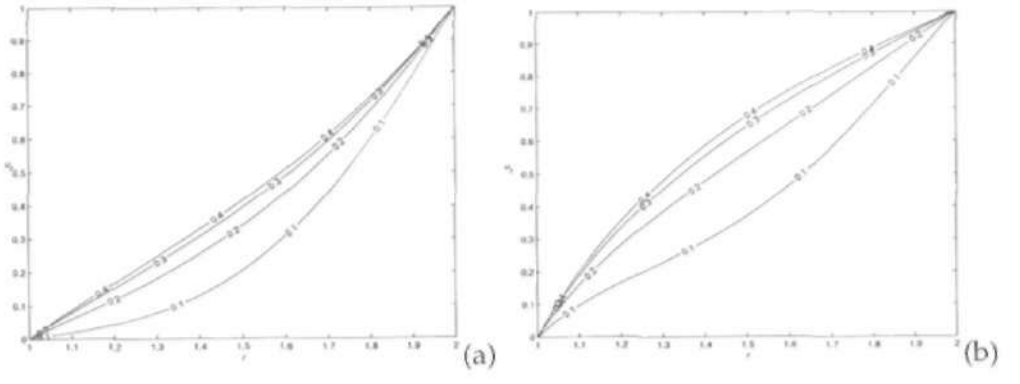


Figure 4.14: Profile of the fluid phase velocity u_f showing the effect of time with $K = 0$ and $K = 1$ represented by a and b respectively ($\mathcal{K} = 50.0$, $R_v = 1.0$, $R_c = 0.25$ and $\mathcal{H}a = 2$).

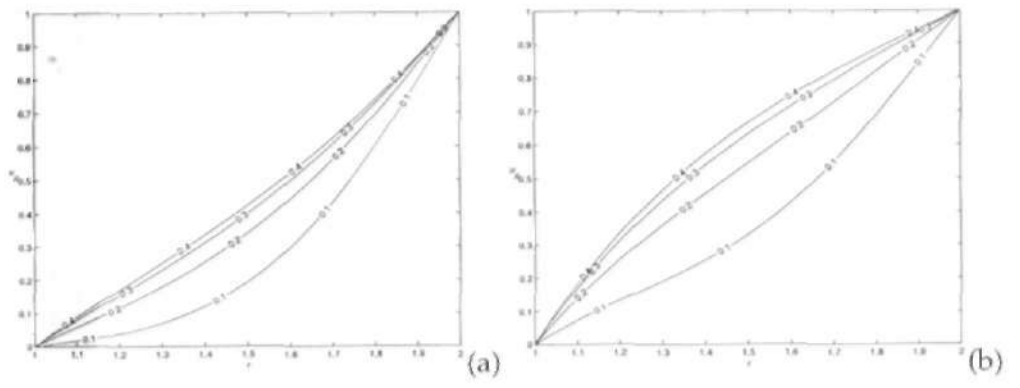


Figure 4.15: Profile of the particle phase velocity u_p showing the effect of time with $K = 0$ and $K = 1$ represented by a and b respectively ($\mathcal{K} = 50.0$, $R_v = 1.0$, $R_c = 0.25$ and $\mathcal{H}a = 2$).

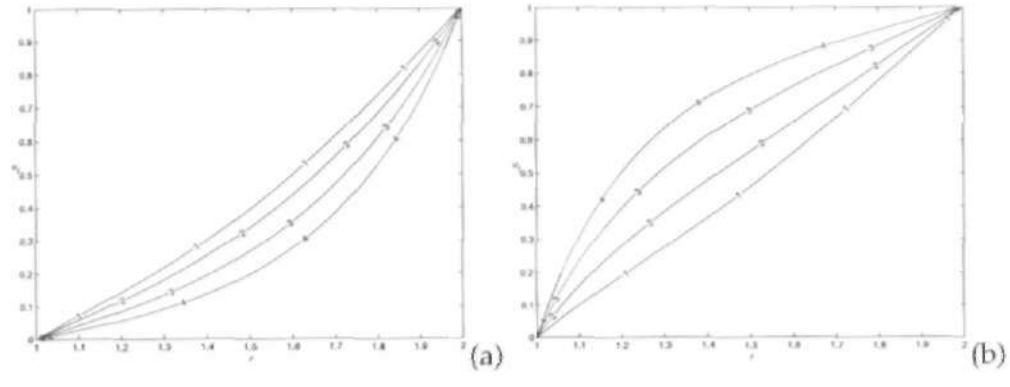


Figure 4.16: Profile of the fluid phase velocity u_f showing the effect of $\mathcal{H}a$ with $K = 0$ and $K = 1$ represented by a and b respectively ($\mathcal{K} = 50.0$, $R_v = 1.0$, $R_c = 0.25$ and $\eta = 0.5$).

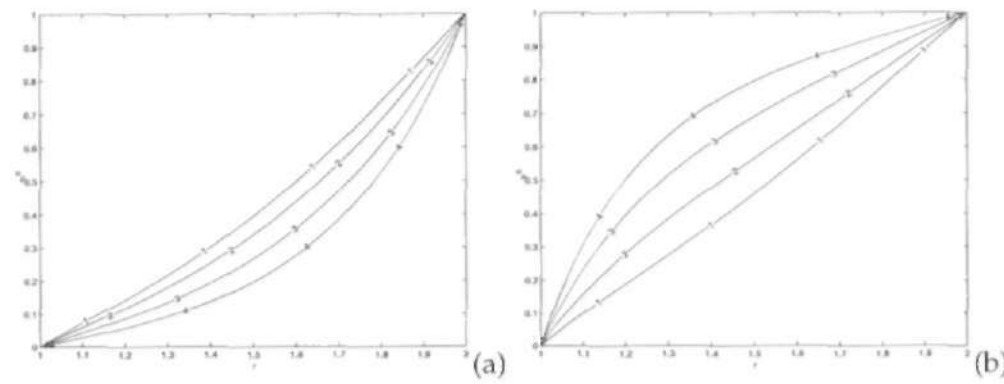


Figure 4.17: Profile of the fluid phase velocity u_p showing the effect of $\mathcal{H}a$ with $K = 0$ and $K = 1$ represented by a and b respectively ($\mathcal{K} = 50.0$, $R_v = 1.0$, $R_c = 0.25$ and $\eta = 0.5$).

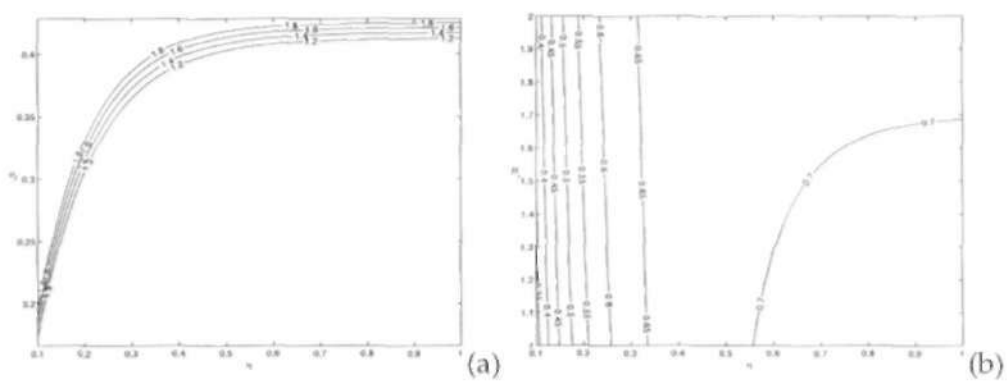


Figure 4.18: Profile of the fluid phase velocity u_f showing the effect of R_v and η with $K = 0$ and $K = 1$ represented by a and b respectively ($\mathcal{K} = 50.0$, $r = 1.5$, $R_c = 0.25$, $\mathcal{H}a = 2.0$ and $\eta = 0.5$).

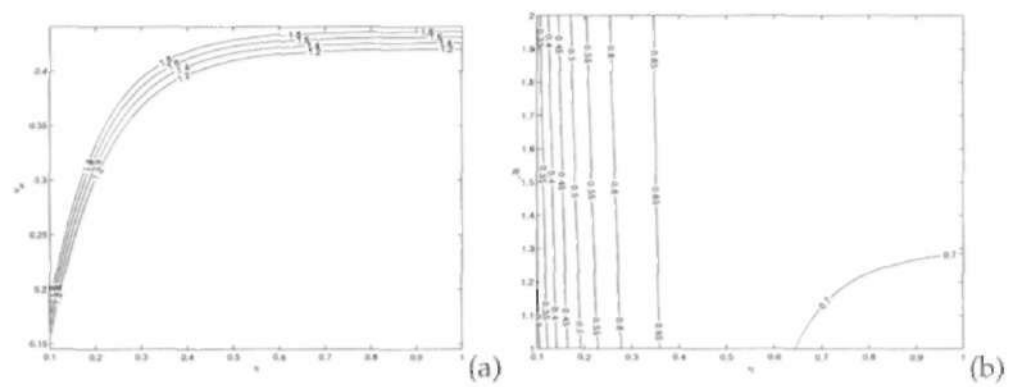


Figure 4.19: Profile of the fluid phase velocity u_p showing the effect of R_v and η with $K = 0$ and $K = 1$ represented by a and b respectively ($\mathcal{K} = 50.0$, $r = 1.5$, $R_c = 0.25$, $\mathcal{H}a = 2.0$ and $\eta = 0.5$).

480026

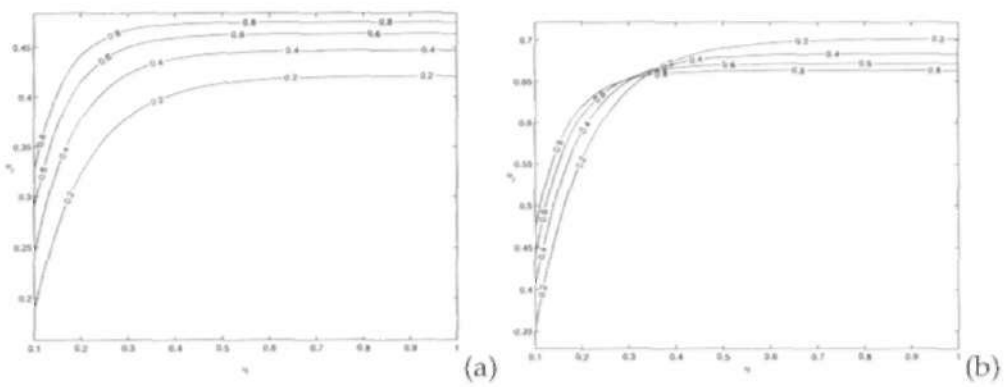


Figure 4.20: Profile of the fluid phase velocity u_f showing the effect of R_c and η with $K = 0$ and $K = 1$ represented by a and b respectively ($\mathcal{K} = 50.0$, $r = 1.5$, $R_v = 1.0$, $\mathcal{H}a = 2.0$ and $\eta = 0.5$).

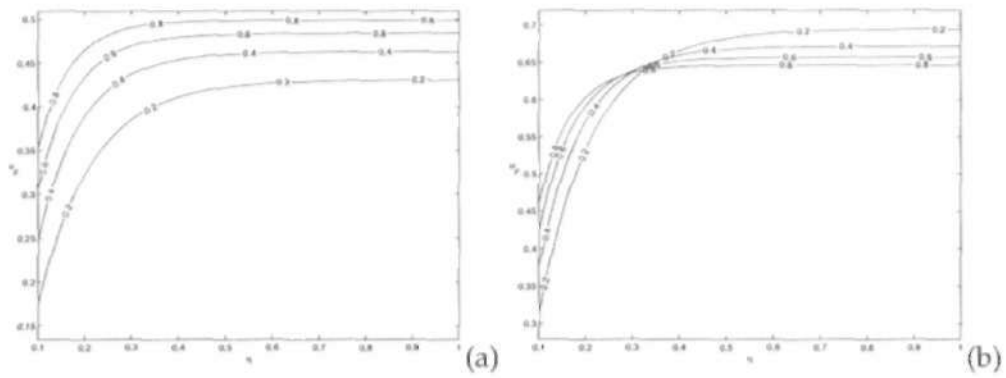


Figure 4.21: Profile of the particle phase velocity u_p showing the effect of R_c and η with $K = 0$ and $K = 1$ represented by a and b respectively ($\mathcal{K} = 50.0$, $r = 1.5$, $R_v = 1.0$, $\mathcal{H}a = 2.0$ and $\eta = 0.5$).

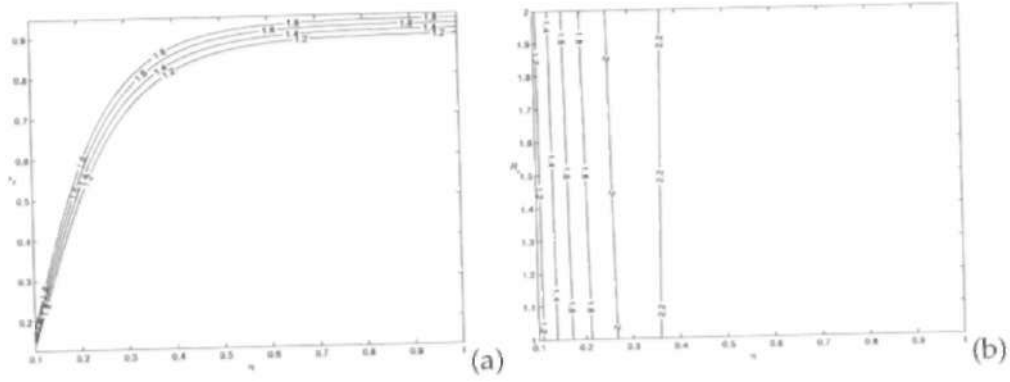


Figure 4.22: Variation of the fluid phase skin friction on the outer surface of the inner cylinder ($r = 1$) showing the effect of R_v and η ($\mathcal{K} = 50.0$, $\mathcal{H}a = 2.0$ and $R_c = 0.25$).

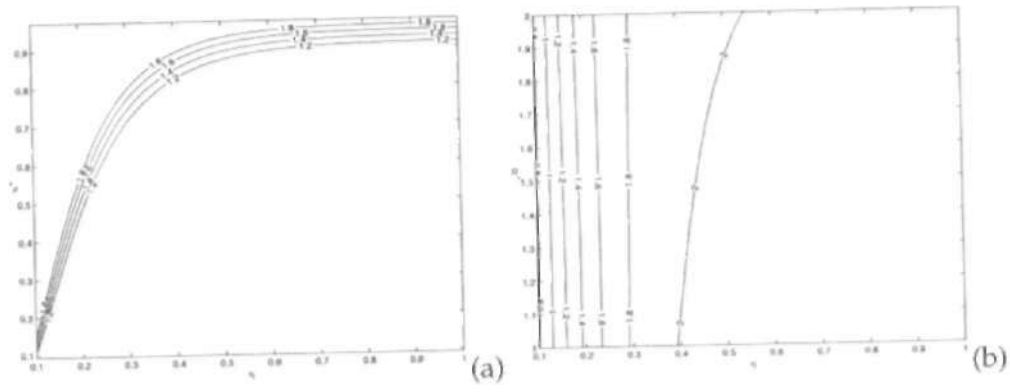


Figure 4.23: Variation of the particle phase skin friction on the outer surface of the inner cylinder ($r = 1$) showing the effect of R_v and η ($\mathcal{K} = 50.0$, $\mathcal{H}a = 2.0$ and $R_c = 0.25$).

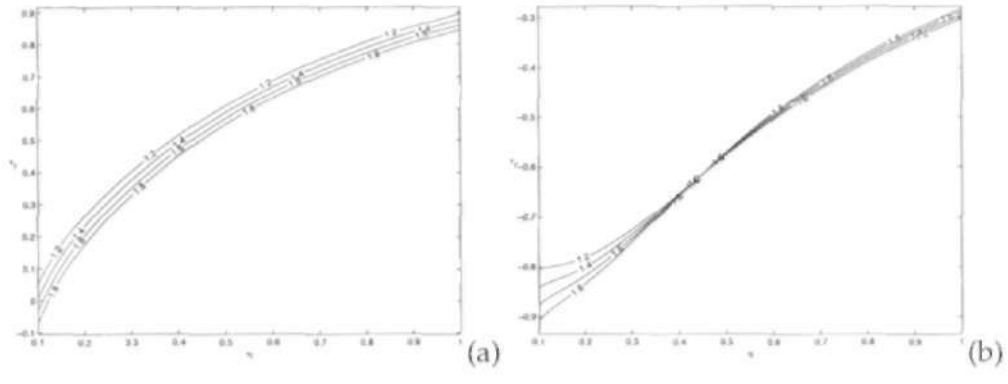


Figure 4.24: Variation of the fluid phase skin friction on the inner surface of the outer cylinder ($r = 2$) showing the effect of R_v and η ($\mathcal{K} = 50.0$, $\mathcal{H}a = 2.0$ and $R_c = 0.25$).

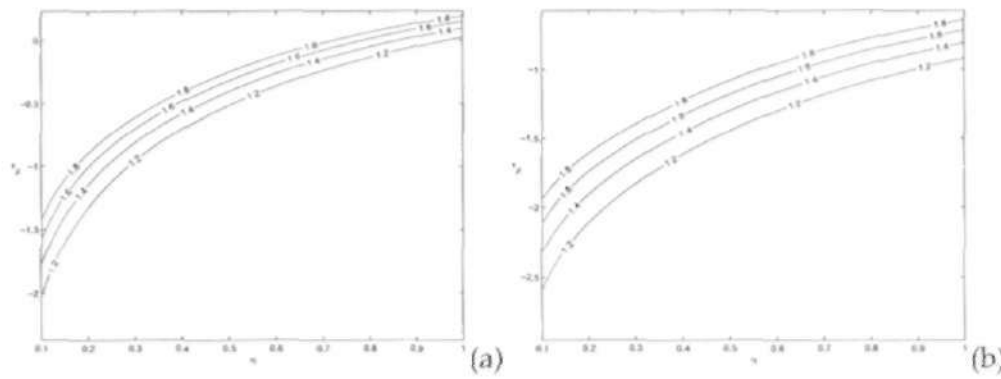


Figure 4.25: Variation of the particle phase skin friction on the inner surface of the outer cylinder ($r = 2$) showing the effect of R_v and η ($\mathcal{K} = 50.0$, $\mathcal{H}a = 2.0$ and $R_c = 0.25$).

4.3 CONCLUDING REMARKS

In this chapter, we have employed the combination of the Laplace transform technique, D'Alembert's and Riemann-sum approximation methods to obtain the solutions of unsteady MHD two-phase flow of fluid-particle suspension in both the parallel plate channel and the annular gap of two concentric cylinders. We have considered the effect of various dimensionless parameters occuring in the problem such as the Hartmann number, the viscosity ratio and the ratio of the substance quantity of mixture on the flow field. It is observed that both the velocity of the fluid phase and the particle phase decrease with increase in Hartmann number.

The skin friction for both the fluid and the particle phases decreases with time on both plates until a steady state is reached, it is also observed to decrease with increase in the particle viscosity on the moving plate while an opposite behaviour has been noticed on the stationary plate. For the annulus, the skin frictions at the opposite cylinders are seen to be of opposite sign; at the outer surface of the inner cylinder it is positive and negative at the inner surface of the outer cylinder. The results obtained demonstrates the reliability of the Riemann-sum approximation method as comparisons made with those obtained using the implicit finite difference method shows consistency between the two.

CHAPTER 5

MHD FREE CONVECTIVE FLOW

Free convection flow field is a self-sustained flow driven by the presence of a temperature gradient. This is opposed to a forced convection flow where external means are used to provide the flow. As a result of the temperature difference, the density field is not uniform. Buoyancy will therefore induce a flow current due to the gravitational field and the variation in the density field. In general, a free convection heat transfer is usually much smaller compared to a forced convection heat transfer, it is therefore important only when no external flow exists.

The effect of magnetic field on the free-convective flow has been presented by Georgantopoulos et al. (1979) and Raptis and Singh (1983) for the cases of the magnetc field being fixed relative to the fluid and the plate respectively. Singh and Singh (1989) extended the classical Rayleigh problem to the case of the hydromagnetic free-convective flow of an electrically conducting and incompressible viscous fluid past an infinite vertical naturally permeable wall in a rotating system. Ferdows et al. (2004) analysed free convection flow with variable suction in the presence of thermal radiation while Alam et al. (2006) studied Dufour and Soret effect with variable suction on unsteady MHD free

convection flow along a porous plate. Singha and Deka (2006) investigated the unsteady viscous incompressible free convection flow of an electrically conducting fluid between two heated vertical parallel plates in the presence of a uniform magnetic field applied transversely to the flow. Jha (2001) examined the combined effect of natural convection and uniform transverse magnetic field on the Couette flow of an electrically conducting fluid between two parallel plates for the impulsive motion of one of the plates. Recently, an exact analysis of the natural convection in unsteady Couette flow of a viscous incompressible fluid confined between two vertical parallel plates in the presence of thermal radiation was performed by Narahari (2009).

Entropy generation due to fluid flow and heat transfer inside a horizontal channel made of two parallel plates under the effect of transverse magnetic field was numerically investigated by Damseh et al. (2008). Aldoss et al. (1996) investigated analytically the effect of a radial magnetic field on the flow and heat transfer characteristics of mixed convection from a horizontal circular cylinder. Using Green's function method, Al-Nimr and Alkam (1999) presented analytical solutions for transient MHD fully developed natural convection in open-ended vertical concentric annuli. The analytical solutions for fully developed MHD natural convection flow in open-ended vertical porous channels was presented by Al-Nimr and Hader (1999), while the effect of magnetic field on natural convection in a vertical cylindrical annulus was studied by Sankar et al. (2006). The numerical study to understand the effect of rotation on the axisymmetric

flow driven by buoyancy in an annular cavity formed by two concentric vertical cylinders which rotate about their axis with different angular velocities was conducted by Venkatachalappa et al. (2001). Weng and Chu (1996) carried out a numerical study of the effects of thermal radiation on the heat transfer of steady natural convection in a participating fluid contained inside a cylindrical annulus.

More recently, Ravi and Singh (2011) considered the natural convective flow of a polar fluid in open-ended vertical concentric annuli. Despite the vast amount of works that has been done on the free-convective flow under different conditions, little work seems to have been carried out on the MHD free-convective Couette flow. We therefore considered the MHD free convective Couette flow between two parallel vertical porous plates. We also carry out a theoretical analysis of an unsteady MHD free convective flow of a viscous incompressible and electrically conducting fliud between two concentric vertical cylinders considering thermal boundary condition of the second kind at the outer surface of the inner cylinder. The solution of the governing equations has been obtained by using a Laplace transform technique. The effect of the various flow parameters entering into the problem such as Prandtl number, Grashof number and the suction/injection parameter on the temperature, velocity, rate of heat transfer and the skin friction are presented graphically and discussed.

5.1 MHD FREE CONVECTIVE COUETTE FLOW WITH SUCTION AND INJECTION[1]

This section considers the unsteady MHD free convective Couette flow of a viscous incompressible electrically conducting fluid between two parallel vertical porous plates. Both cases of the applied magnetic field being fixed either to the fluid or to the moving porous plate are considered. The skin friction have been seen to decrease with both suction and injection on the surface of the moving plate when the channel is being cooled, while on the stationary plate, the magnitude of the skin friction increases with injection.

5.1.1 Mathematical Analysis

The motion of an unsteady two-dimentional viscous, incompressible and electrically conducting fluid filling the gap between two parallel vertical infinite porous plates is considered. The two porous plates are located on the z'-axis and extend from $x' = -\infty$ to ∞ and $z' = -\infty$ to ∞. The fluid flows between the two porous plates in the x'-direction which is taken along the vertical porous plate in the upward direction and the z'-axis is taken to be normal to the porous plate. A uniform magnetic field B_0 is assumed to be acting perpendicular to the porous plates. At time $t \leq 0$, the fluid and the porous plate are assumed to be at rest and at temperature T_0. When $t > 0$ the left porous plate begins to move in its own plane with a velocity Ut^n where U is a constant and its temperature

[1]Jha and Apere (2011b) Published in
Trans. ASME J. Heat Transfer **133** 092501 (2011) ; doi: 10.1115/1.4003902

instatanoeusly rises or falls to T_w. Under the usual Boussinesq approximation, the governing equations are

$$\frac{\partial u'}{\partial t} - w_0 \frac{\partial u'}{\partial z'} = \nu \frac{\partial^2 u'}{\partial z'^2} + g\xi(T' - T_0) - \frac{\sigma B_0^2}{\rho} u' \tag{5.1}$$

$$\frac{\partial T'}{\partial t} - w_0 \frac{\partial T'}{\partial z'} = \frac{\kappa}{\rho C_p} \frac{\partial^2 T'}{\partial z'^2}, \tag{5.2}$$

where w_0 is the normal velocity of suction or injection at the plate according as $w_0 > 0$ or $w_0 < 0$ respectively. $w_0 = 0$ represents the case of non-permeable plates. The initial and boundary conditions for the problem are

$$\begin{aligned} u' &= 0,\ T' = T_0,\quad for\ 0 \le z' \le h;\ at\ t \le 0 \\ u' &= Ut^n,\ T' = T_w,\ when\ z' = 0\ at\ t > 0 \\ u' &= 0,\ T' = T_0,\ when\ z' = h\ at\ t > 0 \end{aligned} \tag{5.3}$$

Eq. (5.1) is valid when the magnetic field is fixed relative to the fluid, if the magnetic lines of force are fixed relative to the moving porous plate, we must account for the relative motion, then eq. (5.1) can be replaced with

$$\frac{\partial u'}{\partial t} - w_0 \frac{\partial u'}{\partial z'} = \nu \frac{\partial^2 u'}{\partial z'^2} + g\xi(T' - T_0) - \frac{\sigma B_0^2}{\rho}(u' - Ut^n) \tag{5.4}$$

Eq. (5.1) and (5.4) are combined together to obtain one single equation

$$\frac{\partial u'}{\partial t} - w_0 \frac{\partial u'}{\partial z'} = \nu \frac{\partial^2 u'}{\partial z'^2} + g\xi(T' - T_0) - \frac{\sigma B_0^2}{\rho}(u' - KUt^n), \tag{5.5}$$

where

$$K = \begin{cases} 0 & \textit{when } B_0 \textit{ is fixed relative to the fluid} \\ 1 & \textit{when } B_0 \textit{ is fixed relative to the moving porous plate} \end{cases}$$

The flow described by eq. (5.5) is the general representation of the velocity distribution for the Couette flow between infinite parallel vertical porous plates of any conducting medium due to the movement of the left porous plate in the presence of free-convective currents. In order to analyse the specific flow profiles, we have considered the case when $n = 0$, which corresponds to the impulsive motion. Introducing the following dimensionless quantities in eqs. (5.2)–(5.5); $z = z'/h$, $u = u'/U$, $\eta = t\nu/h^2$, $\mathcal{H}_a = B_0 h\sqrt{\sigma/\nu\rho}$, $\mathcal{S} = w_0 h/\nu$, $Pr = \mu C_p/\kappa$, $Gr = g\xi(T_w - T_0)h^2/U\nu$, *and* $\theta = (T' - T_0)/(T_w - T_0)$. We now have

$$\frac{\partial \theta}{\partial \eta} - \mathcal{S}\frac{\partial \theta}{\partial z} = \frac{1}{Pr}\frac{\partial^2 \theta}{\partial z^2} \tag{5.6}$$

$$\frac{\partial u}{\partial \eta} - \mathcal{S}\frac{\partial u}{\partial z} = \frac{\partial^2 u}{\partial z^2} - \mathcal{H}_a^2(u - K) + Gr\theta, \tag{5.7}$$

and also the following dimensionless initial and boundary conditions.

$$\begin{aligned} u &= 0,\ \theta = 0,\quad for\ 0 \le z \le 1\ \ at\ \eta \le 0; \\ u &= 1,\ \theta = 1,\ \ when\ z = 0\ \ at\ \eta > 0 \\ u &= 0,\ \theta = 0,\ \ when\ z = 1\ \ at\ \eta > 0. \end{aligned} \tag{5.8}$$

The solutions of eqs. (5.6) and (5.7) can be obtained by using the Laplace transforms technique as follows:

$$\frac{d^2\bar{\theta}}{dz^2} + \mathcal{S}Pr\frac{d\bar{\theta}}{dz} - sPr\bar{\theta} = 0 \tag{5.9}$$

$$\frac{d^2\bar{u}}{dz^2} + \mathcal{S}\frac{d\bar{u}}{dz} - (\mathcal{H}_a^2 + s)\bar{u} = -Gr\bar{\theta} - \frac{\mathcal{H}_a^2 K}{s}. \tag{5.10}$$

The solutions of eqs. (5.9) and (5.10) are respectively:

$$\bar{\theta}(z,s) = \frac{1}{s}\frac{sinh(\delta(1-z))}{sinh(\delta)}\exp(-\frac{\mathcal{S}Pr}{2}z) \tag{5.11}$$

$$\begin{aligned} \bar{u}(z,s) &= [Acosh(\psi z) + Bsinh(\psi z)]\exp(-\frac{\mathcal{S}}{2}z) + \frac{\mathcal{H}_a^2 K}{s(\mathcal{H}_a^2 + s)} \\ - &\quad \frac{Gr}{2ssinh(\delta)}\left[\frac{\exp(\delta(1-z))}{C} - \frac{\exp(-\delta(1-z))}{D}\right] \\ \times &\quad \exp(-\frac{\mathcal{S}Pr}{2}z), \end{aligned} \tag{5.12}$$

where

$$A = \frac{1}{s} - \frac{\mathcal{H}_a^2 K}{s(\mathcal{H}_a^2+s)} + \frac{Gr}{2ssinh(\delta)}\left[\frac{\exp(\delta)}{C} - \frac{\exp(-\delta)}{D}\right] \tag{5.13}$$

$$\begin{aligned} B &= -A\frac{cosh(\psi)}{sinh(\psi)} - \frac{\mathcal{H}_a^2 K}{s(\mathcal{H}_a^2+s)sinh(\psi)}\exp(\frac{S}{2}) + \frac{Gr}{2ssinh(\delta)sinh(\psi)} \\ &\times \left[\frac{1}{C} - \frac{1}{D}\right]\exp((\frac{S}{2}(1-Pr)) \end{aligned} \tag{5.14}$$

$$C = \left(\delta + \frac{SPr}{2}\right)^2 - \mathcal{S}\left(\delta + \frac{SPr}{2}\right) - (\mathcal{H}_a^2 + s) \tag{5.15}$$

$$D = \left(\delta - \frac{SPr}{2}\right)^2 + S\left(\delta - \frac{SPr}{2}\right) - (\mathcal{H}_a^2 + s) \tag{5.16}$$

$$\delta = \sqrt{\left(\frac{SPr}{2}\right)^2 + sPr} \tag{5.17}$$

$$\psi = \sqrt{\left(\frac{S}{2}\right)^2 + (\mathcal{H}_a^2 + s)}. \tag{5.18}$$

Using the Riemann-sum approximation method to determine the temperature and the velocity in the time domain, we have as follows:

$$\theta(z,\eta) = \frac{e^{\gamma\eta}}{\eta}\left[\frac{1}{2}\bar{\theta}(z,\gamma) + Re\sum_{k=1}^{N}\bar{\theta}(z,\gamma+\frac{ik\pi}{\eta})(-1)^k\right] \tag{5.19}$$

$$u(z,\eta) = \frac{e^{\gamma\eta}}{\eta}\left[\frac{1}{2}\bar{u}(z,\gamma) + Re\sum_{k=1}^{N}\bar{u}(z,\gamma+\frac{ik\pi}{\eta})(-1)^k\right]. \tag{5.20}$$

5.1.2 Rate of Heat Transfer and Skin Friction

The rate of heat transfer which is represented by the Nusselt number Nu and the skin friction τ are similarly obtained by differentiating the temperature and the velocity, respectively, with respect to z as follows:

By nature

$$Nu = -\frac{d\theta}{dz} = \frac{e^{\gamma\eta}}{\eta}\left[\frac{1}{2}\bar{\theta}_1(z,\gamma) + Re\sum_{k=1}^{N}\bar{\theta}_1(z,\gamma+\frac{ik\pi}{\eta})(-1)^k\right] \tag{5.21}$$

$$\tau = \frac{du}{dz} = \frac{e^{\varepsilon\eta}}{\eta}\left[\frac{1}{2}\bar{u}_1(z,\gamma) + Re\sum_{k=1}^{N}\bar{u}_1(z,\gamma+\frac{ik\pi}{\eta})(-1)^k\right], \tag{5.22}$$

where

$$\begin{aligned}\bar{\theta}_1(z,s) &= -\mathcal{S}P_r\frac{sinh(\delta(1-z))}{2ssinh(\delta)}\exp((-\mathcal{S}Pr/2)z)\\ &- \frac{cosh(\delta(1-z))}{ssinh(\delta)}\exp((-\mathcal{S}Pr/2)z)\end{aligned} \tag{5.23}$$

$$\begin{aligned}\bar{u}_1(z,s) &= -\frac{\mathcal{S}}{2}\exp(-\frac{\mathcal{S}z}{2})\left[Acosh(\psi z) + Bsinh(\psi z)\right]\\ &+ \psi\exp(-\frac{s\mathcal{S}z}{2})\left[Asinh(\psi z) + Bcosh(\psi z)\right]\\ &+ \frac{Gr}{2ssinh(\delta)}\Big[\exp(-(\delta+\frac{\mathcal{S}Pr}{2})z)\frac{\exp(\delta)}{C}(\delta+\frac{\mathcal{S}Pr}{2})\\ &+ \exp((\delta-\frac{\mathcal{S}Pr}{2})z)\frac{\exp(-\delta)}{D}(\delta-\frac{\mathcal{S}Pr}{2})\Big].\end{aligned} \tag{5.24}$$

Eqs. (5.21) and (5.22) represents the general expressions for the rate of heat transfer and skin friction respectively between different fluid layers amidst the two porous plates. The rate of heat transfer and the skin friction on the two porous plates can then be calculated by setting $z = 0$ and $z = 1$ in eqs. (5.23) and (5.24).

5.1.3 Validation of the Method

In order to validate the accuracy of the Riemann-sum approximation method, we set out to find the solution of the steady state, which should coincide with the transient solution at large time. The expression for the steady state temperature and the velocity distribution u at this state is obtained by setting $\partial()/\partial t$ in eqs. (5.7) and (5.8) to zero. We now obtain the following ordinary differential equations

$$\frac{1}{Pr}\frac{d^2\theta_s}{dz^2} + \mathcal{S}\frac{d\theta_s}{dz} = 0 \tag{5.25}$$

$$\frac{d^2u_s}{dz^2} + \mathcal{S}\frac{du_s}{dy} = \mathcal{H}_a^2(u - K) - Gr\theta_s, \tag{5.26}$$

. The solutions of eqs. (5.25) and (5.26) using the boundary condition (5.8) are

$$\theta_s = \frac{sinh(\mathcal{S}Pr/2(1-z))}{sinh(\mathcal{S}Pr/2)}\exp(-\frac{\mathcal{S}Pr}{2}z) \tag{5.27}$$

$$
\begin{aligned}
u_s &= [A_1 cosh(\psi_1 z) + B_1 sinh(\psi_1 z)] \exp(-\frac{S}{2}z) + K \\
&- \frac{Gr}{2sinh(SPr/2)} \left[\frac{\exp(SPr/2(1-z)}{C_1} + \frac{\exp(-SPr/2(1-z))}{\mathcal{H}_a^2} \right] \\
&\times \exp(-\frac{SPr}{2}z), \qquad (5.28)
\end{aligned}
$$

where

$A_1 = 1 - K + \frac{Gr}{2sinh(SPr/2)} \left[\frac{\exp(SPr/2)}{C_1} + \frac{\exp(-SPr/2)}{\mathcal{H}_a^2} \right]$,

$B_1 = -A_1 \frac{cosh(\psi_1)}{sinh(\psi_1)} - \frac{K}{sinh(\psi_1)} \exp(\frac{S}{2}) + \frac{Gr}{2sinh(SPr/2)sinh(\psi_1)}$

$\times \left[\frac{1}{C_1} + \frac{1}{\mathcal{H}_a^2} \right] \exp((\frac{S}{2}(1-Pr))$

$C_1 = S^2Pr^2 - S^2Pr - \mathcal{H}_a^2$ and $\psi_1 = \sqrt{(\frac{S}{2})^2 + \mathcal{H}_a^2}$.

The results obtained for the velocity and the skin friction for the steady state are found to be in excellent agreement with those of eqs. (5.9) and (5.10) when the value of η is large. Also, the numerical values of the velocities obtained in this problem in the absence of suction and injection was compared with those obtained analytically by Jha (2001) in Table I. The excellent agreement between the two numerical values is evident in the Table 9.1.

5.1.4 Results and Discussion

In order to have a physical insight into the problem, a MATLAB programme is written to compute and generate the graphs for the temperature, velocity, rate of heat transfer and the skin friction for different values of the dimensionless parameters. Some representative results are presented in the form of line graphs in Figures 5.1-5.11 to interpret the effects of these parameters. A comparative

Table 5.1: Numerical values of the velocity obtained analytically in Jha's problem and that of Riemann-sum approximation method when $Gr = 10$, $Pr = 7$ and $\mathcal{S} = 0$ in the present problem

η	z	K	*Velocity* (u)			
			Jha (2001)'s *Result*		*Present Result*	
			$\mathcal{H}_a = 2$	$\mathcal{H}_a = 5$	$\mathcal{H}_a = 2$	$\mathcal{H}_a = 5$
0.2	0.2	0	0.7483	0.4379	0.7479	0.4375
		1	0.9665	1.0538	0.9667	1.0563
	0.4	0	0.4701	0.1752	0.4707	0.1752
		1	0.7878	0.9905	0.7884	0.9935
	0.6	0	0.2595	0.0638	0.2595	0.0639
		1	0.5766	0.8792	0.5772	0.8820
	0.8	0	0.1129	0.0202	0.1129	0.0202
		1	0.3312	0.6361	0.3317	0.6389
0.4	0. 2	0	0.8372	0.4715	0.8350	0.4696
		1	1.0681	1.0879	1.0669	1.09117
	0.4	0	0.5927	0.2148	0.5928	0.2149
		1	0.9301	1.0309	0.9313	1.0367
	0.6	0	0.3600	0.8898	0.3601	0.0898
		1	0.6975	0.9059	0.6986	0.9116
	0.8	0	0.1666	0.0311	0.1666	0.0311
		1	0.3975	0.6475	0.3984	0.6533

analysis is made when necessary between the cases of the magnetic field being fixed to the fluid and to the moving porous plate; this is depicted on the left and right panels respectively of the affected figures. It is obvious from eqs. (5.11) and (5.19) that the dimensionless temperature does not depend on the Grashof number Gr, the Hartmann number $\mathcal{H}_a$ and K. Hence, the variation of the temperature profiles are carried out on time η, the Prandtl number Pr and the suction/injection parameter $\mathcal{S}$ as shown in Figures 5.1 and 5.2. The variation of the temperature with respect to time is shown in Figure 5.1, we observe that the temperature increases with η until it finally reaches its steady state. The temperature is also observed to be higher near the left plate ($z = 0$) than at the

right plate ($z = 1$), this is due to the temperature raise of the left plate ($z = 0$). The variation of the temperature with both the Pr and the $\mathcal{S}$ at the centre of the channel ($z = 0.5$) is illustrated in Figure 5.2. It is observed that as Pr increases, the tempearature decrease and a further increase makes the temperature to tend to zero. This is because fluids with high Pr have a small thermal conductivity and high viscosity, which normally result into low heat penetration and a reduced thermal layer. Similarly, temperature is seen to decrease as $\mathcal{S}$ increases.

The velocity profile when the left plate is being cooled by the free convection currents is shown in Figure 5.3. This figure shows that the velocity is always positive and increases with time. It is at its peak on the impulsively started porous plate and decreases gradually to zero at the stationary plate, this behaviour is same for $K = 0$ and $K = 1$. In Figure 5.4, the velocity profile is shown for a plate that is being heated, a flow reversal is observed in this case as negative values of the velocity is obtained at all times. This phenomenon is due to the free convective currents which is moving within the channel, during this movement, the flow is opposed to these currents and hence there is a reverse flow in the channel. Figures 5.5 and 5.6 shows the effect of the Hartmann number on the flow velocity for both the cooling and the heating of the moving porous plate respectively. The velocity is noticed to decrease with an increase in $\mathcal{H}_a$ when $K = 0$ for both the cooling and heating of the porous plate, the reverse is the case when $K = 1$. It is observed in Figure 5.5 that the velocity increase with injection and decrease with suction for the cooling of the porous plate. This is in

total contrast to the heating of the porous plate as noticed in Figure 5.6. The rate of change of velocity with respect to S is observed to be higher when $K = 1$.

The combined effect of the Gr and S on the velocity at the middle of the channel ($z = 0.5$) is shown in Figure 5.7. The velocity increases as Gr increases positively and decreases as Gr increases negatively. The behaviour of S towards the velocity is influenced by the status of the porous plates; whether it is being cooled or heated. For the case when the porous plate is being cooled ($Gr > 0$), the velocity decreases as S increases, while for the heating ($Gr < 0$) the velocity is seen to increase. In the absence of convection current ($Gr = 0$), the velocity of the fluid is observed to be non-zero, this is the reaction of the fluid to the impulsive movement of the porous plate.

The rate of heat transfer on the two plates, which is represented by the Nusselt number Nu is presented in Figures 5.8 and 5.9. On the moving porous plate ($z = 0$) in Figure 5.8, Nu is observed to increase with injection and decrease with suction. Whereas, Pr has a dual effect on Nu depending on whether the channel is subjected to suction or injection. It has an increasing effect when the channel is being injected and a decreasing effect when the channel is subjected to suction. Contrarily, on the stationary porous plate ($z = 1$) as observed in Figure 5.9, Nu increases with suction and decreases with injection, while it increases with Pr notwithstanding whether the channel is subjected to suction or injection. The skin friction on the surface of the porous plates is presented in Figures 5.10 and 5.11. The skin friction decreases with both suction and injection on

the surface of the moving plate when the channel is being cooled ($Gr > 0$) as observed in Figure 5.10, while on the stationary plate, the τ increases with injection and decreases with suction for the heating of the channel. It is noticed that the effect of suction on the stationary plate is to suppress τ.

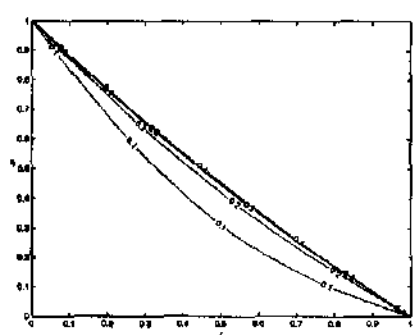


Figure 5.1: Temperature profile θ showing the effect of η ($Pr = 0.71$ and $\mathcal{S} = 0.5$.

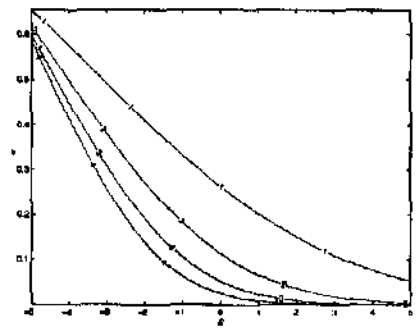


Figure 5.2: Temperature profile θ showing the effect of Pr and S at $\eta = 0.1$ at $z = 0.5$

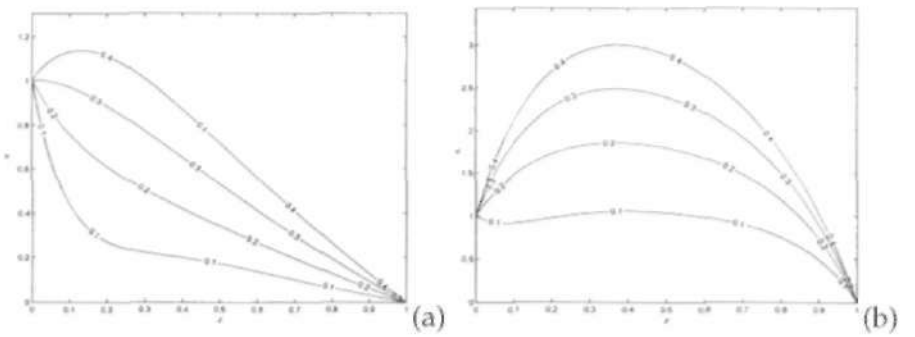


Figure 5.3: Velocity profile u for the cooling of the plate showing the effect of η with $K = 0$ and $K = 1$ represented by a and b respectively ($Pr = 0.71$, $\mathcal{S} = 0.5$, $Gr = 10$ and $\mathcal{H}_a = 2$).

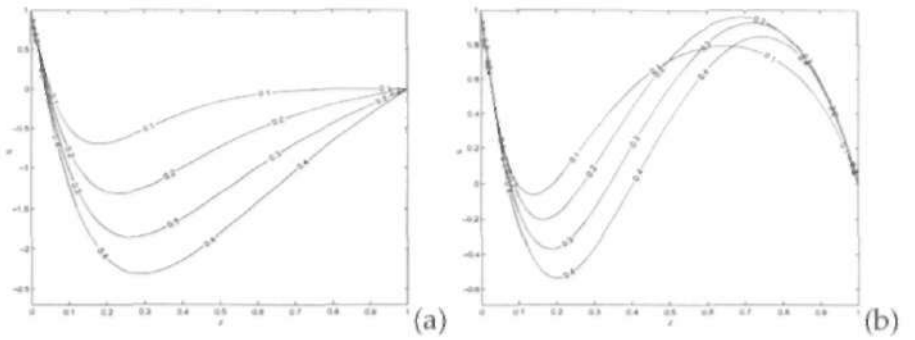


Figure 5.4: Velocity profile u for the heating of the plate showing the effect of time η with $K = 0$ and $K = 1$ represented by a and b respectively ($Pr = 0.5$, $\mathcal{S} = 0.5$, Gr=-10 and $\mathcal{H}_a = 2$).

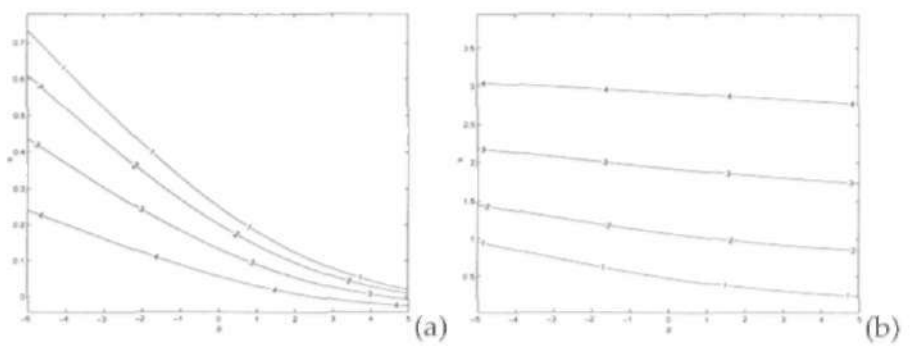


Figure 5.5: Velocity profile u for the cooling of the plate showing the effect of $\mathcal{H}_a$ and $\mathcal{S}$ with $K = 0$ and $K = 1$ represented by a and b respectively ($Gr = 10$, $Pr = 0.7$, $z = 0.5$ and $\eta = 0.1$).

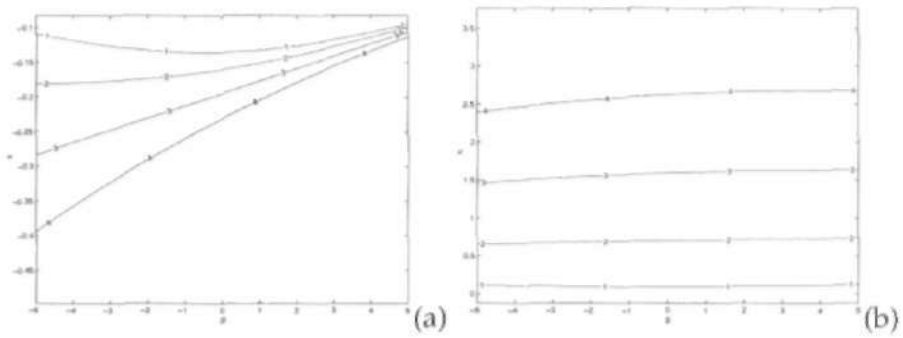


Figure 5.6: Velocity profile u for the heating of the plate showing the effect of $\mathcal{H}_a$ and $\mathcal{S}$ with $K = 0$ and $K = 1$ represented by a and b respectively ($Gr = -10$, $Pr = 0.71$, $z = 0.5$ and $\eta = 0.1$.

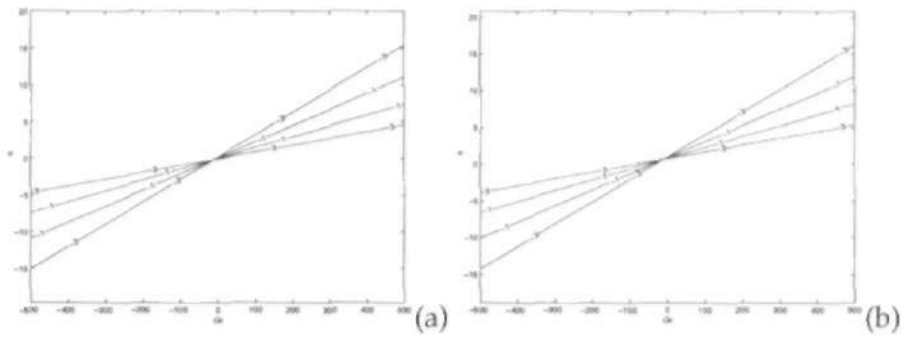


Figure 5.7: Velocity profile u showing the effect of Gr and S with $K = 0$ and $K = 1$ represented by a and b respectively ($z = 0.5$, $Pr = 0.71$, $\eta = 0.1$ and $\mathcal{H}_a = 2$).

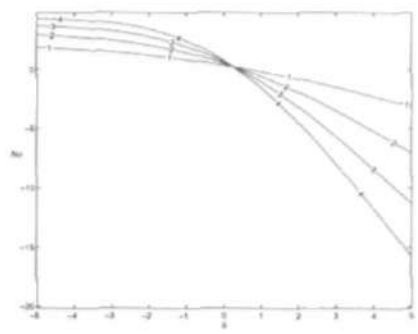


Figure 5.8: Rate of heat transfer at $z = 0$ showing the effect of Pr and S at $\eta = 0.1$.

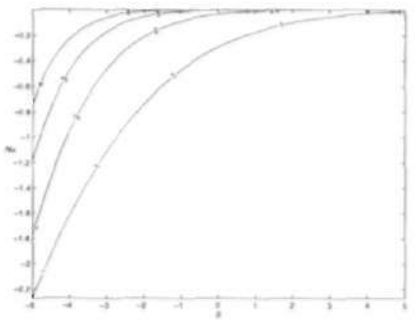


Figure 5.9: Rate of heat transfer at $z = 1$ showing the effect of Pr and S at $\eta = 0.1$.

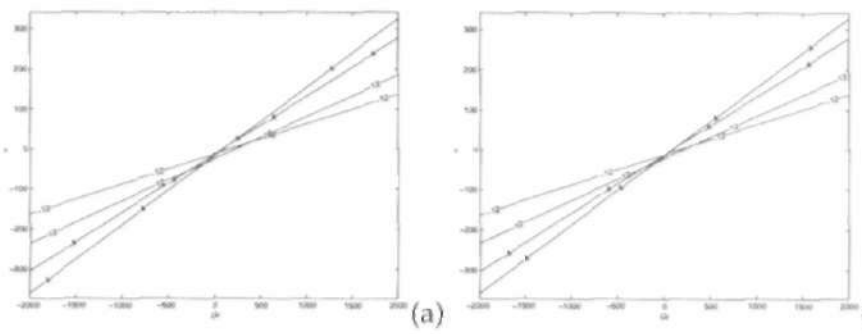


Figure 5.10: Skin friction on the plate at $z = 0$ showing the effect of Gr and S with $K = 0$ and $K = 1$ represented by a and b respectively ($Pr = 0.71$, $\eta = 0.1$ and $\mathcal{H}_a = 2$).

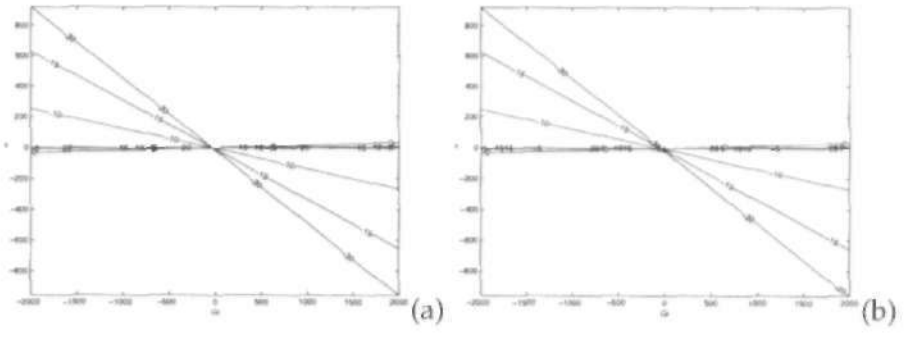


Figure 5.11: Skin friction on the plate at $z = 1$ showing the effect of Gr and S with $K = 0$ and $K = 1$ represented by a and b respectively ($Pr = 0.71$,$\eta = 0.1$ and $\mathcal{H}_a = 2$).

5.2 MHD TRANSIENT FREE CONVECTIVE FLOW IN A VERTICAL ANNULUS WITH THERMAL BOUNDARY CONDITION OF THE SECOND KIND[2]

The problem of MHD free convective flow within the annulus of two concentric cylinders is analysed in this section. The transient free-convection current is set up within the annulus due to the sudden imposition of constant heat flux at the outer surface of the inner cylinder, while the inner surface of the outer cylinder is maintained at constant temperature. In order to capture the present physical situation, the thermal boundary condition of the second kind is used at the outer surface of the inner cylinder, while the thermal boundary condition of the first kind is utilized at the inner surface of the outer cylinder. The results obtained are compared with the steady state solutions which have been obtained separately.

5.2.1 Mathematical Analysis

We consider the MHD free convection motion of a viscous, incompressible and electrically conducting fluid filling the gap between two vertical concentric cylinders of infinite length. The z'-axis is assumed to be on the axis of the cylinders in the vertical direction and r'-axis is on the radial direction. The fluid flow between the two cylinders in the presence of magnetic field acting perpendicular to the flow direction. Initially, ($t < 0$), the fluid and the annular surfaces are at the same tempeature T_0 and there is no fluid motion. At time $t > 0$,

[2]Jha and Apere (2012a) Published in
Trans. ASME J. Heat Transfer **134** 042502 (2012) ; doi: 10.1115/1.4005109

heat is supplied at a constant rate to the fluid trapped between the two cylinders through the inner cylinder ($r = a$) while the inner surface of the outer cylinder ($r = b$) is maintained at constant temperature T_0 which causes the transient natural convection inside the annulus. Since the cylinders are of infinite length and the flow is fully developed, all physical variables are functions of r' and t. The walls of the cylinders are assumed to be electrically non-conducting. The magnetic Reynolds number is assumed to be very small which corresponds to negligible induced magnetic field compared to the externally applied one, therefore, the uniform magnetic field $\vec{B}$ is a constant $\vec{B} \equiv (B_0, 0, 0)$ and is considered as the total magnetic field acting on the fluid. It is assumed that no applied, polarisation voltage exists and the Hall effects of MHD are negligible. Also, all fliud properties are assumed to be temperature independent, while the viscous and Joule dissipation terms are neglected. See Figure 5.12 for the schematic diagram of the problem. Under the usual Boussinesq approximation, the present problem is governed by the following equations

$$\frac{\partial T'}{\partial t} = \frac{\kappa}{\rho C_p}\left[\frac{\partial^2 T'}{\partial r'^2} + \frac{1}{r'}\frac{\partial T'}{\partial r'}\right] \tag{5.29}$$

$$\frac{\partial u'}{\partial t} = \nu\left[\frac{\partial^2 u'}{\partial r'^2} + \frac{1}{r'}\frac{\partial u'}{\partial r'}\right] - \frac{\sigma B_0^2}{\rho}u' + g\xi(T' - T_0) \tag{5.30}$$

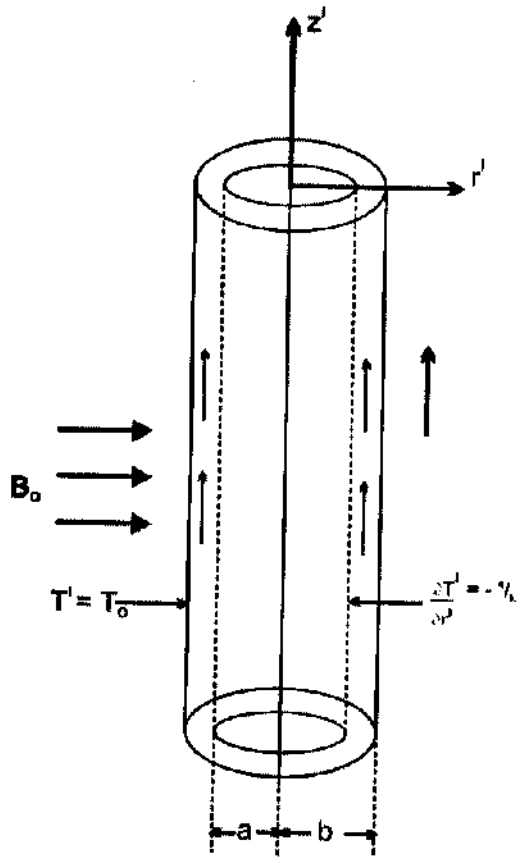


Figure 5.12: Schematic of the problem

The initial and boundary conditions for the problem are

$$\begin{aligned} u' &= 0,\ T' = T_0, \quad a \le r' \le b \text{ and } t \le 0, \\ u' &= 0,\ \frac{\partial T'}{\partial r'} = -\Omega/\kappa, \quad \text{at } r' = a, t > 0; \\ u' &= 0,\ T' = T_0, \quad \text{at } r' = b,\ t > 0. \end{aligned} \tag{5.31}$$

5.2.2 Solution of the Problem

Introducing the following dimensionless quantities in eqs. (5.29) - (5.31);

$$r = r'/a,\ u = \frac{u'\kappa\nu}{g\xi\Omega a^3},\ \eta = \nu t/a^2,\ \theta = \frac{(T'-T_0)\kappa}{\Omega a},\ Pr = \mu C_p/\kappa, \mathcal{H}a = B_0 a\sqrt{\sigma/\nu\rho}$$

and $\varsigma = b/a$

Eq. (5.29) and (5.30) can then be written in dimensionless form as

$$\frac{\partial\theta}{\partial\eta} = \frac{1}{Pr}\left[\frac{\partial^2\theta}{\partial r^2} + \frac{1}{r}\frac{\partial\theta}{\partial r}\right] \tag{5.32}$$

$$\frac{\partial u}{\partial\eta} = \frac{\partial^2 u}{\partial r^2} + \frac{1}{r}\frac{\partial u}{\partial r} - \mathcal{H}a^2 u + \theta \tag{5.33}$$

subject to the following dimensionless initial and boundary conditions

$$\begin{aligned} u &= 0,\ \theta = 0, \quad 1 \le r \le \varsigma \text{ and } \eta \le 0, \\ u &= 0,\ \frac{\partial\theta}{\partial r} = -1, \quad \text{at } r = 1, \eta > 0; \\ u &= 0,\ \theta = 0, \quad \text{at } r = \varsigma,\ \eta > 0. \end{aligned} \tag{5.34}$$

The solutions of eqs. (5.32) and (5.33) and the corresponding boundary conditions (5.34) can be obtained using the Laplace transforms technique as follows:

$$\frac{d^2\bar{\theta}}{dr^2} + \frac{1}{r}\frac{d\bar{\theta}}{dr} - sPr\bar{\theta} = 0 \tag{5.35}$$

$$\frac{d^2\bar{u}}{dr^2} + \frac{1}{r}\frac{d\bar{u}}{dr} - (s + \mathcal{H}a^2)\bar{u} = -\bar{\theta} \tag{5.36}$$

The boundary condition now becomes

$$\bar{u} = 0, \ \frac{d\bar{\theta}}{dr} = -s^{-1} \ at \ r = 1, \ and \ \bar{u} = \bar{\theta} = 0 \ at \ r = \varsigma, \tag{5.37}$$

The solution of eq. (5.35) together with the boundary condition (5.37) is

$$\bar{\theta}(r,s) = A_1 I_0(\gamma_1 r) + A_2 K_0(\gamma_1 r), \tag{5.38}$$

from where we obtain,

$$\frac{\partial\bar{\theta}}{\partial r} = \gamma_1[A_1 I_1(\gamma_1 r) - A_2 K_1(\gamma_1 r)] \tag{5.39}$$

Eq. (5.39) and the boundary condition (5.37) are used to calculate A_1 and A_2, while the solution of eq. (5.36) is

$$\bar{u}(r,s) = A_3 I_0(\delta r) + A_4 K_0(\delta r) + \frac{A_1 I_0(\gamma_1 r) + A_2 K_0(\gamma_1 r)}{(\delta^2 - \gamma_1^2)}, \tag{5.40}$$

where $\gamma_1 = \sqrt{sPr}$, $\delta = \sqrt{s+M^2}$, $A_1 = -\frac{K_0(\gamma_1\varsigma)}{\gamma_1 sC}$, $A_2 = \frac{I_0(\gamma_1\varsigma)}{\gamma_1 sC}$, $A_3 = \frac{K_0(\delta\varsigma)C_1}{C_3(\delta^2-\gamma_1^2)}$, $A_4 = -\frac{I_0(\delta\varsigma)C_1}{C_2(\delta^2-\gamma_1^2)}$,

$C = K_0(\gamma_1\varsigma)I_1(\gamma_1) + K_1(\gamma_1)I_0(\gamma_1\varsigma)$, $C_1 = A_1 I_0(\gamma_1) + A_2 K_0(\gamma_1)$, $C_2 = I_0(\delta\varsigma)K_0(\delta) - K_0(\delta\varsigma)I_0(\delta)$.

Eqs. (5.38) and (5.40) are inverted using the Riemann-sum approximation as follows:

$$\theta(r,\eta) = \frac{e^{\gamma\eta}}{\eta}\left[\frac{1}{2}\bar{\theta}(r,\gamma) + Re\sum_{k=1}^{N}\bar{\theta}(r,\gamma+\frac{ik\pi}{\eta})(-1)^k\right] \tag{5.41}$$

$$u(r,\eta) = \frac{e^{\gamma\eta}}{\eta}\left[\frac{1}{2}\bar{u}(r,\gamma) + Re\sum_{k=1}^{N}\bar{u}(r,\gamma+\frac{ik\pi}{\eta})(-1)^k\right]. \tag{5.42}$$

5.2.3 Rate of Heat Transfer and Skin Friction

The rate of heat transfer which is represented by the Nusselt number (Nu) is obtained by differentiating the temperature with respect to r as follows:

$$Nu = \frac{d\theta}{dr}\Big|_{r=\varsigma} = \frac{e^{\gamma\eta}}{\eta}\left[\frac{1}{2}\bar{\theta}_1(r,\gamma) + Re\sum_{k=1}^{N}\bar{\theta}(r,\gamma+\frac{ik\pi}{\eta})(-1)^k\right], \tag{5.43}$$

where

$$\bar{\theta}_1(r,s) = \gamma_1[A_1 I_1(\gamma_1 r) - A_2 K_1(\gamma_1 r)]. \tag{5.44}$$

The rate of heat transfer on the inner surface of the outer cylinder is obtained by substituting $r = 2$ in eq. (5.44).

The skin friction τ is defined as $\frac{\partial u}{\partial r}$, it is obtained by differentiating equation (5.42) with respect to r as

$$\tau = \frac{\partial u}{\partial r} = \frac{e^{\varepsilon\eta}}{\eta}\left[\frac{1}{2}\bar{u}_1(z,\gamma) + Re\sum_{k=1}^{N}\bar{u}_1(z,\gamma+\frac{ik\pi}{\eta})(-1)^k\right], \tag{5.45}$$

where

$$\bar{u}_1(r,s) = \delta[A_3 I_1(\delta r) - A_4 K_1(\delta r)] + \gamma[\frac{A_1 I_1(\gamma r) - A_2 K_1(\gamma r)}{(\delta^2-\gamma^2)}]. \tag{5.46}$$

Equation (5.45) represents the general expression for the skin friction between different fluid layers between the two cylinders. The skin frictions at the outer surface of the inner cylinder ($r = 1$) and that at the inner surface of the outer cylinder ($r = 2$) can then be obtained from eq. (5.45).

5.2.4 Steady State

The expression for the steady state velocity distribution u_s is obtained by setting $\partial()/\partial\eta$ in eqs. (5.32) and (5.33) to zero. We then obtain the following ordinary differential equation as

$$\frac{d^2\theta_s}{dr^2} + \frac{1}{r}\frac{d\theta_s}{dr} = 0 \tag{5.47}$$

$$\frac{d^2u_s}{dr^2} + \frac{1}{r}\frac{du_s}{dr} - \mathcal{H}a^2 u = -\theta_s. \tag{5.48}$$

The solutions of eqs. (5.47) and (5.48) together with the boundary condition (5.34) are

$$\theta_s(r) = -ln(r) + ln(\varsigma) \tag{5.49}$$

$$u_s(r) = D_1 I_0(\mathcal{H}_a r) + D_2 K_0(\mathcal{H}_a r) - \frac{1}{\mathcal{H}a^2}[ln(r) - ln(\varsigma)], \tag{5.50}$$

where

$$D_1 = -\frac{K_0(\varsigma\mathcal{H}a)[ln(1) - ln(\varsigma)]}{\mathcal{H}a^2[K_0(M)I_0(\varsigma\mathcal{H}a) - K_0(\varsigma\mathcal{H}a)I_0(\mathcal{H}a)]} \tag{5.51}$$

$$D_2 = \frac{I_0(\varsigma\mathcal{H}a)[ln(1) - ln(\varsigma)]}{\mathcal{H}a^2[K_0(\mathcal{H}a)I_0(\varsigma\mathcal{H}a) - K_0(\varsigma\mathcal{H}a)I_0(\mathcal{H}a)]}. \tag{5.52}$$

The numerical values of the velocity obtained analytically for the steady state are compared with those of the transient state obtained using the Riemann-sum approximation method in Table I. The values of $\mathcal{H}a$ and Pr used to generate the results in the Table are 2 and 0.71 respectively. We observed in Table I that at a particular point in the annulus, the transient velocity increases with time until it reaches its steady state. The values of the transient state velocity when $\eta = 10.0$ are observed in Table I to coincides with the steady state values. It can then be concluded that, there is an excellent agreement between the Riemann-sum approximation method and the analytical method.

5.2.5 Results and Discussion

From the solution, we observe that the temperature is dependent on the time and the Prandtl number, while the velocity depends on time, Prandtl number and the Hartmann number. Numerical solution for the temperature, velocity, skin friction and the rate of heat transfer are computed from the semi-analytical solution with the help of MATLAB 7.2, the results are depicted graphically in Figures 5.13-5.20 for various values of time, Prandtl number and the Hartmann

Table 5.2: Comparison of the numerical values of the transient state velocity obtained using the Riemann-sum approximation method and the steady state velocity obtained analytically when $\mathcal{H}a = 2$ and $Pr = 0.71$

η	r	*Velocity*	
		Transient State	*Steady State*
0.2	1.2	0.0106	0.0234
	1.4	0.0109	0.0275
	1.6	0.0077	0.0218
	1.8	0.0038	0.0115
0.4	1.2	0.0180	0.0234
	1.4	0.0205	0.0275
	1.6	0.0158	0.0218
	1.8	0.0082	0.0115
10.0	1.2	0.0234	0.0234
	1.4	0.0275	0.0275
	1.6	0.0218	0.0218
	1.8	0.0115	0.0115

number. The behaviour of the temperature with respect to time and the Prandtl number are shown in Figures 5.13 and 5.14. The figures shows an exponential decrease in the fluid temperature from the outer surface of the inner cylinder to zero on the inner surface of the outer cylinder. The temperature is seen to increase with time in Figure 5.13, while it decreases with an increase in Prandtl number in Figure 5.14. This is expected as fluids with high Prandtl number have a small thermal conductivity and high viscosity, which normally result into low heat penetration and a reduced thermal layer.

Figures 5.15–5.17 shows the velocity profile, the fluid velocity is observed to be parabolic in these figures with maximum velocity shifted towards the outer surface of the inner cylinder due to the asymmetric heating of the annular surfaces. In Figure 5.15, we noticed that the velocity increases with time on

the outer surface of the inner cylinder until it reaches its equilibrium value and then decreases to zero on the inner surface of the outer cylinder. An increase in the Prandtl number leads to a decrease in velocity as seen in Figure 5.16, this is physically true because as Pr increases, the thermal diffusivity of the fluid decreases causing weak convection current, hence a reduction in velocity. Similarly, we observe in Figure 5.17 that increasing values of the Hartmann number results into a decrease in the fluid velocity. This is due to the retarding nature of the Lorentz force which slow down the motion of the fluid. The effect of time and the Prandtl number on the flow velocity is seen to be more pronounced at small values of the two parameters.

The contour graph of the rate of heat transfer is depicted in Figure 5.18, we noticed in this contour that the rate of heat transfer increases with the Prandtl number and decreases with time on the inner surface of the outer cylinder. The increase in the Nu as the Pr increases is expected, as Pr increases the thermal diffusivity of the fluid decreases thereby causing weak penetration of heat (that is, accumulation of heat causing high temperature gradient), this results into high Nu. The variation of the skin friction with respect to Hartmann number $\mathcal{H}a$ and time η is depicted in Figures 5.19 and 5.20. The skin friction decreases with $\mathcal{H}a$ and increases with η on the outer surface of the inner cylinder, while an increase with Hartmann number and a decrease with time is seen on the inner surface of the outer cylinder. This is physically correct as the Hartmann number decreases the velocity which invariably led to a reduction in the velocity

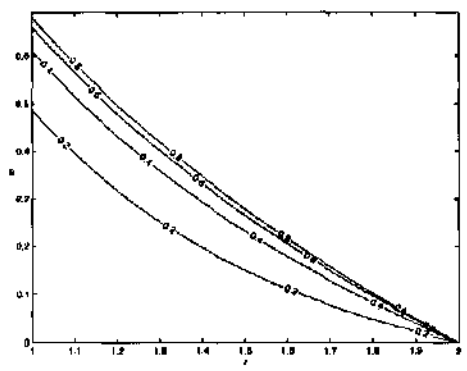


Figure 5.13: Temperature profile θ showing the effect of η with $Pr = 0.71$ and $\mathcal{H}a = 2$.

gradient (skin friction). The numerical results obtained for the steady state for both the temperature and the velocity are compatible with the transient ones at large values of time.

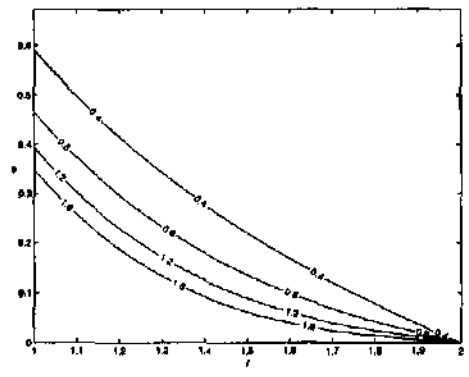


Figure 5.14: Temperature profile θ showing the effect of Pr with $\eta = 0.2$ and $\mathcal{H}a = 2$.

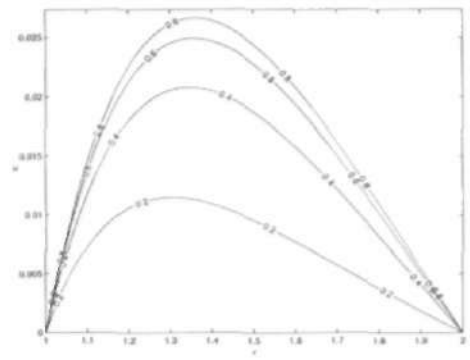


Figure 5.15: Velocity profile u showing the effect of η with $Pr = 0.71$ and $\mathcal{H}a = 2.0$.

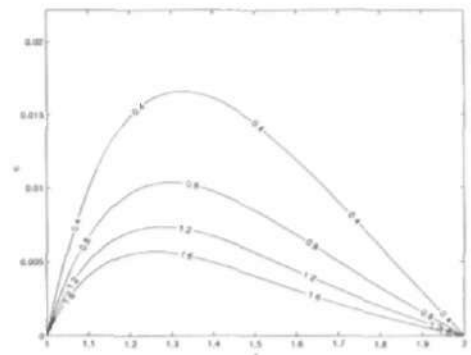


Figure 5.16: Velocity profile u showing the effect of Pr with $\eta = 0.2$ and $\mathcal{H}a = 2$.

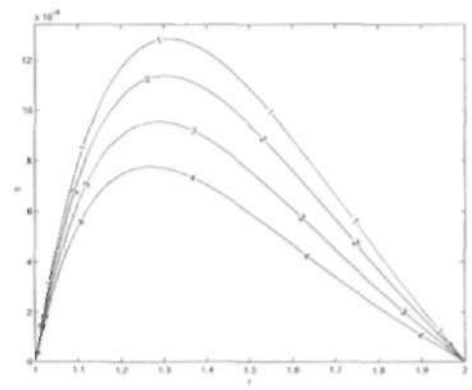


Figure 5.17: Velocity profile u showing the effect of $\mathcal{H}a$ with $Pr = 0.71$ and $\eta = 0.2$.

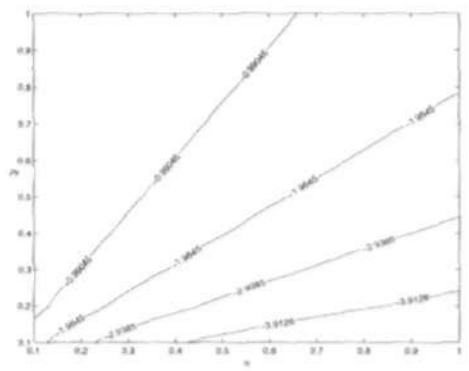


Figure 5.18: Contour graph of the rate of heat transfer at the inner surface of the outer cylinder ($r = 2$) showing the effect of Pr and η.

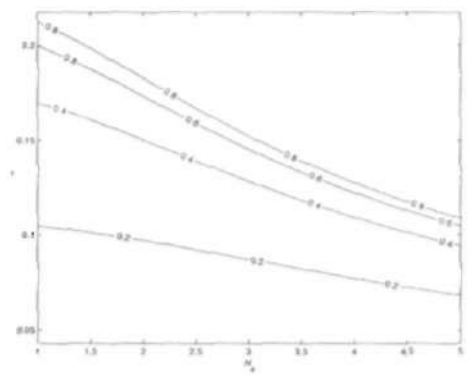


Figure 5.19: The skin friction at the outer surface of the inner cylinder ($r = 1$) showing the effect of $\mathcal{H}a$ and η.

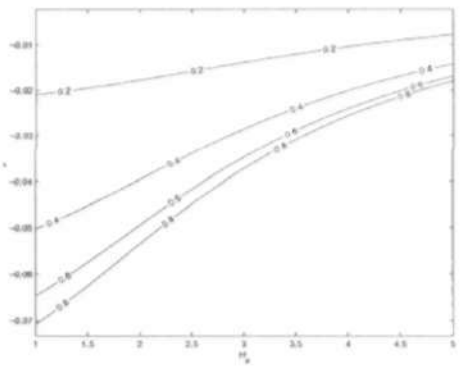


Figure 5.20: The skin friction at inner surface of the outer cylinder ($r = 2$) showing the effect of $\mathcal{H}a$ and η.

5.3 CONCLUDING REMARKS

This chapter investigated the unsteady MHD free convective Couette flow of a viscous incompressible electrically conducting fluid between two parallel porous plates and in two concentric cylinders. Using the Riemann sum approximations method, one can solve the transformed governing equations and consider the effects of flow parameters such as Ha, Pr, S and Gr on the flow behaviour and the dependence of the temperature, velocity, rate of heat transfer and skin friction on these parameters. The main deductions of the Chapter are as follows:

a. The velocity increases as Gr increases positively and decreases as Gr is increased negatively.

b. For the case when the porous plate is being cooled ($Gr > 0$), the velocity decreases as S increases, while for the heating ($Gr < 0$) the velocity is seen to increase.

c. The rate of heat transfer Nu decreases with increasing values of both the suction/injection parameter and the Prandtl number on the moving plate.

d. The skin friction decreases with both suction and injection on the surface of the moving plate when the channel is being cooled, while on the stationary plate, the skin friction increases with injection.

CHAPTER 6

SUMMARY, CONCLUSIONS AND FUTURE DIRECTIONS

6.1 SUMMARY

This dissertation has investigated the flow of viscous incompressible fluid in a channel formed by either two parallel plates or an annulus formed by two concentric cylinders under different physical situations. The different physical situations considered include: MHD Couette flow in both the parallel plates channel and in an annulus, MHD two-phase Couette flow as well as MHD free convective flow. The dissertation also factored the effect of Hall and ion-slip currents, rotation and transpiration in some of the problems.

The system of partial differential equations describing the different flow problems has been formulated and unified closed form expressions are obtained for both cases of the applied magnetic field being fixed to either the fluid or the moving wall where applicable. The Laplace transform techniques are used to reduce the system of partial differential equations to ordinary differential equations; the resulting boundary value problems are then solved analytically where possible or the Riemann-sum approximation method where direct inversion is difficult. The implicit finite difference method is used to verify

the Riemann-sum approximation method. MATLAB programmes are written to compute and generate the graphs for the velocities and the skin frictions.

6.2 CONCLUSIONS

This dissertation is devoted to the mathematical analysis and solutions of the MHD flow of an incompressible Newtonian fluids in two different types of geometries. In Chapters 2, we have studied the MHD Couette flow in a parallel plates channel; while Chapter 3 deals with flow in an annular channel. Chapters 4 deals with the problem of two-phase flow while Chapter 5 examined MHD free convective flow. We have investigated the effect of different dimensionless parameters on the flow regime. From our investigations, our contributions to knowledge are the following:

a. The velocity increases with Ha when the magnetic field is fixed relative to the moving wall.

b. Injection has an increasing effect on both the primary velocity and the magnitude of the secondary velocity while suction has the opposite effect.

c. The effect of both the Hall and ion-slip parameters is to increase the primary velocity and reduce the secondary velocity.

d. Fixing the magnetic field relative to the moving wall always results into the phenomenon of backflow on the secondary velocity in the presence of Hall and ion-slip currents.

e. The skin frictions at the opposite walls are seen to be of opposite sign; at the stationary wall it is positive and negative at the moving wall.

f. The skin friction decreases with both suction and injection on the surface of the moving wall.

g. The velocity of the fluid phase and the particle phase decrease with increase in Hartmann number.

h. The skin friction for both the fluid and the particle phases decreases with time on both walls.

i. The skin friction is also observed to decrease with increase in the particle viscosity on the moving wall while an opposite behaviour was been noticed on the stationary wall.

j. The velocity increases as Gr increases positively and decreases as Gr is increased negatively.

k. For the case when the porous plate is being cooled ($Gr > 0$), the velocity decreases as S increases, while for the heating ($Gr < 0$) the velocity is seen to increase.

l. The rate of heat transfer Nu decreases with increasing values of both the suction/injection parameter and the Prandtl number on the moving plate.

m. The skin friction decreases with both suction and injection on the surface of the moving plate when the channel is being cooled, while on the stationary

480026

plate, the skin friction increases with injection.

6.3 FUTURE DIRECTIONS

From this dissertation, there are several apparent options available for future research in thie field of MHD. Our focus on future research will be directed towards these questions. The magnetic fields studied in this dissertation are not sufficiently strong to create an induced field, therefore, we expect that future study will capture the strong field limit and eventually consider the cases were the magnetic field will be the dominant factor in the analysis. Further, there has been some development in the area of MHD recently, we will also direct our research to the field of MHD in fusion plasma which has generated a lot of interest in the scientific community. On the whole, we have only scratched the surface of all the different effects and possible configurations in the study of MHD. We list below a few of the extensions that we find to be the most interesting, which is not a complete list of all the possibilities but gives an idea of how much more research is still available in the field of MHD.

6.3.1 Induced Magnetic Field

We have neglected the induced magnetic field in this dissertation by assuming a small magnetic Reynolds number. However, in a system where the magnetic field strengths are sufficiently large, some induced field will be created within the channel (Sutton and Sherman 1965). For a realistic analysis, these induced magnetic field must be accounted for. Investigations considering the effect

of the induced magnetic field have been carried out by Mazumder (1977b); Soundalgekar and Uplekar (1986); Mazumder et al. (1976) and Niranjan et al. (1990) amongst others. We intend to consider the effect of induced magnetic field in future research.

6.3.2 Non-Newtonian Fluid

This dissertation aimed at providing analytical solutions; to that effect, we have assumed the fluids to be Newtonian and incompressible in order to simplify the analysis. The Navier-Stokes equation bocome complicated when MHD flow of realistic interest (turbulent, chemically reacting, multiconstituents and/or non-Newtonian) are considered. The governing equations become highly non-linear and it is almost impossible to obtain analytical solution for non-Newtonian fluids taking all the aforementioned factors into account. However, with the advent of high powered supercomputers and the persistent study of higher accuracy, approximate solutions to the MHD equations of non-Newtonian fluids can be obtained. We intend to probe further into the true behaviour of MHD considering non-Newtonian fluids in the nearest future. Some of the literature on non-Newtonian fluids include those of Oldroyd (1951); Hayat et al. (1999); Rajagopal (1983) and Erdogan (1995) amongst others.

6.3.3 Compressible Fluid

Gases are normally modeled as incompressible fluids in both microscopic and macroscopic calculations as long as the pressure changes are less than about

20 per cent of the mean pressure. (See Geankoplis (1993) and Denn (1980)). However, for flow that experiences a significant variatiions in density, the assumptions of incompressibility cannot hold. For example, when dealing with gases at higher velocities and liquids with large pressure changes; significant variations in density can occur. We have to account for the change in density in the analysis if accurate results are to be obtained. We intend to continue our studies of MHD flow by investigating a more general case of fluid beyond the assumptions of incompressibility. Analysis on the compressible MHD flow have been carried out by some authors like those of Yee and Sjögreen (2003) and Gasol et al. (2000).

6.3.4 MHD in Fusion Plasma

Having it in mind that the major use of MHD is in plasma physics, we hope to redirect our attention to that area in the nearest future. The growth of MHD instabilities in toroidal fusion devices can be prevented or reduced by the control of conducting walls and external magnetic field. Also, strong magnetic fields may be used to confine rings or columns of hot plasma that (it is hoped) will be held long enough for thermonuclear fusion to occur and for net power to be generated.[1] Most fusion power scenarios require wall stabilisation to reach high fusion power density and low recirculating power. The research area that is of interest to the larger scientific community includes the fields of space research

[1] Available online at
http://www.pma.caltech.edu/Courses/ph136/yr2004/0418.1.K.pdf

and nonlinear dynamics.[2] It will enhance the understanding of basic non-linear MHD phenomena, like mode-mode interaction, which is relevant to a large variety of plasmas. We intend to carry out numerical simulations of MHD flows in complex, electrically coupled geometries for fusion applications.

[2]Available online at
http://researchprojects.kth.se/index.php/kb_7943/io_9195/io.html

APPENDIX I

List of constants used to define the velocity and the skin friction in Chapter 2

$$A_1 = \frac{\mathcal{H}_a^2 K}{m^2}(e^{-m\eta} - 1),\ A_2 = \frac{\mathcal{H}_a^2 K}{m},$$
$$A_3 = \frac{\mathcal{H}_a^2 K}{m^2}\left[e^{-m\eta} + \eta m - 1\right],\ A_4 = \frac{\mathcal{H}_a^2 K(\alpha + i\gamma)}{m}$$

$$f_1(x_1,x_2,x_3) = \frac{1}{2}\Bigg[\Big(x_1 + \frac{x_2}{\sqrt{x_3}}\Big)\exp(x_2\sqrt{x_3})\operatorname{erfc}\Big(\frac{x_2}{2\sqrt{x_1}} + \sqrt{x_1 x_3}\Big)$$
$$+ \Big(x_1 - \frac{x_2}{\sqrt{x_3}}\Big)\exp(-x_2\sqrt{x_3})\operatorname{erfc}\Big(\frac{x_2}{2\sqrt{x_1}} - \sqrt{x_1 x_3}\Big)\Bigg]$$

$$f_2(x_1,x_2,x_3) = \frac{1}{2}\Bigg[\exp(x_2\sqrt{x_3})\operatorname{erfc}\Big(\frac{x_2}{2\sqrt{x_1}} + \sqrt{x_1 x_3}\Big)$$
$$+ \exp(-x_2\sqrt{x_3})\operatorname{erfc}\Big(\frac{x_2}{2\sqrt{x_1}} - \sqrt{x_1 x_3}\Big)\Bigg]$$

$$
\begin{aligned}
f_3(x_1,x_2,x_3) &= \frac{1}{2}\Bigg[\exp(x_2\sqrt{x_3})\mathrm{erfc}\Big(\frac{x_2}{2\sqrt{x_1}}+\sqrt{x_1x_3}\Big)\Big(\frac{1}{\sqrt{x_3}}+x_1\sqrt{x_3}+x_2\Big)\\
&- \sqrt{x_3}\exp(-x_2\sqrt{x_3})\mathrm{erfc}\Big(\frac{x_2}{2\sqrt{x_1}}-\sqrt{x_1x_3}\Big)\Big(\frac{1}{\sqrt{x_3}}+x_1\sqrt{x_3}-x_2\Big)\\
&- \frac{2}{\sqrt{\pi x_1}}\exp\Big(\frac{-x_2^2}{4}-x_1x_3\Big)\Bigg]
\end{aligned}
$$

$$
\begin{aligned}
f_4(x_1,x_2,x_3) &= -\frac{1}{2}\Bigg[\sqrt{x_3}\exp(x_2\sqrt{x_3})\mathrm{erfc}\Big(\frac{x_2}{2\sqrt{x_1}}+\sqrt{x_1x_3}\Big)\\
&- \sqrt{x_3}\exp(-x_2\sqrt{x_3})\mathrm{erfc}\Big(\frac{x_2}{2\sqrt{x_1}}-\sqrt{x_1x_3}\Big)\\
&+ \frac{2}{\sqrt{\pi x_1}}\exp\Big(\frac{-x_2^2}{4}-x_1x_3\Big)\Bigg]
\end{aligned}
$$

$$
f_5(x_1,x_2) = \mathrm{erfc}\Big(\frac{x_2}{2\sqrt{x_1}}\Big)
$$

$$
f_6(x_1,x_2) = -\frac{1}{\sqrt{\pi x_1}}\exp\Big(-\frac{x_2^2}{4x_1}\Big)
$$

REFERENCES

Abramowitz, M. and Stegun, I. A., editors (1965). *Handbook of Mathematical Functions, with Formulas, graphs and Mathemathecal Tables.* Dover, New York.

Ahmad, N. and Kumari, S. (2009). Effect of Hall current on steady MHD Couette flow in a rotating system. *Int. J. Theoretical and Appl. Mech.*, 4:1–16.

Al-Nimr, M. A. and Alkam, M. (1999). Magnetohydrodynamics transient free convection in open-ended vertical porous annuli. *Journal of Thermophysics and Heat Transfer*, 13:256–265.

Al-Nimr, M. A. and Hader, M. A. (1999). MHD free convection flow in open-ended vertical porous channels. *Chemical Engineering Science*, 54:1883–1889.

Alam, M. S., Rahman, M. M., and Samad, M. A. (2006). Dufour and soret effects on unsteady MHD free convection and mass transfer flow past a vertical plate in a porous medium. *Nonlinear Analysis: Modeling and Control*, 11:271–226.

Aldoss, T. K., Ali, Y. D., and Al-Nimr, M. A. (1996). MHD mixed convection from a horizontal circular cylinder. *Numerical Heat Transfer*, 30:379–396.

Antimirov, M. Y. and Kolyshkin, A. A. (1984). Nonstationary MHD flow in an annular channel in a radial magnetic field. *Magnetohydrodynamics*, 20:285–288.

Aruna Prasad, T. B. and Venkatasiva Murthy, K. N. (1991). Transient flow in a rotating porous annulus due to suction at the walls. *ZAMM - Journal of Applied Mathematics and Mechanics/Zeitschrift für Angewandte Mathematik und Mechanik*, 42:605–613.

Attia, H. A. (2005a). MHD Couette flow with temperature dependent viscosity and the ion-slip. *Tamkang J. Sci. and Engng.*, 8:11–16.

Attia, H. A. (2005b). Unsteady Couette flow with heat transfer considering ion-slip. *Turk J. Phys.*, 29:379–388.

Avilla, M., Marques, F., Lopez, J. M., and Meseguer, A. (2007). Stability control and catastrophic transition in a forced Taylor-Couette system. *J. Fluid Mech.*, 590:471–496.

Banks, W. H. H. and Zaturska, M. B. (1992). On flow through a porous annular

pipe. *Physics of Fluids*, 4:1131–1141.

Bearman, A. S. (1953). Laminar flow in channels with porous walls. *J. Appl. Phys.*, 24:1232–1235.

Bearman, A. S. (1958). Laminar flow in an annulus with porous walls. *J. Appl. Phys.*, 29:71–75.

Chamkha, A. J. (1998). Effects of particulate diffusion on the compressible boundary layer flow of a two-phase suspension over a horizontal surface. *Trans. ASME, J. Fluids Engineering*, 1201:146–151.

Chamkha, A. J. (2000). Unsteady laminar hydromagnetic fluid-particle flow and heat transfer in channels and circular pipes. *International Journal of Heat and Fluid Flow*, 21:740–746.

Chamkha, A. J. and Ramadan, H. M. (1998). Analytical solutions for free convection flow of a particulate suspension past an infinite vertical surface. *Int. J. Engng Sci.*, 36:49–60.

Chandran, P., Saccheti, N. C., and Singh, A. K. (1993). Effect of rotation on unsteady hydromagnetic Couette flow. *Astrophys. Space Sci.*, 202:1–10.

Churchill, R. V. (1972). *Operational Mathematics*. McGraw-Hill, Kogashuka, 3rd, Int. student edition.

Damseh, R., Al-Odatand, M. Q., and Al-Nimr, M. A. (2008). Entropy generation during fluid flow in a channel under the effect of transverse magnetic field. *Heat and Mass Transfer*, 44:897–904.

Das, S., Maji, S. L., and Jana, R. N. (2009). Unsteady MHD Couette flow in a rotating system. *Mathematical and Computer Modelling*, 50:1211–1217.

Datta, N. and Dalai, D. C. (1995). Pulsatile flow and heat transfer of a dusty fluid through an infinitely long annular pipe. *International Journal of Multiphase Flow.*, 21:515–528.

Debnath, L., Ray, S. C., and Chatterjee, A. K. (1979). Effect of Hall current and rotation on unsteady hydromagnetic flow past a porous plate in a rotating system. *ZAMM - Journal of Applied Mathematics and Mechanics/Zeitschrift für Angewandte Mathematik und Mechanik*, 59:469–471.

Deka, R. K. (2008). Hall effects on MHD flow past an accelerated plate. *Theoret. Appl. Mech.*, 35:333–346.

Denn, M. M. (1980). *Process Fluid Mechanics*. Prentice Hall, Englewood Clifs, NY.

Dizaji, A. F., Salimpour, M. R., and Jam, F. (2008). Flow field of a third grade

non-Newtonian fluid in the annulus of rotating concentric cylinders in the presence of magnetic fields. *J. Math. Anal. Appl.*, 337(632–645).

Drew, D. A. (1983). Mathematical modelling of two-phase flow. *Ann. Rev. Fluid Mech.*, 15:261–291.

Dubner, H. and Abate, J. (1968). Numerical inversion of Laplace transforms by relating them to the Fourier Cosine transform. *JACM*, 15:115–123.

Ellahi, R., Hayat, T., Mahomed, F. M., and Zeeshan, A. (2009). Analytic solutions for MHD flow in an annulus. *Commun Nonlinear Sci Numer Simulat*, 15:1224–1227.

Erdogan, M. E. (1995). Plane surface suddenly set in motion in a non-Newtonian fluid. *Acta Mech.*, 108:179–187.

Fayzullyev, F. (1966). Computer, laminarnoye dvijeniye mnogofaznih sredb trboprovodah izd. *FAN, Taşkent*.

Ferdows, M., Sattar, M. A., and Siddiki, M. N. A. (2004). Numerical approach on parameters of the thermal radiation interaction with convection in boundary layer flow at a vertical plate with variable suction. *Thammasat Int. J. of Sci. and Tech.*, 9:19–28.

Fitzpatrick, R. (2011). Newtonian dynamics. Lecture Notes.

Fleisch, D. A. (2008). *A Student's Guide to Maxwell's Equations*. Cambridge University Press.

Fornberg, B. (1998). *A Practical guide to pseudospectral methods*. Cambridge University Press.

Gadiraju, M., Peddieson, J., and Munukutla, S. (1992). Exact solutions for two-phase vertical pipe flow. *Mech. Res. Commun.*, 19:7–13.

Gasol, A., Passot, T., and Sulem, P. L. (2000). On the reduced MHD for compressible fluids. *RevMexAA (Serie de Conferencias)*, 9:80–82.

Geankoplis, C. J. (1993). *Transport Processes and Unit Operators*. Prentice Hall, Englewood Clifs, NY, 3rd edition.

Georgantopoulos, G. A., Doukas, C. N., Kafousias, N. G., and Goudas, C. L. (1979). Hydromagnetic free convection effects on the Stokes problem for an infinite vertical plate. *Letters Heat Mass Trans.*, 6:397–404.

Ghosh, S. and Ghosh, A. K. (2008). On hydromagnetic rotating flow of a dusty fluid near a pulsating plate. *Comp. Appl. Math.*, 27:1–30.

Ghosh, S. K. (1993). Unsteady hydrodynamic flow in a rotating channel with

oscillatory pressure gradient. *J. Phys. Soc. Jpn*, 62:3893–3905.

Ghosh, S. K. and Pop, I. (2003). Hall effects on unsteady hydromagnetic flow in a rotating system with oscillatory pressure gradient. *Int. J. Appl. Mech. Eng.*, 8:43–56.

Ghosh, S. K. and Pop, I. (2004). Hall effects on MHD Couette flow in a rotating environment. *Int. J. Appl. Mech. Eng.*, 9:293–304.

Gidaspow, D. (1986). Hydrodynamics of fluidization and heat transfer: Super computing modelling. *Appl. Mech. Rev.*, 39:1–23.

Gireesha, B. J., Bagewadi, C. S., and Kumara, B. C. P. (2007). Flow of unsteady dusty fluid under varying pulsatile pressure gradient in anholonomic co-ordinate system. *EJTP*, 14:9–16.

Globe, S. (1959). Laminar steady-state Magnethydrodynamic flow in an annular channel. *Physics of Fluids*, 2:404–407.

Gupta, R. K. and Gupta, S. C. (1975). Couette flow of a dusty gas between two infinite coaxial cylinders. *Indian J. Pure Appl. Math.*, 6:56–67.

Guria, M., Jana, R. N., and Ghosh, S. K. (2006). Unsteady Couette flow in a rotating system. *Int. J. Non-Linear Mech.*, 41:838–843.

Guria, M., Jana, R. N., and Ghosh, S. K. (2009). Oscillatory Couette flow in the presence of an inclined magnetic field. *Meccanica*, 556-559.

Hartmann, J. (1937). Hg-dynamics in a homogeneous magnetic field, Part I. *Mathematical Physics Journal, Copenhagen*, 15(6).

Hartmann, J. and Lazarus, F. (1937). Experimental investigations on the flow of mercury in a homogeneous magnetic field. *K. Dan Vidensk. Selsk. Mat. Fys. Medd.*, 15.

Hayat, T., Asghar, S., and Siddique, A. M. (1999). On the moment of plane disk in a non-Newtonian fluid. *Acta Mech.*, 136:125–131.

Jain, R. K. and Mehta, K. N. (1962). Laminar hydromagnetic flow in an annulus with porous walls. *Physics of Fluids*, 5:1207–1211.

Jana, R. N., Data, N., and Mazumder, B. S. (1977). Magnetohydrodynamic Couette flow and heat transfer in a rotating system. *J. Phys. Soc. Jpn*, 42:1034–1039.

Jha, B. K. (2001). Natural convection in unsteady MHD Couette flow. *Heat and Mass Transfer*, 37:329–331.

Jha, B. K. and Apere, C. A. (2010a). Combined effect of Hall and ion-slip currents

of an unsteady MHD Couette flow in a rotating system. *J. Phys. Soc. Jpn.*, 79:124401/1–9.

Jha, B. K. and Apere, C. A. (2010b). Unsteady MHD Couette flow in an annuli: The Riemann-sum approximaion approach. *J. Phys. Soc. Jpn.*, 79:124403/1–5.

Jha, B. K. and Apere, C. A. (2011a). Hall and ion-slip effect on unsteady MHD Couette flow in a rotating system with suction and injection. *J. Phys. Soc. Jpn*, 80:114401.

Jha, B. K. and Apere, C. A. (2011b). Magnetohydrodynamics free convective Couette flow with suction and injection. *Trans. ASME J. Heat Transfer*, 133:1–12.

Jha, B. K. and Apere, C. A. (2011c). Time-dependent MHD Couette flow in a rotating system. *ZAMM - Journal of Applied Mathematics and Mechanics/Zeitschrift für Angewandte Mathematik und Mechanik*, 91:832–842.

Jha, B. K. and Apere, C. A. (2011d). Unsteady MHD two-phase Couette flow of fluid-particle suspension in an annulus. *AIP Advances*, 1:042121.

Jha, B. K. and Apere, C. A. (2012a). Magnetohydrodynamic transient free convective flow in a vertical annulus with thermal boundary condition of the second kind. *Trans. ASME J. Heat Transfer*, 134:042502.

Jha, B. K. and Apere, C. A. (2012b). Time-dependent MHD Couette flow of rotating fluid with Hall and ion-slip currents. *Appl. Math. Mech. -Engl. Ed.*, 33:399–410.

Katagiri, M. (1962). Flow formation in Couette motion in Magnetohydrodynamics. *J. Phys. Soc. Jpn*, 17:393–396.

Latipov, K. S. (1963). O nekotorih zadaçah neustanovivşixsya teçeniy dvuh komponentnih sred. *Izv. AN UzSSR Ser. Teh. Nauk*, 4:21–29.

Leveque, R. J. (2007). *Finite Difference Methods for Ordinary and Partial Differential Equations, Steady State and Time Dependent Problems*. SIAM.

Makinde, O. D., Bég, O. A., and Takhar, H. S. (2009). Magnetohydrodynamic viscous flow in a porous medium cylindrical annulus with an applied radial magnetic field. *Int. J. Appl. Math. and Mech.*, 5:68–81.

Makinde, O. D. and Chinyoka, T. (2010). MHD transient flows and heat transfer of dusty fluid in a channel with variable physical properties and Navier slip condition. *Comp. Math. Appl.*, 60:660–669.

Makinde, O. D. and Chinyoka, T. (2011). Numerical study of unsteady hydromagnetic generalised Couette flow of a reactive third grade fluid with

asymmetric convective cooling. *Computers and Math. with Appl.*, 61:1167–1179.

Mandal, G. and Mandal, K. K. (1983). Effect of Hall current on MHD Couette flow between thick arbitrarily conducting plate in a rotating system. *J. Phys. Soc. Jpn*, 52:470–477.

Mazumder, B. S. (1977a). Combined effect of Hall current and rotation on hydromagnetic flow over an oscillating porous plate. *Int. J. Engng Sci.*, 15:601–606.

Mazumder, B. S. (1977b). Effect of wall conductance on hydromagnetic flow and heat transfer in a rotating channel. *Acta Mech.*, 28:85–99.

Mazumder, B. S. (1991). An exact solution of an oscillatory Couette flow in a rotating system. *Trans. ASME J. Appl. Mech.*, 58:1104–1107.

Mazumder, B. S., Gupta, A. S., and Datta, N. (1976). Hall effect on combined free and forced convective hydromagnetic flow through a channel. *Int. J. Engng Sci.*, 14:285–292.

Muhuri, P. K. (1963). Flow formation in Couette motion in Magnetohydrodynamics with suction. *J. Phys. Soc. Jpn.*, 18:1671–1675.

Muzychka, Y. S. and Yovanovich, M. M. (2006). Unsteady viscous flows and Stokes first problem. *Proceedings of IMECE*, 14301:1–11.

Nag, S. K., Jana, R. N., and Datta, N. (1979). Couettte flow of a dusty gas. *Acta Mech*, 33:179–187.

Nandi, S. (1973). Steady hydromagnetic viscous flow in an annulus with porous walls. *PAGEOPH*, 105:825–835.

Nanousis, N. D., Georgantopoulos, G. A., and Papaioannou, A. I. (1980). Hydromagnetic free convection flow in the Stokes problem for a porous vertical limiting surface with constant suction. *Astrophys. Space Sci.*, 70:370–377.

Narahari, M. (2009). Natural convection in unsteady Couette flow between two vertical parallel plates in the presence of constant heat flux and radiation. *Proc of the 11th WSEAS Int. Conf. on Math. and Comp Methods in Sci. and Engng.*, pages 73–78.

Niranjan, S. S., Soundalgekar, V. M., and Takhar, H. S. (1990). Free convection effects on MHD horizontal channel flow with Hall currents. *IEEE Trans. on Plasma Sci.*, 18:177–183.

Oldroyd, J. G. (1951). The motion of an elastico-viscous liquid contained between coaxial cylinders 1. *Quart. J. Mech. Appl. Math.*, 4:271–282.

Ozoe, H. and Maruo, E. (1987). Magnetic and gravitational natural convection of melted silicon:Two-dimensional numerical computations for the rate of heat transfer. *J.S.M.E.*, 30:774–784.

Pai, S. I. (1962). *Magnetogasdynamics and Plasma Dynamics*. Springer, Berlin.

Rahmatulin, H. A. (1956). Osnovi gidrodinamiki vzaimopronikayuşih dvijeniy. *Prikladnaya Matematika i Makanika*, 20:56–65.

Rajagopal, K. R. (1983). Longitudinal and torsional oscillations of a rod in a non-Newtonian fluid,. *Acta Mech.*, 49:281–285.

Ram, P. C. (1995). Effects of Hall and ion-slip currents on free convective heat generating flow in a rotating fluid. *Int. J. Energy Research*, 19:371–376.

Raptis, A. and Singh, A. K. (1983). MHD free convection flow past an accelerated vertical plate. *Int. Comm. Heat and Mass Trans.*, 10:313–321.

Rashmi, S., Kavitha, V., Roohi, B. S., Gurumurthy, Gireesha, B. J., and Bagewadi, C. S. (2007). Unsteady flow of a dusty fluid between two oscillating plates under varying constant pressure gradient. *Novi Sad J. Math.*, 37:25–34.

Ravi, S. K. and Singh, A. K. (2011). Natural convection of a polar fluid in vertical concentric annuli. *Int. J. Appl. Math and Mech.*, 7:70–81.

Recebli, Z. and Kurt, H. (2008). Two-phase steady flow along a horizontal glass pipe in the presence of magnetic and electric fields. *International Journal of Heat and Fluid Flow*, 29:263–268.

Saffman, P. G. (1962). On the stability of laminar flow of a dusty gas. *J. Fluid Mech.*, 13:120–128.

Sankar, M., Venkatachalappa, M., and Shivakumara, I. S. (2006). Effect of magnetic field on natural convection in a vertical cylindrical annulus. *Int. J. of Engng. Sci.*, 44:1556–1570.

Schlichting, H. (1965). *Boundary Layer Theory*. McGraw-Hill New York.

Seth, G. S., Ansari, M. S., and Nandkeolyar, R. (2011). Effects of rotation and magnetic field on unsteady Couette flow in a porous channel. *J. Appl. Fluid Mech.*, 4:95–103.

Seth, G. S. and Jana, R. N. (1980). Unsteady hydromagnetic flow in a rotating channel with oscillating pressure gradient. *Acta Mech.*, 37:29–34.

Seth, G. S., Jana, R. N., and Maiti, M. K. (1982). Unsteady hydromagnetic Couette flow in a rotating system. *Int. J. Engng Sci.*, 20:989–889.

Seth, G. S., Nandkeolyar, R., Mahto, N., and Singh, S. K. (2009). MHD Couette

flow in a rotating system in the presence of an inclined magnetic field. *Appl. Math. Sci.*, 3:2919–2932.

Shojaefard, M. H., Noorpoor, A. R., and Avanesians, A. (2005). Numerical investigation of flow control by suction and injection on a subsonic airfoil. *Am J. Appl Sci.*, 20:1474–1480.

Simon, R. M., Strout, M. T., and Weiss, G. H. (1972). Numerical inversion of Laplace transforms with application to percentage labelled experiments. *Comput. Biomed. Res.*, 6:596–607.

Singh, A. K. (1983). MHD free convection flow in the Stokes problem for a porous vertical plate in a rotating system. *Astrophys. Space Sci.*, 162:283–289.

Singh, A. K. (1984). Stokes problem for a porous vertical plate with heat sinks by finite difference method. *Astrophys. Space Sci.*, 103:241–248.

Singh, A. K. and Kumar, N. (1983). Unsteady hydromagnetic Couette flow. *Wear*, 89:125–129.

Singh, A. K., Sacheti, N. C., and Chandran, P. (1994). Transient effects on Magnetohydrodynamics Couette flow with rotation: Accelerated motion. *Int. J. Engng Sci.*, 35:133–139.

Singh, A. K. and Singh, J. N. (1989). Transient MHD free convection in a rotating system. *Astrophys. Space Sci.*, 34:123–123.

Singh, J. and Dube, S. N. (1973). Unsteady flow of a dusty fluid through a circular pipe. *Indian J. Pure Appl. Math.*, 6:69–79.

Singh, S. K., Jha, B. K., and Singh, A. K. (1997). Natural convection in vertical concentric annuli under a radial magnetic field. *Heat and Mass Transfer*, 32:399–401.

Singha, N. G. and Deka, P. N. (2006). Skin-friction for unsteady free convection MHD flow between two heated vertical parallel plates. *Theoret. Appl. Mech.*, 33:259–280.

Soundalgekar, V. M. (1979). Free convection effects on the flow past a vertical oscillating plate. *Astrophysics and Space Science*, 64:165–172.

Soundalgekar, V. M. and Uplekar, A. G. (1986). Hall effects in MHD flow with heat transfer. *Trans. on Plasma Sci.*, PS-14:579–583.

Subotic, M. and Lai, F. C. (2010). Flows and their stabilty in rotating cylinders with a porous lining. *Trans. ASME, J. Fluids Eng.*, 132:051201.

Sukumaran, A. K., Reji, R. V., and Santhosh, K. S. (2010). Fluid flow simulations

within rotating annulus. *Proc. of the 37th Nat. & 4th Conf. on Fluid Mech. and Fluid Power*, AM4:1–10.

Sutton, G. and Sherman, A. (1965). *Engineering Magnetohydrodynamics*. McGraw-Hill New York.

Takhar, H. S., Ali, M. A., and Soundalgekar, V. M. (1989). Stability of MHD Couette flow in a narrow gap annulus. *Applied Scientific Research*, 46:1–24.

Taylor, G. I. (1923). Stability of a viscous liquid contained between two rotating cylinders. *Phil. Trans. Royal Society*, A223:289–343.

Tillack, M. S. and Morley, N. B. (1998). *Standard Handbook for Electrical Engineers: Magnetohydrodynamics*. McGraw-Hill New York.

Tiwari, R. and Singh, K. (1983). Effect of Hall current on unsteady hydromagnetic boundary layers in rotating dusty fluid. *Indian J. Pure Appl. Math.*, 14:159–165.

Tsangaris, S., Kondaxakis, D., and Vlachakis, N. W. (2006). Exact solution of the Navier-Stokes equations for the pulsating Dean flow in a channel with porous walls. *Int. J. Engng Sci.*, 44:1498–1509.

Tsangaris, S. and Vlachakis, N. W. (2007). Exact solution for the pulsating finite gap Dean flow. *Appl. Math. Mod.*, 31:1899–1906.

Tzou, D. Y. (1997). *Macro to Microscale Heat Transfer: The Lagging Behaviour*. Taylor and Francis, Washington.

Venkatachalappa, M., Sankar, and Natarajan, A. A. (2001). Natural convection in an annulus between two rotating cylinders. *Acta Mech.*, 147:173–196.

Verma, P. D. and Bansal, J. L. (1969). Laminar flow in an annulus with porous walls of different permeability. *Proc. Natn. Inst. Sci. India*, 35:77–93.

Wang, C. Y. (1971). Pulsative flow in a porous channel. *Trans. ASME: Ser. E J. Appl. Mech.*, 38:553–555.

Wang, C. Y. (1989). Exact solutions of the unsteady Navier–Stokes equations. *Appl. Mech. Rev.*, 42:s269–s282.

Wang, C. Y. (1991). Exact solutions of the steady state Navier–Stokes equations. *Ann. Rev. Fluid Mech.*, 23:159–177.

Weir, A. D. (1976). Axisymmetric convection in a rotating sphere, I. Stress-free surface. *J. Fluid Mech.*, 75:49–79.

Weng, L. C. and Chu, H. S. (1996). Combined natural convection and radiation in a vertical annulus. *Heat and Mass Transfer*, 31:731–379.

Widder, D. V. (1941). *Laplace Transform (Mathematical Series)*. Princeton Univ Pr,

1st edition.

Yee, Y. C. and Sjögreen, B. (2003). Divergence free high order filter methods for the compressible MHD equation. *Proc. of the Int. Conf. on High Performance Sci. Computing, March 10-14, 2003, Hanoi, Vietnam.*

Zaturska, M. B. and Banks, W. H. H. (1995). Suction-driven flow in a porous pipe. *ZAMM - Journal of Applied Mathematics and Mechanics/Zeitschrift für Angewandte Mathematik und Mechanik*, 75:21–30.